Functional validation of human rare missense variants associated with body fat distribution and cardiometabolic risk

Liang Dong

Murray Edwards College

University of Cambridge

April 2021

This thesis is submitted for the degree of Doctor of Philosophy

Declaration

This thesis is the result of my own work and includes nothing which is the outcome of work done in collaboration except as declared in the Preface and specified in the text. I further state that no substantial part of my thesis has already been submitted, or, is being concurrently submitted for any such degree, diploma or other qualification at the University of Cambridge or any other University or similar institution except as declared in the Preface and specified in the text. It does not exceed the prescribed word limit for the relevant Degree Committee.

Summary

Liang Dong

Functional validation of human rare missense variants associated with body fat distribution and cardiometabolic risk

Body fat distribution is a predictor of metabolic and cardiovascular disease independent of body mass index (BMI) and is heritable. To understand the genetic determinants of the differences observed in fat distribution in the general population, genome-wide association studies (GWAS) have emerged as an extremely useful approach and have convincingly associated many single nucleotide polymorphisms (SNPs) with body fat distribution. Unfortunately, it has proven very difficult to link specific genes or genetic variants with these findings, reducing their translational impact. However, massive increases in the size of human genetic studies have increased the power of studies to confidently link rare missense (coding) variants with a range of phenotypes. In collaboration with colleagues in the MRC Epidemiology Unit in Cambridge, we recently identified rare missense variants in *ALK7* (p.I195T and p.N150H), *CALCRL* (p.L87P), *PLIN1* (p.L90P) and *PDE3B* (p.R783X) which were associated with a favourable body fat distribution and with protection from cardiometabolic disease, while a variant in gene *PNPLA2* (p.N252K) was associated with an adverse phenotype (*1*).

To understand the roles of these genes, initial loss-of-function studies were carried out using siRNA-mediated knockdown in 3T3-L1 (pre)adipocytes, as all the genes are expressed in adipose tissue and have been at least loosely implicated in the regulation of intracellular lipolysis. In this cell model, *Plin1* depletion resulted in an increase in basal lipolysis while isoproterenol stimulated lipolysis was suppressed. *Pnpla2* depletion, on the other hand, impaired lipolysis under both basal and stimulated conditions. *Alk7* or *Calcrl* knockdown resulted in a consistent decrease in lipolysis while the impact on adipogenesis was variable. Depletion of *Pde3b* did not have any impact on adipogenesis or lipolysis.

Subsequent studies focussed on functional analysis of a subset of the specific missense variants. mRNA expression of the *PNPLA2* p.N252K variant was lower in the heterozygous carriers of the mutant allele than in homozygous wild-type allele carriers, although notably the variant retained its ability to target lipid droplets and also its catalytic activity. Functional analysis of the *ALK7* variants indicated that the p.I195T variant failed to initiate signal transduction upon stimulation with known ligand Nodal, while the impact of the p.N150H mutant was far more subtle. Meanwhile, the *PLIN1* p.L90P variant seemed to manifest a stronger interaction with HSL compared to wild type in the basal state. However, further investigation suggested that this variant suppressed stimulated lipolysis while the ability to promote lipid accumulation was unaffected.

Collectively, these findings provide some early insights into the potential impact of variants convincingly linked with altered body fat distribution and metabolic disease risk, but further work is required to more clearly understand exactly how they affect adipogenesis and/or lipolysis and thereby modify fat distribution and disease risk *in vivo*.

Acknowledgements

First and foremost, I would like to express my special thanks of gratitude to my supervisor, Prof David Savage, who offered me the great opportunity to work on this project. His continuous support and invaluable guidance drove me during the research and dissertation preparation. I am extremely grateful for his considerable amount of patience throughout the entire journey. It has been a great privilege and honour to work and study under his supervision.

I am very grateful to Dr Satish Patel, for sharing his comprehensive knowledge and insightful perspectives, which provided valuable input every step of the way. I would also like to thank Dr Luca Lotta for the human genetic studies, which has laid the groundwork for the project. Thanks must be extended to Dr Koi Ni Lim for performing the 3' RACE; the members of the MRC Epidemiology Unit for providing the PBMC samples; Dr Martina Schweiger for sending the YFP-tagged PNPLA2 construct; Dr Nuno Rocha and Alice Williamson for sharing materials for the bioassays of ALK-7.

I wish to express my sincere thanks to all the members of the Savage group for their scientific advice and cherished friendship. I am fortunate to have worked in such an enjoyable environment with all the fun we had in the past few years. Special thanks to the admin team in the IMS, who worked swiftly to make the institute COVID secure during the first national lockdown.

最后，我首先要感谢父母对我无条件的支持与鼓励，他们对我的信任和期许是促使我完成学业的动力之一。千言万语都无法表达我对父母的感激之情，简言之就是：我爱你们！其次我要感谢丈夫一路以来的陪伴，一起经历生活的五味杂陈，一同见证学业的高低起伏。很幸运遇到你，相信我们的未来会更加美好！再次要感谢公婆助力，你们辛苦了！最后的最后，我要感谢小米粒和小老虎为我带来的欢乐，尤其是在论文撰写阶段，真的很舍不得你们，希望你们平安舒适。

Table of Contents

Abbreviations

Acronym	Definition
β-AR	β-adrenergic receptor
aa	Amino acid
ABHD5	α/β hydrolase domain-containing protein 5
AC	Adenylyl cyclase
ACC	Acetyl-CoA carboxylase
ACTR-I (ALK-2)	Activin receptor type-1 (activin receptor-like kinase 2)
ACTR-IB (ALK-4)	Activin receptor type-1B (activin receptor-like kinase 4)
ACTR-IC (ALK-7)	Activin receptor type-1C (activin receptor-like kinase 7)
ACTR-IIB	Activin receptor type-2B
ADIPOQ	Adiponectin
ADM	Adrenomedullin
AGPAT	1-acylglycerol-3-phosphate acyltransferase
AMH (MIS)	Anti-Müllerian hormone (Müllerian inhibitory substance)
AMPK	AMP-activated protein kinase
ANOVA	Analysis of variance
ANP	Atrial natriuretic peptide
ATGL (PNPLA2, $iPLA_2\zeta$)	Adipose triglyceride lipase (patatin-like phospholipase domain-containing protein 2, calcium-independent phospholipase $A_2\zeta$)
ATP	Adenosine triphosphate
B2M	Beta-2-microglobulin
BAT	Brown adipose tissue
BiFC	Bimolecular fluorescence complementation
BMAT	Bone marrow adipose tissue
BMI	Body mass index
BMP	Bone morphogenetic protein
BMPR-1A (ALK-3)	BMP receptor type-1A (activin receptor-like kinase 3)
BMPR-1B (ALK-6)	BMP receptor type-1B (activin receptor-like kinase 6)
BSA	Bovine serum albumin
C/EBP	CCAAT/enhancer binding protein
CALCRL (CRLR)	Calcitonin gene-related peptide type 1 receptor (calcitonin receptor-like receptor)
cAMP	Cyclic adenosine monophosphate
CCPG	Constitutive coactivator of PPARγ
cDNA	Complementary DNA
cGI-PDE	cGMP-inhibited cyclic nucleotide phosphodiesterase
cGMP	Cyclic guanosine monophosphate
CGRP	Calcitonin gene-related peptide
CNS	Central nervous system
Co-Smad	Common mediator Smad
CpG	5’-C-phosphate-G-3’
$cPLA_2$	Cytosolic phospholipase A_2
CREB	cAMP response element-binding protein

CRIPTO (TDGF1)	Teratocarcinoma-derived growth factor 1
CT	Computed tomography
Ct	Threshold cycle
CTR	Calcitonin receptor
ddNTP	Dideoxynucleotide triphosphate
DEXA	Dual-energy X-ray absorptiometry
DG	Diglyceride
DGAT	Diacylglycerol acyltransferase
DMEM	Dulbecco's Modified Eagle's Medium
dNTP	Deoxynucleoside triphosphate
Dox	Doxycycline
DPBS	Dulbecco's phosphate buffered saline
ECD	Extracellular domain (ectodomain)
ECL	Extracellular loop
EM	Electron microscopy
ER	endoplasmic reticulum
ERK	Extracellular signal-regulated kinase
ERRα (NR3B1)	Estrogen-related receptor α (nuclear receptor subfamily 3 group B member 1)
ESE	Exonic splicing enhancer
ESS	Exonic splicing silencer
EV	Empty vector
EWAS	Epigenome-wide association studies
EWAT	Epididymal WAT
FA	Fatty acid
FABP4	Fatty acid-binding protein 4
FASN	Fatty acid synthase
FAT (CD36)	Fatty acid translocase (cluster of differentiation 36)
FATP	Fatty acid transport protein
FBS	Fetal bovine serum
FFA	Free fatty acid
FOXO1	Forkhead box protein O1
FPLD	Familial partial lipodystrophy
FRET	Förster resonance energy transfer
FSP27 (CIDEC)	Fat-specific protein of 27 kDa (cell death-inducing DFF45-like effector C)
FTO	Fat mass and obesity associated
G0S2	G0/G1 switch protein 2
GC	Guanylyl cyclase
GDF	Growth and differentiation factor
gDNA	Genomic DNA
GFP	Green fluorescent protein
G_i	Inhibitory regulatory G-protein
GLUT (SLC2)	Glucose transporter (solute carrier family 2)
GPAT	Glycerol-3-phosphate acyltransferase
GPCR	G protein-coupled receptor
GPR81	G protein-coupled receptor 81

G_s	Stimulatory G-protein
GTP	Guanosine triphosphate
GWAS	Genome wide association studies
HFD	High-fat diet
HIF3A	Hypoxia-inducible factor 3α
HLPDA	Hypoxia-inducible lipid droplet-associated protein
HPRT1	Hypoxanthine-guanine phosphoribosyltransferase
HRP	Horseradish peroxidase
HSL	Hormone sensitive lipase
IBMX	3-isobutyl-1-methylxanthine
ICL	Intracellular loop
IGF-1	Insulin-like growth factor 1
IL-6	Interleukin 6
IR	Insulin receptor
IRES	Internal ribosome entry site
IRS	Insulin receptor substrate
JNK	c-Jun N-terminal kinase
KO	Knockout
KRB	Krebs-Ringer buffer
LB	Luria broth
LD	Lipid droplet
LDL	Low-density lipoprotein
LEP	Leptin
LPL	Lipoprotein lipase
LTR	Long terminal repeat
LYPLAL1	Lysophospholipase-like protein 1
M-MLV	Moloney Murine Leukaemia Virus
MAF	Minor allele frequency
MAPK	Mitogen-activated protein kinase
MCP-1 (CCL2)	Monocyte chemoattractant protein 1 (C-C motif chemokine 2)
MEF	Mouse embryonic fibroblast
MEK	Mitogen-activated protein kinase kinase
MG	Monoglyceride
MGL	Monoglyceride lipase
miRNA	MicroRNA
MRI	Magnetic resonance imaging
MSRA	Mitochondrial peptide methionine sulfoxide reductase
mTORC1	Mammalian target of rapamycin complex 1
NA	Numerical aperture
NAFLD	Non-alcoholic fatty liver disease
NC	Negative control
NCS	Newborn calf serum
NHR	N-terminal hydrophobic region
NHS	National Health Service
NLSD	Neutral lipid storage disease
NLSDI (CDS)	Neutral lipid storage disease with ichthyosis (Chanarin-Dorfman syndrome)

NLSDM	Neutral lipid storage disease with myopathy
NO	Nitric oxide
NPR-A	Atrial natriuretic peptide receptor 1
PAP	Phosphatidic acid phosphatase
PAT	Perilipin, ADRP and TIP47
PBMC	Peripheral blood mononuclear cell
PC	Phosphatidylcholine
PCR	Polymerase chain reaction
PCSK9	Proprotein convertase subtilisin/kexin type 9
PCYT1A (CCTα)	Choline-phosphate cytidylyltransferase A
PDE	Phosphodiesterase
PE	Phosphatidylethanolamine
PGC-1α	PPARγ coactivator-1α
PI	Phosphatidylinositol
PI3K	Phosphoinositol-3 kinase
PIP_3	Phosphatidylinositol-3,4,5-triphosphate
PKA	Protein kinase A
PKB (AKT)	Protein kinase B (serine/threonine-protein kinase)
PKC	Protein kinase C
PKG	Protein kinase G
PLIN	Perilipin
PPA	Posterior-probability of association
PPARγ	Peroxisome proliferator-activated receptor γ
PPIA	peptidyl-prolyl cis-trans isomerase A (cyclophilin A)
PS	Phosphatidylserine
qPCR	Real-time quantitative PCR
R-Smad	Receptor-regulated Smad
RACE	Rapid amplification of cDNA ends
RAMP	Receptor activity modifying protein
RBP4	Retinol-binding protein 4
RCP	Receptor component protein
RT	Room temperature
rtTA	Reverse Tet transactivator
SAT	Subcutaneous adipose tissue
SBE	Smad-binding element
SCD	Stearoyl-CoA desaturase
SD	Standard deviation
SE	Sterol ester
siRNA	Small interfering RNA
SIRT1	NAD-dependent protein deacetylase sirtuin-1
SKR3 (ALK-1)	Serine/threonine-protein kinase receptor R3 (activin receptor-like kinase 1)
SM	Sphingomyelin
Smad	Mothers against decapentaplegic homologue
SNAP	Soluble N-ethylmaleimide sensitive factor attachment protein
SNARE	SNAP receptor
SNP	Single nucleotide polymorphism

SP	Signal peptide
SPINK1	Pancreatic secretory trypsin inhibitor
SREBP1	Sterol regulatory element-binding protein 1
SVF	Stromovascular fraction
T2D	Type 2 diabetes
TFAP2B	Transcription factor AP-2-beta
TG	Triglyceride
TGF-β	Transforming growth factor-β
TGFR-1 (ALK-5)	TGF-β receptor type-1 (activin receptor-like kinase 5)
TM	Transmembrane
Tm	Melting temperature
TNF-α	Tumour necrosis factor-α
TRB-3	Tribbles homologue 3
TRE	Tetracycline-response element
TSOD	Tsumura Suzuki Obese Diabetes
UV	Ultra-violet
VAT	Visceral adipose tissue
VLDL	Very low-intensity lipoprotein
WAT	White adipose tissue
WHO	World Health Organization
WHR	Waist-to-hip ratio
WPRE	Woodchuck hepatitis virus post-transcriptional regulatory element
WT	Wild type
YFP	Yellow fluorescent protein

Amino acids

Amino acid	3-letter code	1-letter code
Alanine	Ala	A
Arginine	Arg	R
Asparagine	Asn	N
Aspartic acid (aspartate)	Asp	D
Cysteine	Cys	C
Glutamic acid (glutamate)	Glu	E
Glutamine	Gln	Q
Glycine	Gly	G
Histidine	His	H
Isoleucine	Iso	I
Leucine	Leu	L
Lysine	Lys	K
Methionine	Met	M
Phenylalanine	Phe	F
Proline	Pro	P
Serine	Ser	S
Threonine	Thr	T
Tryptophan	Trp	W
Tyrosine	Tyr	Y
Valine	Val	V

1 General Introduction

1.1 Obesity and cardiometabolic diseases

Obesity, which is described as excessive accumulation of body fat, has already become a global public health problem with the estimated worldwide prevalence having nearly tripled (from 15% of adults to almost 40%) between 1975 and 2016, according to the World Health Organization (WHO) (*2*, *3*) (https://www.who.int/news-room/fact-sheets/detail/obesity-and-overweight). The severe health impact of being overweight or obese is indicated in at least 2.8 million deaths per year worldwide being attributed to these problems based on a WHO report in 2017 (https://www.who.int/features/factfiles/obesity/en/). Life expectancy is predicted to be shortened by a fifth and a third of a year for females and males, respectively, by the middle of the 21st century (*4*). Based on past and present trends, it is projected that more than half of the global population will be obese by 2030 (*5*). Taking the UK as an example, obesity and its related diseases place an enormous financial burden on the National Health Service (NHS) which may cost an estimated £22.9 billion per year by 2050 (*4*). The rise in the prevalence of obesity in both children and adults is mainly attributable to technological advances which have reduced the prices for food and drink production, especially for less nutritious food, and promoted sedentary lifestyles (*6*).

Not only can obesity lead to poor quality of life due to lower earnings and lower probability of employment, but it can also contribute to the development of serious chronic diseases, such as diabetes, cardiovascular diseases and some cancers (*4*, *7*). Among them all, cardiovascular disease is the top single cause of death globally, which ultimately indicates obesity as a strong predictor of mortality (*3*, *4*, *8*) (https://www.who.int/news-room/fact-sheets/detail/cardiovascular-diseases-(cvds)). Besides, being obese is also associated with greater risk of developing metabolic syndrome, which is defined as a group of conditions that co-occur, including diabetes, hypertension, hypertriglyceridemia, hyperglycaemia and increased central adiposity (*9*). Data shows that the incidence of metabolic syndrome often runs in parallel with the prevalence of obesity and type 2 diabetes (T2D) (*10*). Although it is difficult to collect global data since the criteria varies slightly between different organizations,

metabolic syndrome was estimated to affect one quarter of the global population based on the same report published in 2018 (*10*).

As a widely used measurement for obesity, body mass index (BMI) is calculated as an individual's body weight (kilogram, kg) divided by the square of body height (metre, m). Adult subjects with a BMI between 25 and 30 kg/m^2 are considered as overweight, while those over 30 kg/m^2 are obese (*11*). As body composition varies by age and gender, BMI for children and teens is often expressed as BMI-for-age in relation to others from the same age and gender group. Overweight is therefore defined as BMI between the 85th percentile and the 95th percentile, and obesity is above the 95th percentile of the same age and gender (*12*). Although BMI can be used as an indicator for overall adiposity, it does not distinguish between lean mass and fat mass, nor does it indicate fat mass distribution. Numerous techniques are available for measurement of body fat, dual-energy X-ray absorptiometry (DEXA) is particularly useful to determine body fat composition and distribution in large population studies (*11*). Other imaging techniques such as computed tomography (CT) and magnetic resonance imaging (MRI) could also provide quantitative information on local fat storage (*11*, *13*). Several studies have shown that independent of BMI, body fat distribution plays an important role in relation to comorbid conditions associated with obesity since it was first described in 1956 (*14*–*16*). Particularly central adiposity which has been shown to be positively associated with incidents of T2D, cardiovascular risk and risk of death, independent of general adiposity (*17*–*20*). In a longitudinal Swedish population study, the authors have found that the ratio of waist to hip circumferences showed a stronger association with cardiovascular disease risk than BMI (*21*, *22*). Similar conclusion was drawn from a study in a Finnish population (*23*). Furthermore, large hip and thigh circumferences have been implicated in the association with a lower risk of T2D in the Hoorn study based on a Dutch population, independently of BMI (*24*).

1.2 Body fat distribution and cardiometabolic risk

The most popular anthropometric measurement for body fat distribution is the ratio of waist to hip circumferences, widely known as the waist-to-hip ratio (WHR), which is specifically

designed to focus on intra-abdominal fat (*11*, *25*). The proposed mechanism explaining the causality between body fat distribution and cardiometabolic risk is the location and regulation of adipose tissue (*8*). It is well acknowledged that individuals carrying greater upper body fat (apple or android body shape – high WHR) have increased cardiometabolic risk, whereas subjects with fat stored in the lower body (pear or gynoid body shape – low WHR) have less risk (Figure 1.1) (*15*, *25*, *26*). Besides the profile of the transcriptome and proteome, the secretome response in adipose tissue to environmental signals is largely depot-dependent, which could contribute to the risk of disease development (*27*).

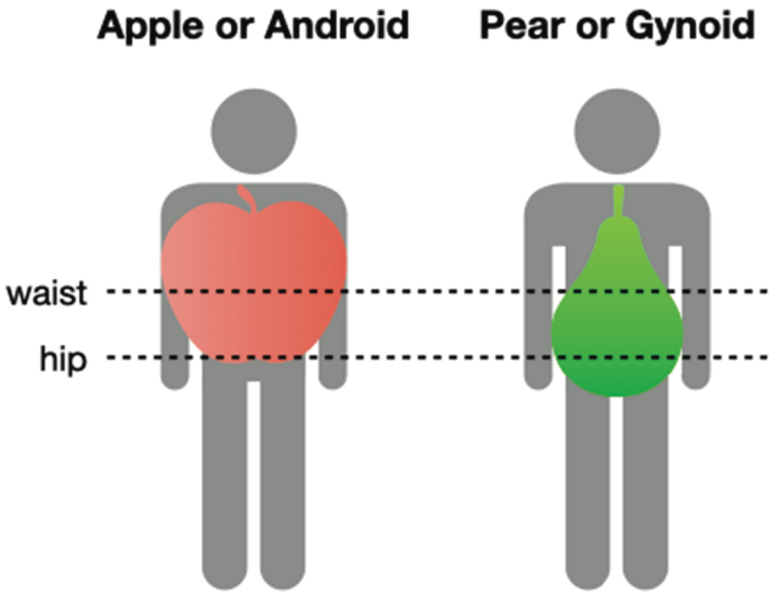

Figure 1.1 Waist-to-hip ratio (WHR) is used as a measurement for body fat distribution. Increased upper body fat (apple or android body shape) indicates a higher cardiometabolic risk (left), whereas fat accumulated in the lower body (pear or gynoid body shape) is considered as having less risk (right).

1.2.1 Adipose tissue anatomy and distribution

Adipose tissue is the primary site for fat storage that drives lipid distribution, and also a highly active metabolic and endocrine/paracrine organ (*28–31*). The tissue is primarily composed of adipocytes but also consists of a stromovascular fraction (SVF) which contains preadipocytes, fibroblasts, endothelial cells, as well as macrophages and other immune cells (*28–31*). A

number of cytokines termed adipokines are secreted from the adipose tissue to communicate with other distant organs such as the brain, liver, skeletal muscle and pancreas in order to modulate systemic metabolism (*29*, *32*, *33*).

In general, adipose tissue can be morphologically divided into white adipose tissue (WAT) and brown adipose tissue (BAT). In humans, BAT is abundant in newborns and located predominantly in the interscapular and supraclavicular area. It decreases in adults and only accounts for approximately 4% of total fat mass (*27*, *32*, *33*). Brown adipocytes contain multiple small lipid droplets and many mitochondria and the main function of BAT is for non-shivering thermogenesis upon prolonged cold exposure (*29*, *32*). In contrast to adult human BAT, rodent BAT depots are well-defined within the interscapular, perirenal, and periaortic regions (*34*). In addition, species-specific differences between human and mouse BAT have been noted, such as their responses to β3 adrenergic activation or glucocorticoid stimulation (*35*). Beige or brite adipose tissue is a form of BAT, which is dispersed within WAT (*27*, *29*). It has the capability of transforming into brown-like adipocytes when induced by cold exposure and/or adrenergic stimulation (*27*, *29*). Consequently, expansion of BAT results in increased thermogenesis, lipid oxidation, as well as reduced adiposity, at least in rodent models (*36*). In fact, multiple lines of evidence suggested that human BAT more closely resembles to murine beige/brite adipose tissue than to the classic BAT of mice based on gene expression signatures (*37*, *38*).

Unlike brown adipocytes, a typical white adipocyte contains a large unilocular lipid droplet in the cytoplasm, which occupies most of the cell volume. The size of adipocytes varies between 25 and 200 μm in diameter, depending on the amount of lipid loaded in the lipid droplet (*29*). WAT represents more than 95% of total body fat and is distributed throughout the whole body (*27*). Broadly speaking, there are two major types of WAT, subcutaneous adipose tissue (SAT) can usually be found beneath the skin, and visceral adipose tissue (VAT) which is mostly around internal organs (Figure 1.2) (*33*, *39*). In addition, there is bone marrow adipose tissue (BMAT) in bone marrow, dermal WAT within the reticular dermis of the skin, and other types of WAT that are located in the retro-orbital and periarticular regions (*39–41*).

SAT contributes more than 80% of all adipose tissue and resides in both upper and lower body, mostly in the subscapular, abdominal and gluteo-femoral areas (Figure 1.2) (*39*, *42*). It is considered as a 'safe' site for lipid storage that also secretes anti-inflammatory adipokines to exert its protective metabolic effect, although higher upper body SAT mass has been shown to be associated with adverse cardiometabolic risk factors (*36*, *43*). In fact, upper body SAT can be subdivided into superficial and deep layers, the latter behaves more like VAT and is more metabolically active than the former (*41*). Intra-abdominal fat is considered as VAT, including mesenteric, omental and retroperitoneal adipose tissue, which are located around the intestines, stomach and kidney, respectively (Figure 1.2) (*42*). Compared to SAT, VAT is known to have an unfavourable effect on metabolic health (*36*). Additionally, fat can accumulate ectopically in intramuscular, pericardial and intrahepatic areas within the visceral cavity which are also found to affect the susceptibility to obesity-related comorbidities (*39*, *42*, *44*). The difference between SAT and VAT in terms of their impact on metabolism has been tested directly in animals and humans by adipose tissue removal or transplantation. Surgically removing the omentum together with adjustable gastric banding, but not subcutaneous abdominal adipose tissue, improves long-term glucose and insulin profiles in patients with obesity (*45*, *46*). Transplantation of SAT from donor mice to the visceral region of recipient mice results in whole-body glucose metabolism improving with decreased body weight and fat content, while transplantation of VAT to a subcutaneous region did not seem to have a detrimental effect on metabolism in mice (*47*).

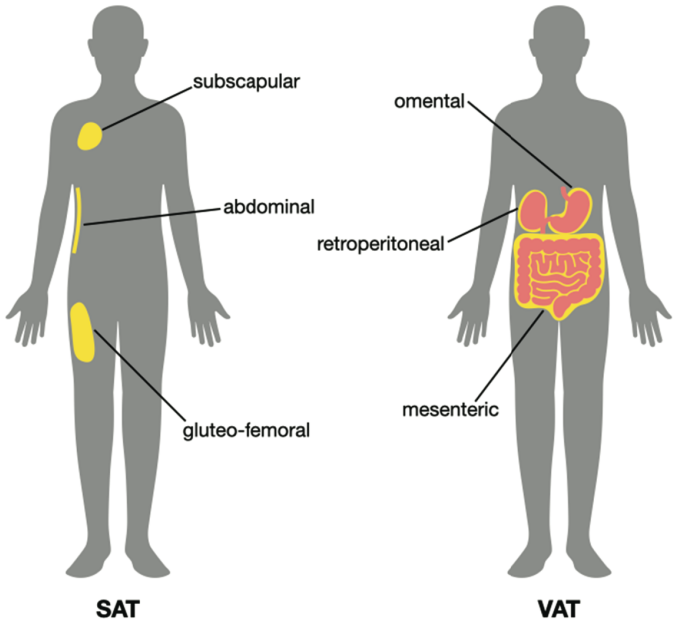

Figure 1.2 The main white adipose tissue (WAT) depots in humans. Subcutaneous adipose tissue (SAT, left) and visceral adipose tissue (VAT, right) are the two major WAT depots in humans. SAT mostly resides in the subscapular (on the upper back), abdominal (around the waist) and gluteo-femoral (thigh) regions. Intra-abdominal VAT mainly includes omental (near the stomach), retroperitoneal (surrounding the kidney) and mesenteric (intestinal area) adipose tissue.

1.2.2 White adipose tissue development

The appearance of adipose tissue can be traced back to before birth, starting approximately from the 14th week of gestation in a human foetus (*48*). In the order of the timing of appearance, it is first noticeable in the head and neck regions, then in the thorax and abdomen, and last in the upper and lower limbs (*48*). Although no significant difference in adipose tissue distribution was observed between genders, fat accumulation in terms of both adipocyte size and number seems to be divergent from one depot to another towards the end of gestation, indicating prenatal heterogeneity of adipose tissue (*48*, *49*). The size of adipocytes increases dramatically during the first year after birth, especially in SAT (*49*). Gender differences in fat content start to show from the second year of puberty, at which point substantial SAT is deposited in the upper body in males and in the lower body in females (*49*).

Lineage tracing approaches via labelling or transgenic reporter strains has been applied in mice in order to provide some insights into the ontogenesis of various fat depots. Most adipose tissue in general is thought to be derived from the mesoderm during embryonic development, although different layers of mesoderm give rise to different white adipose depots (*50*). Moreover, at least three subpopulations of white preadipocytes in mice have been identified with distinct gene expression profiles and unique metabolic properties using a combination of clonal analysis and lineage tracing *in vivo*, suggesting the developmental and functional heterogeneity of white adipocytes within the same depot (*51*).

In both humans and mice, apart from the differences in early embryonic developmental gene expression profiles such as genes of the homeobox and forkhead box families between the abdominal subcutaneous and visceral fat depots, heterogeneity also exists within VAT between mesenteric and omental preadipocytes (*52*, *53*). Although these two depots are located in close vicinity, the molecular signature of the former is similar to SAT (*53*). Similarly, at least four subtypes of mesenchymal progenitor cells have been identified from human SAT explants using single-cell sequencing (*54*). It is concluded that these subtypes give rise to white and beige adipocytes, as well as subtypes that differ in key adipokine expression, such as leptin and adiponectin (*54*). Taken together, these analyses in both species indicate that inherent regional differences in molecular signatures, leading to diverse developmental pathways, might contribute differently to fat distribution and cardiometabolic risk (*55*).

1.2.3 White adipose tissue function

The functions of WAT include lipid synthesis, storage and breakdown, as well as adipokine secretion. Excess energy is stored in the form of neutral lipids, primarily triglycerides (TGs), in lipid droplets in adipose tissue through lipogenesis. Under conditions of food deprivation or high energy demand, TGs are broken down to glycerol and fatty acids (FAs) through lipolysis. The released products are carried in the bloodstream and delivered to other tissues that utilize FAs as energy substrates for β-oxidation in mitochondria, with glycerol transported to the liver for gluconeogenesis (*29*, *31*, *56*). Thus, WAT plays a vital role in keeping the balance between fatty acid storage and release in response to nutritional status and energy demands.

As an endocrine organ, WAT also secrets a range of peptides, termed adipokines, that lead to various biological events including the regulation of appetite, insulin sensitivity and immunological responses (*31*, *56*, *57*). Although WAT in all depots seems to share many functions, the depots manifest intrinsic differences in lipid handling and signalling that affect metabolic health (*58*, *59*). For example, uptake of dietary FAs is generally more efficient in omental than in abdominal SAT (*60*, *61*). Similarly, upper body subcutaneous fat stores FAs more efficiently than in lower body SAT (*61*, *62*). Depot specific differences have been observed in lipolytic rates which will be discussed further in section 1.2.3.3.

1.2.3.1 Adipogenesis

The expansion of adipose tissue can be achieved either by increasing the size of existing adipocytes, termed hypertrophy, or by hyperplasia meaning the formation of new adipocytes (*63*). The differentiation of committed preadipocytes to mature adipocytes is defined as adipogenesis (*29*, *64*). This process can be further divided into distinct stages based on *in vitro* studies: mesenchymal precursor, committed preadipocyte, growth-arrested preadipocyte, mitotic clonal expansion, terminal differentiation and mature adipocyte (*65*). Since adipogenesis is important in the development of adipose tissue, the regulation of adipogenesis on a transcriptional level has been studied intensively. As a result, a number of transcription factors involved in the process have been identified with peroxisome proliferator-activated receptor γ (PPARγ) being the master regulator of adipogenesis (*63*). PPARγ expression is induced by CCAAT/enhancer binding protein (C/EBP) β and δ at an early stage of clonal expansion (*63*). PPARγ induces the expression of C/EBPα, which in turn promotes the transcription of PPARγ (*29*). Therefore, PPARγ and C/EBPα regulate one another reciprocally to regulate the expression of numerous additional genes that are involved in the development of mature adipocytes (*57*, *66*).

Adipocyte hypertrophy, independent of BMI, is ultimately associated with insulin resistance (*67*). Enlarged adipocytes are reported to become hypoxic which triggers a proinflammatory response, ultimately leading to adipose tissue dysfunction (*68*, *69*). The size of adipocytes is depot-dependent, and it is key in responding to lipid storage capacity, which subsequently

has an impact on metabolic health (*8*, *63*). As indicated in *in vitro* studies, enlargement of subcutaneous abdominal adipocytes is associated with increased systematic insulin resistance and inflammation, whereas small adipocytes are important in preventing obesity-related metabolic syndromes (*67*, *70*, *71*). In the context of obesity, the size of adipocytes from subcutaneous, omental and mesenteric adipose tissue are all enlarged, and subcutaneous adipocytes are larger than omental adipocytes in women (*72*).

It is believed that the total number of adipocytes is determined by the number of preadipocytes in early life and is not likely to change in adulthood but about 10% of adipocytes are renewed annually (*73*). However, hyperplasia happens when growth in adipocyte size reaches a plateau and may largely be limited by availability of preadipocytes to undergo differentiation or by the number of mesenchymal cells available for trans-differentiation into preadipocytes (*57*, *74*). Studies of adipocyte development suggest that there are regional differences in the capacity of preadipocytes to proliferate between SAT and omental VAT in obese subjects, which may influence depot-specific fat accumulation (*75*). Recruitment of new preadipocytes to differentiate in SAT can have a protective effect against metabolic syndrome by taking up excess lipid thereby limiting ectopic fat deposition (*31*, *41*, *74*, *76*). Moreover, a larger proportion of small adipocytes and lower level of *PPARG* gene expression is observed in SAT from insulin-resistant than insulin-sensitive obese subjects, indicating that an impairment in differentiation could associate with obesity-related insulin resistance (*77*). In fact, activation of PPARγ by agonists (such as thiazolidinediones) promotes differentiation of preadipocytes in abdominal subcutaneous fat but not omental adipose tissue, despite similar expression of PPARγ in both depots (*78*). This results in an increment in adiposity in subcutaneous regions, leading to an improvement in insulin sensitivity in type 2 diabetic patients despite a reduction in WHR (*79*, *80*).

1.2.3.2 Lipogenesis

Besides energy storage, an important purpose of TG synthesis in adipose tissue is to avoid ectopic fat accumulation so that the body can be protected from peripheral insulin resistance (*9*, *29*). TG stored in adipocytes is synthesized by esterification of three FAs to a glycerol

backbone. After a meal, circulating TGs incorporated within chylomicrons or very low-density lipoproteins (VLDLs) are hydrolysed by lipoprotein lipase (LPL) to release FAs for uptake into adipocytes (Figure 1.3) (*29*). FA uptake is facilitated mainly by FA translocase (FAT, also known as CD36), FA transport proteins (FATPs) and FA-binding protein 4 (FABP4) (*81–83*). Glycerol is either produced by glycolysis from glucose that is transported via glucose transporters (GLUT1 and GLUT4, synonyms are SLC2A1 and SLC2A4, respectively), or glyceroneogenesis (Figure 1.3) (*84–86*). The biochemical process of TG synthesis involves stepwise acylation reactions catalysed by different enzymes after FAs and glycerol are converted to FA acyl-CoAs and glycerol 3-phosphate, respectively (Figure 1.3) (*87*). This process starts with addition of the first FA by glycerol-3-phosphate acyltransferase (GPAT) to form lysophosphatidic acid, the second FA is then added by 1-acylglycerol-3-phosphate acyltransferase (AGPAT) to form phosphatidic acid, which is subsequently converted to diglyceride (DG) by phosphatidic acid phosphatase (PAP). TG is finally made by addition of the last FA to DG through diacylglycerol acyltransferase (DGAT) (*88*).

Another pathway for TG synthesis is *de novo* lipogenesis whereby surplus dietary carbohydrate not stored as glycogen can be converted to fat, albeit this is relatively less frequent compared to the dietary fat driven pathway described above (Figure 1.3) (*58*, *89*). FAs can be synthesized *de novo* from glucose via acetyl-CoA (*87*, *89*). This process involves several enzymes, such as acetyl-CoA carboxylase (ACC), fatty acid synthase (FASN) and stearoyl-CoA desaturase (SCD), to generate a diverse FA pool (Figure 1.3) (*90*). Since both TG synthesis pathways employ glucose-derived elements, they are influenced by elevated glucose in the bloodstream and glucose-induced insulin action as well as lipogenic gene expression (*87*, *89*, *91*). Thus, glucose uptake plays a pivotal role in determining TG storage.

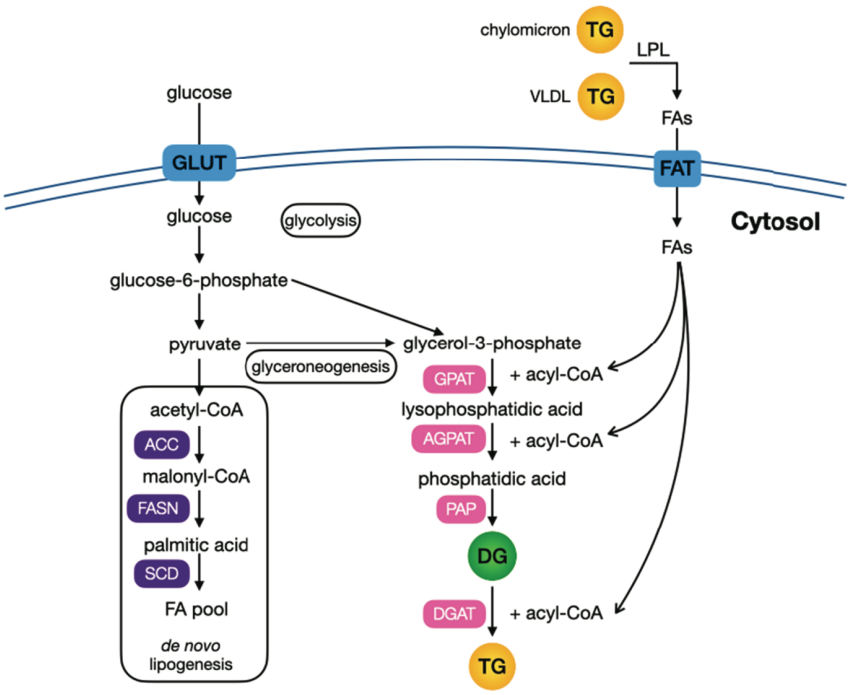

Figure 1.3 The lipogenic pathways. FA and glycerol are activated to become acyl-CoA and glycerol-3-phosphate, respectively. The FA used to synthesise TG is mostly from circulating lipids. However, FAs can also be synthesised from glucose with the *de novo* lipogenesis pathway. Glycerol is produced in the early stage of glycolysis or via glyceroneogenesis.

TG synthesis is also depot dependent due to differences in glucose and FA uptake in different depots. When expressing regional glucose uptake per kilogram fat mass, the rate of glucose uptake is higher in VAT than SAT *in vivo* (*92*). *In vitro* study also shows that glucose uptake, as well as the GLUT4 protein level, is greater in omental adipose tissue than SAT (*93*, *94*). On the contrary, insulin-stimulated glucose uptake is reduced in omental adipose tissue from individuals with central obesity compared with the ones with peripheral obesity owing to their reduced insulin sensitivity (*93*). Similarly, FA uptake studies using radiolabelled tracers followed by adipose tissue biopsy also demonstrate the differences between SAT and VAT in relation to body fat distribution. Direct uptake of circulating FAs is greater in SAT in the postabsorptive state, whereas postprandial FA uptake is higher in intra-abdominal VAT (*60*, *95*). Besides, the activity of proteins facilitating FA uptake also contributes to depot-dependent TG storage. For example, studies have shown that increased LPL activity positively correlates with SAT TG storage and expansion to reduce lipid accumulation in VAT and ectopic tissues, and thus lower cardiometabolic risk (*96*, *97*).

1.2.3.3 Lipolysis

Intracellular lipolysis occurs on the surface of the lipid droplet within the cytoplasm of the adipocyte, whereas intravascular lipolysis leads to the hydrolysis of vascular TG by LPL (*98*–*100*). During increased energy demand, TG is hydrolysed with liberated FAs and glycerol available for release into the circulation. The newly released FAs can be taken up by peripheral organs and used as an energy source and oxidised (*101*). FAs can also be used as a substrate for lipid synthesis and act as cell signalling intermediates (*101*). Meanwhile, circulating glycerol is utilised by the liver and participates in processes of glucose utilisation or production (*101*).

In WAT, lipolysis is controlled through a series of events including the engagement of receptor-mediated signal transduction, enzymatic activation and protein translocation for lipid mobilisation from lipid droplets. Furthermore, it is a dynamic process that is highly regulated by neuroendocrine signals, positively by catecholamine and negatively by insulin signalling, and is under tight nutritional control (Figure 1.4) (*98*). This thereby controls the flux of FAs in the circulation as dysregulation of lipolysis can lead to the accumulation of excessive FAs in non-adipose tissue such as liver and skeletal muscle, which is likely to cause lipotoxicity and promote insulin resistance (*102*). Therefore, lipolytic regulation is of great importance in the maintenance of FA storage and release (*98*).

As shown in Figure 1.4, catecholamines stimulate lipolysis via the second messenger cyclic adenosine monophosphate (cAMP) and protein kinase A (PKA) pathway. Catecholamine binds to β-adrenergic receptors (β-ARs) located on the plasma membrane. The β-ARs are coupled to stimulatory G-proteins (G_s) that activate adenylyl cyclase (AC) which leads to increased intracellular levels of cAMP, thereby promoting PKA activity (*100*, *102*, *103*). PKA phosphorylates perilipin-1 (PLIN1), a lipid droplet-associated protein, to release α/β hydrolase domain-containing protein 5 (ABHD5), which binds to adipose triglyceride lipase (ATGL). ATGL is the rate-limiting enzyme that initiates lipolysis and hydrolyses TG into DG and a FA. PKA also phosphorylates hormone sensitive lipase (HSL) to promote its translocation

from the cytosol to the surface of the lipid droplet and its interaction with PLIN1. It then catalyses the hydrolysis of DG into monoglyceride (MG) and produces the second FA. Monoglyceride lipase (MGL) hydrolyses MG to produce glycerol and the third and final FA (Figure 1.4) (*102*). In addition, AC activity can also be induced by protein kinase C (PKC), which may in turn promote lipolysis via subsequent elevation of cAMP levels (*104*, *105*). Other evidence shows that PKC activates the mitogen-activated protein kinase (MAPK) pathway, in particular via extracellular signal-regulated kinases (ERKs) to increase the lipolytic activity of HSL by phosphorylation (*105*, *106*). Phosphorylation of HSL and PLIN1 can also be activated via the cyclic guanosine monophosphate (cGMP) and protein kinase G (PKG) pathway mediated by atrial natriuretic peptide (ANP) through binding with the atrial natriuretic peptide receptor 1 (NPR-A), leading to stimulated lipolysis (Figure 1.4) (*102*, *107*).

Insulin, an anabolic hormone, is a well-known negative regulator of intracellular lipolysis (Figure 1.4). Insulin binds and triggers the autophosphorylation of the insulin receptor (IR) which is located on the plasma membrane (*108*). Phosphorylated IR subsequently activates insulin receptor substrates (IRSs) via phosphorylation to initiate phosphoinositol-3 kinase (PI3K) signalling (*108*). PI3K catalyses the production of the second messenger phosphatidylinositol-3,4,5-triphosphate (PIP_3), which in turn activates protein kinase B (PKB, also known as AKT). It is thought that PKB phosphorylates and activates phosphodiesterase 3B (PDE3B) to degrade cellular cAMP leading to reduced activity of PKA, thus inhibiting lipolysis (Figure 1.4) (*102*, *105*, *109*–*111*). An alternative pathway sensing lactate derived from glucose was proposed a decade ago, implying a less direct approach to mediate insulin-induced inhibition of lipolysis. Lactate activates an inhibitory G-protein (G_i) -coupled receptor 81 (GPR81) to inhibit AC thus reducing cAMP production to suppress lipolysis eventually (*112*). Activation of AMP-activated protein kinase (AMPK) also shows anti-lipolytic activity, yet it remains controversial (*113*–*115*). AMPK is a widely expressed serine/threonine kinase that responds to regulatory signals (*114*). It has been reported that activation of PKA promotes the phosphorylation of AMPK to increase lipolysis *in vitro* (*116*). On the other hand, AMPK has been shown to have opposing effects on ATGL and HSL activity (*114*).

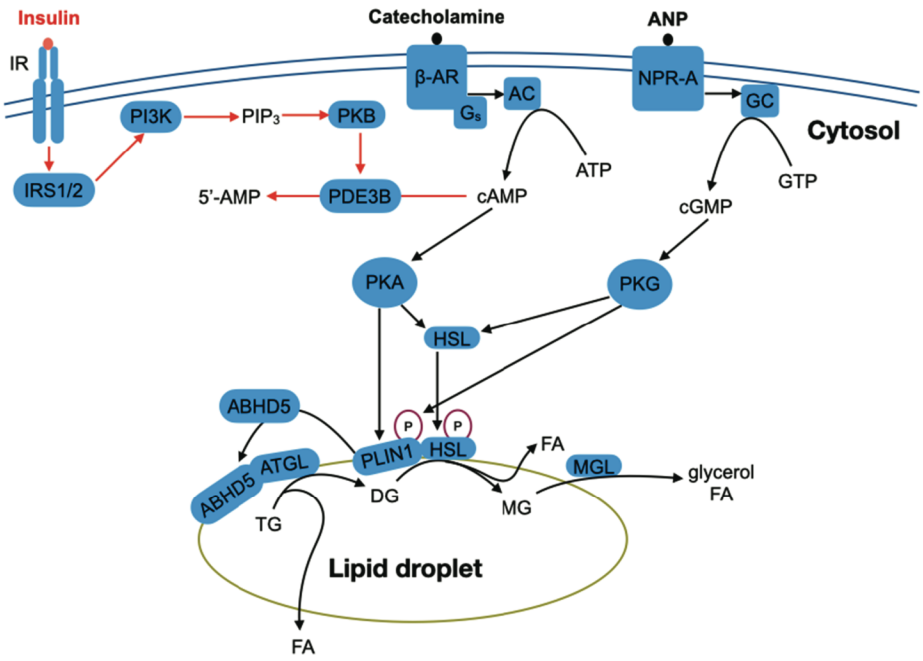

Figure 1.4 Hormonal control of intracellular lipolysis in adipocytes. The pathways for stimulating lipolysis are indicated by black arrows, while the inhibitory pathway is indicated by red arrows. ATP, adenosine triphosphate; GTP, guanosine triphosphate.

Regional variation in lipolytic activity is widely acknowledged. VAT possesses a higher lipolytic response to catecholamine stimulation, and weaker anti-lipolytic action to insulin compared to SAT (*98*, *117*, *118*). Similarly, visceral and subcutaneous abdominal fat depots are more responsive to lipolytic stimuli than the subcutaneous gluteo-femoral fat depot, the latter offers protection against cardiometabolic disease (*119*, *120*). Large hypertrophic subcutaneous adipocytes, which are associated with greater metabolic risk, also display increased lipolytic activity (*121*). As a combined consequence of greater FA incorporation, elevated lipolysis, decreased anti-lipolytic effect of insulin, intra-abdominal adipose tissue has a higher turnover of FAs than lower body adipose tissue (*8*, *122*). One contributor to the regional differences is the difference in the expression and activity of many proteins involved in the lipolytic machinery and signalling pathways. For instance, it has been reported that the expression of perilipin-1 protein is higher in omental than abdominal subcutaneous AT (*123*). Depending on their anatomic position, FAs released from SAT are drained through systemic veins, whereas those from VAT are exported straight to the portal circulation, ultimately

leading to insulin resistance, thus linking VAT to the risk of developing the metabolic syndrome (*26*, *39*, *98*, *124*).

1.2.3.4 Adipokines

As part of the endocrine system, adipose tissue synthesizes and secretes a wide range of biologically active compounds that participate in the modulation of systemic metabolism and inflammation by regulating appetite, lipid metabolism, glucose homeostasis, insulin sensitivity and vascular integrity in different organs (*29*, *33*, *125*). Regional difference in the pattern of peptide secretion exists to exert various paracrine and autocrine roles in specific depots. In general, VAT expresses higher level of cytokines than SAT in obese patients (*126*). Furthermore, the size of adipocytes is an important determinant for secretion of several adipokines (*127*). Very large hypertrophic adipocytes are dysregulated and often associated with impaired cytokine secretion shifting towards proinflammatory adipokines (*127*). This could be one explanation for the correlation of body fat distribution to the pathophysiological outcome and development of cardiometabolic diseases (*128*).

Among all the adipokines, leptin and adiponectin are the most recognised and well-characterised. Leptin signalling through its leptin receptor primarily acts on the brain to control food intake (*8*, *29*). The secretion of leptin is subjected to nutritional and hormonal cues, such that circulating levels of leptin rise with weight gain and decline upon prolonged starvation (*129*). There is a strong positive correlation between circulating leptin levels and body fat percentage or BMI (*130*, *131*). Particularly when comparing with omental adipose tissue, the leptin secretion rate is much higher in SAT because of a combination of larger adipocytes and greater gene expression (*132*, *133*).

Unlike leptin, circulating levels of adiponectin show an inverse relationship with BMI or visceral adiposity and a positive correlation with insulin sensitivity (*134–136*). Adiponectin is abundantly expressed in mature adipocytes, and its concentration in plasma is extremely high compared to other cytokines and hormones (*137*). Adiponectin forms high molecular weight multimers and is reported to signal through adiponectin receptors in the liver to reduce hepatic gluconeogenesis, and in muscle to increase FA oxidation, in order to exert its insulin-

sensitizing effect (*138–140*). It is also reported to be an anti-inflammatory protein which has a protective role against cardiovascular disease (*141*, *142*).

There are many more putative hormones secreted from adipocytes reported to affect insulin resistance. For example, resistin which is mainly secreted by visceral macrophages may play a role in the pathogenesis of cardiometabolic diseases (*41*, *143*). Retinol-binding protein 4 (RBP4) is preferentially expressed in VAT, its circulating level positively correlates with intra-abdominal fat mass as well as adipocyte size and metabolic risk factors (*144*, *145*). Visfatin and omentin are both identified as VAT-specific cytokines, although their relationships with insulin sensitivity are quite the opposite (*134*, *146*). The expression of visfatin is correlated with visceral fat mass and BMI (*41*, *139*). Recently it has been shown to induce chronic inflammation in adipocytes and ultimately induce insulin resistance (*147*). On the contrary, plasma omentin levels negatively correlated with metabolic risk factors (*146*, *148*).

Adipose tissue hypertrophy promotes the recruitment of immune cells, as well as the release of proinflammatory cytokines, such as tumour necrosis factor-α (TNF-α), interleukin 6 (IL-6), monocyte chemoattractant protein 1 (MCP-1, synonym CCL2), among many others (*149*). Increased expression of proinflammatory cytokines increases expression and phosphorylation of MAPKs, such as c-Jun N-terminal kinase (JNK), which impairs insulin signalling by hindering IRS1 phosphorylation on tyrosine residues to propagate signals to PKB, more in omental adipose tissue than SAT (*150*). *In vivo* studies have suggested that SAT contributes approximately 15-35% of systemic IL-6 concentrations in human, but its release from gluteal SAT is significantly less than from abdominal SAT, indicating a regional difference in the contribution to secreted proinflammatory cytokines (*151*, *152*). In response to adipose tissue expansion and remodelling, macrophages infiltrate adipose tissue and have been observed to cluster around dying adipocytes in crown-like structures, which represents adipose tissue inflammation – one of the factors linking obesity to insulin resistance (*149*). Macrophage infiltration was detected to a greater extent in omental adipose tissue compared to SAT in individuals with central adiposity (*153*).

Apart from adipokines, other bioactive factors released from adipose tissue also display depot-specific features. Lipid mediators such as palmitoleic acid, mostly derived from *de novo*

lipogenesis, is more abundant in the upper arm and thigh than the abdominal region in SAT linking a beneficial effect with fat distribution (*154*). However, the effect of palmitoleic acid on cardiovascular disease risk is not clear yet (*154*).

1.2.4 Lipid droplets

Lipid droplets (LDs) can form in nearly all cell types across species, from bacteria to mammals. The number and size of LDs vary among different cell types or even between individual cells in the same cell type (*155*). The diameter of a LD can range from 20 nm in nonadipocytes to more than 100 μm in a white adipocyte (*156*). Discovered in the nineteenth century by light microscopy, LDs were originally considered as inactive vesicles for lipid storage (*157*, *158*). It was not until 1991 when the protein perilipin-1 was identified to be specifically associated with the periphery of LDs and subjected to hormonal stimulation, that LDs started to gain recognition as dynamic cytoplasmic organelles which participate in lipid metabolism (*157*–*159*). The majority of LDs are cytosolic, but they may also be present in the nucleus.

1.2.4.1 Structure

A LD is composed of a hydrophobic core filled with neutral lipids, predominantly in the form of TG and sterol ester (SE), surrounded by a monolayer of phospholipids containing LD-associated proteins (Figure 1.5) (*155*, *157*, *158*). Neutral lipids are stored at various ratios in the hydrophobic core depending on the cell type. For example, mainly TGs are stored in LDs in adipocytes, while SEs are the main components in steroidogenic cells. Other lipids include retinyl esters in retinosomes and cholesterol esters in macrophages that are referred to as foam cells (*155*, *157*).

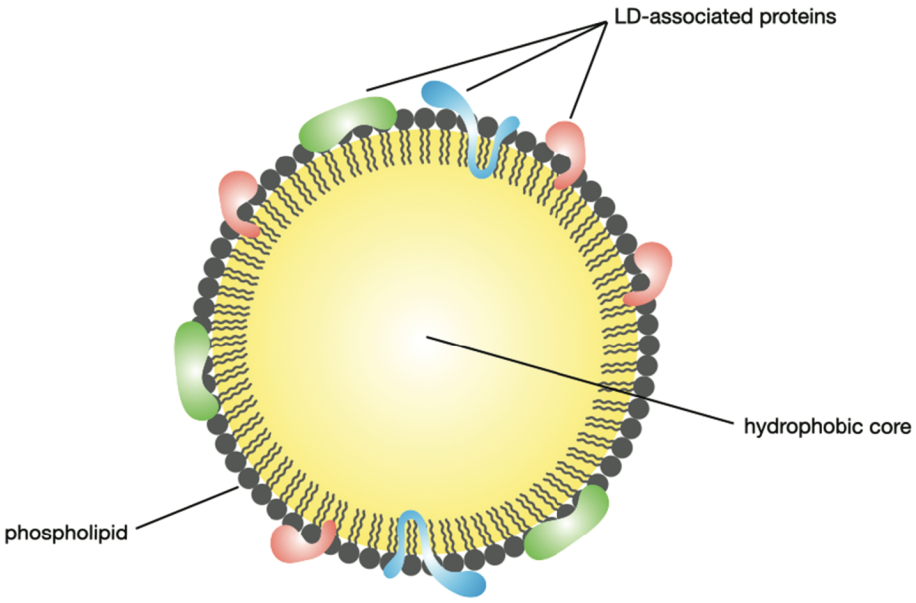

Figure 1.5 Lipid droplet structure. Lipid droplets (LDs) consist of a hydrophobic core, mostly in the form of triglyceride (TG) and sterol ester (SE), surrounded by a phospholipid monolayer with various proteins embedded.

The phospholipid monolayer provides a barrier for separating the hydrophobic core from the aqueous environment in the cytosol. Phosphatidylcholine (PC) is the most abundant constituent of the LD monolayer, followed by phosphatidylethanolamine (PE), phosphatidylinositol (PI), phosphatidylserine (PS), sphingomyelin (SM) and other minor phospholipids such as phosphatidic acid, in the order of abundancy (*155*). Alterations in phospholipid composition and shape, as well as LD-associated proteins, in response to various physiological conditions, suggests a key role of the LD monolayer in controlling the dynamics of LDs.

1.2.4.2 Biogenesis

LDs in prokaryotes are believed to be derived from plasma membrane, but the mechanism of LD formation in eukaryotes is incompletely understood (*160*). However, LDs are often found to be in close contact with the endoplasmic reticulum (ER) in many cell types, as shown in multiple studies using electron microscopy (EM) (*161–165*). Besides, there is evidence that

some proteins involved in TG synthesis such as DGAT and GPAT are partially or fully translocated from the ER to the surface of a LD as it forms (*163*, *166*). Therefore, a few LD formation models have been proposed based on the concept that LDs originate from the ER.

The most supported model suggested that neutral lipids are likely to diffuse between the two phospholipid leaflets of the ER membranes. As *de novo* lipid synthesis proceeds, neutral lipid aggregates and forms a lens-like structure between the ER bilayer. When lipid accumulation reaches a critical concentration, the lens bulges and buds into the cytosol from the cytoplasmic surface of the ER to form a nascent LD (*167*). Alternatively, the lens could be 'excised' from both leaflets of the ER bilayer as a bicelle to release a LD, known as the hatching mechanism (*168*). Majority of LDs are observed to be physically associated with the ER in yeast, while in mammalian cells some LDs seems to bud off completely from the ER, thus it remains to be established if all LDs bud off the ER or some may in fact remain connected (*163*, *166*). Also, the directional regulation of a newly formed LD to bud and move towards the cytosol remains unknown (*155*, *162*, *167*).

Vesicular budding is another model that proposes LDs could originate at specific locations on the ER, from vesicles containing both leaflets of ER membrane is formed but still remains tethered to the cytoplasmic side of the ER (*167*). Neutral lipids are synthesized by neutral lipid-synthesizing enzymes to fill the vesicle bilayer gradually. The ER membrane enclosed in the vesicle could be fused with the LD membrane, or used as a compartment for any hydrophilic proteins found in the LD core (*167*).

In some cases, the accumulation of lipids between ER leaflets was not observed using freeze-fracture electron microscopy, and the fact that LDs always lie adjacent to a ER bilayer challenges the models proposed. The authors described a pair of ER membranes partially enclosing the LD as an egg cup holding an egg (*169*). Based on this observation, an 'eggcup' model was proposed, in which a LD is formed within a cup-shaped region of the ER (*169*). Whether the LD membrane is derived from ER membranes in this model needs further investigation.

1.2.4.3 Growth

Existing LDs need to expand to harbour more lipids, but the mechanism of LD growth is not fully understood. Evidence that most of the enzymes regulating lipid synthesis localise on the ER supports one possible mechanism, namely that neutral lipids are synthesised and transferred from the ER to adjacent LDs to facilitate the growth of LDs (*155*, *157*, *170*). The growth of LDs in this model is hypothesized to be achieved by permanent attachment to the ER by membrane continuities, followed by lipid transportation by carriers or by homotypic fusion between multiple nascent LDs (*155*, *170*). It is recognised that SNAREs (SNAP receptors, soluble N-ethylmaleimide sensitive factor attachment protein receptors) are required for the fusion of vesicles with phospholipid bilayer, so their role in mediating LD fusion can be envisaged (*171*). However, more experimental studies are still needed to support this model.

The other possible mechanism of LD expansion is by lipid transfer (*156*, *157*). It has been revealed that fat-specific protein of 27 kDa (FSP27, as known as CIDEC) is highly enriched at LD-LD contact sites (*172*, *173*). As a result, directional net transfer of neutral lipid from smaller to larger LDs occurs, driven by the greater internal pressure in the smaller LD and mediated by FSP27 (*172*). Exactly how this process happens remains unclear.

Meanwhile, phospholipid remodelling is also essential to accommodate rapid changes from LD expansion on the surface, in particular through additional synthesis of PC. The rate-limiting enzyme for PC synthesis is choline-phosphate cytidylyltransferase A (PCYT1A, also known as CCTα). It has been reported that PCYT1A tightly binds to LD during LD expansion, but findings from our group and others suggested that it is confined in the nucleus and only translocates from the nucleoplasm to the nuclear envelope by sensing membrane packing defects primarily (*174–176*).

1.2.4.4 Targeting

A LD proteomic analysis suggested that more than 150 proteins are associated with LDs, including structural proteins, membrane trafficking proteins, lipases and enzymes for lipid

synthesis (*156*, *177*, *178*). Until now, the mechanism for protein targeting on LDs is still under investigation. Due to the nature of the phospholipid monolayer, LD-associated proteins can be structurally divided into three classes: peripherally associated proteins, lipid anchored proteins, and monotopic integral membrane proteins (*170*). For instance, perilipins are peripherally associated with LDs via a common amphipathic helical structure and modulate lipid homeostasis by controlling the access of lipases to neutral lipids in the hydrophobic core (*179*). Lipid anchored proteins such as small GTPases are crucial regulators of membrane trafficking that control vesicle formation and motility (*155*, *170*, *180*). As a member of the monotopic integral membrane proteins, proteins required for TG synthesis and LD expansion such as GPAT4 incorporate into the LD via their hydrophobic domain (*155*, *166*). Some proteins are associated with LDs indirectly by interaction with other LD-bound proteins, such as HSL which interacts with PLIN1 (*157*, *181*).

1.2.4.5 Interaction

Using a combination of confocal and lattice light sheet spectral imaging methods, LDs have been visualised to be in close proximity to other cellular organelles, including the ER, mitochondria, Golgi, lysosomes and peroxisomes in different nutritional states (*182*). The interaction of LDs with almost all the other organelles indicates its multitude of functions in lipid metabolism. As mentioned, LD-ER contact is involved in lipid synthesis. The association of LDs with mitochondria and peroxisomes is for fatty acid oxidation, while that with lysosomes is for degradation of LDs, termed lipophagy (*160*, *183*). Exactly how these contact sites function remains an open question.

1.2.4.6 Dysregulation

The LD is the main organelle for maintaining lipid deposition and mobilisation, as well as buffering against excess FA flux and ER stress (*160*, *184*). Hydrolysed neutral lipids are utilised for β-oxidation, membrane synthesis, and the generation of signalling molecules in order to regulate lipid distribution and energy balance (*162*). Dysregulation of LD homeostasis has been implicated in the pathogenesis of many metabolic disorders. Obesity, as mentioned

previously, is characterised by excessive storage of lipids, while lipodystrophy is caused by inability to store lipids in LDs in specialised adipocytes (*160*, *185*). Both conditions are often accompanied by other metabolic traits such as ectopic lipid accumulation in non-adipose tissues and insulin resistance that leads to tissue dysfunction including non-alcoholic fatty liver disease (NAFLD) and atherosclerosis (*157*, *160*, *186*). Given the various functions of LD-associated proteins and the different processes they are involved in, any abnormality such as gene mutations or changes in protein content could modulate the pathophysiological role of LDs. For instance, Chanarin-Dorfman syndrome (CDS), also known as neutral lipid storage disease with ichthyosis (NLSDI), is a rare autosomal recessive disease caused by mutations in the *ABHD5* gene (*187*). These mutations inhibit binding with ATGL which is required in order to initiate lipolysis, explaining the massive TG accumulation seen in several tissues in patients (*188*). Understanding the mechanisms regulating LD function could help to understand the pathogenesis of cardiometabolic diseases.

1.3 Determinants of body fat distribution

1.3.1 Age and gender

Undoubtedly age and gonadal hormones play roles in determining body fat distribution. Generally speaking, women accumulate more SAT in the gluteo-femoral areas, whereas men in VAT although they have a lower average body fat percentage (*189*). With aging, postmenopausal women tend to build up more visceral fat in the abdominal region, resulting in a similar body shape to men (*190*–*193*). According to a longitudinal study in middle-aged Swedish women, there is a significant mean increase in waist circumference of about 0.7 cm per year and a decrease in hip circumference up to the age of 56 (*194*). The ratio between SAT and VAT areas is significantly higher in females than males but decreases beyond the age of 60 in both genders (*195*). Redistribution of body fat, especially rapid accumulation of intra-abdominal fat and gradual loss of SAT in the lower body over time, is associated with changes in metabolic variables in older subjects, leading to an increased cardiometabolic morbidity (*196*–*199*).

Although little is known about the shift from peripheral to a more central fat deposition with aging, gonadal hormones have been suggested to direct body fat distribution. VAT mass negatively correlates with circulating testosterone concentration in men (*200*). Administration of testosterone to middle-aged men with abdominal obesity for three or nine months in different studies results in a decreased visceral fat mass, WHR and an improvement of metabolic profiles (*201*, *202*). On the contrary, treating obese postmenopausal women on calorie restriction with nandrolone decanoate with weak androgen activity over nine months results in subcutaneous abdominal fat loss, but visceral fat gain (*203*). Apart from reducing adipogenesis, testosterone seems to elevate lipolysis in order to reduce abdominal visceral fat mass in men (*204*). Oestrogen is implicated in gynoid fat accumulation in females, mainly via binding with oestrogen receptors in adipose tissue, the expression of which is reduced in VAT in males but not in females (*39*, *205*). Due to the falling level of oestrogen during the perimenopausal transition, visceral adiposity starts to rise in women (*206*). Menopausal oestrogen deficiency is associated with increased intra-abdominal body fat and many adverse changes in metabolic parameters, including increased TG levels with higher LPL activity on omental adipocytes, as well as elevated glucose and insulin levels (*207*, *208*). Furthermore, studies in transgender adults with cross-hormone administration for 12 months shows a profound effect on body fat distribution (*209*). The exact mechanism of sex steroid modulation of body fat distribution has yet to be identified.

1.3.2 Environment and genetics

Obesity can be simply explained as energy imbalance that occurs when an individual consumes more calories or burns fewer calories. The constant increase in the prevalence of obesity is often accompanied by the remarkable transition from a nutritionally challenging to an obesogenic environment with readily available calorie-dense foods and decreased physical activity (*210*). However, this modern obesogenic environment cannot be the sole driver of the obesity pandemic since not everyone in such an environment is obese. Moreover, variations as to how people respond to the environment exist, which is reflected as body fat distribution and risks of developing obesity related health problems. Therefore, genetic variation could also contribute to the difference between individuals, which is called heritability (*211*). There is evidence that genes account for more variance of all

circumferences and WHR in women than in men, indicating sexual dimorphism of genetic effects on body fat distribution (*212*). The analysis of familial aggregation such as twin studies is considered to be an informative method to distinguish the effect of shared genes from a shared environment regarding a specific trait or disease risk (*211*, *213*). For instance, data from the Swedish Adoption/Twin Study of Aging have estimated the genetic variation in WHR to be 28% in males and 49% in females (*214*). Other studies have indicated that genetic factors influence body fat distribution with higher heritability for abdominal visceral fat than that for the subcutaneous fat depot (*215*–*217*).

To understand the fundamental contribution of genetic variants to differences in phenotypes, genomics studies such as genome wide association studies (GWAS), exome sequencing studies and candidate gene studies are employed to identify the association between genetic loci and disease traits. GWAS searches for genetic markers in the population in a hypothesis-free manner, which would lead to a better understanding of the biology of disease in order to facilitate the development of novel treatment strategies (*218*, *219*). Exome sequencing studies involve the sequencing of protein coding regions in the genome, while the goal of candidate gene studies is to identify gene mutations of a specific disease by comparing the case group to the control group. More about genomic studies will be discussed in the following section.

1.3.3 Epigenetics

In order to understand the underlying molecular basis of body fat distribution, particularly in the modulation of regional adiposity, modifications in regulatory pathways via epigenetic mechanisms have gained more and more attention in recent years (*220*). Epigenetics is the study of changes in gene activity and expression without alterations in the DNA sequence on a chromosome, such changes in chromatin remodelling can be achieved typically by DNA methylation or histone modification (*221*). DNA methylation status, mostly at 5'-C-phosphate-G-3' (CpG) islands, in specific loci has been implicated in the association with functional changes in a depot-specific manner, as presented in a methylation analysis study between subcutaneous abdominal and gluteal fat samples (*222*). Characterisation of abdominal and gluteal adipose tissue samples obtained from female volunteers has shown

that apart from a depot-specific gene expression pattern, genes upregulated in abdominal adipose tissue samples were generally associated with CpG hypomethylation, whereas those downregulated were in general hypermethylated (*222*). Differences in the ratio of hyper/hypomethylation in genes were also observed between abdominal SAT and omental VAT in both non-obese and obese subjects in multiple independent cohorts (*223*). A more recent study provides further evidence of differential gene expression and DNA methylation in adipocytes isolated from paired SAT and VAT of individuals with a normal BMI, more strikingly at transcription factor and developmental genes that are fundamental to adipocyte function (*224*).

Epigenome-wide association studies (EWAS) have identified CpG loci with methylation associated with multiple parameters for adiposity and risk factors for obesity related diseases (*225*, *226*). In a paired analysis of obese women before and after gastric bypass and significant weight loss, more DNA methylation was observed in subcutaneous abdominal adipose tissue before the weight loss, and there is less robust differential methylation of CpG sites in the intra-abdominal omental adipose tissue (*227*). Most CpG sites are mapped to genes that are associated with obesity, T2D and related traits (*227*). Similar studies comparing differential DNA methylation profiles in isolated subcutaneous abdominal white adipocytes from post-obese women two years after gastric bypass with BMI-matched never-obese women, suggests a CpG hypomethylation but an enrichment of differentially methylated sites in genes involved in adipogenesis in post-obese women (*228*).

1.3.4 Genomics studies

As mentioned above, there are a few approaches that have been utilised by researchers to investigate the association between genetic variants and disease susceptibility. Among them, GWAS emerged as a fundamental tool to determine the association of single nucleotide polymorphisms (SNPs), which is the most common type of genetic variation, with complex traits such as body fat distribution (*229*, *230*). It has detected more than 10,000 SNPs that are significantly associated with a broad range of diseases and traits over the last decade (*218*). However, nearly 90% of all phenotype-associated hits from GWAS are located in the non-coding region near or within a gene (*229*). These SNPs can potentially affect the

transcriptional regulation of downstream targets or alter splice sites, thus potentially affecting the expression/function of the gene, although the function and causality are not straightforward (*229*). Therefore, follow-on studies, particularly fine-mapping of SNP-trait associations, are often required to narrow down the region of association to identify one or more causal variants (*218*). In fact, for most of these variants the effect on overall disease risk is rather small (*218*, *231*). Furthermore, common diseases and complex traits such as body fat distribution are often multifactorial (*232*). Hence, much work has been focused on detecting variants with lower frequencies but larger impact on disease risk in order to identify the missing heritability (*219*).

The *FTO* (fat mass and obesity associated) gene is the first locus identified to have an association with risk of obesity using GWAS approach (*233*). Since then, nearly 300 loci have been discovered for obesity-related traits from multiple GWAS based on different populations (*234*). Similarly, the first meta-analysis of GWAS has identified two loci near *TFAP2B* (transcription factor AP-2-beta) and *MSRA* (mitochondrial peptide methionine sulfoxide reductase) that are strongly associated with waist circumference, and another genetic variant near *LYPLAL1* (lysophospholipase-like protein 1) that was strongly associated with WHR in women only (*235*). With the increasingly large size of cohorts, 526 variants and risk alleles that are associated with body fat distribution in humans have been reported so far according to the EBI GWAS catalog (*236*) (https://www.ebi.ac.uk/gwas/efotraits/EFO_0004341). Gene expression enrichment has suggested that BMI-associated loci are mostly enriched in the brain and central nervous system and involved in the control of energy intake, whereas genes that are associated with WHR adjusted for BMI are enriched in peripheral tissues including adipose tissue, indicating that body fat distribution is regulated in local depots (*219*, *234*, *237*, *238*). The fact that the majority of the identified loci for WHR do not overlap with that for BMI, suggests that the regulation of body fat distribution is independent of general obesity (*234*).

1.4 Coding variants

Most genetic variants captured from GWAS typically have a minor allele frequency (MAF) greater than 1% (*218*). As population-based sample sizes are increasing, GWAS are able to detect rare coding variants with a MAF below 0.5% which also have strong associations with diseases and traits. These rare coding variants are mostly missense variants, where amino acid (aa) changes could result in a mild dominant or dominant-negative effect, thus are more functionally relevant than many common non-coding variants (*239*). Therefore, the study of rare coding variants can facilitate fine-mapping approaches for causal variant identification and provide strong evidence for the causal role of the gene (*1*). Since these variants are usually population-specific and difficult to impute, their study requires large, homogenous samples and direct genotyping (*1*). The UK Biobank is such a population-based prospective cohort with approximately 500,000 individuals aged 40 to 69 when recruited between 2007 and 2010 in the UK (*240*). Detailed phenotypic information is accessible and genotype data have been collected on all participants, which allow the discovery of new genetic associations for complex traits (*241*). Follow-up functional studies of these rare coding variants, and the genes in which they are located, will extend fundamental knowledge of the genetic contribution to disease risk.

To identify likely-causal nonsynonymous genetic variant and genes implicated in the regulation of body fat distribution, Dr Luca Lotta and colleagues conducted a genome-wide association scan of 37,435 directly-genotyped, rare nonsynonymous variants with BMI-adjusted WHR in 450,562 European ancestry participants of UK Biobank (*1*). In the main analysis, they have identified six associations at the genome-wide level of statistical significance ($p < 5x10^{-8}$) in genes at least 1 Mb apart from each other (*1*). Additional fine-mapping analyses provided strong statistical evidence for the causal association of rare nonsynonymous variants of *ALK7* (three signals), *CALCRL* (two signals), *PLIN1* (one signal), and *PDE3B* (three signals) in the main analysis (*1*). The minor alleles of these variants were associated with lower WHR and larger hip circumference with protection from cardiovascular or metabolic disease (*1*).

At *ALK7*, there was evidence that the rare p.I195T (rs56188432, MAF = 0.2%) and the low frequency missense variant p.N150H (rs55920843, MAF = 1.2%) were in the 99% credible set with posterior-probability of association (PPA) > 99% (*1*). Therefore, the *ALK7* locus was

identified as causal gene for body fat distribution and both p.I195T and p.N150H as causal variants for the signals (*1*). Similarly, *CALCRL* p.L87P (rs61739909, MAF = 0.3%), *PLIN1* p.L90P (rs139271800, MAF = 0.1%) and *PDE3B* p.R783X (rs150090666, MAF = 0.1%) were all identified as the most likely causal variants for the signals at corresponding loci (*1*).

Since all four genes implicated in the main analysis are abundantly expressed in SAT and VAT and a review of functional evidence revealed links between each of the four encoded proteins in the regulation of intracellular lipolysis, Lotta et al. conducted follow-up associated analyses of all genetic variation within regions 1Mb either side of the key genes regulating the lipolysis pathway and also estimated associations of the burden of rare nonsynonymous variants in these genes (*1*). These key regulators are *PNPLA2* (encodes the main enzyme for TG hydrolysis), *ABHD5* (encodes the activator of PNPLA2), *G0S2* (encodes the inhibitor of PNPLA2), *LIPE* (encodes the main enzyme for DG hydrolysis), and *MGLL* (encodes the main enzyme for MG hydrolysis) (*1*). They identified an association led by a missense variant p.N252K (rs140201358, MAF = 1.4%) in *PNPLA2*, encoding adipose triglyceride lipase (ATGL), with lower BMI and smaller hip circumference, as well as higher risk of T2D and coronary artery disease (*1*). This variant was also in the 99% credible set, supporting a likely-causal association (PPA > 99%) (*1*).

The study conducted by Lotta et al. provides human genetic evidence of a link between intracellular lipolysis, fat distribution and its cardiometabolic complications in the general population. In the next section, I will summarise previous findings on each of these genes.

1.4.1 Activin receptor type-1C (ACTR-1C, ALK7)

1.4.1.1 Overview

The transforming growth factor-β (TGF-β) superfamily contains over 30 family members (*242*). The superfamily can be subdivided into two functional groups, firstly the TGF-β-like group that includes TGF-βs, activins, Nodal and some growth and differentiation factors (GDFs), and secondly the bone morphogenetic protein (BMP)-like group comprised of BMPs, most GDFs

and anti-Müllerian hormone (AMH, also known as Müllerian inhibitory substance, MIS) (*242*). Members in the superfamily are ubiquitously expressed in a wide range of tissues and are involved in a variety of cellular processes such as cell proliferation, differentiation, development and apoptosis (*242*, *243*). TGF-β superfamily ligands are small secreted signalling molecules that transduce their signals by binding to heteromeric complexes of the receptors on the cell surface, thereby activating intracellular Smad (mothers against decapentaplegic homologue) transcriptional regulators in order to regulate gene expression in the nucleus (Figure 1.6) (*242*, *244*). These receptors can be classified as type I and type II transmembrane serine/threonine receptor kinases. An active ligand/receptor complex is composed of two type I receptors, two type II receptors and a dimeric ligand (*242*). The two types of receptor kinases are interdependent as type I receptor kinase requires type II receptor kinase to bind ligand, and the latter requires the former to signal (*245*). Typically, type II receptor kinase is constitutively active which, upon ligand binding, recruits and activates type I receptor kinase through phosphorylation to initiate downstream signalling pathways (*242*).

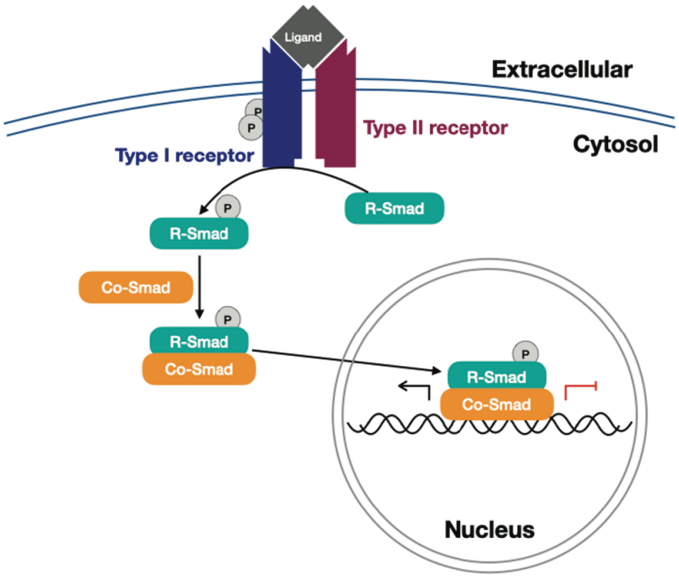

Figure 1.6 Schematic overview of the TGF-β signalling pathway. Upon dimeric ligand binding, constitutively active type II receptor kinase phosphorylates type I receptor kinase, which activates receptor-regulated Smad (R-Smad) by phosphorylation. Phosphorylated R-Smad forms a complex with common mediator Smad (Co-Smad). The resulting Smad complex translocates to the nucleus to regulate the expression of specific target genes. Positive reactions are indicted by black arrows while the red line indicates inhibitory reaction.

Type I receptors are classified into three main groups according to their sequence similarities. The first group includes serine/threonine-protein kinase receptor R3 (SKR3, also known as ALK-1) and activin receptor type-1 (ACTR-1, as known as ALK-2), which interact with different TGF-β-like ligands (*246*). The second group comprises the BMP receptors BMP receptor type-1A (BMPR-1A, also refers to ALK-3) and BMP receptor type-1B (BMPR-1B, also known as ALK-6) (*246*). The last group consists of the activin receptor type-1B (ACTR-1B or ALK-4), the TGF-β receptor type-1 (TGFR-1, or ALK-5), and the Nodal/activin receptor type-1C (ACTR-1C, also known as ALK-7) (*246*). Generally speaking, the TGF-β and activin specific receptors activate Smad2 and Smad3, whereas Smad1, Smad5 and Smad8 are activated by the BMP specific receptors for downstream signalling transduction (*244*).

Being one out of the seven type I receptors, *Alk7* was originally cloned from rats as an orphan receptor (*247–250*). The human *ALK7* cDNA was first isolated from a human brain complementary DNA (cDNA) library in 2001 and the gene is positioned on chromosome 2q24.1-q3 (*251*). The expression of ALK-7 was detected predominantly in the central nervous system (CNS), but is also enriched in other tissues such as adipose tissue and the pancreas (*250*, *252*). Apart from the full-length ALK-7, there are three other isoforms generated by alternative splicing of the *ALK7* gene which have been identified from human placenta (*253*). These spliced variants are expressed throughout pregnancy and their expression is developmentally regulated (*253*).

1.4.1.2 Structure

Human *ALK7* encodes for a protein with 493 amino acids (Figure 1.7 A) (*253*, *254*). Like other type I receptors, full-length ALK-7 contains a signal peptide, an extracellular domain (ECD, as known as ectodomain) with approximately 100 residues, a single-spanning transmembrane (TM) domain of approximately 20 residues, followed by an intracellular domain (Figure 1.7 A) (*244*, *254*). The intracellular domain is distinguished by a regulatory glycine-serine rich domain, known as the GS region, that lies upstream of the cytoplasmic kinase domain (Figure

1.7 A) (*244*). In fact, type I and type II receptors are structurally related and share sequence similarity in the ECD and kinase domains (*244*). Structures of four of the seven mammalian type I receptors have been reported, but the ALK-7 structure has yet to be characterised (*255*). However, some general insights can be drawn from other family members as to the domain structure, as well as the structural basis for activation of ALK-7.

A three-finger toxin fold is observed in the ECD which presents a common pattern in all type I receptors (*243*, *255*, *256*). The three-finger toxin fold comprises five stranded β sheets with an extended loop connecting β-strands (Figure 1.7 B) (*255*, *257*). In addition, ten cysteines forming five disulphide bonds within the ECD enable distinctive ligand binding modalities (Figure 1.7 B) (*255*, *257*). Structures of the complex of ligands with ECD from multiple type I receptors suggest ligand binding specificity, although the full extent regarding the selectivity over ligands has not been elucidated (*255*).

Based on crystal structures of the cytoplasmic domain of another type I receptor ALK-5, the GS region, which is a highly conserved juxtamembrane segment, forms a helix-loop-helix structure that harbours the sites for phosphorylation by type II receptors in the loop region (*258*, *259*). The receptor itself maintains an inactive form by forming an inhibitory wedge between the GS region and kinase domain (*246*, *258*, *259*). Phosphorylation at the GS loop disrupts the conformation by creating a binding site for Smad substrate, hence activates the receptor and enhances its kinase activity (*259*). Indeed, it has been shown that replacing the threonine residue at position 194 in the GS region with aspartate elicits the maximum activity of ALK-7 due to the elevated autophosphorylation activity (Figure 1.7) (*248*, *260*). On the other hand, replacement of lysine with arginine at residue 222 in the kinase domain eliminates the intrinsic kinase activity of ALK-7 (Figure 1.7) (*248*, *260*). Although structural information for receptor/Smad complex is absent, the specificity of their interaction has been investigated by generating receptor chimeras or site-directed mutants (*261–265*). It appears that the L45 loop of nine amino acids situated in the kinase domain of ALK-5 determines the Smad2 signalling specificity (Figure 1.7) (*261*, *262*, *264*). Since a similar structural element has been identified within other type I receptors to specify their corresponding Smad interactions, one can postulate that the equivalent region within ALK-7 would have the same role since the kinase domain of ALK-7 shares great similarity with that of ALK-5 and ALK-4 (*261*, *262*, *264*,

266). Nonetheless, evidence of the precise interaction between ALK-7 and Smads is still required.

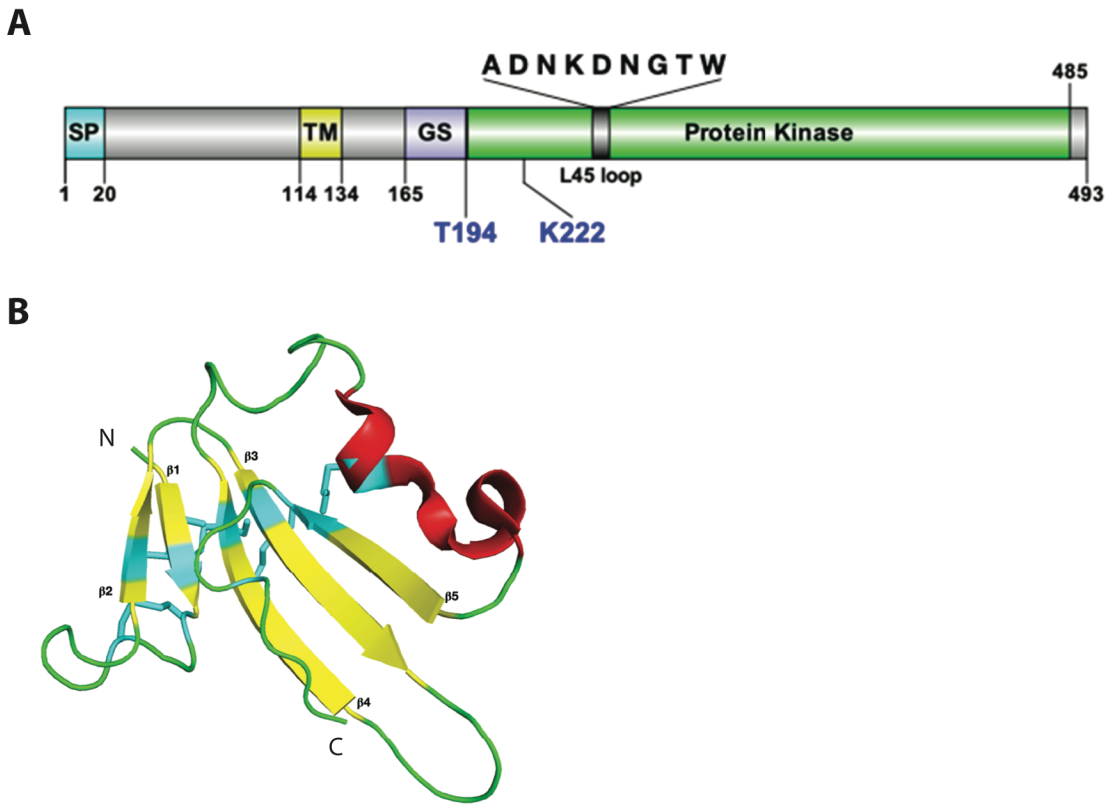

Figure 1.7 Structural domains of human type I receptors. (A) The human ALK-7 protein consists of a signal peptide (SP), a single transmembrane (TM) domain, followed by a GS domain and a protein kinase domain. Mutation of T194 to aspartic acid results in elevated kinase activity while replacement of K222 with arginine impairs signalling activity. The L45 loop of 9 amino acids for Smad2 specificity in the protein kinase domain is also indicated. The domain graph was generated by GPS (*249*). (B) The secondary structure of the three-finger toxin fold of ALK-5 (PDB: 2PJY) (*252*). Five disulphide bonds are labelled in cyan and β sheets are labelled in yellow. The helix is labelled in red and the loops are in green. The cartoon representation was generated by PyMOL.

1.4.1.3 Function

ALK-7 responds to ligands Nodal, activin B, activin AB and GDF-3 upon heterodimerisation with activin receptor type-2B (ACTR-IIB) (*267–270*). It is also suggested that ALK-7 may be a putative receptor for activin E (*271*). In addition to the traditional ligand/receptor complex, a coreceptor teratocarcinoma-derived growth factor 1 (CRIPTO, also known as TDGF1) has been

found to be required for Nodal signalling, where it antagonises activin and blocks activin signalling (*272*, *273*). However, whether CRIPTO is necessary for ALK-7 activation in Nodal signalling remains debatable, although the responsiveness of ALK-7 was greatly enhanced in the presence of CRIPTO (*274*, *275*). Once ALK-7 is phosphorylated and activated, receptor-regulated Smads (R-Smads), Smad2 and Smad3, are subsequently phosphorylated and form a complex with a common mediator Smad (Co-Smad), named Smad4; the complex then translocates to the nucleus to regulate downstream gene expression (*276*).

As described earlier, ALK-7 is detected in a wide range of tissues, but most abundantly in the nervous system and other tissues implicated in metabolic regulation, such as adipose tissue including both WAT and BAT, and pancreatic islets (*267*, *277*). The mRNA expression of *ALK7* is reduced in obese subjects and correlated negatively with several metabolic parameters in a sibling pair study, suggesting a potential role for ALK-7 in maintaining a healthy lean condition, or at least in the regulation of metabolism and adipose tissue function (*252*, *269*, *278*). Characterisation of mice lacking *Alk7* globally or specifically in adipocytes shows that they are resistant to diet induced obesity mainly due to increased energy expenditure, but partially develop insulin resistance and liver steatosis (*268*, *277*). It is proposed that ALK-7 signalling facilitates fat accumulation under nutrient overload and promotes catecholamine resistance by suppressing β-AR expression and signalling in WAT during a high-fat diet (HFD) (*277*). On the other hand, under nutrient stress ALK-7 also functions as a sensor to regulate the adaptation of BAT to nutrient availability (*279*). ALK-7 also negatively regulates glucose-stimulated insulin release in pancreatic β-cells through an effect of activin B on Ca^{2+} signalling (*280*). Expression of ALK-7 is downregulated in human hearts from patients with hypertrophic cardiomyopathy, as well as in hypertrophic animal hearts, indicating a protective role of ALK-7 against the development of pathological cardiac hypertrophy (*281*).

Apart from its role in the maintenance of metabolic homeostasis, it is evident that ALK-7 is also a suppressor of tumorigenesis and metastasis by triggering apoptosis and impairing adhesion and proliferation in cancer cells (*282–284*). Interestingly *ALK7* is a target gene of a transcriptional coactivator which is highly expressed in regulatory T cells (*285*). Upregulation of the activin/ALK-7 signalling axis amplifies the suppressive function of regulatory T cells in antitumor immune responses, indicating a potential role for ALK-7 in immunity (*285*). These

findings uncover a wider role played by ALK-7 as a potential anticancer immunotherapeutic target.

1.4.2 Calcitonin gene-related peptide type 1 receptor (CALCRL)

1.4.2.1 Overview

The calcitonin family is a group of peptide hormones encompassing calcitonin, calcitonin gene-related peptide (CGRP), amylin, adrenomedullin (ADM), and adrenomedullin 2 (ADM2, also referred as intermedin) (*286*). Family members share structural similarities but are responsible for diverse biological functions. Calcitonin is secreted by thyroid parafollicular cells to prevent hypercalcemia and promote bone formation, while amylin is released from pancreatic β-cells postprandially and has been implicated in the regulation of energy homeostasis by inhibiting food intake (*287–290*). CGRP is abundant in the CNS, particularly in sensory neurons where its function is associated with neurogenic inflammation (*289*, *291*). ADM and ADM2 are both found in endothelial cells and presents vasodilatory properties that may have potential role in cardiovascular systems (*289*, *291*).

Functions of these hormone peptides are acted via activation of their corresponding receptors, either calcitonin receptor (CTR) or calcitonin gene-related peptide type 1 receptor (CALCRL, also known as calcitonin receptor-like receptor, CRLR), along with a single transmembrane domain accessory protein named receptor activity modifying protein (RAMP) 1, 2 or 3. CTR itself preferably responds to calcitonin, but can also associate with RAMPs in response to amylin and CGRP (*289*). Unlike CTR, CALCRL alone does not respond to any ligand, but binds to specific ligand when forming complex with individual RAMP through heterodimerisation (*291*). An additional receptor component protein (RCP) interacts with CALCRL directly and couples the CGRP receptor, but it is only required for CGRP-mediated signal transduction pathway (*292–294*).

CALCRL was originally isolated as an orphan receptor for ADM from rat lung (*295*). The first human *CALCRL* cDNA was cloned from the cerebellum in 1995 and has been shown to be

expressed predominantly in adipose tissue, cardiovascular and respiratory systems (*296*, *297*). CALCRL is a G protein-coupled receptor (GPCR) and mainly located on the plasma membrane. It requires co-expression of RAMPs to form a functional receptor in order to initiate various signalling pathways. When heterodimerised with RAMP1, CALCRL/RAMP1 complex serves as a CGRP receptor, while RAMP2 and RAMP3 interact with CALCRL to respond to ADM, forming AM_1 and AM_2 receptor, respectively (*298–300*). It appears that AM_2 receptor is more potent than AM_1 or CGRP receptor in response to ADM2 (*289*). The regulation of the heterodimerization of specific RAMPs with CALCRL is still unclear, although competition between different RAMPs to interact with CALCRL has been proposed (*291*).

1.4.2.2 Structure

Human *CALCRL* is located on chromosome 2 (2q32.1), its cDNA encodes for a protein with 461 amino acids (Figure 1.8 A) (*301*). CALCRL is a class B GPCR that belongs to the secretin family (*302*). GPCRs of this family are characterised by a unique ECD that plays an important role in ligand binding, which contains 100 – 160 residues at the N-terminus with three disulphide bonds, followed by a seven TM helix motif (Figure 1.8 A and B) (*254*, *300*, *303*, *304*).

Crystal structures of CALCRL-RAMPs ECD heterodimer bound with CGRP or ADM have been deposited to reveal the interaction between CALCRL and RAMPs, as well as peptide binding, but the structure of CALCRL alone has not been solved yet due to its nature as an integral membrane protein (*300*, *305*, *306*). Although CGRP and ADM share the same binding site on CALCRL, the difference in the shape of the binding pocket formed between CALCRL-RAMP1 or CALCRL-RAMP2 ECDs suggests ligand specificity (*300*, *305*). Taking advantage of cryo-EM, the structure of a CGRP receptor in complex with CGRP coupled with G_s protein has been determined which provides insights into ligand binding and the active interaction between receptor components (Figure 1.8 C) (*307*). It reveals that the N-terminus of CGRP binds in the receptor core, while the side chains of its C-terminus interacts with the receptors ECDs (Figure 1.8 C) (*307*). Moreover, it also suggests that the CALCRL-RAMP1 interaction is essential for ligand binding and presentation to the CGRP receptor core (*307*).

The first 38 residues of CALCRL immediately downstream of the signal peptide have been shown to be involved in the binding with ligands and interaction with RAMP1 (Figure 1.8 C) (*308*). It has been indicated that glycosylation at N123 in the ECD is essential for ligand binding and signal transduction in the presence of RAMPs (*309*). Flow cytometric analysis has demonstrated that the region from TM1 through TM5 is crucial for the translocation of RAMPs to the plasma membrane (*310*). The single transmembrane domain of RAMP1 interacts with TM3, TM4 and TM5 of CALCRL, primarily via van der Waals interactions but may also do so through hydrogen bond formation (Figure 1.8 C) (*307*). Molecular modelling of the second intracellular loop (ICL2) (residues 236 – 255) between TM3 and TM4 reveals a binding pocket for G protein by conformational change upon activation (Figure 1.8 B and C) (*294*, *304*). This has been confirmed by molecular dynamic stimulation, demonstrating that ICL2 interacts with the C-terminus of RAMP1 with G protein stimulation (*307*). Additional systematic substitution of all residues in ICL2 suggests that H238 and K249 are essential for the CGRP-stimulated cAMP response, since H238 is involved in cell-surface expression, and K249 may interact with the G protein (Figure 1.8 B) (*294*). Residues in the second extracellular loop (ECL2) ensure the stable packing of ECL2, which is crucial for the activation of the receptor by CGRP and its downstream signalling (Figure 1.8 C) (*307*). This loop is further stabilised by RAMP1 (Figure 1.8 C) (*307*). ECL3 (residues 355 – 367) between TM6 and TM7 is more important in responding to ADM rather than CGRP in terms of stimulating cAMP production (*311*). The cytoplasmic C-terminal tail from residue 388 has been shown to be crucial in ADM-mediated cAMP production and receptor internalisation, but not essential in the binding with ADM (*312*). Residues 390 – 399, which are located in helix eight, are involved in G_s coupling and cell surface expression of AM_1 receptor, while residues 414 – 417 are responsible for G_i coupling (*312*, *313*).

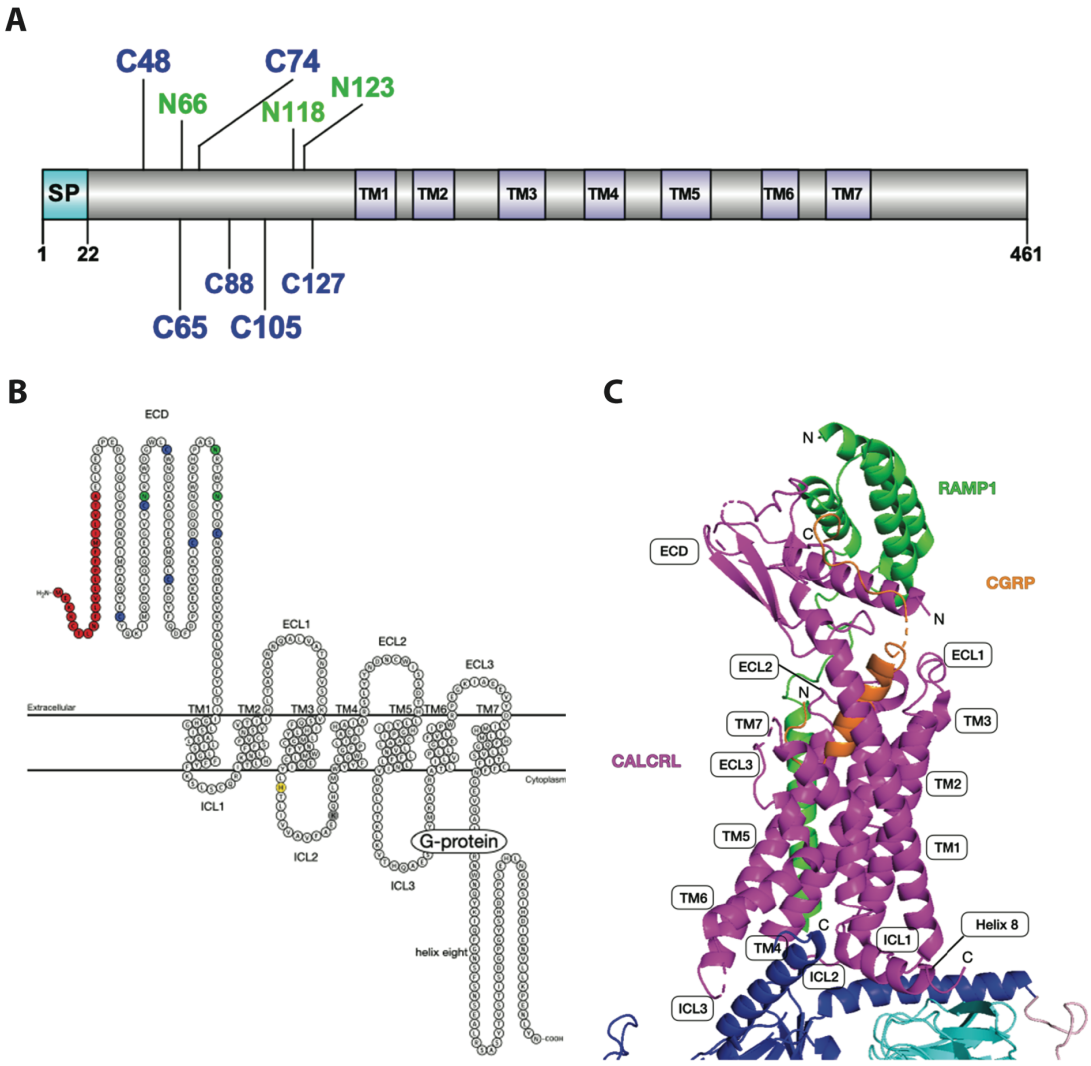

Figure 1.8 Domain structure of the human CALCRL and CGRP receptor. (A) The human CALCRL consists of 461 amino acid residues. The main features such as signal peptide (SP) and seven transmembrane domains are indicated. Six cysteines, forming three disulphide bonds, are highlighted in blue. Three glycosylation sites are labelled in green. The domain graph was generated by GPS (*249*). (B) Two-dimensional topology of the human CALCRL. SP is labelled in red. Cysteines are highlighted in blue and the glycosylation sites in green. Residues H238 and K249 in ICL2 for cell surface expression and G-protein interaction are highlighted in yellow and grey, respectively. The illustration of CALCRL and RAMP1 was produced by Protter (*299*). (C) The cryo-EM structure of CGRP/CALCRL/RAMP1/G_s complex (PDB: 6E3Y) (*302*). The colour scheme is consistent in the figure. Part of the G protein subunits is shown in blue (G_α), cyan (G_β) and light pink (G_γ). The cartoon representation was generated by PyMOL.

1.4.2.3 Function

Generally speaking, as a GPCR, CALCRL interacts with G proteins to initiate signal transduction. In response to ligands, most biological effects of CALCRL-RAMP receptors are involved in cAMP or nitric oxide (NO) production (Figure 1.9) (*314*, *315*). In human coronary artery

smooth muscle cells, the endogenous expression of CALCRL and its co-receptor RAMP1 or RAMP2 are downregulated by the proinflammatory cytokine TNF-α in a time and dose dependent manner, thus reducing cAMP levels (*316*). On the contrary, dexamethasone, a type of glucocorticoid, increases the mRNA expression of *CALCRL* and *RAMP1*, resulting in a significant increase of intracellular cAMP production in the vascular smooth muscle cells (*317*). cAMP activates PKA, which in turn promotes the phosphorylation of many PKA substrates, such as ERKs and cAMP response element-binding proteins (CREBs) (Figure 1.9) (*318*, *319*). The activation of PKA is also involved in the control of ATP-dependent potassium channels leading to vasodilation, as well as the generation of NO (Figure 1.9) (*291*, *320*). Other downstream signalling pathways include activation of PI3K and PKB activities (Figure 1.9) (*318*, *321*, *322*). Furthermore, CALCRL based receptors display different potencies not only for ligands, but also for diverse pathways in response to their corresponding ligands to exert their distinctive roles (*318*). This ligand pharmacological preference is allosterically influenced by RAMP, which modifies the conformation of CALCRL to allow different binding states (*298*, *323*, *324*).

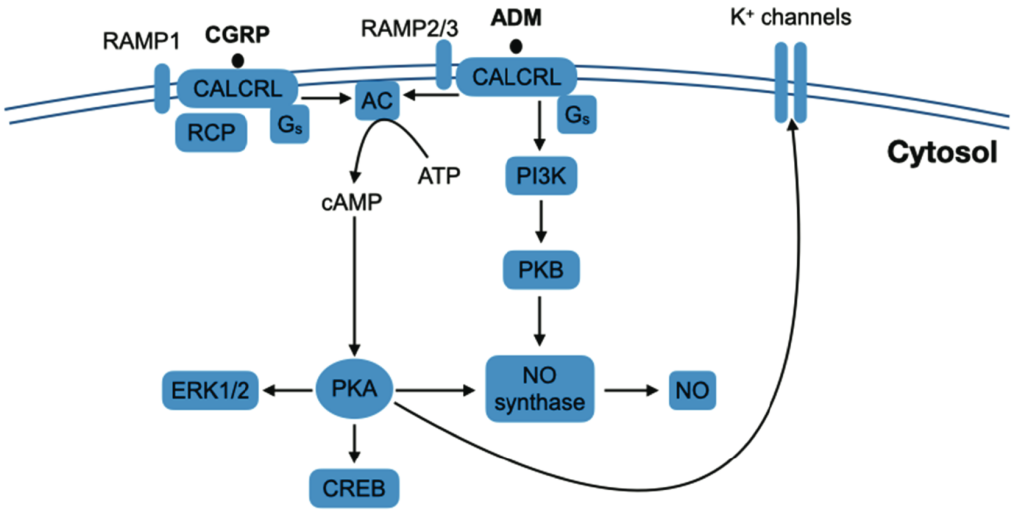

Figure 1.9 CALCRL and its receptor components mediate intracellular signalling pathways in response to CGRP (CGRP receptor) or AM (AM_1/AM_2 receptor). Ligands (CGRP or ADM) bind to CALCRL/RAMP receptor complex to increase cAMP levels, resulting in the activation of PKA which subsequently phosphorylates multiple downstream targets, such as ERKs, CREB or K^+ channels. The generation of NO is mediated by the phosphorylation of NO synthase by PKA or PKB.

It is well accepted that CGRP and its receptors are important in the transmission of pain, therefore CGRP receptor (CALCRL-RAMP1) has been targeted for the treatment of migraine by preventing CGRP ligand binding (*325–327*). In addition, studies in rats and mice suggest a role of CGRP in the development of obesity and insulin resistance, indicating that CGRP action could be a therapeutic target (*328*, *329*). As part of the signalling receptor, one intronic SNP rs696574 in the *CALCRL* gene has been identified in association with hypertension among women in a Japanese cohort, suggesting a role in vascular homeostasis, which may be related to the role of ADM in cardiovascular pathologies (*315*, *330*). However, the importance of CALCRL in relation to cardiometabolic disease needs to be further explored.

1.4.3 Perilipin 1 (PLIN1)

1.4.3.1 Overview

As described in previous sections, cytoplasmic LDs play an important role in the regulation of lipid homeostasis by storing TGs as a source of energy substrates or precursors for signalling lipids or membrane phospholipid synthesis, as well as cholesterol esters for membrane and steroid hormone synthesis (*331*). To date more than 200 protein components were discovered in association with LDs by proteomic studies and perilipins are the most abundant of those (*331*).

Perilipins are a family of proteins that are predominantly localised on the surface of LDs in nearly all cell types to serve as gatekeepers in the regulation of lipid metabolism (*185*). There are five mammalian perilipins encoded by five perilipin genes in the family, *PLIN1*, *2*, *3*, *4* and *5*, which are numbered in the order of their discovery (*331*). Perilipin 2 and 3 are ubiquitously expressed in nearly all tissue types, whereas the expression of perilipin 1, 4 and 5 are more tissue selective (*185*, *331*). The expression of perilipin 5 is primarily limited to FA oxidizing tissues, such as BAT, cardiac and skeletal muscle, while perilipin 4 is mostly enriched in adipose tissue, with lower levels of expression in skeletal muscle and heart (*185*, *331*). Perilipin 1, on the other hand, is only abundantly expressed in WAT and BAT (*331*). Subcellular localisation of perilipins differs too as perilipin 1 and 2 are mostly localised to LDs while the

others could also be cytosolic or ER enriched (*332*). Moreover, perilipin family members display differential specificity to TG or cholesterol ester cargos (*332*). Perilipin 1, 2 and 5 are found to be preferentially associated with TG-enriched LDs, whereas LDs enriched with cholesterol esters are preferably coated with perilipin 4 (*331*). Perilipin 2 and 3 are also localised to retinoid-filled LDs in hepatic stellate cells and retinal pigment epithelial cells (*331*). This enrichment and distribution pattern of perilipins indicates the specialised regulatory function of individual perilipins for lipid metabolism in a tissue-specific manner (*185*).

Perilipin 1 was first detected in rat epididymal adipocytes and found to be associated with LDs in 1991 (*159*). The authors also showed that rat perilipin is phosphorylated by PKA upon lipolytic stimulation (*159*). This discovery has been considered as a milestone in the understanding of lipid metabolism. The cDNA of rat perilipin was then isolated from a rat adipocyte cDNA expression library two years later (*333*).

The human *PLIN1* gene is localised to chromosomal region 15q26 and its cDNA was not isolated until 1998 (*334*). The *PLIN1* gene is predicted to encode four mRNA splice variants termed *PLIN1a*, *PLIN1b*, *PLIN1c* and *PLIN1d*, however only the expression of the first three isoforms have been confirmed (*333*, *335*, *336*). PLIN1a, the longest isoform of PLIN1, and PLIN1b are both highly expressed in adipocytes while PLIN1c is only expressed in steroidogenic cells (*333*, *336*). PLIN1a has been the focus of most previous studies, and it will be referred to as PLIN1 in the following sections and chapters for simplicity.

1.4.3.2 Structure

Members of the perilipin family share two conserved domains at the N terminus, starting with a hydrophobic PAT (Perilipin, ADRP and TIP47) domain consisting of approximately 100 amino acids, followed by an 11-mer amphipathic helical repeat, meaning that the sequences form amphipathic helices with three helical turns for each 11 amino acids, which varies in length (*179*, *185*, *331*). The C-terminal region of the perilipins are more divergent but still share a similar domain containing a putative 4-helix bundle (*179*, *185*, *331*).

The human *PLIN1* cDNA encodes a full-length protein with 522 amino acids (Figure 1.10 A) (*334*). As the most abundantly expressed phosphoprotein in adipocytes, human PLIN1 has five established PKA phosphorylation sites, as opposed to six in mouse PLIN1, although phosphoproteomic studies in 3T3-L1 and primary murine adipocytes found as many as 27 phosphorylated serine and threonine residues, some of which are potentially targeted by PKA (Figure 1.10 A) (*254*, *337*). It is difficult to understand the structural basis as to how PLIN1 assembles onto the LDs due to the lack of a crystal structure of PLIN1. However, mutagenesis strategies have been employed to study the structural impact on the function of PLIN1. Mouse PLIN1 was detected when isolated LDs were subjected to alkaline carbonate solution indicating that its association with LDs is mediated through hydrophobic interactions, suggesting the hydrophobic domains of mouse PLIN1 may be embedded into the core of the LDs to anchor the protein (*338*). Thus, a series of truncated mutations of murine PLIN1 have been generated and examined, showing that the central 25% of the protein is essential to target and anchor the protein to LDs (*338*). There are three sequences with approximately 20 moderately hydrophobic amino acids within the region that are found to cooperate to direct the targeting of mouse PLIN1 to LDs, although deletion of any single hydrophobic sequence or any combination of them only shows reduced targeting without eliminating its association with LDs (*338*, *339*). The complete abolition of LD targeting was only observed when all three hydrophobic sequences were removed alongside the 11-mer repeat region (*339*). Indeed the 11-mer repeat region of human PLIN1 has more recently been shown to mediate LD targeting (Figure 1.10 A) (*179*). Surprisingly, the highly conserved PAT domain is rather dispensable in promoting TG storage but does provide a binding site for HSL since it contains a PKA phosphorylation site at position 81 (Figure 1.10 A) (*340–343*). Phosphorylation of the other two N-terminal PKA sites in murine PLIN1 at position 222 and 276, as well as S81, has been shown to facilitate the docking of HSL onto the surface of LDs and maximal HSL-mediated lipolysis (*341*, *344*, *345*). Furthermore, the acidic motif (residues 290 – 321), which is unique in PLIN1, is responsible for the interaction with FSP27 to facilitate LD enlargement (*346*).

The only available structural information for the perilipin family is the crystal structure of the C-terminus of the mouse homologue PLIN3 (*347*, *348*). It revealed that the C-terminus is formed by a 4-helix bundle, an α/β domain that consists of two helices and two β sheets, and a deep hydrophobic cleft in between (Figure 1.10 B) (*347*). This hydrophobic cleft is conserved

in the perilipin family and suggests binding to a hydrophobic peptide, protein or a small molecule (*347*). The β sheets that stabilise the 4-helix bundle at the extreme C terminus, on the other hand, are unlikely to be present in PLIN1 due to one extra exon in the gene (*185*, *349*). The unique feature of the C-terminus of PLIN1 indicates a distinct function of the gene. Sequential deletion of C-terminal portions of mouse PLIN1 also reduced TG storage, especially the removal of the portion containing three other consensus serine residues 433, 492 and 517 for PKA phosphorylation of murine PLIN1, equivalent to positions 436, 497 and 522 in human PLIN1 (*340*). Hence it was proposed that the C-terminus of PLIN1 functions as a shield to facilitate TG storage by preventing the access of lipases to the LDs (*340*). This could be explained by the fact that PLIN1 binds ABHD5 on a C-terminal sequence (aa 382 – 429 of murine PLIN1) thus restricting the interaction between ABHD5 and ATGL to suppress the rate of basal lipolysis when TG storage is favoured (*350*). Phosphorylation of S492 and S517 of mouse PLIN1 releases ABHD5 and thereby enables the interaction of ABHD5 with ATGL to initiate TG hydrolysis (*351*). In particular, the phosphorylation site S517 has been considered as the master regulator of PKA-dependent lipolysis as it is essential for PKA-stimulated lipolytic actions (*352*). In addition to lipolysis, chronic stimulation of β-adrenergic receptors induces the fragmentation of large perinuclear LDs into microlipid droplets to increase surface area available to lipases and dispersion throughout the cytoplasm, suggesting a remodelling of LDs which is demonstrated to be mediated by phosphorylation of S492 by PKA (*353*).

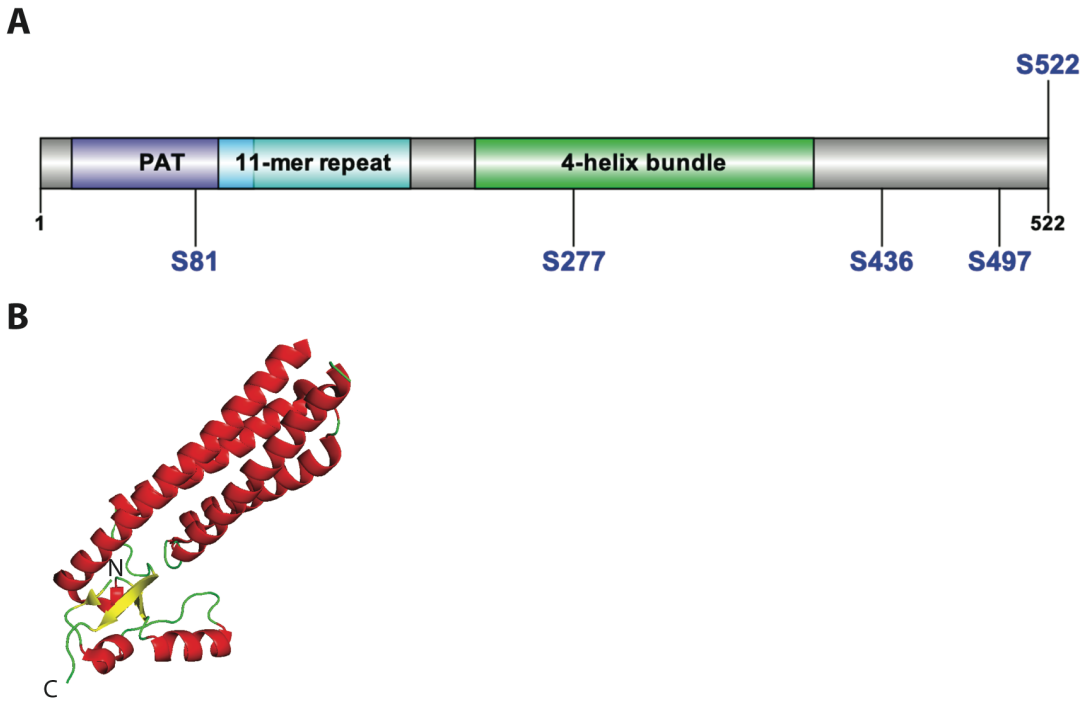

Figure 1.10 Domain structure of selected members of the perilipin family. (A) Domain structure of the human PLIN1. The highly conserved PAT domain is located at the N-terminus of PLIN1, followed by an 11-mer repeat helical motif. The 4-helix bundle is localised to the C-terminus of PLIN1. Human PLIN1 has five PKA phosphorylation sites, which are indicated in blue. The domain graph was generated by GPS (*249*). (B) The secondary structure of the C-terminus mouse PLIN3 (PDB: 1SZI) (*342*). The helices are labelled in red while the β sheets are labelled in yellow. The cartoon representation was generated by PyMOL.

1.4.3.3 Function

It is well established that PLIN1 is essential to attenuate intracellular lipolysis to promote TG storage under basal or fed conditions and to enhance lipolysis under stimulated or fasting conditions in times of energy demand (*331*). The function of PLIN1 is subject to posttranslational modification, which means the role of PLIN1 shifts from storage to mobilisation of stored neutral lipids upon phosphorylation by PKA (*344*). As described above, a 'barrier' is formed by unphosphorylated PLIN1 to restrict the access of lipase thus inhibiting TG hydrolysis which leads to increased TG content (*354*). Upon stimulation such as during energy deprivation, cellular cAMP levels rise which triggers the activation of PKA. Activated PKA in turn phosphorylates PLIN1 and HSL to release ABHD5, which subsequently binds to ATGL to initiate TG hydrolysis, converting TGs to DGs as well as releasing FAs. Meanwhile, phosphorylated HSL is recruited to the surface of LDs via interactions with N-terminal

phospho-sequences in PLIN1, which is essential for hydrolysing ATGL-derived DGs to MGs and releasing additional FAs (*185*). MGL mediates the final step of lipolysis by cleaving off FAs from MGs to release glycerol (*331*). However, since MGL is thought to be a soluble cytosolic protein, the mechanism that controls MGL activity and whether or not PLIN1 is involved is currently unknown (*331*, *355*).

Apart from its role in coordinating TG storage and hydrolysis, PLIN1 is also involved in the regulation of LD size (*185*). For example, studies have suggested that PLIN1 increases the average size of LDs and facilitates the formation of unilocular adipocytes through its interaction with FSP27 (*346*, *356*). Lipid exchange and transfer mediated by FSP27 was enhanced by the formation of heterodimers of PLIN1-FSP27, which may promote lipid transfer pore formation/expansion, thus increasing the lipid transfer rate (*346*). On the contrary, other findings demonstrate that overexpression of PLIN1 in 3T3-L1 adipocytes diminishes LD size by inhibiting FSP27 expression, suggesting there probably is a critical balance among PLIN1, FSP27 and LD surface pools for an optimised LD size for TG storage and mobilisation (*185*, *357*).

To investigate the physiological role of PLIN1, global *Plin1* knockout (KO) mice have been generated and their metabolic phenotype has been characterised (*358*, *359*). These mice have a normal body weight but are lean with reduced adipose mass and smaller adipocytes (*358*, *359*). Corresponding to the role of PLIN1 in regulating intracellular lipolysis, isolated adipocytes from *Plin1* KO mice show elevated basal lipolysis and attenuated stimulated lipolysis (*358*, *359*). When fed with a HFD, *Plin1* null mice are resistant to diet induced obesity (*358*, *359*). They also manifest an increased metabolic rate but gradually develop glucose intolerance and peripheral insulin resistance with aging (*359*).

Molecular characterisation of several PLIN1 frameshift variants found in humans shows that these mutants fail to suppress basal lipolysis in adipocytes because of their inability to bind with ABHD5 (*360*, *361*). Similar to some of the phenotypes displayed in *Plin1* null mice, patients carrying heterozygous PLIN1 frameshift mutations suffer from partial lipodystrophy characterised by the loss of SAT primarily in the lower limbs, severe dyslipidaemia, liver steatosis and insulin-resistant diabetes (*361–364*). These PLIN1 frameshift mutations co-

segregate in families thereby defining familial partial lipodystrophy (FPLD) type 4 (FPLD4) (*364*). However, whether heterozygous *PLIN1* variants that are predicted to result in *PLIN1* haploinsufficiency should be reported as causative of FPLD4 has been questioned (*365*).

1.4.4 Phosphodiesterase 3B (PDE3B)

1.4.4.1 Overview

Cyclic nucleotides, such as cAMP and cGMP are intracellular second messengers that play a key role in the modulation of intracellular signal transduction (*366–368*). They are produced by adenylyl and guanylyl cyclases (ACs and GCs), respectively, through the activation of GPCRs (*366*, *368*). Signalling pathways mediated by these second messengers are involved in the regulation of various critical physiological processes in cells, including but not limited to cell proliferation and apoptosis, inflammatory and stress responses, and cardiac muscle contraction (*368*). Thus, the concentration of second messengers is strictly controlled to ensure rapid and precise responses to stimuli (*369*).

Cyclic nucleotide phosphodiesterases (PDEs) are a group of enzymes that hydrolyse the 3' phosphate bond of cyclic nucleotides to produce inactive 5'-AMP and 5'-GMP in order to terminate second messenger signals (*366*, *370*). The PDE superfamily contains 11 members encoded by 21 genes in the human genome, with an estimation of more than 100 mRNA products due to alternative splicing (*366*, *370*, *371*). They share a conserved catalytic domain at the C-terminus, but the sequences of regulatory N-terminal regions vary between family members (*370*). Depending on the affinity and specificity of their substrates, the PDE superfamily can be further classified into three categories: those that specifically hydrolyse cAMP (PDE4, PDE7 and PDE8); those that are cGMP specific (PDE5, PDE6 and PDE9); and those that exhibit dual specificity (PDE1, PDE2, PDE3, PDE10 and PDE11) (*368*, *370*). The signalosome hypothesis suggests that different PDE isoforms in various subcellular locations contribute to compartmentalised regulation of cyclic nucleotide signalling pathways (*368*).

PDE3 was previously named as cGMP-inhibited cyclic nucleotide phosphodiesterase (cGI-PDE) since it presents a higher affinity to cAMP and the hydrolysis of cAMP is inhibited by cGMP *in vivo* (*371–375*). There are two subfamily members, PDE3A and PDE3B, which are encoded by two separate genes (*367*). Both of them are widely expressed in all tissues, but the former is abundant in the cardiovascular system and platelets, while the latter is enriched in adipose tissue, liver and pancreatic β-cells (*367*, *370*, *376*, *377*).

1.4.4.2 Structure

First cloned in 1996, the human *PDE3B* gene is located on chromosome 11p15.2 (*378*). Its cDNA encodes a protein of 1112 amino acids with a mass of 124 kDa (Figure 1.11 A) (*378*). The crystal structure of the conserved catalytic domain (aa 654 to 1073) in complex with an inhibitor revealed a 44-aa insertion from R755 to S798, which is a distinguishing feature from other PDEs (Figure 1.11 A and B) (*254*, *379*, *380*). Lacking clear secondary structural information, the role of this insertion remains to be established (*368*, *379*). It is widely acknowledged that either zinc or magnesium occupies two metal binding sites in most of the PDEs, where they coordinate with two invariant histidines (H741 and H821) and two invariant aspartic acid (D822 and D937) residues (Figure 1.11 B) (*370*). For PDE3B, however, a combination of magnesium and manganese was required for its optimal catalytic activity (*379*). Furthermore, the ability of PDE3B to bind both cAMP and cGMP, as well as binding with selective inhibitors via hydrogen bonds with a conserved residue Q988, was confirmed based on structural modelling (*379*).

PDE3B is predominantly localised in the ER and is also associated with the plasma membrane and caveolae in adipocytes, hepatocytes and cardiac myocytes (*375*, *381–385*). This membrane association property is indicated by the N-terminal hydrophobic regions (NHRs), including NHR1 for membrane insertion, which contains six putative transmembrane helices, and NHR2 for efficient membrane targeting, which contains a small hydrophobic domain of approximately 50 residues (Figure 1.11 A) (*368*, *386*). The regulatory domain at the N-terminus also includes multiple phosphorylation sites for PKA and PKB in response to hormonal stimulation (Figure 1.11 A) (*366*, *387*).

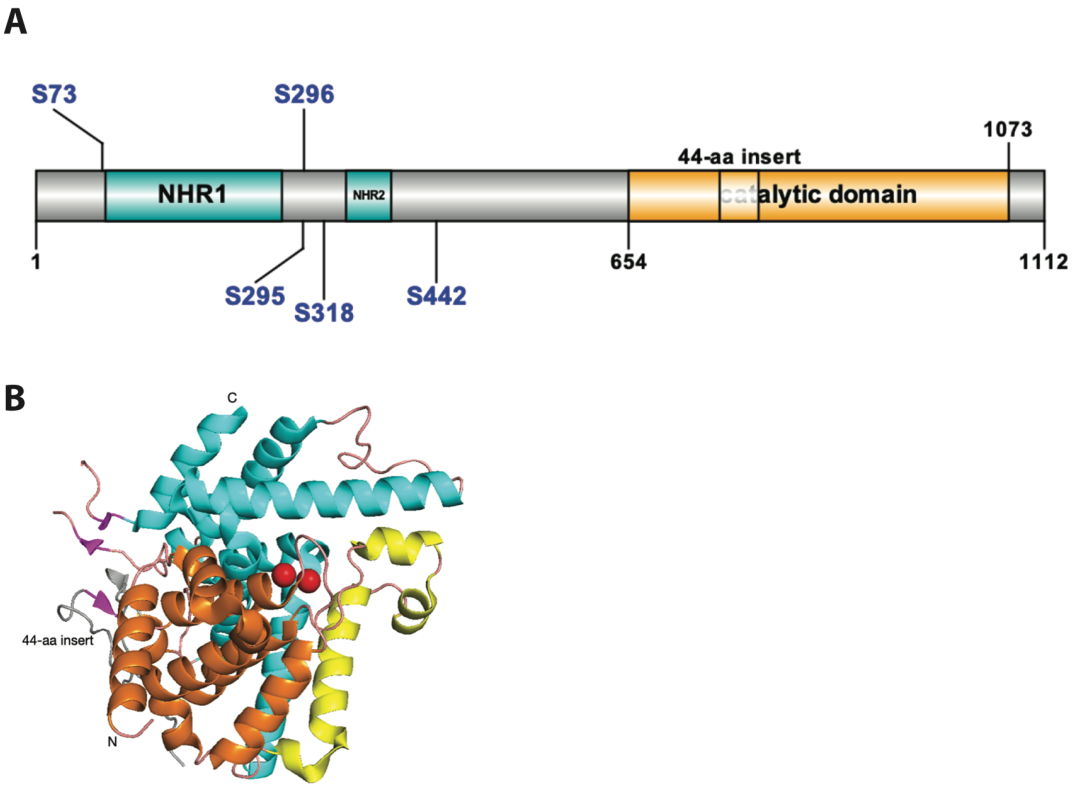

Figure 1.11 Domain structure of the human PDE3B. (A) The schematic diagram of the human PDE3B. The NHRs (N-terminal hydrophobic regions) in PDE3B are localised at the N-terminus of PDE3B. A unique 44-aa insertion is embedded in the conserved catalytic domain at the C-terminus. The putative phosphorylation sites for PKA or PKB are labelled in blue. The domain graph was generated by GPS (*249*). (B) The secondary structure of the catalytical domain of human PDE3B (PDB: 1SO2) (*374*). The catalytic domain of PDE3B is mainly composed of α helices. They form three subdomains labelled in orange, yellow and cyan. The unique 44-residue insertion is labelled in grey. Two magnesium ions are presented as red spheres. The cartoon representation was generated by PyMOL.

1.4.4.3 Function

Intensive studies have focused on the role of PDE3B in the regulation of whole-body energy homeostasis, through hormonal stimuli such as insulin, insulin-like growth factor 1 (IGF-1) and leptin (*367*). As mentioned previously, activation of PDE3B by insulin is the principal mechanism to inhibit intracellular lipolysis. In adipose tissue, the anti-lipolytic effect of insulin is associated with activation of PI3K and PKB, resulting in the phosphorylation of PDE3B, which plays a crucial role in the short-term negative feedback loop to control intracellular cAMP levels (*366*, *388*). Reduced cAMP leads to attenuated cAMP dependent PKA activity,

which in turn decreases the phosphorylation of PKA substrates PLIN1 and HSL in the lipolytic machinery. In addition, PDE3B can be phosphorylated directly by PKA in response to cAMP-enhancing agents such as isoproterenol (*374*, *389*, *390*). PKA mediated phosphorylation of PDE3B also promotes its binding with 14-3-3 protein and protects itself from inactivation by phosphatase (*391*). PDE activities are in general decreased with obesity, with a particularly strong negative correlation between PDE3 activity and BMI (*392*). This correlation was observed in isolated omental but not in subcutaneous adipocytes from obese patients (*392*). Thus, decreased PDE3B activity resulting in a diminished anti-lipolytic effect of insulin could be a contributing factor to the enhanced lipolysis observed in VAT in obese subjects.

PDE3B has also been shown to be involved in hepatic glycogenolysis and glucose stimulated insulin secretion in pancreatic β-cells. For instance, circulating insulin stimulates the synthesis and release of IGF-1 from liver, IGF-1 subsequently binds to its own receptors on the surface of β-cells and activates PDE3B to reduce the β-cell cAMP concentration *in vitro*, possibly through a PI3K mediated pathway (*393*, *394*). As a result, the local reduction of cAMP inside β-cells leads to suppression of insulin secretion. A similar PI3K-PDE3B-cAMP pathway has been reported for leptin signalling via hypothalamic PDE3B activation in leptin-sensitive neurons in order to control food intake and body weight (*395*–*397*).

Pde3b KO mice were found to be protected from obesity, the WAT of which shows a browning phenotype with elevated metabolic rate due to activation of the cAMP dependent AMPK signalling pathway, indicating that PDE3B and/or its downstream signalling molecules might potentially be new therapeutic targets for treating obesity (*398*). Although a PDE3B specific inhibitor has not been reported, PDE3 selective inhibitors such as cilostazol, milrinone, cilostamide and enoximone, among others, have been utilised for cardiovascular therapies (*386*, *399*). The first two compounds are currently available on the market to help patients improve myocardial contractility, but both exhibit serious side effects (*400*).

1.4.5 Adipose triglyceride lipase (ATGL, PNPLA2)

1.4.5.1 Overview

TGs stored in lipid droplets in WAT are the primary energy reservoir in cells. The hydrolysis of TG provides glycerol and FAs to other tissues for energy production. For decades, HSL has been considered to be the sole enzyme regulating lipolysis due to its broad substrate specificity, including TGs, DGs, MGs and cholesteryl esters (*401–403*). Surprisingly, HSL KO mice fail to present an obese phenotype but still release a substantial amount of glycerol and FAs *in vitro* despite TG lipase activity being reduced to 40% in WAT, suggesting that the function of HSL in hydrolysing TG may be compensated by another enzyme (*404*). Additionally, instead of TG, massive DG accumulation in various tissues was observed in HSL deficient mice further corroborating the existence of an alternative TG lipase (*402*). In 2004, three independent groups published the discovery of a novel enzyme that mainly degrades TG, named desnutrin, calcium-independent phospholipase A_2 ζ (iPLA$_2$ζ), and adipose triglyceride lipase (ATGL), respectively (*405–407*). These are identical proteins now generally recognised as ATGL.

ATGL is encoded by the *PNPLA2* gene, which is short for patatin-like phospholipase domain-containing protein 2 (*406*). It belongs to a family of PNPLA proteins containing nine members, which share a patatin domain (Pfam01734) that is named after patatin which was initially discovered in potato tubers (*407*, *408*). Members of the family display diverse lipid hydrolase activities with different substrate specificities and play critical roles in lipid metabolism and energy homeostasis (*408*, *409*). In this thesis, the nomenclature *PNPLA2* and ATGL will be used for gene and protein, respectively. ATGL is widely expressed in all human tissues but is highly enriched in adipose tissue where it catalyses the first step in the hydrolysis of TG (*410*). In adipocytes, ATGL is mostly localised to the ER-related membranes in the cytoplasm, although a small portion of ATGL forms a complex with its inhibitor G0/G1 switch protein 2 (G0S2) in the cytosol (*411*, *412*).

1.4.5.2 Structure

The human *PNPLA2* gene is located on chromosome 11p15.5. The cDNA of human ATGL encodes for a protein with 504 amino acids (Figure 1.12) (*406*). The human ATGL protein shares 86% homology with murine ATGL (*407*, *410*). The three-dimensional structure of ATGL remains to be determined, but crystal structures of an isoenzyme of patatin Pat17 and human cytosolic phospholipase A_2 ($cPLA_2$) have been published (*413–415*). Based on the shared features between ATGL and $cPLA_2$, it is predicted that the N-terminal of the ATGL protein has a three-layer α/β/α sandwich overlapping the patatin domain (residues 10 – 178) (Figure 1.12) (*254*, *414*, *416*). According to the molecular structure of Pat17, the central β-sheet is essentially sandwiched between α-helices front and back in the three-layer α/β/α sandwich fold (*414*). A typical α/β hydrolase fold has a catalytic serine-aspartate dyad, which in ATGL consists of S47 located in the GXSXG motif and D166 within the DXG/A motif (Figure 1.12) (*410*, *416*). *In vitro* studies show that the change from serine to alanine in the GXSXG motif results in impaired lipase activity (*417*). The glycine-rich sequence is of great importance in stabilising the active site during substrate cleavage by S47 (*414*). The patatin domain within the α/β/α sandwich fold also interacts with a number of co-factors, for instance ABHD5, G0S2, hypoxia-inducible lipid droplet-associated protein (HLPDA), to regulate ATGL activity (*409*, *412*, *418*).

The C-terminal part of ATGL consists mostly of α-helical and loop regions with a hydrophobic stretch (residues 315 – 360), which is involved in the localisation to lipid droplets and the regulation of enzyme activity (Figure 1.12) (*409*, *410*, *416*, *419*). In particular, phosphorylation of T372 within the hydrophobic stretch of murine ATGL, equivalent to T370 of human ATGL, has been shown to prevent lipid droplet targeting (Figure 1.12) (*420*). Two other putative phosphorylation sites in human ATGL are S404 and S428, corresponding to murine S406 and S430 (Figure 1.12) (*180*). Studies suggest that phosphorylation at murine S406 is mediated by PKA and/or AMPK, leading to enhanced ATGL activity to promote lipolysis (*421*, *422*).

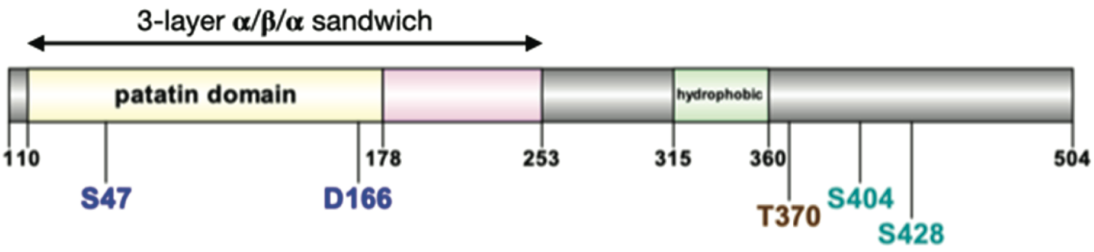

Figure 1.12 Domain organisation of the human ATGL. The ATGL protein comprises a three-layer α/β/α sandwich motif at the N-terminus and a C-terminal part. The patatin domain contains a catalytic site, S47 and D166 which are labelled in blue. The hydrophobic region, as well as T370, at the C-terminus are involved in LD binding. Two putative phosphorylation sites S404 and S428 are also indicated in the scheme. The domain graph was generated by GPS (*249*).

1.4.5.3 Function

As a member of the patatin family, ATGL exhibits non-specific lipid acyl-hydrolase activity (*408*, *414*). ATGL is well-known for its lipolytic function in adipocytes where it initiates lipolysis by removing a FA from TG to generate DG, which is considered to be the rate-limiting step of lipolysis. The involvement of ATGL in the catabolism of TG is also observed in hepatocytes and cardiomyocytes (*423*, *424*).

Regulation of ATGL activity mainly involves a direct interaction with co-factors (*188*, *418*, *425*, *426*). ABHD5 also belongs to the α/β hydrolase superfamily but itself does not exhibit lipase activity due to the replacement of serine by asparagine in the GXSXG motif (*410*). However, the TG hydrolase activity of ATGL is significantly enhanced (>80%) via direct protein-protein interaction with ABHD5 (*188*). G0S2, on the other hand, directly binds to the patatin domain of ATGL to limit substrate accessibility in order to inhibit lipase activity, thereby controlling TG turnover (*410*). It does not seem like there is competition between ABHD5 and G0S2 in their binding with ATGL (*410*). Similar to G0S2, the role of HILPDA in the attenuation of ATGL activity also involves direct interaction of both proteins, although it has a relatively low affinity compared to G0S2 (*418*).

Intracellular lipid dysmetabolism, leading to accumulation of neutral lipids in various organs and tissues, causes a rare autosomal recessive disease named neutral lipid storage disease

(NLSD) (*427*). Two distinct clinical phenotypes of NLSD, NLSD with ichthyosis (NLSDI, also known as CDS) and NLSD with myopathy (NLSDM), are caused by mutations in *ABHD5* and *PNPLA2*, respectively (*187*, *428–430*). Neutral lipid accumulation in multiple tissues in the affected individuals results from impaired lipolytic fat degradation, not from increased free fatty acid (FFA) uptake or TG synthesis rate (*188*). Mutations in ABHD5, either by single amino acid substitution or protein truncation, are associated with NLSDI due to their incapability of activating ATGL for TG hydrolysis (*188*). Whereas *PNPLA2* mutations found in diagnosed NLSDM patients are predicted to encode mutated or truncated ATGL proteins resulting in a defective patatin domain or hydrophobic domain, respectively (*431*). Mutation within the protein either reduces the lipid droplet targeting thus leading to low activity of lipid droplet associated ATGL, or impairs the enzyme activity, therefore causing the loss of ATGL function in TG catabolism (*431*).

Similarly, genetic deletion of ATGL in mice also results in the accumulation of TG in multiple tissues (*432*). Interestingly these mice are not or only moderately obese, and resistant to diet induced obesity (*432*). Moreover, they also demonstrate improved glucose tolerance and insulin sensitivity, which could be explained by reduced lipotoxicity in ectopic tissues, suggesting that the inhibition of ATGL may have a beneficial impact on metabolic profiles (*432*, *433*). Thus, a small-molecule inhibitor named Atglistatin has been developed specifically targeting ATGL (*434*). However, studies have indicated that Atglistatin inhibits murine but not human lipolysis, so the development of pharmacological inhibitors specific for human ATGL to tackle metabolic diseases remains challenging (*431*, *433*).

1.5 Study aims

The overall aim of my study was to investigate the functional impact of the missense variants reported by Lotta et al. (*1*) using cellular models to provide some insights into their roles in adipocyte biology in order to advance understanding of the mechanisms underlying the association of these ‘genes’ with body fat distribution and the risk of cardiometabolic disease.

As stated previously, all the candidate genes are expressed in adipose tissue and have been at least loosely implicated in the regulation of intracellular lipolysis to some extent. Therefore, the initial aim of the study was to establish the role of *ALK7*, *CALCRL*, *PLIN1*, *PDE3B* and *PNPLA2* in the regulation of adipogenesis and intracellular lipolysis, using a siRNA-mediated knockdown approach in the context of 3T3-L1 adipocytes. The initial findings will be described in Chapter 3.

The study further aimed to highlight the functional consequences of the specific rare coding variants of *ALK7*, *PLIN1* and *PNPLA2* by *in vitro* overexpression experiments. These results will be presented in Chapters 4 and 5.

Functional studies on *PDE3B* and *CALCRL* missense variants are being undertaken by other members of the laboratory (*PDE3B*) and/or external collaborators (*CALCRL*). These studies are ongoing, and their results are not presented in this thesis.

2 Materials and Methods

2.1 Cloning

2.1.1 Primer design

Oligonucleotide primers complementary to template DNA were designed for polymerase chain reaction (PCR). Ideally primers between 18 to 24 bases with a guanine (G) and cytosine (C) content between 40% to 60% were selected. Usually, primers terminating on a 3' G or C were selected to promote binding to the template. The designed primer pairs had optimal melting temperatures (Tm) in the range of 50 to 60°C with a maximum difference of 5°C between them. For restriction cloning, enzyme sites were added to the 5' ends of a primer and 3 to 6 bases of nucleotides were added upstream of the site to assist in restriction digestion.

For site-directed mutagenesis, the primers containing desired mutations were designed using the online QuikChange Primer Design Programme (https://www.agilent.com/store/primerDesignProgram.jsp) (Agilent, USA).

All oligonucleotide primers were synthesized by Sigma-Aldrich (UK) and resuspended to 100 µM in nuclease-free water (Thermo Fisher, USA) for storage. Primer sequences used for PCR cloning in this thesis are listed in Appendix 1.

2.1.2 Polymerase chain reaction (PCR)

In general, 20 ng of template DNA was used for PCR amplification by Phusion High-Fidelity DNA polymerase (Thermo Fisher Scientific, USA). In a 50ul reaction, the DNA template was amplified in the presence of 10 µl 5X Phusion HF or GC buffer, 200 µM of each deoxynucleoside triphosphate (dNTP), 0.5 µM of each primer, 3% DMSO, 2 U Phusion DNA polymerase.

A typical PCR program was set up as follows: initial denaturation at 98°C for 30 seconds, followed by 35 cycles of 10 seconds of denaturation at 98°C, 30 seconds of annealing at 65°C (temperature varied depending on the Tm of the primer pair) and an extension time of 15 seconds per 1 kb amplicon at 72°C, and a final extension at 72°C for 10 minutes. The reaction was performed on a ProFlex PCR System (Applied Biosystems, Thermo Fisher Scientific, USA).

2.1.3 Agarose gel electrophoresis

Agarose gel electrophoresis is a widely used procedure for DNA separation by size through an agarose matrix. Generally, 0.8 – 1% agarose gels were prepared by dissolving an appropriate amount of UltraPure Agarose (Thermo Fisher Scientific, Invitrogen, USA) in a given volume of TAE buffer (CIMR stock) and heating up in a microwave until the agarose powder was fully dissolved. SYBR Safe DNA Gel Stain (Thermo Fisher Scientific, USA) was diluted to a final concentration of 0.005% (v/v) in the molten agarose for DNA detection and poured into a gel tray with well comb in place and allowed to solidify at room temperature (RT). The gel was then loaded with 10 – 50 µl of samples, together with 7 – 10 µl of HyperLadder 1 kb (Bioline, UK) as a marker. Gel electrophoresis was performed in TAE buffer at 100 V for 30 minutes. DNA fragments were visualised under ultra-violet (UV) light using either ChemiDoc MP Imaging System (Bio-Rad, USA) or G:BOX Chemi XL Gel Documentation System (Syngene, UK).

2.1.4 DNA purification and gel extraction

For downstream application, amplified PCR fragments were purified from PCR reaction using PureLink PCR Purification Kit (Thermo Fisher Scientific, USA) according to the manufacturer's guide.

For purification of DNA fragments from agarose gels, the DNA bands were visualised using the Safe Imager Blue-Light Transilluminator (Thermo Fisher Scientific, USA) and excised using a scalpel. The agarose piece was dissolved in an optimal pH buffer by gentle heat and the DNA extracted using the PureLink Quick Gel Extraction Kit (Thermo Fisher Scientific, USA) as per the manufacturer's manual. DNA was eluted in 30 µl nuclease-free water and quantified using

NanoDrop 1000 Spectrophotometer (Thermo Fisher Scientific, USA). Absorbance at 230, 260 and 280 nm was recorded.

2.1.5 Restriction enzyme digestion and alkaline phosphatase treatment

Restriction digestion of 1.5 – 3 µg DNA was performed in a 50 µl reaction using 1.5 – 3 U FastDigest restriction enzymes (Thermo Fisher Scientific, USA) in the presence of 5 µl 10X FastDigest buffer (Thermo Fisher Scientific, USA). The reaction was typically incubated at 37°C for 1 hour before heating to 65°C or 80°C for 5 minutes to inactivate the enzyme.

When linearizing plasmid vector for cloning, FastAP Thermosensitive Alkaline Phosphatase (Thermo Fisher Scientific, USA) was also included in the reaction to dephosphorylate the vector and avoid its re-circularisation during ligation.

The digested DNA fragment and vector were then purified using PureLink PCR Purification Kit and PureLink Quick Gel Extraction Kit, respectively.

2.1.6 Ligation

Ligations were performed using the Rapid DNA Ligation Kit (Thermo Fisher Scientific, USA) according to the manufacturer's protocol. Typically, ligations were conducted in a 20 µl reaction volume, consisting of 150 ng insert and 50 ng dephosphorylated vector, 4 µl 5X Rapid Ligation buffer, and 5 U T4 DNA ligase. The reaction was left at RT for 15 minutes and the recombinant plasmid was then ready to be transformed into the appropriate bacterial strain.

2.1.7 Bacterial transformation

Typically, 50 ng of recombinant DNA from the ligation mixture (5 µl) was used to transform into 50 µl competent cells. Briefly, competent cells of choice were thawed and incubated with ligation mixture for 30 minutes on ice. The competent cells/DNA mixture was heat shocked at 42°C for 45 seconds and immediately returned on ice for 5 minutes. To allow the bacteria

to grow and express antibiotic resistance proteins, 900 µl of S.O.C. medium (Thermo Fisher Scientific, USA) or Luria broth (LB, CIMR, UK) was added and incubated at 37°C with shaking 250 rpm for 1 hour. Cells were spun down at 2000 rpm for 2 minutes at RT, 800 µl supernatant was discarded. The remaining cells were then re-suspended and plated onto pre-warmed LB agar plates (CIMR, UK) supplemented with the appropriate antibiotic for selection. The plates were left in the 37°C incubator for 16 hours to form colonies.

2.1.8 Colony PCR

Colony PCR with GoTaq Green Master Mix (Promega, USA) was used to screen positive bacterial colonies on agar plates. Colonies were randomly selected using sterile 10 µl filter pipette tip and resuspended in 70 µl LB media to serve as a template for the PCR. A 10 µl reaction normally contained 1 µl cell suspension, 0.5 µM of each primer, 5 µl 2X GoTaq Green Master Mix, topped up with nuclease-free water. The PCR amplification program was set as follows: initial denaturation at 95°C for 2 minutes, followed by 30 cycles of 1 minute of denaturation at 95°C, 1 minute of annealing at 65°C (the exact annealing temperature was primer-dependent) and an extension time of 1 minute per 1 kb amplicon at 72°C, and a final extension at 72°C for 5 minutes. PCR products were separated by agarose gel electrophoresis as described in 2.1.3. Once a positive colony was confirmed, the same cell suspension was selected for amplification and purification of plasmid DNA.

2.1.9 Plasmid DNA purification

Colonies were used to inoculate 3 ml LB containing the appropriate antibiotic in a 14 ml round bottom tube (Falcon, Corning, USA) and agitated at 250 rpm for 16 hours at 37°C. Cells were spun down and plasmid DNA was purified using Wizard Plus SV Miniprep DNA Purification System (Promega, USA) following the manufacturer's instructions and the DNA re-suspended in 50 ul nuclease-free water and quantified using NanoDrop 1000 Spectrophotometer.

In order to obtain high yield of high-quality plasmid DNA for downstream application, the initial 3 ml LB culture was used to inoculate 150 ml LB with the appropriated antibiotic in a 1

L flask and shaken at 250 rpm in a 37°C incubator for 16 hours. Cells were pelleted and plasmid DNA was extracted and purified using HiSpeed Plasmid Maxi Kit (Qiagen, Germany) according to the manufacturer's protocol and typically re-suspended in 500 µl nuclease-free water and quantified using NanoDrop 1000 Spectrophotometer.

2.1.10 Site-directed mutagenesis

QuikChange II XL Site-Directed Mutagenesis Kit (Agilent, USA) was used to introduce a site-specific mutation into a construct. A typical reaction consisted of 50 ng template DNA, 125 ng of each mutagenic primer that containing the desired mutation, 1 µl dNTP mix, 3 µl QuikSolution reagent, 5 µl 10X reaction buffer and 2.5 U *PfuUltra* High Fidelity DNA polymerase, topped up with nuclease-free water to a final volume of 50 µl. PCR cycling started with 1 minute of initial denaturation at 95°C, followed by 18 cycles of denaturation at 95°C for 50 seconds, annealing at 60°C for 50 seconds and elongation at 68°C for 1 minute per kb of the plasmid length, ended with 7 minutes of final extension at 68°C. The PCR product was cooled down and treated with 10 U DpnI restriction enzyme for 1 hour at 37°C in order to remove parental methylated and hemimethylated DNA. 2 – 5 µl of DpnI-treated DNA was transformed into XL10-Gold ultracompetent cells (Agilent, USA) according to the manufacturer's instruction manual. Plasmid DNA was extracted and purified from resulting colonies as describe in 2.1.9. Clones containing the desired mutations were identified by Sanger sequencing (2.1.11). The DNA fragment carrying the mutation(s) was then subcloned into the original cloning vector to avoid additional mutations in other regions of the vector, which could potentially affect downstream experiments. Primers used for site-directed mutagenesis are listed in Appendix 2.

2.1.11 Sanger sequencing

Sanger sequencing is a method to determine the nucleotide sequence of DNA by incorporating fluorescent-labelled dideoxynucleotide triphosphates (ddNTPs) into the sequence of interest. Unlike dNTPs, ddNTPs lack a 3'-hydroxyl group (3'-OH) which is essential for DNA polymerase to continue synthesising the DNA chain. Once a ddNTP has been added

to the chain, an incoming dNTP cannot be added, resulting in the termination of chain elongation that ends with a labelled nucleotide. Thus, this method is also known as the chain termination method.

The mixture of DNA fragments is then separated by size using capillary gel electrophoresis. Since each base carries a particular colour of dye, they can be detected by a laser to generate a chromatograph showing fluorescence intensity in the correct order of the sequence.

All cloned plasmids were sequenced at 5' and 3' ends of genes of interest to verify correct orientation and sequence fidelity. Sequencing was performed using 100 ng plasmid DNA, 0.5 µM primer (forward or reverse), 0.5 µl BigDye Terminator v3.1 Ready Reaction Mix (Thermo Fisher Scientific, USA), 2 µl 5X sequencing buffer (Thermo Fisher Scientific, USA) in 10 µl reaction volume. Thermal cycling was repeated for 25 times with parameters set as follows: denaturation at 95°C for 10 seconds, followed by annealing at 50°C for 5 seconds and extension at 60°C for 4 minutes. The PCR products were purified using AxyPrep Mag DyeClean (Axygen Biosciences, USA) as per the manufacturer's instruction and eluted in nuclease-free water. The DNA solutions were run on a 48-capillary 3730 DNA Analyzer (Thermo Fisher Scientific, USA). Sequencing analysis was performed using Sequencher DNA sequence analysis software (Gene Codes Corporation, USA) against reference sequences that were obtained from Ensembl (http://www.ensembl.org/index.html).

2.2 Cell culture

All reagents were purchased from Sigma-Aldrich (USA) unless otherwise indicated.

2.2.1 Cell maintenance

Growth media used for cell maintenance in this thesis are summarised in Table 2.1.

COS-7 (African green monkey kidney) and HEK293 (Human embryonic kidney 293) cells were purchased from American Type Culture Collection (ATCC, USA). HEK293T cells, which were

used for lentiviral packaging, were also obtained from ATCC and were maintained in the same medium. Routine passaging was performed every 2 – 3 days by rinsing the cells with pre-warmed Dulbecco's phosphate buffered saline (DPBS), followed by treatment with trypsin-EDTA solution. Detached cells were then diluted and re-suspended with an appropriate volume of growth media to a new culture vessel.

Murine 3T3-L1 preadipocytes were obtained from ATCC. Newborn calf serum (NCS) was heat inactivated at 65°C for 30 minutes before use. Mouse embryonic fibroblasts (MEFs) were maintained in the medium as described previously (*435*). Both 3T3-L1 and MEF cells were maintained below 70% confluency.

All cells were tested mycoplasma-free and maintained in a 5% CO_2 humidified chamber at 37°C.

Table 2.1 Cell culture media used for cell maintenance.

Cell line	Medium	Components
COS-7 HEK293 HEK293T	Dulbecco's Modified Eagle's Medium (DMEM)	10% (v/v) FBS (fetal bovin serum) (Thermo Fisher Scientific, USA) 4 mM L-glutamine 1X MEM Non-essential amino acid solution 1 mM sodium pyruvate 100 units/ml penicillin 100 µg/ml streptomycin
3T3-L1	DMEM	10% (v/v) NCS 4 mM L-glutamine 1X MEM Non-essential amino acid solution 1 mM sodium pyruvate 100 units/ml penicillin 100 µg/ml streptomycin
MEF	DMEM	10% (v/v) FBS 4 mM L-glutamine 1X MEM Non-essential amino acid solution 1 mM sodium pyruvate 100 units/ml penicillin 100 µg/ml streptomycin 50 µM 2-mercaptoethanol (Thermo Fisher Scientific, USA) 3 µg/ml puromycin dihydrochloride (Cambridge Bioscience, UK)

2.2.2 Cell preservation and recovery

All cells at 70 – 90% confluency were trypsinised and centrifuged at 200 *x g* at RT for 5 minutes. Cells were resuspended in corresponding serum containing 10% (v/v) DMSO and aliquoted 1

ml to each cryovial. Cryovials containing cells were placed into an isopropanol filled Mr. Frosty freezing container and kept in -80°C freezer for 24 hours. For long term preservation, cells were stored in liquid nitrogen vapour phase.

Cells were thawed by placing the cryovial in a 37°C incubator and transferred to a centrifuge tube containing 9 ml of growth medium, followed by centrifugation at 200 *x g* for 5 minutes at RT to remove DMSO. Cell pellet was resuspended in growth medium and dispersed into an appropriate tissue culture flask. Fresh medium was replaced after 24 hours.

2.2.3 Adipocyte differentiation

To differentiate 3T3-L1 cells into adipocytes, cells were seeded into culture plates and grown to confluency and fed 3T3-L1 preadipocyte medium every 2 - 3 days. At least two days after attaining confluency, differentiation was induced by incubating cells with differentiation medium supplemented with 1 µM insulin (Actrapid, Novo Nordisk, Denmark), 0.5 mM 3-isobutyl-1-methylxanthine (IBMX) and 1 µM dexamethasone for the first 2 days. The medium was replaced with differentiation medium supplemented with 1 µM insulin for another 2 days and then maintained in differentiation medium which was replaced every 2 days until mature adipocytes were developed, which normally took a further 6 – 8 days.

To differentiate MEFs into adipocytes, cells were seeded into tissue culture plates and maintained in growth medium every 2 – 3 days in the presence of appropriate antibiotics until they reached confluency. Medium was replaced 2 days post-confluency and differentiation was induced by incubating MEFs in growth medium supplemented with 8 µg/ml D-pantothenic acid, 8 µg/ml biotin, 1 µM rosiglitazone, 0.5 mM IBMX, 1 µM dexamethasone, and 1 µM insulin for the first 3 days. The medium was then replaced with growth medium with 8 µg/ml D-pantothenic acid, 8 µg/ml biotin, 1 µM rosiglitazone, and 1 µM insulin for a further 3 days. MEFs were maintained in growth medium which was replaced every 3 days until mature adipocytes were developed, which normally took another 6 days.

2.2.4 Transient transfection

Cells were seeded in 12-well tissue culture plate and were transfected with plasmid DNA using Lipofectamine LTX with PLUS Reagent (Thermo Fisher Scientific, USA) according to the manufacturer's manual the following day.

HEK293 cells were seeded in poly-D-lysine-coated 24-well tissue culture plate and were transfected with plasmid DNA using Lipofectamine 3000 Reagent (Thermo Fisher Scientific, USA) following the manufacturer's protocol.

2.2.5 siRNA transfection

Small interfering RNAs (siRNAs) were purchased from Horizon Discovery (UK) and are listed in Appendix 3.

3T3-L1 preadipocytes were seeded in 12-well tissue culture plates and maintained until confluency as described in 2.2.1. Confluent cells were transfected with 30 nM mouse siRNA every 2 – 3 days using Lipofectamine RNAiMAX Transfection Reagent (Thermo Fisher Scientific, USA) according to the manufacturer's protocol. Cells were differentiated until day 9 – 10 as described in 2.2.3.

2.2.6 Stable cell line generation

2.2.6.1 Viral production

HEK293T cells were employed to produce lentivirus. Cells were seeded at approximately 70% confluent in 100 mm tissue culture dishes and transfected on the following day using Lipofectamine LTX with PLUS Reagent. 10 µg of lentiviral plasmid, 7.5 µg of each packaging plasmid (pMDLg/pRRE and pRSV-Rev), 5 µg of pCMV-VSV-G plasmid encoding the envelope, were transfected, together with 1 µg pEGFP as an indicator for transfection efficiency. Medium was replaced with UltraCULTURE Serum-free Medium (Lonza, Switzerland) 24 hours

post-transfection and repeated for a further 3 days. Meanwhile, lentivirus-containing medium was collected and pooled at 48, 72, and 96 hours post-transfection and filtered with 0.45 µm filter (Sartorius, Germany) and concentrated using Centricon Plus-70 (Merck, USA). The concentrated virus was used to infect target cell line or was aliquoted and stored at -80°C until further use.

2.2.6.2 Viral transduction of target cell line

Plin1 knockout (KO) MEFs obtained from Prof Andrew Greenberg (*435*) were seeded in 6-well tissue culture plate at 40% - 50% confluency the day before transduction. Varying amounts of the concentrated lentivirus particles were used to transduce *Plin1* KO MEFs in the presence of 10 µg/ml polybrene (Merck, USA) to enhance infection efficiency. After 24 hours, the virus-containing medium was replaced with fresh growth medium in the presence of 200 µg/ml hygromycin (Merck, USA) to select transduced cells. Stable cell lines were maintained in culture medium containing selection antibiotic.

2.3 Gene expression analysis

2.3.1 RNA extraction

Cultured cells were re-suspended in 350 µl RLT (Qiagen, Germany) supplemented with 1% (v/v) β-mercaptoethanol (Sigma-Aldrich, USA). The cell lysates were homogenised by passing through a QIAshredder (Qiagen, Germany) and the mRNA was purified using the RNeasy Mini Kit (Qiagen, Germany) according to the manufacturer's protocol. The RNA was eluted in 30-50 µl Nuclease-free water and the quality and quantity of the RNA was assessed using the NanoDrop 1000 Spectrophotometer (Thermo Fisher Scientific, USA).

For peripheral blood mononuclear cells (PBMCs), total RNA was extracted from 1 – 2 million cells. PBMCs were resuspended in 100 µl RLT Plus (Qiagen, Germany) supplemented with 1% (v/v) β-mercaptoethanol, and the RNA extracted using RNeasy Plus Micro Kit (Qiagen,

Germany), following the manufacturer's manual. The RNA was eluted in 20 µl nuclease-free water and assessed as above.

2.3.2 Reverse transcription

To eliminate any genomic DNA (gDNA) contamination, the purified RNA was treated with DNase I (Thermo Fisher Scientific, USA), or RQ1 RNase-free DNase (Promega, USA), according to manufacturer's protocol.

In general, a total of 0.4 – 2 µg DNase-treated RNA was reverse transcribed to cDNA using Moloney Murine Leukaemia Virus (M-MLV) reverse transcriptase (Promega, USA). Briefly, RNA was incubated with 0.5 µg Random primers (Promega, USA) at 70°C for 5 minutes to melt secondary structure within the template. To prevent the re-formation of its secondary structure, mixture was placed on ice immediately. In the same tube, 4 µl M-MLV 5X Reaction buffer, 0.5 mM dNTPs, 200 U M-MLV reverse transcriptase, 20 U Recombinant RNasin Ribonuclease Inhibitor, and nuclease-free water were added to a total volume of 20 µl for cDNA synthesis. The reaction was then incubated at 37°C for 1 hour, followed by 15 minutes incubation at 70°C. Alternatively, cDNA was also synthesised from DNase I-treated RNA using the LunaScript RT SuperMix kit (New England Biolabs, USA) following the manufacturer's protocol. Up to 1 µg RNA was mixed with 4 µl 5X LunaScript RT SuperMix and topped up with nuclease-free water to 20 µl in a reaction. The reaction was first incubated at 25°C for 2 minutes for primer annealing, followed by cDNA synthesis at 55°C for 10 minutes and 1-minute heat inactivation at 95°C. Synthesised cDNA was diluted 5 – 10 times in nuclease-free water and stored at -20°C.

2.3.3 Real-time quantitative PCR (qPCR)

Real-time quantitative PCR (qPCR) was performed to determine gene expression at transcriptional level. 2 µl of cDNA of which was used in a 10 µl qPCR reaction. The reaction also contained 0.5 µM gene-specific TaqMan gene expression assay (Thermo Fisher Scientific, USA) or forward and reverse primer with 5'-[6FAM], 3'-[TAMRA]-labelled probe (Sigma-

Aldrich, UK), and 5 µl of either 2X TaqMan Universal PCR Master Mix (Thermo Fisher Scientific, USA) or 2X SYBR Green Master Mix (Thermo Fisher Scientific, USA), respectively.

The PCR was performed on the QuantStudio 7 Flex Real-Time PCR system (Thermo Fisher Scientific, USA). The thermal cycling program started with an initial hold at 50°C for 2 minutes, 95°C for 10 minutes, followed by 40 cycles of PCR stage with alternation between 15 seconds of 95°C and 1 minute of 60°C. An additional melt curve stage was added (15 seconds at 95°C, 1 minute at 60°C followed by 15 seconds at 95°C) when SYBR Green dye was used during amplification. A threshold cycle (Ct) was calculated by the instrument's software (Thermo Fisher Scientific, USA) for each reaction, and mRNA expression was quantified using the standard curve method. The expression of target genes was normalised to that of a housekeeping gene as described in the following chapters. Primers used for qPCR are summarised in Appendix 4.

2.4 Protein analysis

2.4.1 Cell lysate preparation

For harvesting cell lysates, cultured cells were washed twice with ice-cold DPBS and lysed using RIPA buffer (Sigma, USA) supplemented with EDTA-free Protease Inhibitor Cocktail (Roche, Switzerland) and Phosphatase Inhibitor Cocktail Tablets (Roche, Switzerland). The cell suspension was cleared by spinning at 16,100 *x g* at 4°C for 15 minutes. Protein concentration was determined using DC Protein Assay (Bio-Rad, USA) according to the manufacturer's instructions and the assay was measured at 590 – 750 nm with the Asys Expert Plus (Biochrom, UK) or the Infinite M1000 (Tecan, Switzerland) microplate reader. Typically, 10 – 30 µg of protein lysate was denatured in NuPAGE 4X LDS Sample Buffer (Thermo Fisher Scientific, USA), together with 50 mM DTT (Sigma-Aldrich, USA) by heating at 70°C for 10 minutes.

2.4.2 SDS-PAGE and Western blotting

Protein samples were resolved on NuPAGE 4 – 12% Bis-Tris Protein gels (Thermo Fisher Scientific, USA) in 1X NuPAGE MOPS SDS Running Buffer (Thermo Fisher Scientific, USA). The iBlot Gel Transfer system (Thermo Fisher Scientific, USA) was used to transfer protein on to a nitrocellulose membrane. Membranes were blocked in 5% (w/v) dried skimmed milk (Marvel, UK) or 5% (w/v) bovine serum albumin (BSA) dissolved in tris-buffered saline and 0.1% (v/v) Tween-20 (Sigma-Aldrich) (TBST) at RT for 1 hour. Membranes were then probed with appropriate primary antibodies diluted in TBST containing 5% (w/v) BSA or 5% (w/v) dried skimmed milk at 4°C for 16 hours. After three washes in TBST, membranes were incubated with horseradish peroxidase (HRP)-linked IgG antibody (Cells Signalling Technology, USA) in TBST containing 5% (w/v) BSA or 5% (w/v) dried skimmed milk at RT for 1 hour for chemiluminescent detection. After a final TBST washing step, blots were visualised with Immobilon Western Chemiluminescent HRP Substrate (Merck, USA) using ImageQuant LAS 4000 (GE Healthcare, USA). Antibodies used for Western blotting are summarised in Appendix 5.

2.4.3 Densitometry analysis

Levels of protein expression in immunoblots was quantified by densitometry. The intensity of a specific protein band was quantified using ImageQuant TL 8.2 image analysis software (GE Healthcare, USA), according to the manufacturer's manual, and normalised with an internal loading control.

2.5 Fluorescence assays

2.5.1 Fluorescent staining

Cells were seeded onto 13 mm coverslips in a 12-well tissue culture plate and either transfected or differentiated as described in 2.2.4 and 2.2.3, respectively. At the time of harvest, cells were washed twice with PBS (CIMR, UK) before being fixed with 4% formaldehyde (Polysciences, USA) for 15 minutes at RT.

For direct fluorescent imaging of green fluorescent protein (GFP) or yellow fluorescent protein (YFP)-tagged protein, cells were incubated with HCS LipidTOX Deep Red Neutral Lipid Stain (Thermo Fisher Scientific, USA) in PBS at a dilution of 1:1000 for 1 hour to stain lipid droplets. For immunostaining of PLIN1, cells were permeabilised with 0.5% (v/v) Triton-X100 (Sigma-Aldrich, USA) for 10 minutes at RT and washed three times in PBS. Cells were blocked for 1 hour at RT in blocking buffer (3% (w/v) BSA and 0.05% (v/v) Tween-20 in PBS) followed by incubation with primary antibody diluted in blocking buffer for 16 hours at 4°C. The cells were then washed four times with washing buffer (0.1% (w/v) BSA and 0.05% (v/v) Tween-20 in PBS), followed by 1 hour incubation with Alexa Fluro secondary antibody (Thermo Fisher Scientific, USA) which was diluted at 1:1000 in PBS containing 1% (w/v) BSA and 0.05% Tween-20. In order to stain lipid droplets, cells were finally stained with 0.5% (v/v) HCS LipidTOX Deep Red Neutral Lipid Stain in PBS for 1 hour at RT.

All cells were rinsed three times with PBS after lipid droplet staining, and the coverslips were mounted on glass slides using approximately 10 µl ProLong Gold or Diamond Antifade Mountant (or with DAPI) (Thermo Fisher Scientific, USA) and allowed to cure overnight at RT before confocal microscopy. Antibodies and fluorescent dyes used for fluorescent staining are summarised in Appendix 5.

2.5.2 Bimolecular fluorescence complementation (BiFC)

BiFC is a method based on the reconstitution of a fluorescent protein by bringing its non-fluorescent fragments into close proximity, thus enabling it to emit a fluorescent signal (*436*). This association is facilitated by the interaction between the proteins that are fused to these fragments, which allows a direct visualisation of protein-protein interactions in intact cells (*437*). BiFC has been used with a wide range of proteins in many cell types and organisms (*437*). In this particular study, YFP has been split into N-terminal (Yn) and C-terminal (Yc) fragments, and fused with HSL and myc-tagged PLIN1, respectively (Figure 2.1) (*438*).

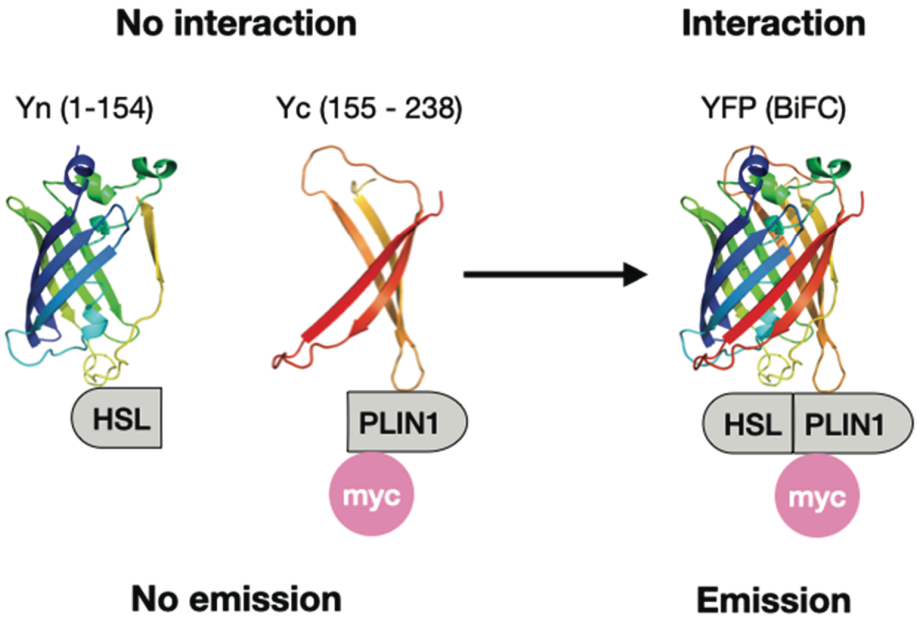

Figure 2.1 Schematic diagram of BiFC. The N-terminal (Yn) and C-terminal (Yc) of YFP (PDB: 1YFP) (*433*) are fused to HSL and myc-PLIN1, respectively. The interaction between HSL and PLIN1 allows the formation of a biomolecular fluorescent complex. The cartoon representation was generated by PyMOL.

3T3-L1 preadipocytes were seeded on coverslips in 12-well tissue culture plate and co-transfected with 500 ng DNA of each plasmid transiently, as described in 2.2.4. Cells were loaded with 400 µM BSA-conjugated oleic acid (Sigma-Aldrich, USA) 4 hours post transfection and incubated for 20 hours at 32°C in a humidified incubator. The medium was replaced with growth medium and stimulated in the absence or presence of 10 µM isoproterenol and 250 µM IBMX for 2 hours in a 30°C to stabilise the protein-protein interaction.

Immunofluorescence staining was performed as describe above in 2.5.1 and confocal imaging was performed as described below in 2.6.

2.6 Confocal microscopy

All images were acquired using a Leica TCS SP8 confocal laser scanning microscope (Germany) with a 63X immersion oil objective lens with a numerical aperture (NA) of 1.4. Sequential scan method was used to acquire images. In general, DAPI or Alexa Fluor 405 secondary antibody

for myc-tagged protein used in the BiFC experiment was excited at 405 nm and emission was detected between 420 and 460 nm. Fluorescent signals for GFP or Alexa Fluor 488 secondary antibody for myc-tagged protein was excited at 488 nm with emission between 490 and 530 nm. As for YFP or BiFC detection, signals were visualised using 514 nm excitation and 520 – 545 nm was used for emission. LipidTOX Deep Red was excited at 633 nm and emission was detected between 640 – 680 nm. 3D z-stack images were acquired at 0.4 µm intervals.

2.7 Image processing and analysis

Confocal images were analysed using Imaris x64 9.2.1 software (Bitplane, Switzerland).

For protein-protein interaction study using BiFC, an average of 16 images were taken randomly from each group and used to quantify BiFC (yellow fluorescence) and myc intensity. The threshold of fluorescence detection was automatically adjusted according to the absolute intensity of each channel. Yellow fluorescence or myc intensity above background was measured using surface module. Total intensity of yellow fluorescence was normalised to total myc intensity.

3D images were used for lipid droplets size measurement in preadipocytes. Lipid droplets were identified by LipidTOX Deep Red staining as described in 5.3.10. The threshold of lipid droplets was determined according to the absolute intensity of the red pixels. The volume of lipid droplets was measured using the spot module.

2.8 Dual-luciferase reporter assay

HEK293 cells were transfected as described in 2.2.4. Transfected cells were starved in serum-free DMEM for 24 hours after 24 hours of transfection, followed by another 24 hours of stimulation by ligand. Cells were then lysed using active lysis procedure, followed by standard protocol outlined by Dual-luciferase reporter assay system provided by Promega (USA).

2.9 Lipolysis assay

2.9.1 Cell treatment

Differentiated 3T3-L1 adipocytes were washed once with pre-warmed DPBS and serum starved with serum-free DMEM medium supplemented with 0.5% (v/v) BSA for 2 hours at 37°C. Cells were then washed once with pre-warmed Krebs-Ringer buffer (KRB), which was consisted of 118.5 mM NaCl, 4.75 mM KCl, 1.92 mM $CaCl_2$, 1.19 mM KH_2PO_4, 1.19 mM $MgSO_4(H_2O)_7$, 25 mM $NaHCO_3$, 10 mM HEPES and 6 mM Glucose with a pH of 7.4, followed by incubation with either basal or lipolytic medium for 3 hours at 37°C. Basal medium was made of KRB containing 4% (w/v) fatty acid free BSA and 6 µM Triacsin C (Enzo Life Sciences, UK), whilst lipolytic medium also contained 10 µM isoproterenol (Sigma-Aldrich, USA).

Differentiated MEF adipocytes were washed once in pre-warmed DPBS and starved with serum-free DMEM medium in the presence of 0.5% (v/v) BSA for 4 hours at 37°C. Serum starved cells were washed once with pre-warmed DMEM without phenol red (Thermo Fisher Scientific, USA) and incubated with phenol red free DMEM supplemented with 4% (w/v) fatty acid free BSA and 6 µM Triacsin C in the absence (basal) or presence (lipolytic) of 10 µM isoproterenol and 250 µM IBMX for 2 hours at 37°C.

2.9.2 Glycerol release assay

The glycerol produced by TG hydrolysis can be measured by coupled enzyme reactions. First glycerol is phosphorylated by glycerol kinase to form glycerol-1-phosphate, which is then oxidised by glycerol phosphate oxidase to hydrogen peroxide (*439*). Peroxidase catalyses the coupling of hydrogen peroxide to produce a quinoneimine dye which shows an absorbance at 540 nm (*439*). After the lipolytic stimulation, the supernatant was collected and centrifuged at 1000 rpm for 5 minutes at 4°C to remove any cellular residues. Cleared medium was diluted and incubated with Free Glycerol Reagent (Sigma-Aldrich, USA) at RT for 15 minutes. Absorbance at 540 nm was measured and glycerol content was calculated using a Glycerol Standard Solution (Sigma-Aldrich, USA) which was served to generate a standard curve.

Meanwhile, cells were harvested for protein quantification assay and western blotting as described above in 2.4. Glycerol release was normalised to total protein amount or lipid content and then further normalised glycerol release from non-stimulated control cells.

2.10 Lipid accumulation quantification

2.10.1 AdipoRed assay

Intracellular lipid accumulation was determined by AdipoRed Assay Reagent (Lonza, Switzerland), according to the manufacturer's instructions. Differentiated 3T3-L1 cells were washed once in DPBS and incubated with 0.5 ml medium containing 3% (v/v) AdipoRed at 37°C for 10 minutes. Fluorescent images were taken using EVOS Cell Imaging System (Thermo Fisher Scientific, USA).

2.10.2 Oil Red O assay

Alternatively, quantification of intracellular lipid accumulation can be measured using Oil Red O assay. Oil Red O stock was prepared by mixing 1 g powder (Sigma-Aldrich, USA) in 400 ml 2-Propanol (Honeywell, Germany) and warming to 56°C for 1 hour, which can be stored at RT for up to a year. Differentiated MEFs were washed once with DPBS and fixed with 10% (v/v) formalin (Sigma-Aldrich, USA) for 1 hour at RT. Meanwhile, Oil Red O working solution was made by mixing 3:2 parts Oil Red O stock and ultrapure water and left to stand for 10 minutes before filtered through a 0.45 µm filter. Fixed cells were washed twice with DPBS and twice with 60% (v/v) 2-Propanol prior to staining with working solution of Oil Red O for 1 hour at RT. Stained cells were de-stained by washing 2 – 3 times with water and replaced with DPBS for imagining using Olympus CKX41 inverted microscope (Japan) connected with a DP20 digital camera (Olympus, Japan). When imaging the whole wells, DPBS was aspirated and images were taken using Epson V550 scanner (Japan). To quantitatively assess adipocyte differentiation, 2-Propanol was added to each well and cells were incubated at RT for 10 minutes on a rocker to elute the dye. Supernatant was then transferred to a 96-well microtiter

plate (Thermo Fisher Scientific, USA), and absorbance was measured at 510 nm on the Infinite M1000 PRO plate reader.

2.11 Statistical analysis

Data are presented as mean standard deviation (SD). Statistical analyses were performed using GraphPad Prism (GraphPad Software, USA). To compare a single parameter between two groups, unpaired two-tailed Student's t-test was used, unless stated otherwise. For comparison between more than two independent groups, analysis of variance (ANOVA) was used. When a significant difference was indicated by ANOVA, post-hoc test was performed for multiple comparisons. In all cases $p < 0.05$ was considered as statistically significant. Significance is shown on all figures with * denotes $p < 0.05$, ** $p < 0.01$, *** $p < 0.001$ and **** $p < 0.0001$, while ns indicates not significant.

3 Loss-of-function studies in 3T3-L1 adipocytes

3.1 Abstract

First a loss-of-function study was performed in 3T3-L1 (pre)adipocytes to evaluate the role of *Alk7*, *Calcrl*, *Plin1*, *Pde3b* and *Pnpla2* in adipocyte biology, including adipogenesis and lipolysis. Silencing of *Plin1* expression via siRNA delivery, partially impaired adipogenesis. Moreover, adipocytes with reduced *Plin1* were resistant to isoproterenol stimulated lipolysis. The depletion of *Pnpla2*, on the other hand, did not seem to affect lipid accumulation and severely attenuated lipolysis. The results varied in terms of adipogenesis when the expression of *Alk7* or *Calcrl* was reduced, but lipolysis was consistently decreased. Depletion of *Pde3b* did not have any impact on 3T3-L1 adipogenesis or lipolysis.

3.2 Introduction

In order to begin to understand how the variants identified by Lotta et al. might affect fat distribution, I performed siRNA mediated knockdown of *Alk7*, *Calcrl*, *Plin1*, *Pde3b* and *Pnpla2* in 3T3-L1 (pre)adipocytes (*1*). The impact of these perturbations on adipogenesis and lipolysis was then assessed.

3.2.1 The 3T3-L1 adipocyte differentiation model

The 3T3-L1 cell line is a widely used model for adipocyte differentiation that was originally derived from the Swiss mouse embryo fibroblast 3T3 line (*440*, *441*). When 3T3 fibroblasts become confluent, the cells undergo growth arrest by contact inhibition, and spontaneously accumulate TG to convert into adipocytes over a period of two to four weeks (*267*, *441*, *442*). Treatment with adipogenic agents such as glucocorticoids and cAMP elevating reagents in the presence of insulin can effectively achieve a complete conversion of 3T3-L1 cells to mature adipocytes within two weeks (*443*). The first step is to induce the commitment of cells to an adipogenic fate by adding a differentiation cocktail that contains dexamethasone, 3-isobutyl-

1-methylxanthine (IBMX) and insulin (*443*). As insulin binding activity rises, additional insulin administration facilitates adipocyte conversion by increasing glucose uptake (*442*, *443*). Differentiated 3T3-L1 adipocytes display similar gene expression profiles to white adipocytes and respond homogeneously to treatments such as siRNA or chemical compounds in experimental conditions, which make them the most commonly used *in vitro* model to study adipocyte biology (*444*).

3.2.2 Role of selected genes in adipocyte biology

In this section, I briefly summarise what is already 'known' about the role of each gene in adipose tissue and metabolism.

3.2.2.1 ALK7

ALK-7 and its type II receptor partner ACTR-IIB, together with the co-receptor CRIPTO, were initially reported to be involved in the transduction of Nodal signalling in mesendoderm formation during vertebrate development in *Xenopus laevis* embryos (*274*). Since then, many studies have focused on the roles of Nodal/ALK-7 signalling in cell survival and proliferation (*266*, *276*, *283*, *445*, *446*). In adipose tissue, ALK-7 was first established as a marker of adipocyte differentiation in 3T3-L1 cells, as well as in mouse primary SVF cells, especially during the late phase of differentiation (*267*). In differentiated adipocytes, activation of ALK-7 suppressed the expression of the master regulators of adipogenesis PPARγ and C/EBPα, which subsequently downregulated the transcription of lipases such as ATGL and HSL, thus reducing lipolysis (*447*, *448*). Furthermore, the inhibition of lipolysis by insulin was also reported to be mediated via the GDF-3/ALK-7 axis in adipose tissue (*270*). It was proposed that GDF-3 is produced and secreted by adipose tissue macrophages upon insulin administration, which also contributes to the activation of ALK-7, resulting in the inhibition of lipolysis and the accumulation of fat mass *in vivo* (*270*).

A list of genetically modified animal models generated to study the role of ALK-7 in maintaining whole body energy homeostasis, as well as cardiac function is presented in Table

3.1. In summary, mice lacking *Alk7*, globally or adipose tissue specifically, manifest enhanced β-AR mediated lipolysis and increased energy expenditure (*277*). In addition, these knockout mice were resistant to diet induce weight gain (*268*, *277*). It has been suggested that ALK-7 functions after food intake to promote excess fat storage in adipocytes by contributing to catecholamine resistance in the context of obesity (*277*, *449*). Although the association of ALK-7 loss-of-function variant with BMI has not been reported in human genetic studies, inhibition of ALK-7 function demonstrated increased energy expenditure based on mouse models (*277*). Therefore, suppression of ALK-7 signalling may be a potential therapy for obesity. Pancreatic islets from *Alk7* knockout mice showed enhanced insulin secretion under sustained glucose simulation, suggesting that ALK-7 may also function as a negative regulator of insulin release (*280*). However, mice lacking *Alk7* globally developed an age-dependent syndrome including liver steatosis, insulin resistance and glucose intolerance (*280*). On the other hand, normal glucose and insulin responses were observed in adipose-specific *Alk7* knockout mice (*277*). A human cohort study indicated that an intronic SNP rs13010956 in the *ALK7* gene had a significant association with metabolic syndrome risk in females and might also be involved in cardiovascular remodelling (*450*). Similar to findings by Lotta et al, recent studies have also showed that the same coding variants in *ALK7* (p.I195T and p.N150H), among others, are associated with a reduced WHR and a lower risk of T2D (*1*, *18*, *451*). Functional characterisation of these variants will be described in the next chapter.

Table 3.1 Overview of genetic animal models of *Alk7*.

Genetic manipulation	Phenotypes compared to WT (unless otherwise stated)	References
Alk7$^{-/-}$ mice	- Normal weight gain and fasting levels of glucose and glucagon - Hyperinsulinemia, reduced insulin sensitivity and glucose intolerance; increased β-cell mass and islet size with aging; higher insulin secretion level upon constant stimulation of high glucose - Liver steatosis - Reduced lipid droplet size in interscapular BAT - Longer ventricular repolarization, more susceptible to ventricular arrhythmia	(*268*, *279*, *280*, *452*)
Alk7$^{-/-}$ mice on HFD	- Normal food intake, reduced weight gain and body fat content, reduced epididymal fat pads with smaller adipocytes - Reduced adipose tissue inflammation - Increased energy expenditure, enhanced mitochondrial biogenesis and FA oxidation, elevated lipolysis	(*268*, *277*)
T.B-*Nidd5/3* mice (obese mice carrying a nonsense mutation in the *Alk7* kinase domain)	compared to Tsumura Suzuki Obese Diabetes (TSOD) mice - Lower body weight, smaller adipocyte size - Increased FA uptake and TG synthesis - Elevated lipolysis, increased energy expenditure - Improved glucose tolerance and insulin sensitivity	(*448*)
Alk7$^{fx/fx}$*::Ap2*^{CRE} mice on HFD (adipose tissue-specific)	- Resistant to diet-induced weight gain, reduced fat mass and adipocyte size - Normal insulin and glucose responses - Reduced adipose tissue inflammation - Increased energy expenditure, enhanced mitochondria biogenesis and FA oxidation, elevated lipolysis	(*277*)
Alk7$^{flox/flox}$::*AdipoQ*^{CreERT2} (tamoxifen inducible Cre) on HFD	- Small increase in body weight, reduced WAT mass - Improved glucose tolerance - Increased energy expenditure	(*449*)

Table 3.1 Overview of genetic animal models of *Alk7* (continued).

Genetic manipulation	Phenotypes compared to WT (unless otherwise stated)	References
Alk7$^{flox/flox}$::*AdipoQ*^{CreERT2} (tamoxifen inducible Cre) with diet switch (from HFD to CD)	- Rapid weight loss, further reduction in WAT mass, smaller LD size in WAT - Reduced AT apoptosis - Improved glucose tolerance - Increased energy expenditure, elevated lipolysis - Reduced AT inflammation	(*449*)
Alk7$^{flox/flox}$::*AdipoQ*^{CreERT2} (tamoxifen inducible Cre) with double diet switch (from HFD to CD, and back to HFD)	- Slower weight gain, slightly less food intake, maintained reduced WAT mass - Reduced insulin sensitivity and glucose tolerance	(*449*)
Ucp1^{CRE}:*Alk7*$^{fx/fx}$ mice (BAT-specific)	- Normal food intake, body weight and body fat composition, reduced LD size in interscapular BAT - Regular energy expenditure - Normal insulin sensitivity - Hypothermia upon fasting	(*279*)
Alk7$^{-/-}$ mice with aortic banding (AB) surgery	- Greater deterioration of cardiac hypertrophy, cardiac dilation and dysfunction	(*281*)
Cardiac-specific *Alk7*-transgentic mice with AB surgery	- Alleviated AB-induced cardiac hypertrophy, cardiac dilation and dysfunction	(*281*)
Type 2 diabetic rats injected with *Alk7* shRNA	compared to diabetic rats - Increased food intake, normal body weight - Reduced aortic stiffness - Improved insulin sensitivity and hyperlipidaemia	(*453*)
RIP1-Tag2 (RT2);Alk7^{tm1b} mice (*Alk7* was inactivated)	compared to RT2/B6 mice - Increased tumour burden and liver metastasis - Reduced apoptosis at early tumorigenesis	(*284*)

3.2.2.2 CALCRL

Prior work has focused on understanding the metabolic role of calcitonin family members in adipose tissue, but much less work has been done on their receptors, such as CALCRL (*328*, *329*, *454*, *455*). Adrenomedullin (ADM), which is known to bind and signal through CALCRL, has been proposed to be an anti-adipogenic factor since depletion of ADM results in enhanced differentiation *in vitro* (*456*). ADM also functions as an autocrine/paracrine factor in adipose tissue, although the effect of CALCRL mediated ADM signalling pathways in the regulation of adipocyte differentiation and lipid metabolism is controversial (*98*, *314*, *322*). In differentiated 3T3-F442A cells, ADM exposure inhibited β-adrenergic stimulated lipolysis via a NO-dependent mechanism, which can be explained by NO-induced oxidation of the β-agonist isoproterenol (*314*). In contrast, increased lipolysis was observed in differentiated rat adipocytes treated with ADM in a dose-dependent manner (*322*). ADM enhanced isoproterenol stimulated lipolysis, possibly via PKA-mediated HSL activation and translocation, along with increased ERK phosphorylation which leads to elevated HSL phosphorylation and activity (*322*). ADM has also been reported to enhance glucose uptake through the PI3K/PKB pathway *in vitro* (*322*). Further work is required to confirm and reconcile these data.

As listed in Table 3.2, studies of *Calcrl* KO mice focused on embryonic and vascular development (*457–460*). Homozygous *Calcrl* knockout mice died at midgestation, suggesting that *Calcrl* is essential for survival (*457*). Studies in rat adipose tissue have shown upregulation of *Calcrl* mRNA in response to HFD feeding in VAT, suggesting a functional association of CALCRL mediated signalling pathways and weight gain (*461*). However, the exact role of CALCRL in adipocyte biology is still largely unknown.

Table 3.2 Overview of genetic mouse models of *Calcrl*.

Genetic manipulation	Phenotypes compared to WT (unless otherwise stated)	References
Calcrl$^{-/-}$	- Embryos failed to survive by mid-gestation - Hydrops fetalis - Cardiovascular defects	(*457*, *458*)
Calcrl$^{LoxP/-}$*Tie2Cre*$^{+}$ (heterozygotes lacking *Calcrl* specifically in endothelial cells)	- Delayed embryonic lethality compared to *Calcrl*$^{-/-}$ mice - Interstitial oedema - Embryonic lymphedema, reduced lymphatic endothelial cell proliferation	(*458*)
Calcrl$^{fl/fl}$*/CAGGCre-ER*^{TM} (temporal *Calcrl*$^{-/-}$ in adult mice)	- Lymphatic insufficiency in multiple organs	(*459*)
Calcrl$^{fl/fl}$*/CAGGCre-ER*^{TM} (temporal *Calcrl*$^{-/-}$ in adult mice) on western diet	- Reduced body weight and impaired intestinal lipid absorption	(*459*)
Calcrl$^{fl/fl}$*/Prox1-CreER*^{T2} (lymphatic endothelium-specific)	- Intestinal lymphangiectasia, systematic lymphatic insufficiency	(*460*)

Abnormal circulating levels of CALCRL ligands, such as CGRP and ADM, have been observed in obese and diabetic patients (*462–469*). Interestingly, ADM concentrations in the blood and the mRNA expression of *CALCRL*, together with receptor activity-modifying proteins *RAMP2* and *RAMP3*, were reported to be significantly elevated in omental adipose tissue from pregnant women with gestational diabetes mellitus compared with those with normal glucose tolerance with similar BMI, in response to excessive ADM production, suggesting a possible role for CALCRL mediated ADM signalling in the development of insulin resistance (*468*). Gene expression analysis in VAT isolated from prepubertal children demonstrates that *CALCRL* expression is downregulated in obese children (*470*). Collectively, these findings hint at biologically meaningful actions of CALCRL in adipose tissue.

Another variant in the regulatory region of the *CALCRL* locus (rs1569135) was identified in a GWAS meta-analysis of WHR adjusted for BMI (*238*, *471*). Moreover, expression of *CALCRL* in isolated abdominal SAT correlated with adipocyte hyperplasia, suggesting that *Calcrl* may influence the size and number of adipocytes in WAT, which could then alter fat distribution

(*472*). The site of the rare missense mutation L87 is not conserved but is located at the tip of a β-strand close to strictly conserved residues C88 and C127 in the extracellular domain where CALCRL interacts with RAMPs for ligand binding (Figure 3.1) (*1*, *254*, *473*). The intramolecular disulphide bond created by C88 and C127 stabilises the β-strand which is in close contact with RAMP2 (*1*, *300*). The mutation p.L87P might partially destabilise the β-strand, potentially resulting in disrupted interaction with RAMPs, thus affecting ligand binding and downstream signalling (*1*).

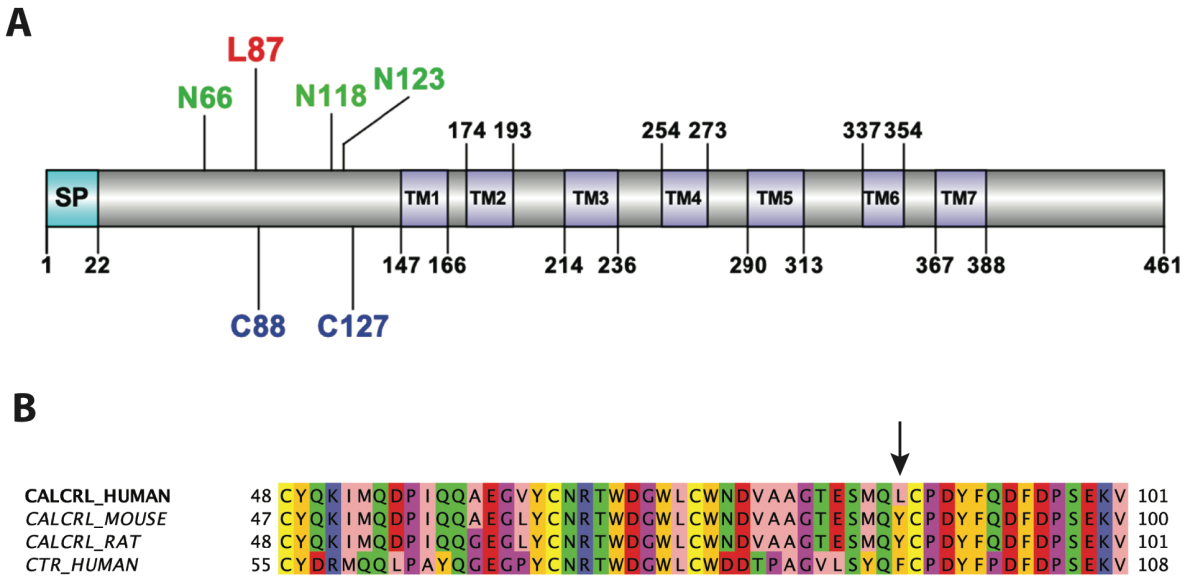

Figure 3.1 Location of the human CALCRL p.L87P variant. (A) Domain structure of human CALCRL. Human CALCRL consists of 461 amino acid residues. The signal peptide (SP) and seven transmembrane domains (TMs) are illustrated. There are three putative sites for glycosylation, N66, N118 and N123, which are labelled in green. The mutant site at residue 87 is labelled in red. Two cysteine residues, C88 and C127, participating in a disulphide bond are also indicated. (B) Sequence alignment of a CALCRL segment from representative species and the calcitonin receptor. The site of the mutated residue is indicated by an arrow. The domain structure was generated by GPS (*249*), and the sequence alignment was generated using Jalview (*468*).

3.2.2.3 PLIN1

PLIN1 is located on the surface of LDs in adipocytes as well as steroidogenic cells (*336*, *474*, *475*). The mRNA of *Plin1* is undetectable in 3T3-L1 preadipocytes, but markedly induced upon

differentiation (*474*). The master regulator of adipocyte differentiation PPARγ, especially PPARγ2, has been shown to regulate the expression of PLIN1 (*474*). PPARγ dependent PLIN1 expression is activated by the constitutive coactivator of PPARγ (CCPG) but blocked by tribbles homologue 3 (TRB-3) (*476*, *477*). *PLIN1* is also a target gene of estrogen-related receptor α (ERRα, or NR3B1 short for nuclear receptor subfamily 3 group B member 1), which is activated by PPARγ coactivator-1α (PGC-1α) (*475*). Reduction of PLIN1 expression was observed when 3T3-L1 adipocytes were treated with TNF-α, which partially contributes to TNF-α induced TG lipolysis (*478*, *479*). Under physiological conditions such as obesity, macrophages within WAT release TNF-α to suppress the expression of PLIN1 and increase the release of FFAs which ultimately contributes to systemic lipotoxicity (*185*, *480*).

As described in Chapter 1, PLIN1 functions as a scaffolding protein on the surface of LDs to regulate the access of lipases to substrates. The role of PLIN1 in adipose tissue metabolism has been investigated by deletion or overexpression in mice, as summarised in Table 3.3. As expected, ablation of *Plin1* led to increased basal and decreased stimulated lipolysis in adipocytes and these mice were protected from diet induced obesity (*358*, *359*). Surprisingly, overexpression of *Plin1* specifically in adipose tissue also resulted in mice being resistant to diet induced obesity, increased FA oxidation and elevated whole-body energy expenditure (*357*, *481*). Further investigation has indicated that the observed phenotype in *Plin1* transgenic mice might be due to the induction of a BAT-like phenotype in WAT caused by decreased expression of FSP27 (*357*).

Table 3.3 Overview of genetic mouse models of *Plin1*.

Genetic manipulation	Phenotypes compared to WT (unless otherwise stated)	References
Plin1$^{-/-}$	- Higher food intake but maintained normal body weight, less body fat and smaller adipocyte size - Elevated basal lipolysis and impaired stimulated lipolysis, higher metabolic rate, increased β-oxidation - Glucose intolerance and insulin resistance with aging - Developed cardiac hypertrophy and failure - Increased adipose tissue macrophages and inflammation	(*358*, *359*, *482–486*)
Plin1$^{-/-}$ on HFD	- Resistant to diet-induced obesity - Increased oxygen consumption	(*358*, *359*)
Lepr$^{db/db}$*/Plin1*$^{-/-}$	compared to *Lepr*$^{db/db}$*/Plin*$^{+/+}$ mice - Reversed obesity - Increased metabolic rate	(*358*)
PLIN1 or *Plin1* Tg (adipose-specific overexpression of human or mouse PLIN1)	- Normal body weight - Impaired stimulated lipolysis	(*357*, *481*)
PLIN1 or *Plin1* Tg (adipose-specific overexpression of human or mouse PLIN1) on HFD	- Reduced fat mass and body weight, reduced adipocyte size; normal food intake - Increased energy expenditure, BAT-like WAT - Decreased lipolysis - Improved glucose tolerance	(*357*, *481*)

Only a limited number of studies have reported a potential association of *PLIN1* expression with obesity in humans, the findings are however not conclusive (*487–489*). One study showed that the expression of perilipin-1 from abdominal SAT, at both mRNA and protein levels, was positively correlated with obesity, defined by percentage body fat (*488*). In contrast, other studies have reported a decrease in PLIN1 expression in abdominal SAT in obese compared to non-obese subjects (*123*, *487*, *489*). In fact, some depot and gender specific variations in PLIN1 expression have been observed in obese subjects (*487*). For example, abdominal subcutaneous *PLIN1* mRNA expression was higher than in omental AT in

obese subjects, and the protein level was higher in obese male subjects compared to obese women (*487*). A study investigating regional differences in the expression and subcellular distribution of PLIN1 in females revealed a reduced expression in obese versus lean subjects, and in abdominal subcutaneous versus omental AT in women with obesity, but significantly more PLIN1 was localised in the lipid fraction in obese versus lean subjects (*123*). PLIN1 expression also negatively correlates with average adipocyte volume and basal lipolytic rate (*123*). Additionally, the expression of PLIN1 in adipose tissue, both omental and SAT, from obese subjects matched for BMI correlates positively with insulin sensitivity (*490*). Recent studies also found a decrease in the expression of the *PLIN1* gene under the regulation of circulating microRNAs (miRNAs), particularly miR-642b, in obese children (*491*). Despite the conflicting findings, these studies support the idea that there is some relationship between the expression or distribution of PLIN1 and the obese phenotype (*492*).

FPLD4, an autosomal dominant form of lipodystrophy, is associated with specific mutations in the *PLIN1* gene (*493*). However, only a few SNPs in the *PLIN1* locus, including both intronic and exonic variants, have been identified to be associated with metabolic syndrome risk in humans (*494–500*). It is noteworthy that the association of some variants shows a gender difference and not all alleles are polymorphic in all populations (*492*). Therefore, identification of causal PLIN1 variants that alter metabolic outcomes remains a challenge (*492*).

3.2.2.4 PDE3B

PDE3B is the dominant isoform of phosphodiesterase in adipocytes that mediates the anti-lipolytic action of insulin. Studies of *Pde3b* gene regulation have shown that its promoter activity and mRNA expression are both increased upon differentiation in 3T3-L1 cells (*501*, *502*). It appears that the expression of PDE3B requires PPARγ in mice (*503*). Additionally, studies have shown that the transcriptional regulation of *Pde3b* expression is controlled by CREB during 3T3-L1 differentiation (*504*). However, TNF-α treatment in 3T3-L1 adipocytes was found to downregulate PDE3B expression (*502*). Indeed TNF-α expression was found to be higher in obese subjects and to be involved in the development of insulin resistance (*505*,

506). TNF-α can stimulate lipolysis by activating the MAPK-ERK pathway to downregulate PDE3B expression, resulting in an elevation of cAMP levels and the activation of PKA in human adipocytes (*507*).

Many approaches have been utilised to study the role of PDE3B in maintaining whole-body energy homeostasis *in vivo* and *in vitro*. These methods include studies of genetically modified mice and cellular models for functional characterisation in response to insulin and adrenergic stimulation. As shown in Table 3.4, global KO of *Pde3b* in mice resulted in complex metabolic profiles, both beneficial and non-beneficial (*377*, *384*, *398*, *508*). Compared to WT counterparts, these mice were protected from diet induced weight gain with smaller WAT mass and decreased adipose tissue inflammation (*377*, *398*, *509*). As mentioned in Chapter 1, a WAT beiging phenotype was also observed in *Pde3b* KO mice, accompanied by increased mitochondrial biogenesis and energy dissipation (*398*). Non-beneficial alterations noted in *Pde3b* KO mice include increased TG content in the liver and signs of insulin resistance indicated by the reduced ability of insulin to lower glucose levels (*509*).

Table 3.4 Overview of genetic mouse models of *Pde3b*.

Genetic manipulation	Phenotypes compared to WT (unless otherwise stated)	References
Pde3b$^{-/-}$	- Smaller adipocyte size - Increased TG content in liver - Increased stimulated lipolysis, elevated mitochondrial biogenesis, increased metabolic rate - Insulin resistance - Protected from ischemia-reperfusion injury - Decreased adipose tissue inflammation	(*377*, *384*, *398*, *509*)
Pde3b$^{-/-}$ on HFD	- Reduced adipose tissue inflammation and macrophages - Less weight gain, reduced WAT mass - Improved glucose tolerance - WAT browning	(*377*, *398*)
apoE$^{-/-}$*/Pde3b*$^{-/-}$ *Ldlr*$^{-/-}$*/Pde3b*$^{-/-}$	compared to *apoE*$^{-/-}$ or *Ldlr*$^{-/-}$ mice - Reduced plaque formation in aorta	(*377*)
Pde3b$^{-/-}$ treated *with* β3-adrenergic agonist	- Reduced body weight and epididymal WAT (EWAT), smaller adipocyte size - Increased mitochondrial biogenesis, higher oxygen consumption, elevated lipid oxidation - BAT-like EWAT	(*398*, *510*)
RIP (rat insulin promoter)-*Pde3b* Tg (pancreatic β-cell-specific overexpression)	- Impaired insulin secretion and glucose tolerance - Enlarged islets	(*511*)

In a high throughput siRNA screen, in primary human adipocytes differentiated from preadipocytes, to identify new genes affecting adipogenesis and/or fat storage, *PDE3B* was highlighted as one of the hits that increased lipid accumulation (*512*). Consistent with Lotta et al.'s findings, a study investigating predicted loss-of-function variants has reported that carriers with the same PDE3B variant (p.R783X) manifest reduced coronary artery disease risk (*1*, *513*). As illustrated in Figure 3.2, the R783 residue is located in a 44-aa insertion, which is unique in the PDE3 family. This nonsense variant generates a premature truncation in the catalytic domain and is thus strongly predicted to exhibit a loss of function (Figure 3.2) (*1*).

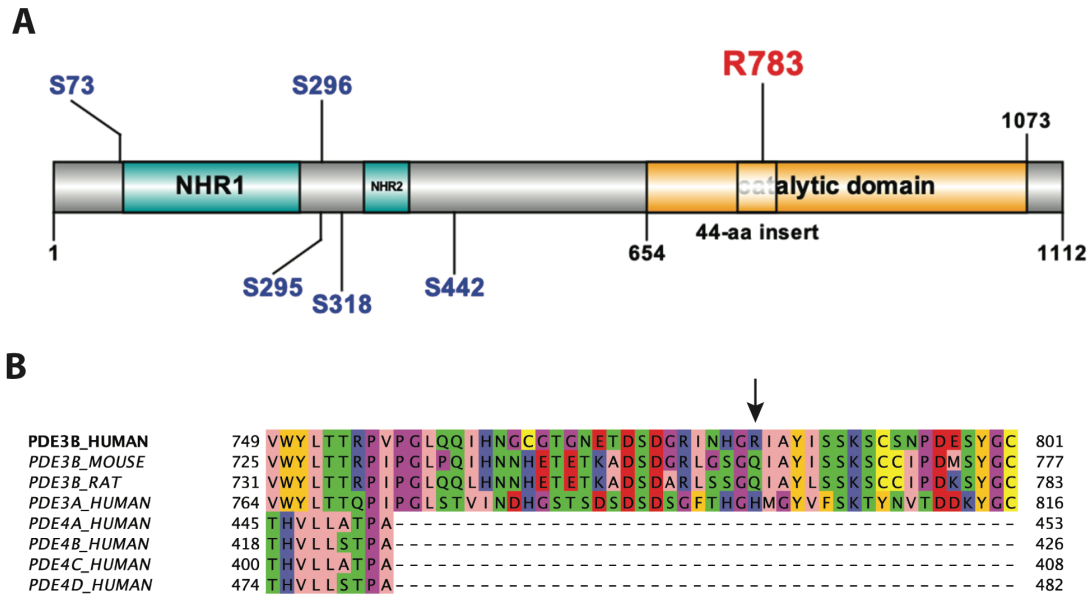

Figure 3.2 Location of the human PDE3B p.R783X variant. (A) Domain graph of human PDE3B. Human PDE3B has 1112 residues. The two N-terminal hydrophobic regions (NHRs) and a catalytic domain at the C terminus are presented. Five putative phosphorylation sites at positions 73, 295, 296, 318 and 442 are labelled. The variant site is located in the 44-aa insert and labelled in red. (B) Sequence alignment of PDE3B segments from selected species, human PDE3A and PDE4 isoforms. The arrow indicates the mutated site R783. Domain graph was generated by GPS (*249*), sequence alignment was performed with Jalview (*468*).

3.2.2.5 PNPLA2

Various studies have been conducted to demonstrate the important role that ATGL plays in the regulation of LD turnover in mammalian cells, in both adipocytes and non-adipocyte cells (*403*). In adipose tissue, ATGL is the rate-limiting enzyme that catalyses the first step of TG hydrolysis, which comprises three sequential enzymatic reactions releasing one FA at each step, along with the production of DG, MG and glycerol (*410*).

The regulation of ATGL expression and enzyme activity on both transcriptional and post-transcriptional levels has been studied by a number of groups. It has been shown that *Pnpla2* is a target for transcriptional activation by PPARγ and both mRNA and protein expression of ATGL was increased by PPARγ agonists but inhibited by a PPARγ antagonist (*514*, *515*). In addition, at least two forkhead box protein O1 (FOXO1) binding sites were found in the promoter region of *Pnpla2*, indicating that the transcription of the *Pnpla2* gene is directly regulated by FOXO1 (*516*). This regulatory effect was further enhanced by NAD-dependent

protein deacetylase sirtuin-1 (SIRT1), which deacetylates and activates FOXO1 (*517*). The mRNA level of *Pnpla2* in mouse WAT was induced by fasting and downregulated upon refeeding (*405*). Increased *Pnpla2* expression was also observed in 3T3-L1 adipocytes in response to glucocorticoids, whereas isoproterenol, TNF-α, insulin and mammalian target of rapamycin complex 1 (mTORC1) decrease its expression (*405*, *514*, *516*, *518*, *519*).

However, the mRNA level of *PNPLA2* does not always correlate with its lipase activity. For example, both isoproterenol and TNF-α stimulate lipolysis whilst suppressing the expression of ATGL (*518*). The discrepancy between enzyme expression and activity can be explained by post-translational regulation (*99*). As mentioned in Chapter 1, ATGL is post-translationally modified by phosphorylation at several putative phosphorylation sites either by PKA or AMPK to increase its activity (*114*, *421*, *422*). ATGL activity is also regulated through protein-protein interaction with its co-activator ABHD5, or inhibitors G0S2 and HILPA. Furthermore, as a negative feedback mechanism, lipid intermediates generated during lipolysis such as long-chain acyl-coenzyme A inhibit ATGL activity in order to protect cells from lipotoxicity (*520*).

As indicated in Table 3.5, numerous genetically modified mouse models, either by genetic knockout or transgenic overexpression, have been generated to study the pathophysiological role of ATGL in a variety of tissues over the past 15 years. In general, systemic and adipocyte specific ATGL KO mice manifest improved glucose homeostasis. However, the contribution of ATGL to adipocyte lipolysis and whole-body energy homeostasis in humans is not as clear as in rodents (*431*). Genetic association studies showed a trend of decreased plasma FFA concentrations in rare *PNPLA2* variants carriers, but the effect was not significant (*521*). Even so the effect towards lower FFA levels was most pronounced in the p.N252K group, which is consistent with a haplotype analysis elucidating a significant association between SNPs of *PNPLA2* and levels of FFAs (*521*, *522*). Functional predication and validation of this variant will be described in the next chapter.

Table 3.5 Overview of genetic mouse models of *Pnpla2*.

Genetic manipulation	Phenotypes compared to WT (unless otherwise stated)	References
Pnpla2$^{-/-}$	- Increased body weight and fat mass, higher TG content in multiple tissues - Diminished stimulated lipolysis, reduced energy expenditure - Improved glucose tolerance and insulin sensitivity - Reduced FA mobility during exercise - Impaired cardiac function - Hypothermia - BAT hypertrophy and hyperplasia, normal BAT mitochondrial function	(*523–528*)
Pnpla2$^{-/-}$ on HFD	- Early mortality - Resistant to diet induced obesity, reduced WAT mass	(*432*)
C57/B16 injected with *Pnpla2* shRNA	- Normal body weight and fat mass - Increased liver weight, liver steatosis - Decreased FA oxidation	(*423*)
C57/B16 injected with *Pnpla2* shRNA on HFD	- Normal body weight, reduced gonadal fat mass - Increased liver weight, liver steatosis	(*423*)
AAKO (Adipose-specific *Pnpla2*$^{-/-}$)	- Increased body weight and fat mass - Decreased lipolysis and lipid oxidation, reduced oxygen consumption and energy expenditure - Hypothermia - Improved hepatic insulin sensitivity, smaller liver and less hepatic TG content - BAT hypertrophy	(*422*, *528–530*)
AAKO (Adipose-specific) on HFD	- Increased body weight and fat mass, increased adipocyte size - Decreased lipolysis and lipid oxidation - BAT hypertrophy - Smaller liver and less hepatic TG content, reduced liver inflammation	(*422*, *530*)
ATGLLKO (liver-specific)	- Increased liver mass with higher TG content, developed progressive hepatic steatosis, decreased liver FA oxidation, increased number of lipolysosomes - Lipid droplet accumulation in cholangiocytes	(*531*)
β-*Atgl*-KO (β-cell specific)	- Normal food intake and body weight - Impaired glucose-stimulated insulin secretion, reduced insulinaemia	(*532*, *533*)

Table 3.5 Overview of genetic mouse models of *Pnpla2* (continued).

Genetic manipulation	Phenotypes compared to WT (unless otherwise stated)	References
β-*Atgl*-KO (β-cell specific) on HFD	- Reduced insulinaemia, glycaemia, enhanced insulin sensitivity - Enlarged islet size, increased islet TG accumulation - Reduced lipolysis decreased mitochondrial oxidation - Reduced body weight gain and fat mass; increased energy expenditure	(*532*, *533*)
Pnpla2$^{-/-}$ on methionine-choline-deficient diet	- More severe liver steatosis - Reduced WAT loss - Reduced non-HSL hydrolase activity	(*534*)
Pnpla2$^{-/-}$ injected with lipopolysaccharide	- Increased liver inflammation - Higher mortality - Hypothermia	(*534*)
ATGL-ko/CM (*Pnpla2*$^{-/-}$ in all tissues except cardiac muscle)	compared to *Pnpla2*$^{-/-}$ mice - No TG accumulation in cardiac muscle - Reduced FA mobilisation during exercise	(*527*)
ic*Atgl*KO (cardiomyocyte-specific)	- Increased cardiac TG content, myocardial interstitial fibrosis, heart hypertrophy and dysfunction, reduced myocardial FA oxidation - Impaired ATP synthesis on mitochondrial function	(*424*)
SMAKO (skeletal muscle-specific)	- Increased intramyocellular TG accumulation - Normal body weight, fat mass and muscle weight - Normal food intake, energy expenditure and FA oxidation - Unaffected mitochondrial morphology and insulin response	(*535*)
iBAKO (BAT-specific)	- Normal body weight - BAT hypertrophy and hyperplasia.	(*528*)
ATGLiKO (intestine-specific)	- Normal body weight and food intake - Increased TG accumulation in small intestines, higher faecal fat weight - Decreased FA oxidation - Delayed cholesterol absorption	(*536*)

Table 3.5 Overview of genetic mouse models of *Pnpla2* (continued).

Genetic manipulation	Phenotypes compared to WT (unless otherwise stated)	References
Ob/ob with *Pnpla2* overexpression	- Normal body weight - Reduced hepatic TG content and FFA - Increased FA oxidation	(*537*)
aP2-Pnpla2 Tg (adipose-specific overexpression)	- Normal body weight and fat mass - Increased lipolysis, elevated energy expenditure	(*538*)
aP2-Pnpla2 Tg (adipose-specific overexpression) on HFD	- Leaner, resistant to diet-induced obesity, decreased adipocyte size, reduced TG content - Increased insulin sensitivity	(*538*)
Ckm (muscle creatine kinase)-*ATGL* Tg (skeletal muscle-specific overexpression)	- Reduced intramyocellular TG content - Normal body weight, fat mass and muscle weight - Normal food intake and energy expenditure - Unaffected mitochondrial morphology and insulin response	(*535*)
AKO/cTg (*Pnpla2*$^{-/-}$ with cardiomyocyte-specific overexpression) on HFD	- Resistant to diet induced obesity, reduced WAT mass - Hypophagia - Enlarged BAT - Improved insulin sensitivity	(*432*)
DAKO (adipose-specific *Pnpla2*$^{-/-}$ and *Lipe*$^{-/-}$)	- Developed liposarcomas - Severely reduced lipolysis - Hypothermia - WAT-like BAT	(*539*)
iDKO (intestine-specific *Pnpla2*$^{-/-}$ and *Abhd5*$^{-/-}$)	- Normal body weight and food intake - Normal faecal output and lipid composition - Increased intestinal lipid accumulation - Improved hepatic steatosis	(*540*)

3.3 Materials and Methods

3.3.1 Cell culture

The 3T3-L1 preadipocytes were cultured and differentiated to mature adipocytes as described in 2.2.1 and 2.2.3, respectively.

To investigate the expression profile of selected genes of interest during the course of 3T3-L1 differentiation, cells were harvested when preadipocytes reached confluency (day -2), two days post-confluency (day 0), and every 3 days from day 0 until day 12 for mRNA and protein analysis.

3.3.2 siRNA transfection

Consecutive gene knockdown in 3T3-L1 cells was performed as described in 2.2.5. A list of commercially available siRNAs used in this study is shown in Appendix 3. Cells were either harvested on day 9 (second set of experiments) or day 10 (first set of experiments) to validate the knockdown efficacy. The ability to accumulate lipids in cells was assessed and the cells were either treated with basal or lipolytic medium for glycerol release assays on the same day.

3.3.3 AdipoRed assay

Differentiated 3T3-L1 adipocytes were washed in DPBS once and incubated with 0.5 ml medium containing 3% (v/v) AdipoRed Assay Reagent for 10 minutes in a 37°C incubator. Fluorescence of the AdipoRed stain as a quantification of lipid accumulation was measured by excitation at 485 nm and emission at 572 nm with an Infinite M1000 plate reader. Fluorescent images were taken using an EVOS Cell Imaging System.

3.3.4 Glycerol release assay

3T3-L1 preadipocytes were differentiated to mature adipocytes until day 9 (second set of experiments) or day 10 (first set of experiments) and transfected with siRNA throughout the course of differentiation. Cells were serum starved and treated with either basal or lipolytic medium as described in 2.9.1. Supernatant (media) was collected for the glycerol release assay as described in 2.9.2. Glycerol release was normalised to total cellular protein and then further normalised to negative control (NC) siRNA-treated cells.

3.3.5 Real-time quantitative PCR (qPCR)

Cells were lysed in 350 µl RLT supplemented with 1% (v/v) β-mercaptoethanol and kept at -80°C until all samples were collected for RNA extraction. Isolation of RNA and cDNA synthesis was performed as described in 2.3.1 and 2.3.2, respectively. cDNA was diluted and used as a template for qPCR to assess gene expression as described in 2.3.3. The primers used in this study are listed in Appendix 4. The mRNA expression of target genes was normalised to the expression of peptidyl-prolyl cis-trans isomerase A (also known as cyclophilin A, *Ppia*), a housekeeping gene. When studying the expression profile of all genes, the relative mRNA expression on specific days was further normalised to its corresponding expression level on day 0. Knockdown efficiencies for target genes were calculated as percent fold change in normalised mRNA expression relative to NC siRNA treated cells.

3.3.6 Western blotting

Cell lysates were prepared, and equal amounts subjected to SDS-PAGE followed by western blotting as described in 2.4.1 and 2.4.2. Details of antibodies used in this study are provided in Appendix 5.

3.4 Results

3.4.1 Expression profiles of target genes

To confirm that 3T3-L1 adipocytes are a valid cellular model for this study, I first aimed to verify expression of the genes of interest in these cells at different time points during the course of differentiation. The mRNA expression of target genes was assessed by qPCR, along with *Pparg2* as a classical indicator of adipogenesis. As expected, *Pparg2* expression was induced after the addition of differentiation cocktail at day 0 and continued to rise until day 12 (Figure 3.3 A). Likewise, the mRNA expression of all selected genes also increased upon 3T3-L1 differentiation except *Calcrl*, which was detected in both preadipocytes and adipocytes without substantial changes (Figure 3.3 A). Furthermore, *Plin1* and *Pde3b* were highly expressed in mature adipocytes towards the end of the differentiation protocol, compared with *Alk7* and *Pnpla2* (Figure 3.3 A). The expression of *Calcrl* in adipocytes remained similar to that in preadipocytes (Figure 3.3 A).

Protein expression at different stages during 3T3-L1 adipogenesis was validated by western blotting. As a marker for mature adipocytes, FABP4 expression was first detected on day 3 and remained high when the experiment was terminated at day 12 (Figure 3.3 B). As shown in Figure 3.3 B, expression of PPARγ2 (top band) was observed from day 3 and peaked on day 6, but gradually decreased until day 12. The same pattern was observed for ALK-7 (Figure 3.3 B). Similarly, ATGL expression declined after day 6, when the expression was first detected (Figure 3.3 B). The protein expression of PLIN1 also revealed an upward trend from day 6 and kept increasing until day 12 (Figure 3.3 B). Expression of these target genes was universally undetectable in preadipocytes. Due to a lack of suitable antibodies against CALCRL and PDE3B, their protein expression could not be assessed by western blotting. Therefore, expression validation of these two targets was measured by qPCR alone in subsequent studies.

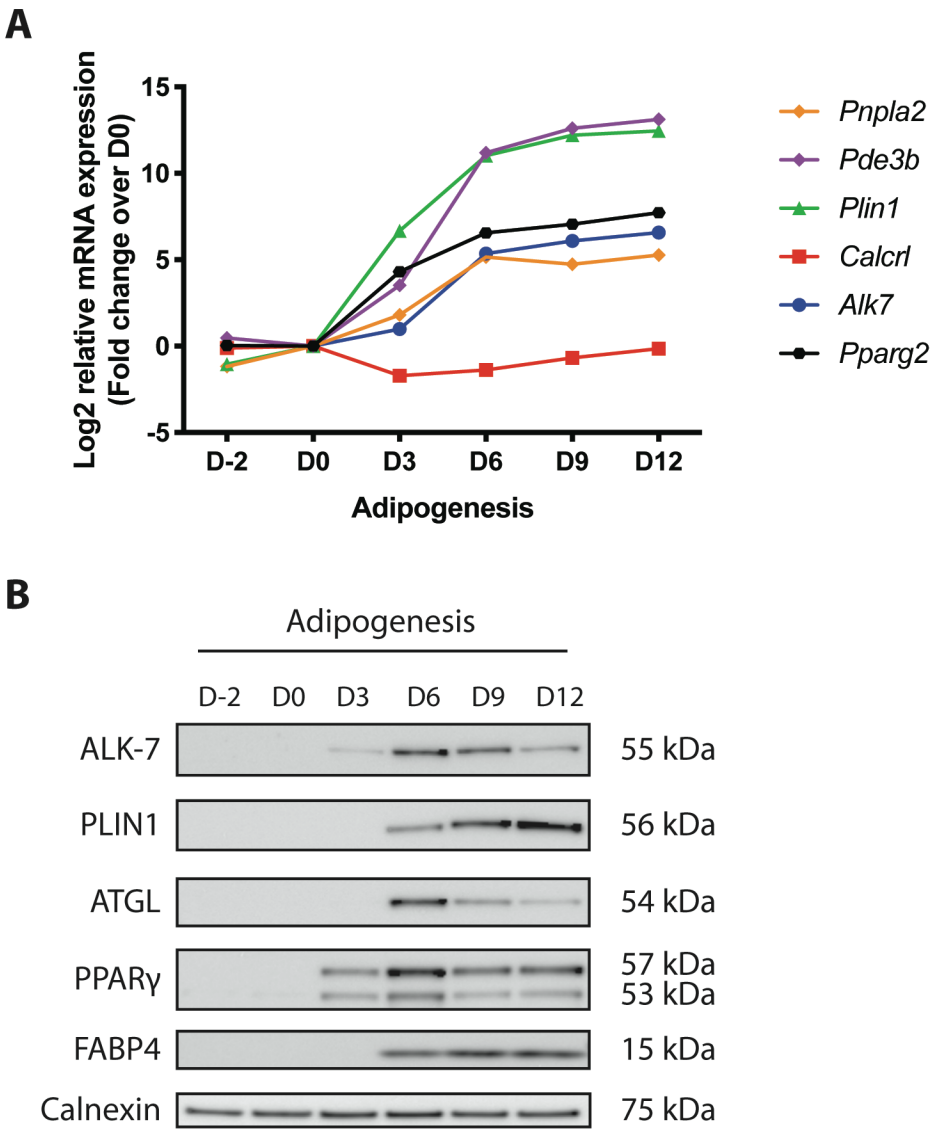

Figure 3.3 Expression profiles of selected genes during 3T3-L1 adipogenesis. (A) The mRNA expression of all selected genes during the differentiation of 3T3-L1 cells. The expression level of individual gene on day 0 (D0) was set to 1. *Pparg2* served as a marker for adipogenesis. All data were log2 transformed. Figures are representative of two independent experiments. (B) Protein expression levels were assessed by western blotting. PPARγ2 was detected as the top band in the PPARγ blot, while the bottom bands represent PPARγ1 expression. FABP4 served as a marker for differentiated adipocytes. Calnexin served as a loading control. Blots are representative of two independent experiments.

3.4.2 The effect of knockdown on adipocyte biology

Having established the expression profile of all candidate genes in 3T3-L1 cells, the role of these genes in adipocyte biology was then investigated using a gene silencing approach.

siRNA mediated knockdown was performed in confluent preadipocytes, as well as from the onset and throughout the course of differentiation until day 9 or day 10. The relative knockdown efficacy by individual siRNAs was determined by qPCR and western blotting.

To assess the effect of knockdown on adipogenesis, accumulated neutral lipids in 3T3-L1 adipocytes were stained with AdipoRed in order to visualise intracellular LDs. The expression of selected adipogenic markers was also determined as an indicator of differentiation capacity. As highlighted in the introduction, all of the target genes have been implicated in the regulation of intracellular lipolysis to at least some extent. Therefore, glycerol release was used as a measure of the lipolytic rate, in order to evaluate the impact of knockdown of these genes on lipolysis. In general, cells were treated with siRNA as described previously and lipolysis assays were performed on either day 9 or day 10, when differentiated adipocytes were incubated in the absence (basal) or presence (stimulated) of 10 µM isoproterenol.

3.4.2.1 Alk7

As illustrated in Figure 3.4 C, knockdown with siAlk7 proved to be efficient as measured by the mRNA expression. The level of *Alk7* in siAlk7 treated cells was reduced to approximately 10% of levels in NC siRNA treated cells. However, the residual *Alk7* mRNA was sufficient to be translated into ALK-7 protein, which was still detected by western blotting, showing an approximately 55% reduction in ALK-7 protein expression compared to the control cells (Figure 3.4 E).

After a series of siRNA treatments before and during the course of differentiation, no visible difference in lipid accumulation was observed between NC siRNA and siAlk7 treated cells according to AdipoRed staining (Figure 3.4 A). In line with findings from lipid accumulation, the mRNA expression of *Pparg2* did not differ between the two groups (Figure 3.4 B).

A glycerol release assay was performed in both cell groups in the absence or presence of isoproterenol. Approximately three- to five-fold increase of glycerol release was observed when cells were treated with isoproterenol, regardless of siRNA treatment (Figure 3.4 D). However, *Alk7* knockdown cells showed reduced glycerol release levels in both basal and

stimulated conditions compared to NC siRNA treated cells, although the difference in isoproterenol stimulated cells did not reach statistical significance (Figure 3.4 D).

Decreased glycerol release in cells transfected with siAlk7 is in keeping with the reduction of a subset of proteins involved in lipolysis (Figure 3.4 E). Phosphorylation of PLIN1 and HSL was lower in *Alk7* knockdown cells than in control cells regardless of stimulation, although total expression of HSL did not seem to differ (Figure 3.4 E). However, the total expression of PLIN1 upon isoproterenol stimulation appeared to be slightly lower in siAlk7 treated cells than that in the control cells (Figure 3.4 E). On the other hand, the expression of rate-limiting enzyme for lipolysis, ATGL, in siAlk7 treated cells remained similar to that in the control cells (Figure 3.4 E). Additionally, the expression of adipogenic markers, such as PPARγ and FABP4, was similar among all groups (Figure 3.4 E).

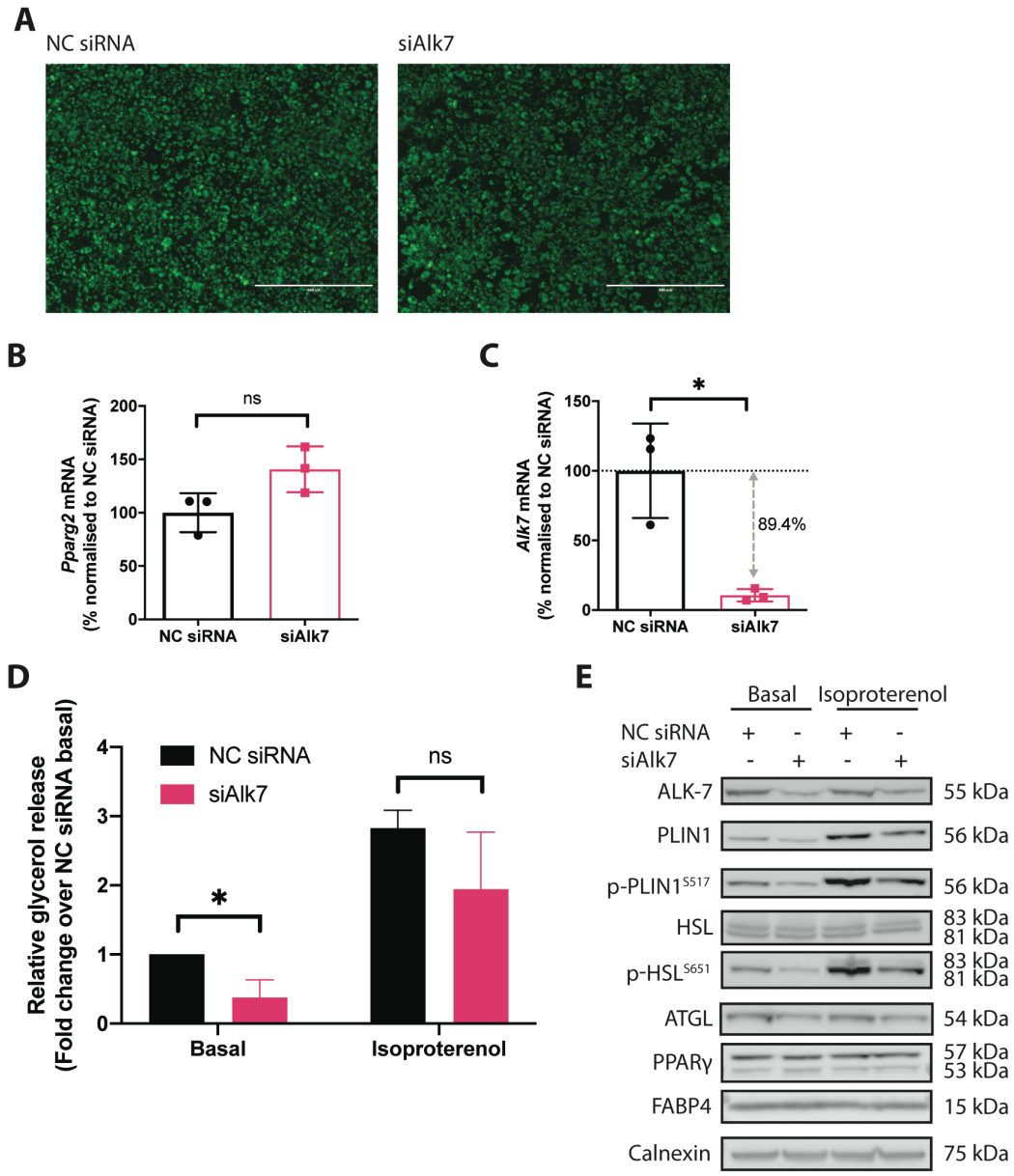

Figure 3.4 Characterisation of the impact of *Alk7* knockdown on 3T3-L1 adipogenesis and lipolysis. (A) Fluorescent microscopy of AdipoRed-stained lipid accumulation in siRNA treated cells. Images are representative of three independent experiments. Scale bars, 400 µm. (B) The mRNA expression of *Pparg2* was not affected by *Alk7* knockdown. (C) The knockdown efficacy of siAlk7 was assessed by qPCR. (D) Glycerol release was measured and normalised to protein amount, and expressed as fold change relative to basal NC siRNA-treated cells. (E) The expression levels of ALK-7 and proteins involved in regulating lipolysis under both basal and stimulated conditions were assessed by western blotting. Blots are representative from three independent experiments. Calnexin served as a loading control. In B to D, results from three independent experiments are presented as mean ± SD. Statistical significance was evaluated by an unpaired t-test. * $P < 0.05$, ns not significant.

Previous studies have reported that mice lacking *Alk7* displayed reduced fat accumulation after a high fat diet, as well as enhanced catecholamine sensitivity (*277*). Considering that the initial findings from the current experiments contradicted previous observations, a second attempt was made to re-examine the impact of silencing *Alk7* expression on adipogenesis and lipolysis (Figure 3.5).

In this set of experiments, the protein expression of ALK-7 was reduced dramatically by approximately 90% via repeated siRNA transfection, as shown in Figure 3.5 D. Unlike results from the previous experiments, lipid accumulation was now reduced in *Alk7* depleted cells compared with NC siRNA treated cells as indicated by AdipoRed staining (Figure 3.5 A). Quantification of the lipid staining revealed that the fluorescent signals were nearly halved in *Alk7* knockdown cells (Figure 3.5 B). Moreover, the expression of PPARγ and FABP4 was also decreased reflecting a reduced differentiation capacity (Figure 3.5 D). Nevertheless, similar to what was observed in Figure 3.4 D, basal lipolysis was suppressed in siAlk7 treated cells and there seems to be a downward trend for glycerol release in response to lipolytic stimulation (Figure 3.5 C). Meanwhile, the expression of proteins involved in intracellular lipolysis, such as PLIN1, HSL and ATGL, were all reduced in cells treated with siAlk7 (Figure 3.5 D). Similarly, phosphorylation of PLIN1 and HSL were both lower in siALK7 transfected cells than that in NC siRNA treated cells, regardless of lipolytic stimulation (Figure 3.5 D).

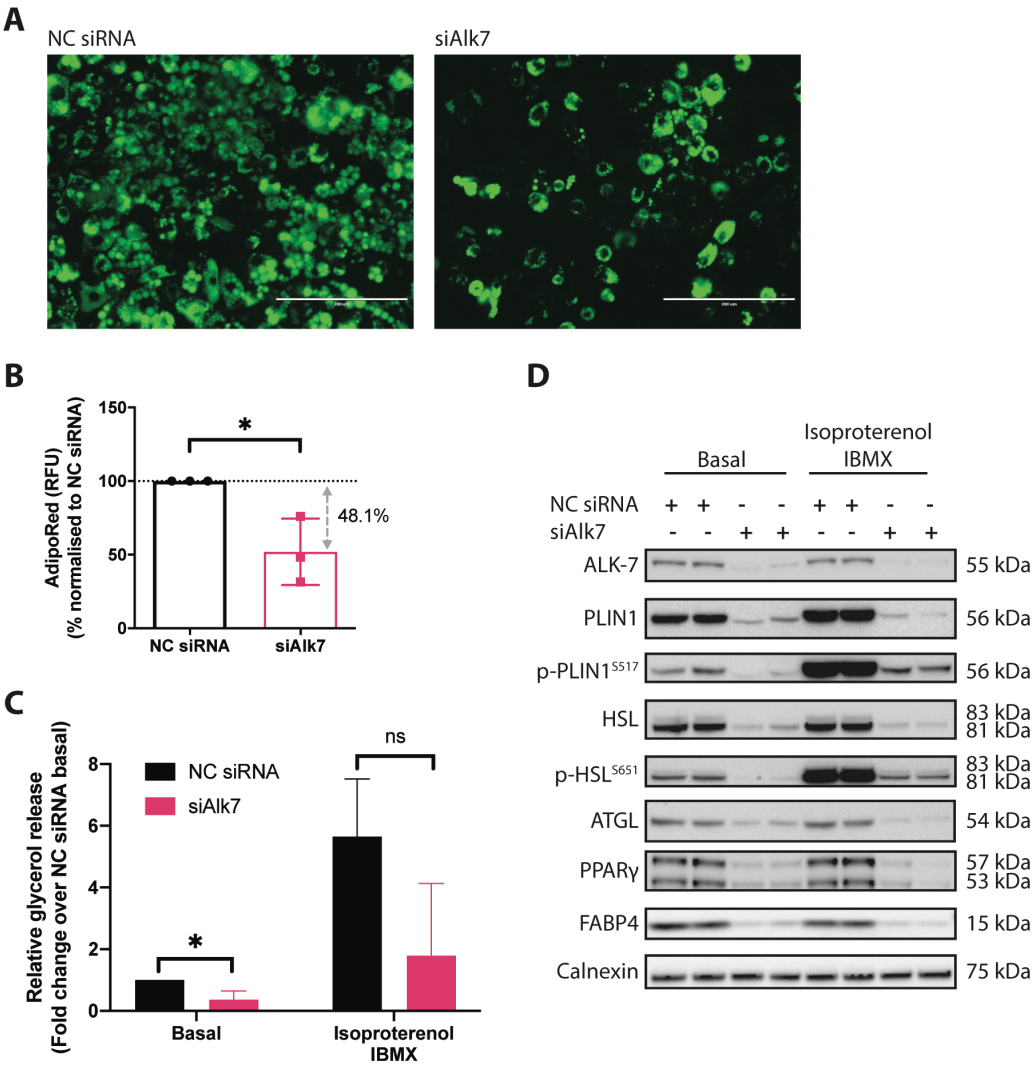

Figure 3.5 Second attempt to characterise the impact of *Alk7* knockdown on 3T3-L1 adipogenesis and lipolysis. (A) Lipid accumulation was reduced in cells treated with siAlk7. Images are representative of three independent experiments. Scale bars, 200 µm. (B) Quantification of AdipoRed fluorescence. Measurements were normalised to and presented as a percentage of NC siRNA. (C) Glycerol release was measured and normalised to protein amount, and presented as fold change to basal NC siRNA. (D) Western blot analysis of the protein expression of ALK-7, lipolytic and adipogenic markers. Calnexin served as a loading control. Blots are representative of three independent experiments. In B and C, results from three independent experiments are presented as mean ± SD. Statistical significance was evaluated by an unpaired t-test. * $P < 0.05$, ns not significant.

3.4.2.2 Calcrl

As mentioned earlier, a suitable antibody to test the knockdown efficacy for CALCRL using western blotting was not found, but the mRNA expression of *Calcrl* was reduced by approximately 85% by siCalcrl transfection in 3T3-L1 cells (Figure 3.6 C). There was no visible difference in lipid accumulation between NC siRNA and siCalcrl treated cells, as assessed by AdipoRed staining (Figure 3.6 A). The analysis of *Pparg2* mRNA expression also showed no significant difference between these two cell groups (Figure 3.6 B).

The effect of *Calcrl* knockdown on lipolysis was also assessed by measuring glycerol released by cells in the culture medium. As indicated in Figure 3.6 D, reduced basal lipolysis was observed after depletion of *Calcrl*, however the difference in isoproterenol stimulated lipolysis was not statistically significant (Figure 3.6 D). Western blotting for ATGL consistently showed a slightly reduced expression in siCalcrl treated cells in both basal and isoproterenol stimulated conditions compared with cells transfected with NC siRNA (Figure 3.6 E). However, the expression of other proteins involved in lipolysis, such as PLIN1 and HSL, as well as their phosphorylated forms, did not appear to be different between NC siRNA and siCalcrl treated cells (Figure 3.6 E).

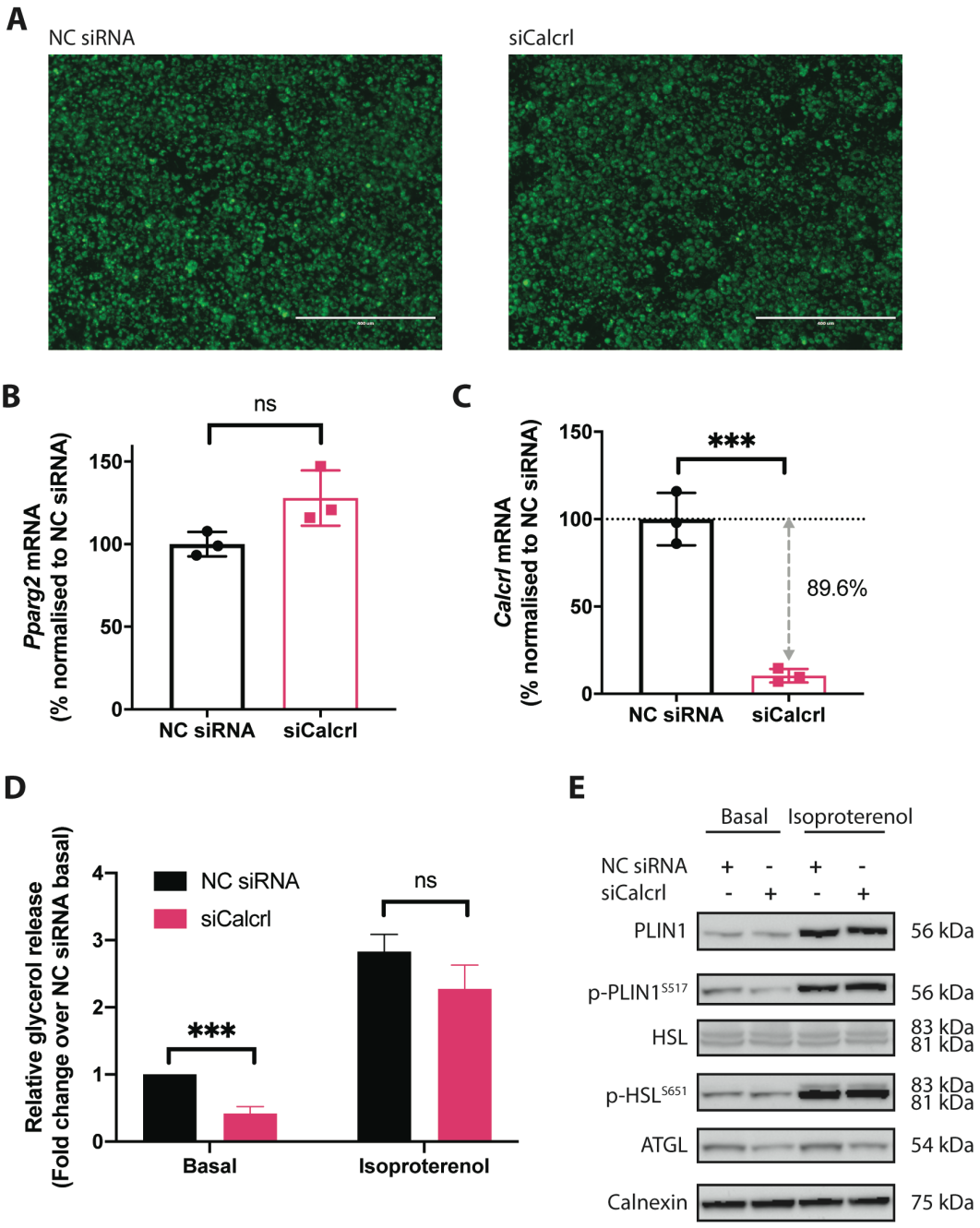

Figure 3.6 The impact of *Calcrl* depletion on adipogenesis and lipolysis in 3T3-L1 cells. (A) AdipoRed staining for lipid accumulation in siRNA treated cells. Images are representative of three independent experiments. Scale bars, 400 µm. (B) The mRNA expression of *Pparg2* was not affected by *Calcrl* knockdown. (C) The expression of *Calcrl* mRNA was significantly reduced. (D) Glycerol release was measured and normalised to protein amount, and presented as fold change relative to NC siRNA basal. (E) The protein expression of PLIN1, HSL and ATGL was analysed by western blotting. Calnexin served as a loading control. Blots are representative of three independent experiments. In B to D, results from three independent experiments are presented as mean ± SD. Statistical significance was evaluated by an unpaired t-test. *** $P < 0.001$, ns not significant.

As listed in Table 3.2, mice with *Calcrl* depletion demonstrated reduced lipid absorption in the intestine, thus affecting body weight gain (*459*). In addition, the complex formed by CALCRL and RAMP is tightly coupled to G_s proteins to increase cellular cAMP production, which in turn activates a number of PKA substrates (*541*). Since the impact of ADM/CALCRL/RAMP on lipid metabolism is still unclear, the same knockdown experiment was repeated to re-examine the role of CALCRL in differentiated 3T3-L1 adipocytes.

The knockdown efficiency of siCalcrl in 3T3-L1 cells in the second set of experiments improved to approximately 98% based on mRNA expression of *Calcrl* (Figure 3.7 C). In this case, lipid accumulation in *Calcrl* knockdown cells was dramatically diminished in contrast to my initial observations (Figure 3.7 A). As a result, quantification of AdipoRed fluorescence in cells transfected with siCalcrl was significantly reduced by approximately 65% compared to NC siRNA treated cells (Figure 3.7 B). Impaired differentiation was also accompanied by reduced expression of *Pparg2* and FABP4 determined by qPCR and western blotting, respectively (Figure 3.7 D and F). Consistent with the results presented in Figure 3.6 D, both basal and stimulated lipolysis were significantly decreased in *Calcrl* knockdown cells compared to NC siRNA treated cells (Figure 3.7 E). Furthermore, the expression of proteins regulating lipolysis, including ATGL, PLIN1 and HSL, as well as the phosphorylation of PLIN1 and HSL, were downregulated in siCalcrl treated cells (Figure 3.7 F).

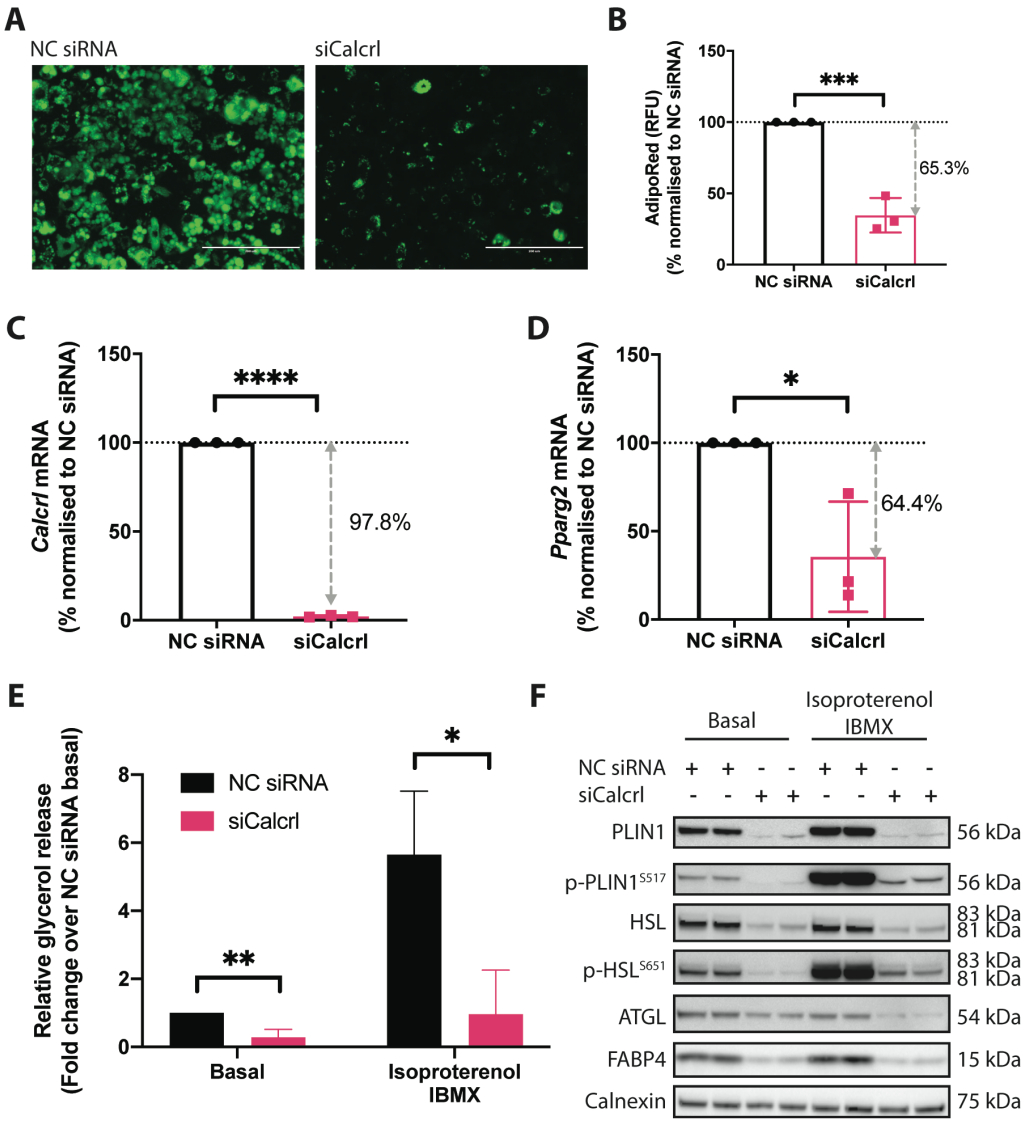

Figure 3.7 Re-evaluation of the impact of *Calcrl* knockdown on 3T3-L1 adipocyte biology. (A) Lipid accumulation was visualised by AdipoRed staining. Images are representative of three independent experiments. Scale bars, 200 µm. (B) AdipoRed fluorescence was quantified and normalised to NC siRNA. Data are presented as percentage of NC siRNA. (C) The knockdown efficacy of siCalcrl was validated by qPCR. (D) The mRNA expression of *Pparg2* was measured by qPCR and normalised to NC siRNA. (E) Glycerol release was measured and normalised to protein amount, and presented as fold change relative to NC siRNA basal. (F) Western blot analysis of the expression of FABP4 and proteins in the lipolytic machinery. Calnexin served as a loading control. Blots are representative of three independent experiments. In B to E, results from three independent experiments are presented as mean ± SD. Statistical significance was evaluated by an unpaired t-test. **** $P < 0.0001$, *** $P < 0.001$, ** $P < 0.01$, * $P < 0.05$.

3.4.2.3 Plin1

PLIN1 is well-known for its role in orchestrating both TG storage and mobilisation, therefore the hypothesis I wanted to test was that depletion of *Plin1* before and during the course of differentiation of 3T3-L1 cells would affect adipogenesis as well as lipolysis. Gene knockdown by siPlin1 resulted in an approximately 90% reduction in the mRNA level, although PLIN1 protein was still detectable by western blotting showing approximately 85% reduction (Figure 3.8 D and F).

Less lipid accumulation was observed in siPlin1 treated cells, which presented apparently smaller LDs (visually), as indicated in AdipoRed stained images (Figure 3.8 A). In addition, the mRNA expression of several adipogenic genes including PPARγ2, adiponectin (*Adipoq*), leptin (*Lep*) and GLUT4 (*Slc2a4*) was also decreased (Figure 3.8 B and C). However, no difference in the protein expression of FABP4 was observed (Figure 3.8 F).

As expected, when quantifying the glycerol release as an indicator for lipolysis, there was a significant increase in basal lipolysis but a decrease in isoproterenol stimulated lipolysis in *Plin1* knockdown cells (Figure 3.8 E). Thus, these cells were noticeably less responsive to isoproterenol stimulation as a result of the elevated basal lipolysis, which is also indicated by reduced phosphorylation of PLIN1 (Figure 3.8 E and F). Due to the depletion of *Plin1*, ABHD5 was presumably destabilised, leading to an observed reduction in its expression (Figure 3.8 F). The expression of ATGL however was not changed compared with NC siRNA treated cells (Figure 3.8 F). There was less phosphorylated HSL in *Plin1* deficient cells when stimulated with isoproterenol despite no change in total HSL expression (Figure 3.8 F).

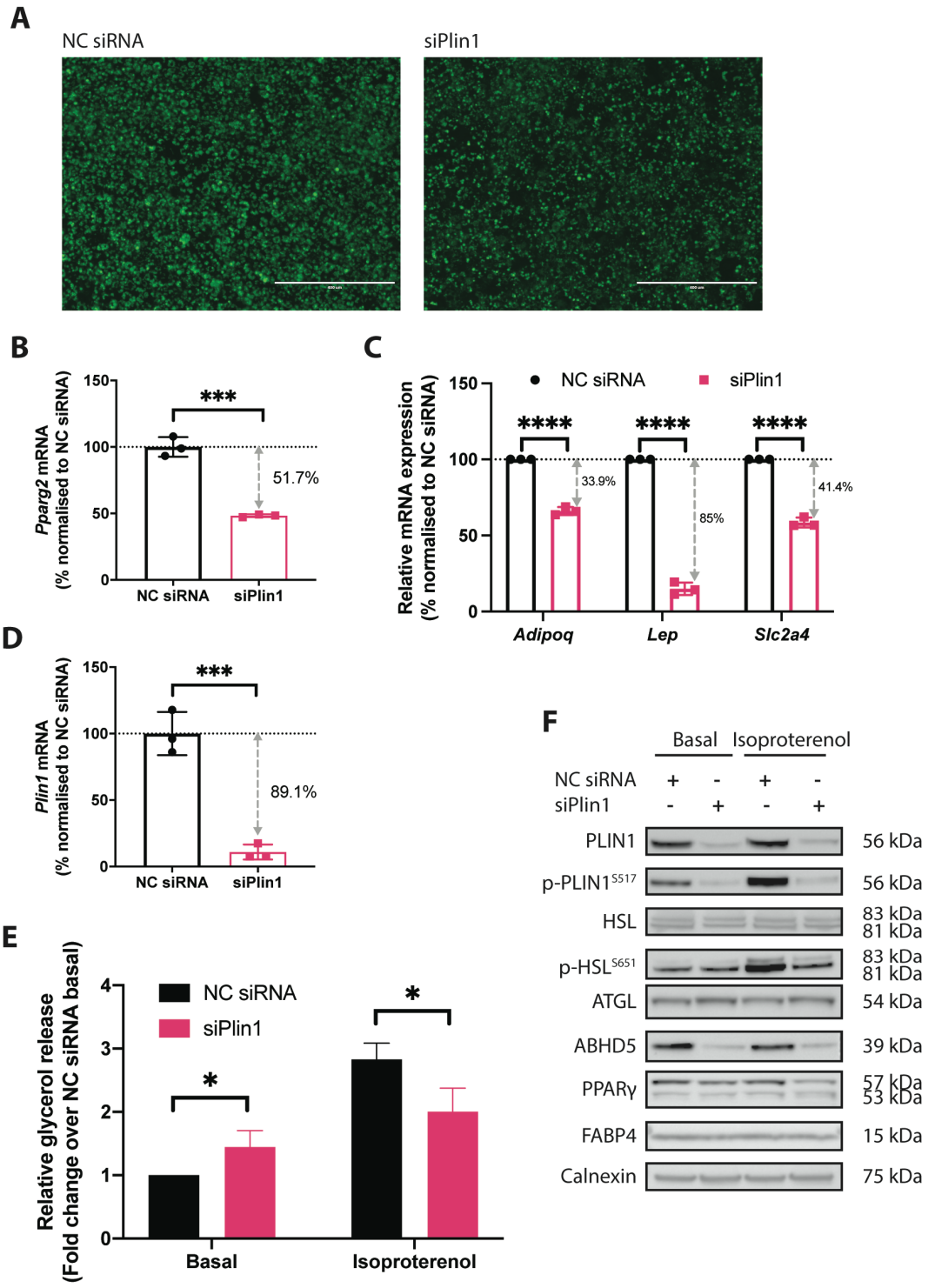

Figure 3.8 The impact of siRNA-mediated knockdown of *Plin1* on 3T3-L1 adipogenesis and lipolysis. (A) Lipid droplets appeared to be smaller in cells with *Plin1* depletion. Images are representative of three independent experiments. Scale bars, 400 µm. (B, C) The expression of adipogenic genes was assessed by qPCR and normalised to NC siRNA. (D) The knockdown of *Plin1* expression by siRNA treatment was measured by qPCR. (E) Glycerol release was measured and normalised to protein amount, and presented as fold change relative to NC siRNA basal. (F) The protein expression of lipolytic and adipogenic genes was analysed by western blotting. Calnexin served as a loading control. Blots are representative of three independent experiments. In B to E, results from three independent experiments are presented as mean ± SD. Statistical significance was evaluated by an unpaired t-test. **** $P < 0.0001$, *** $P < 0.001$, * $P < 0.05$.

3.4.2.4 Pde3b

Repeated knockdown of *Pde3b* by siRNA in 3T3-L1 cells reduced the expression level of *Pde3b* mRNA by approximately 75% (Figure 3.9 C). Unfortunately, as mentioned earlier, knockdown efficacy could not be validated at a protein level due to the lack of a suitable antibody against PDE3B.

There was no significant difference in *Pparg2* mRNA expression between NC siRNA treated cells and siPde3b treated cells (Figure 3.9 B). Similarly, lipid accumulation assessed by AdipoRed staining did not show any visible difference (Figure 3.9 A).

3T3-L1 adipocytes lacking *Pde3b* still responded to isoproterenol stimulation, which is indicated by more than two-fold induction of glycerol release compared to basal lipolysis (Figure 3.9 D). However, these cells showed no change in either basal or isoproterenol stimulated lipolysis when compared with NC siRNA treated cells (Figure 3.9 D). Western blot analysis for proteins involved in the process of lipolysis also indicated no differences upon *Pde3b* depletion (Figure 3.9 E).

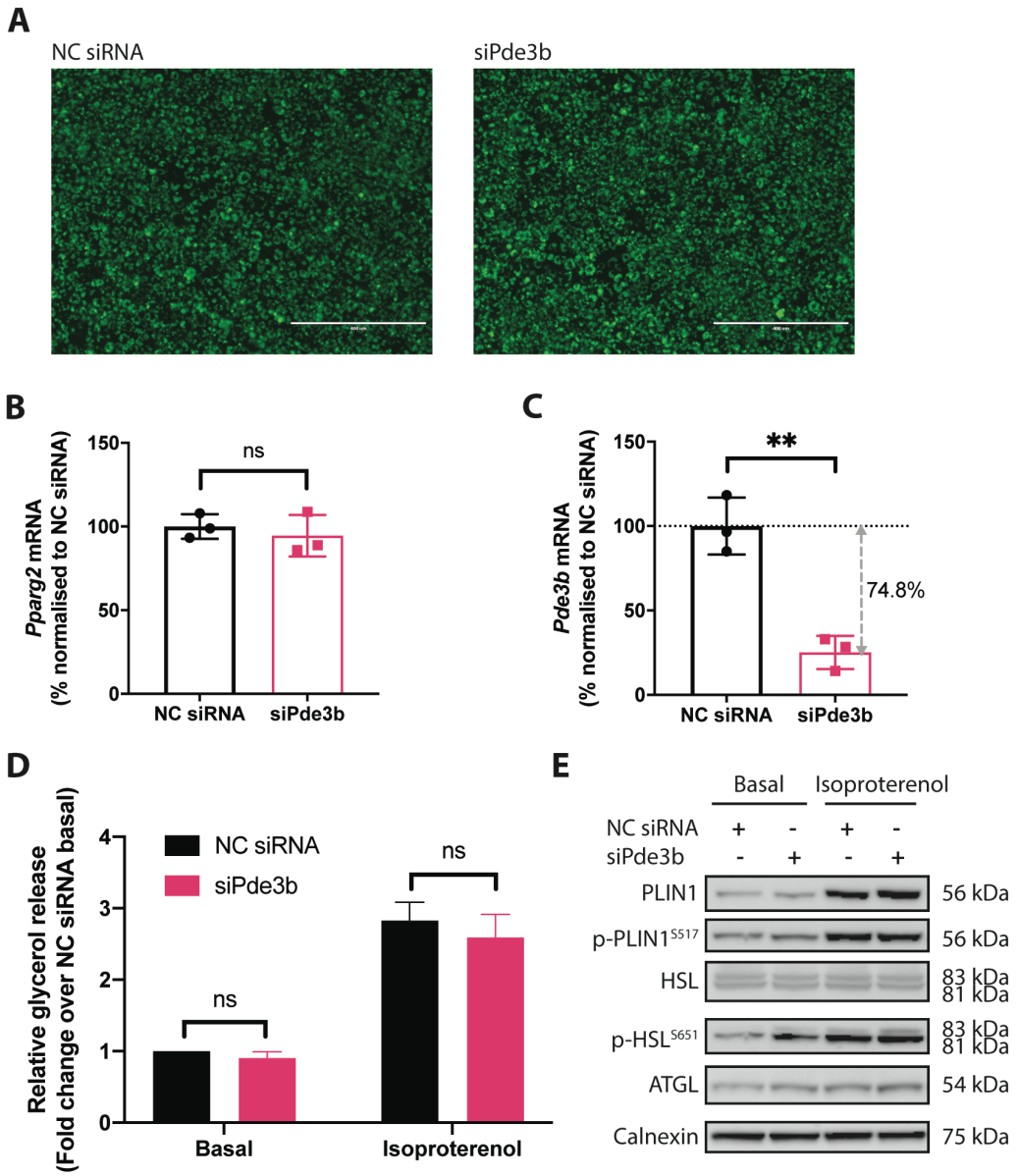

Figure 3.9 The impact of silencing *Pde3b* expression in 3T3-L1 adipocytes. (A) No visible difference in lipid accumulation was observed by AdipoRed staining between NC siRNA and siPde3b treated cells. Images are representative of three independent experiments. Scale bars, 400 µm. (B) The mRNA expression of *Pparg2* was measured and normalised to NC siRNA. (C) The knockdown efficacy of siPde3b was validated by qPCR and normalised to NC siRNA. (D) Glycerol release was measured and normalised to protein amount, and expresed as fold change relative to NC siRNA basal. (E) Western blot analysis of PLIN1, HSL and ATGL in siRNA treated cells. Calnexin served as a loading control. Blots are representative of three independent experiments. In B to D, results from three independent experiments are presented as mean ± SD. Statistical significance was evaluated by an unpaired t-test. ** $P < 0.01$, ns not significant.

3.4.2.5 Pnpla2

Knockdown of *Pnpla2* by siRNA proved to be effective in reducing the mRNA expression by approximately 90%, while the protein expression of ATGL was barely detectable by western blotting (Figure 3.10 C and E). There was no visible difference in lipid accumulation between NC siRNA treated cells and siPnpla2 treated cells, judging from the fluorescent images taken after AdipoRed staining (Figure 3.10 A). The mRNA expression of *Pparg2*, as well as the protein expression of PPARγ and FABP4, did not show a significant difference following siPnpla2 knockdown (Figure 3.10 B and E).

Since ATGL is the rate-limiting enzyme in lipolysis and its role cannot be fully rescued by HSL, it is expected that the loss of ATGL by siPnpla2 treatment would cause a reduction in both basal and stimulated lipolysis (*523*). Indeed, siPnpla2 treated adipocytes showed severely impaired basal lipolysis, as well as a significant reduction in isoproterenol stimulated lipolysis (Figure 3.10 D). Along with attenuated glycerol release, total PLIN1 expression and phosphorylation of PLIN1 were also lower in these cells (Figure 3.10 E). Although total HSL expression did not differ, the phosphorylation of HSL was markedly reduced by *Pnpla2* knockdown in both the basal and stimulated states (Figure 3.10 E).

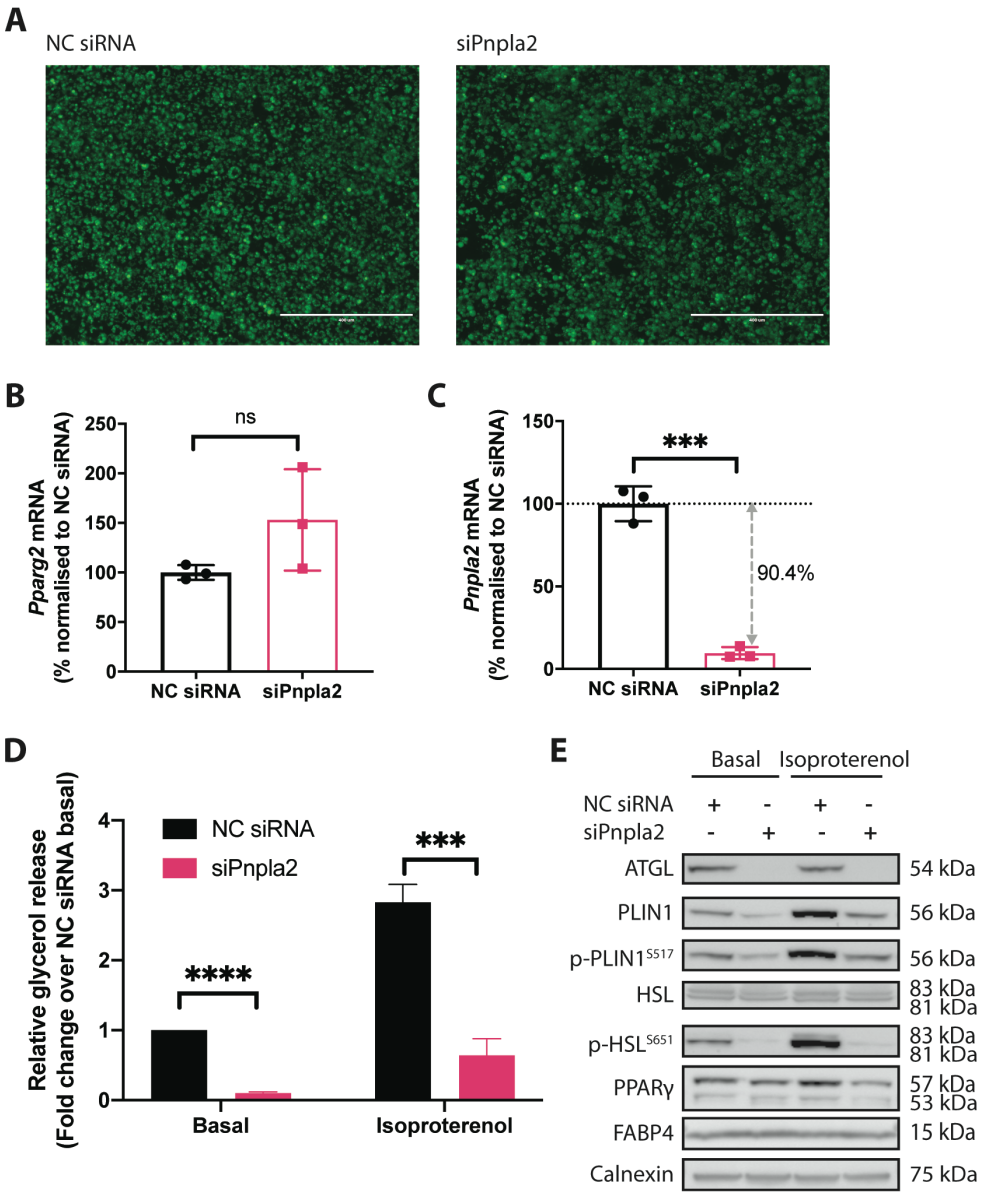

Figure 3.10 The impact of siPnpla2 treatment on 3T3-L1 adipogenesis and lipolysis. (A) Fluorescent images of lipid accumulation by AdipoRed staining. Images are representative of three independent experiments. Scale bars, 400 µm. (B) The mRNA expression of *Pparg2* was determined and normalised to NC siRNA. (C) The knockdown efficacy of siPnpla2 was validated by qPCR and normalised to NC siRNA. (D) Glycerol release was measured and normalised to protein amount, and presented as fold change relative to NC siRNA basal. (E) The knockdown efficacy of ATGL and the expression of PLIN1, HSL, PPARγ and FABP4 in siRNA treated cells was validated by western blotting. Calnexin served as a loading control. Blots are representative of three independent experiments. In B to D, results from three independent experiments are presented as mean ± SD. Statistical significance was evaluated by an unpaired t-test. **** $P < 0.0001$, *** $P < 0.001$, ns not significant.

3.5 Discussion

The main experimental approach described in this chapter was siRNA mediated mRNA knockdown in 3T3-L1 (pre)adipocytes. Transfection of individual siRNAs was performed in preadipocytes followed by consecutive siRNA knockdowns during the course of 3T3-L1 differentiation, in order to maintain a high knockdown efficiency of target genes. Differentiated cells were either stained with AdipoRed as an indicator of lipid accumulation or subjected to glycerol release assays as a measure of lipolytic rates. The role of selected genes in the regulation of adipose biology will be discussed individually in the following sections.

3.5.1 Alk7

Previous studies have suggested that ALK-7 is specifically expressed in the late phases of adipogenesis but is not essential for adipocyte differentiation in mice (*267*, *448*). As indicated by the expression profile in the current study, both mRNA and protein expression of ALK-7 were induced upon 3T3-L1 differentiation, which is consistent with previous findings (*267*, *448*, *542*).

It has been reported that mouse *Alk7* is involved in lipid storage as *Alk7*-null mice were protected from diet induced obesity (*268*, *277*). Especially in fat-specific *Alk7* KO mice, fat accumulation, as well as adipocyte size, were significantly reduced (*277*). Therefore, we anticipated that the adipogenic capacity in siAlk7 transfected 3T3-L1 cells would be reduced. However, the impact of *Alk7* knockdown on 3T3-L1 adipogenesis was inconclusive in the current study due to the difference in results obtained from the two sets of experiments. One possible explanation would be the inconsistency in the knockdown efficacy, which improved to 90% reduction of ALK-7 protein expression in the second set of experiments from 55% in the first set. Therefore, a more striking phenotype was observed in the second set of knockdown assays showing reduced lipid accumulation in siAlk7 transfected adipocytes, resembling the phenotype observed in *Alk7* KO mice (*277*). Although AdipoRed staining

indicates an overall reduced lipid accumulation in *Alk7* knockdown cells, it did not provide any information as to the size of LDs per cell. Therefore, future experiments could be carried out to assess the impact of *Alk7* knockdown on LD size in 3T3-L1 adipocytes, especially since LD size is known to influence the cellular balance between lipolysis and lipid storage. Decreased expression of adipogenic markers such as PPARγ2 and FABP4 also implies an impaired differentiation in cells treated with siAlk7, this however is in conflict with previous reports where upregulation of PPARγ2 was observed in *Alk7* deficient obese mice (*447*, *448*). Also, Yogosawa et al. demonstrated that stably transfecting 3T3-L1 adipocytes (day 5) with a constitutively active mutant of ALK-7 resulted in reduced expression of adipogenic markers PPARγ2 and C/EBPα, although the effect on adipogenesis was not reported (*448*). The same study reported no difference in the expression levels of these transcription factors, when WT ALK-7 was overexpressed compared to empty vector control, suggesting that the WT ALK-7 was inert in these 3T3-L1 adipocytes (*448*). The discrepancy between our result and theirs lies in the experimental conditions, as their gain-of-function analysis was performed in differentiating adipocytes while the loss-of-function in this study was carried out before the onset of differentiation. It could also be explained by the fact that the regulation of adipogenesis by affecting the expression of PPARγ is exerted by many members of the TGF-β superfamily independent of ALK-7, which could potentially become activated/supressed to compensate for ALK-7 depletion (*543*). For example, it has been suggested that GDF-10 secreted from 3T3-L1 cells inhibits adipogenesis by suppressing PPARγ expression through binding with ALK-4/ACVR-IIB and activation of Smad2/3 signalling pathway (*544*, *545*). On the other hand, PPARγ has been shown to be activated by BMP4 via Smad1/5/8 signalling pathway in order to stimulated adipogenesis (*546*). It has recently been suggested that the Smad1/5/8 signalling pathways are activated to prime undifferentiated precursors for adipogenic commitment, while the Smad2/3 pathway suppresses preadipocyte proliferation in 3T3-L1 cells (*547*). However, as the exact mechanisms through which TGF-β superfamily members preferentially regulate adipogenesis remain largely unclear, further studies are required to examine which of these specific signalling pathway(s) regulating adipocyte development are activated or suppressed as a consequence of silencing *Alk7* expression (*543*).

A technical concern when interpreting the data in this study was the difference in cell line passages used in the two separate sets of 3T3-L1 experiments. The 3T3-L1 cell line is an established cell model to study adipogenesis, but some researchers have reported waning of adipogenic potential when passaged extensively (*548*, *549*). The passage numbers for cells used in the first set of experiments were 11, 13 and 15, while the cells used for the second were passaged at 24, 25 and 38. It is likely since the latest set of knockdown experiments were carried out in much later passages, the cells might have had a declined differentiation capacity.

Nevertheless, *Alk7* depletion reduced basal lipolysis in both sets of experiments, although it could be argued that the larger decrease in basal glycerol release in the second set of experiments reflect the already decreased lipid accumulation. There was also a similar downward trend of glycerol release following isoproterenol stimulation in both sets of assays, although both findings did not reach statistical significance. Previous studies have shown that mice lacking *Alk7* displayed elevated basal and stimulated lipolysis when fed on a HFD (*277*). In line with enhanced adrenergic signalling, increased total and phosphorylated HSL was also observed in adipose-specific *Alk7* KO mice, as well as phosphorylated PKA substrates upon stimulation (*277*). Similarly, obese mice carrying a loss of function ALK-7 (R322X) also displayed higher rate of lipolysis with increased expression of major lipases, such as ATGL and HSL (*448*). All evidence suggests that the phenotypic data obtained from *Alk7* KO mouse studies cannot be replicated in our 3T3-L1 cell model. One of the members of the TGF-β superfamily activin B, which signals through ALK-7, has previously been shown to negatively regulate lipolysis in 3T3-L1 adipocytes (*550*). However, another type I receptor ALK-4, which has been shown to be expressed in human and mouse adipose tissue, is also considered to be activated by activin B (*252*, *268*, *279*, *551*, *552*). Therefore, it is possible that ALK-4 could compensate for the loss of ALK-7 under current experimental settings. Collectively, future studies are required to clarify the role of ALK-7 in adipocyte biology with cell culture models due to the complexity of multiple TGF-β signalling pathways. Additional studies may also need an *Alk4* deficient background because of the functional overlap between the two.

3.5.2 Calcrl

Calcrl was expressed in both preadipocytes and adipocytes, in line with previous studies which have shown that *Calcrl* is expressed in a variety of adipocyte cell lines, including 3T3-L1 and 3T3-F442A mouse cell lines, as well as MK427 cells which were derived from rats (*314*, *322*, *461*). Unlike the other genes of interest, the expression of *Calcrl* in 3T3-L1 decreased from day 0 to day 3 and then gradually returned to a similar level to preadipocytes by day 12. This U-shaped expression pattern of *Calcrl* has been reported by others, and a similar pattern was also observed for the expression and secretion of its ligand ADM in 3T3-L1 cells (*461*). Furthermore, during the differentiation of MK427 cells, the mRNA expression of *Calcrl* was lower on day 5 but higher on day 10 compared to day 1 (*322*). This might suggest a potential role of ADM, as well as CALCRL in adipogenesis.

CALCRL has been proven to be essential for survival, and depletion of *Calcrl* in adult mice results in reduced body weight due to impaired lipid absorption in the intestine (*457*, *459*, *460*). However, the role of CALCRL in adipocyte biology has not been established. Since the results from AdipoRed staining in my study were inconsistent, the function of CALCRL in adipogenesis in 3T3-L1 cells remains unclear. Previous studies have reported that ADM inhibits adipogenesis by reducing the expression of adipogenic transcription factors, such as PPARγ2 and C/EBPα in 3T3-F442A cells, although whether the expression of CALCRL was also altered accordingly has not been reported (*456*). Furthermore, CALCRL also acts as a receptor component for other ligands (CGRP, ADM2), the roles of which in adipocyte differentiation have not yet been fully understood. Therefore, further studies will be necessary to dissect CALCRL mediated signalling transduction in 3T3-L1 cells. It should be noted that similar to the *Alk7* knockdown experiments, the discrepancy in adipogenesis between the two sets of experiments in this study could be related to the use of two different passages of 3T3-L1 cells (*548*, *549*).

Even so, *Calcrl* knockdown resulted in a consistent reduction in basal glycerol release, albeit the significantly reduced lipid accumulation in the second set of experiments, could drive the observed decrease in lipolysis. As described in the introduction, CALCRL binds with RAMPs and functions to promote cAMP production when coupled with G_s proteins, which is the main

signalling pathways activated upon ligand binding in adipocytes (*541*, *553*). However, the role of ligands in the regulation of lipolysis is controversial as it varies depending on the experimental conditions such as species, cell types and dosage (*314*, *322*, *554*). Lipolysis assays showed elevated glycerol release in human mesenchymal stem cell derived adipocytes when exposed to exogeneous CGRP or ADM (*554*). Similarly, increased cAMP levels and PKA mediated substrate phosphorylation by treatment with another ligand ADM2 was observed in rat adipocytes derived from stromal vascular cells isolated from SAT (*469*). Therefore, it was implied that the corresponding receptors for the calcitonin family peptides may be responsible for the reported effects (*554*). On the other hand, ADM has also been indicated in the inhibition of β-adrenergic stimulated lipolysis mediated by NO which oxidised isoproterenol to an inactive compound (*314*). Clearly the lipolysis data presented in this work are in agreement with findings from the majority of the previous reports and favour the theory that the lack of *Calcrl* in the pathway may fail to produce adequate cAMP, which could explain the observed reduction in lipolysis. Whether the NO pathway is also altered following the knockdown of *Calcrl* in 3T3-L1 adipocytes could be verified with future work by performing an intracellular cAMP assay or a NO production assay. Although the knockdown by siCalcrl seems to be efficient on the transcriptional level, the lack of information on the protein level may limit the interpretation of the current findings.

3.5.3 Plin1

PLIN1 is located on the surface of LDs and is well known for its fundamental role in the regulation of TG storage and mobilisation. It has been reported that *Plin1* is a target gene of PPARγ (*555*). Therefore, as expected the mRNA expression of *Plin1* in 3T3-L1 cells was greatly induced upon differentiation, following a trend similar to *Pparg2* expression. Although the protein expression of PPARγ gradually decreased towards the late phase of 3T3-L1 adipogenesis, PLIN1 expression on the other hand was stabilised by lipid storage, which is consistent with previous findings (*556*).

Knocking down *Plin1* before the onset, as well as throughout 3T3-L1 differentiation, resulted in diminished lipid accumulation. However, differentiation of adipocytes isolated from *Plin1*

null mice seemed to be normal (*359*). However, it has been described that instead of large LDs, stromovascular cells isolated from subcutaneous fat pads of *Plin1* null mice accumulated tiny LDs when differentiated *in vitro* (*485*). These cells also showed a diminished capacity to fully differentiated into mature adipocytes and a significant reduction in the mRNA expression of adipogenic transcription factors such as *Pparg* and *Cebps* was observed in *Plin1* null adipose tissue, which is in agreement with results from the current study (*485*). Although the exact mechanism by which *Plin1* deficiency leads to reduced adipogenesis is not clear, there are suggestions that a positive feedback loop exists between SREBP1c (sterol regulatory element-binding protein 1c) and PLIN1 during adipogenesis to promote TG synthesis, thus enhancing LD formation (*484*). SREBP1c is a transcription factor which is synthesised as a precursor in the ER membrane, it is then processed by proteases to release its active nuclear form in order to induce the expression of target genes that are involved in FA synthesis (*484*, *557*). The nuclear form of SREBP1c was found to be decreased in *Plin1* null adipose tissue and differentiated MEFs, which was restored by ectopic expression of PLIN1 (*484*). Therefore, disruption of PLIN1 expression may cause decreased SREBP1 activation, leading to reduced lipogenic gene expression (*484*).

Depletion of *Plin1* in 3T3-L1 cells led to elevated basal lipolysis while isoproterenol stimulated lipolysis was significantly reduced, which is expected since PLIN1 acts dually as a suppressor of basal lipolysis and as a substrate of PKA to stimulate lipolysis (*359*). In addition, the elevated basal lipolysis could also be an explanation for the reduced lipid accumulation observed. Lack of PLIN1 on the surface of LDs destabilises ABHD, which explains the reduced expression of ABHD5 in siPlin1 treated cells. This is consistent with what has been reported previously (*351*).

3.5.4 Pde3b

Consistent with findings from previous studies, the mRNA expression of *Pde3b* was indeed induced upon 3T3-L1 differentiation and remained stable until late stages of differentiation (*501*, *502*). Meanwhile, it has also been shown that PDE3B activity correlated with its expression profile (*502*). Since no visible difference was observed in lipid accumulation and the expression of *Pparg2* between NC siRNA and siPde3b treated cells, it suggests that differentiation of 3T3-L1 cells is independent of PDE3B. However, in contrast to the result

from the current study, knocking down *PDE3B* by siRNA in subcutaneous human preadipocytes has been reported to increase lipid accumulation assessed by AdipoRed staining, although no changes in the expression of adipogenic markers, *PLIN1* and *FABP4,* was observed (*512*). The authors explained the phenotype by a shift of the lipogenesis/lipolysis ratio towards lipogenesis after *PDE3B* knockdown. However, the knockdown efficacy was not reported, which could possibly explain the discrepancy between our studies in lipid staining (*512*).

The anti-lipolytic function of PDE3B is exerted by catalysing the breakdown of intracellular cAMP, therefore in theory PKA activities are downregulated leading to suppressed lipolysis. Silencing the expression of *Pde3b* in 3T3-L1 should result in cAMP accumulation leading to higher rates of lipolysis, however this is not what was observed in the current experiment. This was surprising as stimulated lipolysis has been shown to be enhanced in *Pde3b* KO compared to WT mice, as well as in adipocytes obtained from the KO mice, although no difference was observed for basal lipolysis (*509*). Our result is however in line with several *in vitro* studies using either a similar approach or by examining lipolytic rate in differentiated brown adipocytes isolated from *Pde3b* KO mice (*558*, *559*). However, *in vitro* studies did report that insulin stimulated suppression of catecholamine induced lipolysis was partially impaired in 3T3-L1 adipocytes with *Pde3b* knockdown, as well as in *Pde3b* KO brown adipocytes (*558*, *559*). Therefore, several attempts were made to introduce insulin in the glycerol release assay following repeated knockdown by siRNA. The results again showed no significant difference in the insulin suppression of lipolysis between NC siRNA and siPde3b treated cells (data not shown). However, this was largely due to the fact that inhibition of lipolysis with insulin in control cells itself was not consistent, thus further assays could be done to optimise the conditions in order to achieve reliable suppression with insulin. In addition, the assessment of knockdown efficacy at protein level was not possible in our study, while Stöckli et al. reported 94% reduction of PDE3B protein by siRNA mediated knockdown in 3T3-L1 adipocytes, resulting in a small but significant insulin stimulated reduction of catecholamine induced lipolysis (*559*). Therefore, it is necessary to improve knockdown efficiency and a suitable antibody is needed to confirm this.

3.5.5 Pnpla2

As described in Chapter 1, the role of ATGL in TG mobilisation is well established. The mRNA expression of *Pnpla2* was induced during the differentiation of 3T3-L1 cells, which is consistent with findings from previous reports (*406*). Unlike the mRNA expression profile, the protein expression of ATGL fell at the late stages of differentiation in the current experiments, concomitant with the expression of PPARγ. This is expected as it has been shown that *Pnpla2* is a target gene of PPARγ; both mRNA and protein expression of ATGL are positively regulated by PPARγ in mature adipocytes (*514*, *515*). Previous studies have shown that the transcription of *Pnpla2* was also activated by the interaction between PPARγ and transcription factor Sp1 in differentiated adipocytes, while the latter alone acts as a repressor in 3T3-L1 preadipocytes when PPARγ is absent (*560*).

With regard to the role of ATGL in adipogenesis, results from the current study indicates that ATGL is dispensable for the differentiation of 3T3-L1 cells. However, one study has reported that differentiated 3T3-L1 cells with ATGL depletion manifested fewer small LDs than controls, although the size distribution of LDs per cell was not statistically analysed (*561*). As ATGL is the rate-limiting enzyme of lipolysis, glycerol release in cells treated with siPnpla2 was markedly decreased under basal and stimulated conditions, which is in agreement with what was observed from previous studies (*407*).

3.6 Conclusion

In summary, the results from siPlin1 or siPnpla2 treated cells confirmed their roles in regulating lipolysis in adipocytes. Knockdown of *Alk7* or *Calcrl* in 3T3-L1 cells showed reduced basal lipolysis, although their function in adipogenesis requires further clarification. To improve the experimental consistency, we could use CRISPR to knockout *Alk7* or *Calcrl* in 3T3-L1 cells. As both ALK-7 and CALCRL function as receptors for multiple ligands which are involved in diverse signalling pathways, more work on how these receptors are altered in response to particular ligands is required. Reduced expression of *Pde3b* did not show any impact on 3T3-L1 adipogenesis or lipolysis in current experimental setting, which was unexpected as PDE3B is known to be involved in insulin mediated anti-lipolytic action. Further experiments could be performed to achieve more consistent depletion of *Pde3b* and insulin suppression of lipolysis, which are essential for phenotyping assays.

Following on from the results described in this chapter, further functional characterisation for specific missense variants in *ALK7*, *PNPLA2* and *PLIN1* was carried out and will be discussed in the next two chapters.

4 Functional characterisation of PNPLA2 and ALK-7 missense variants associated with altered body fat distribution

4.1 Abstract

The adipogenic and lipolytic defects caused by knockdown of *Pnpla2* and *Alk7* in 3T3-L1 adipocytes were reported in Chapter 3. This chapter will describe functional studies of rare nonsynonymous variants in *PNPLA2* (p.N252K) and *ALK7* (p.I195T and p.N150H) that are associated with altered waist-to-hip ratio (WHR), an anthropometric proxy measure for body fat distribution.

The *PNPLA2* variant is predicted to affect splicing so its mRNA expression level was examined in both homozygous WT allele and heterozygous mutant allele carriers. Quantification of *PNPLA2* mRNA expression from PBMCs by qPCR revealed that the overall mRNA expression of *PNPLA2* was reduced in heterozygous carriers. The PNPLA2 variant was initially characterised by overexpressing the mutant construct in COS-7 cells where it retained the ability to target LDs. Furthermore, the catalytic activity of PNPLA2 did not seem to be affected by the N252K mutation.

In terms of the ALK-7 variants, a luciferase-based reporter assay was conducted in HEK293 cells to reveal the impact of the ALK-7 variants in mediating Smad-dependent signal transduction. Data obtained from the activity assay suggest that the replacement of isoleucine with threonine at residue 195 in ALK-7 abolished the signalling transduction activity, while the mutation N150H seems, if anything, to elevate signalling activity even in the absence of ligand.

4.2 Introduction

4.2.1 Lipid droplet targeting of PNPLA2

As mentioned previously, PNPLA2 catalyses the first hydrolysis reaction of TG in the adipocyte lipolysis pathway. The intracellular localisation of PNPLA2, under basal conditions where the lipolytic rate is low, is generally cytosolic (*412*). Cytosolic PNPLA2 translocates to the surface of LDs upon stimulation, leading to the initiation of lipolysis (*412*). It has been acknowledged that the C-terminal region of PNPLA2, especially the hydrophobic stretch, is important for its localisation to LDs. However, truncation of the C-terminal region including the hydrophobic stretch of PNPLA2 did not completely abolish the ability of the truncated protein (aa 1 – 319) to bind LDs, indicating that the N-terminal region of PNPLA2 also contributes to LD targeting to some extent (*419*).

4.2.2 Predicted functional impact of PNPLA2 variant

We reported the association of a PNPLA2 variant p.N252K with lower BMI but higher WHR, as well as a higher risk of T2D and coronary artery disease (*1*). This rare variant has been reported by other researchers previously, where lower FFA levels were observed in the p.N252K carriers (*521*, *522*). The asparagine residue at position 252 is located at the junction between the three-layer α/β/α sandwich and α-helical and loop regions of the protein (Figure 4.1 A). This residue is highly conserved among orthologues while other residues are also observed in paralogous proteins (Figure 4.1 C) (*1*). The enzyme activity of the variant is predicted to be unaffected since the patatin domain would remain intact. However, the mutation in this variant (c.756C>G) occurs close to the conserved 5' donor splice site, which is typically GU in pre-mRNA, suggesting that this variant could potentially affect splicing (Figure 4.1 B). Indeed, *in silico* prediction shows a higher chance of alternative splicing caused by the creation of an exonic splicing silencer site due to the nucleotide change (*1*).

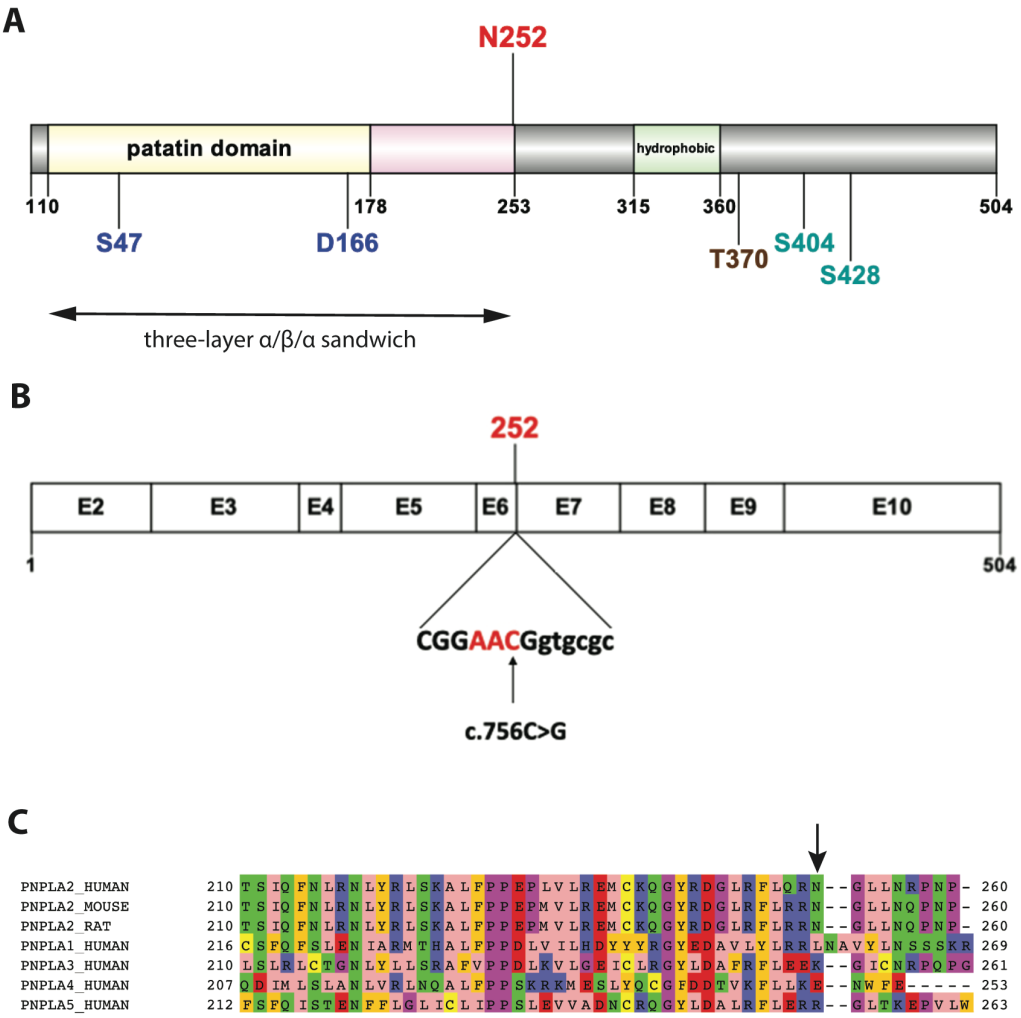

Figure 4.1 The human PNPLA2 p.N252K variant. (A) Domain organisation of human PNPLA2. Human PNPLA2 consists of 504 amino acid residues. The three-layer α/β/α sandwich fold at the N-terminus overlaps the patatin domain, including the putative catalytic dyad labelled as S47 and D166. A hydrophobic stretch at the C-terminus is involved in LD binding. Putative phosphorylation sites, T370, S404 and S428 are also indicated. Location of the missense variant at residue position 252 is labelled in red. (B) Schematic illustration of exon architecture of human PNPLA2. Donor splice site sequence from position -7 to 6 at the splice junction between exon 6 and intron 6-7 is indicated with the exonic sequence in uppercase and intronic sequence in lowercase. Residue position 252 and the WT codon is labelled in red. The arrow indicates the location of the nucleotide substitution for N252K. (C) Sequence alignment of PNPLA2 segments from selected species and the human paralogues. The mutated residue N252 is indicated by an arrow. Domain structure and exon architecture were generated by GPS (*249*), sequence alignment was performed with Jalview (*468*).

4.2.3 Mechanisms of ALK-7 signalling

As described in Chapter 1, ALK-7 is classified as a type I receptor kinase, which forms a heterotetramer with ACTR-IIB, a type II receptor kinase, for downstream signal transduction upon ligand binding (Figure 4.2). ACTR-IIB activates ALK-7 through phosphorylation in the GS domain of ALK-7, leading to a conformational change in ALK-7 that enables ATP binding and ALK-7 subsequently phosphorylates downstream R-Smads (*246*). Based on the preference of ligand/type I receptor kinase, Smad2/3 are phosphorylated by ALK-7 to initiate the canonical Smad signalling pathway (Figure 4.2) (*246*). Activated Smad2/3 form a heterooligomeric complex with Smad4, the resulting Smad complex translocates into the nucleus and interacts with DNA-binding co-factors to regulate the expression of a set of cell-specific genes (Figure 4.2) (*562*). An 8-bp palindromic duplex sequence 5'-GTCTAGAC-3' was originally identified as a high affinity binding site for Smad3 and Smad4 (*563*). It was later discovered that the GTCT motif or its complementary extended sequence CAGA is enough to be recognised by the Smads based on the crystal structures of N-terminal domains of Smad3 and Smad4 (*562*, *564*). Therefore, GTCT or CAGA motifs are referred to as Smad-binding elements (SBEs) or a CAGA box (*562*, *565*). Although low affinity binding of Smad complexes with single SBEs has been observed *in vivo*, most Smad-responsive promotor regions contain concatemers of multiple SBEs for higher and tighter binding affinity (*566*). In mature adipocytes, ALK-7 is reported to downregulate the expression of key adipogenic transcription factors PPARγ and C/EBPα (Figure 4.2) (*448*). Smad signalling pathway has been shown to suppress PPARγ expression, whereas downregulation of C/EBPα might be mediated by directly interaction with Smad complex although the exact mechanism is still unclear (*448*, *567*, *568*).

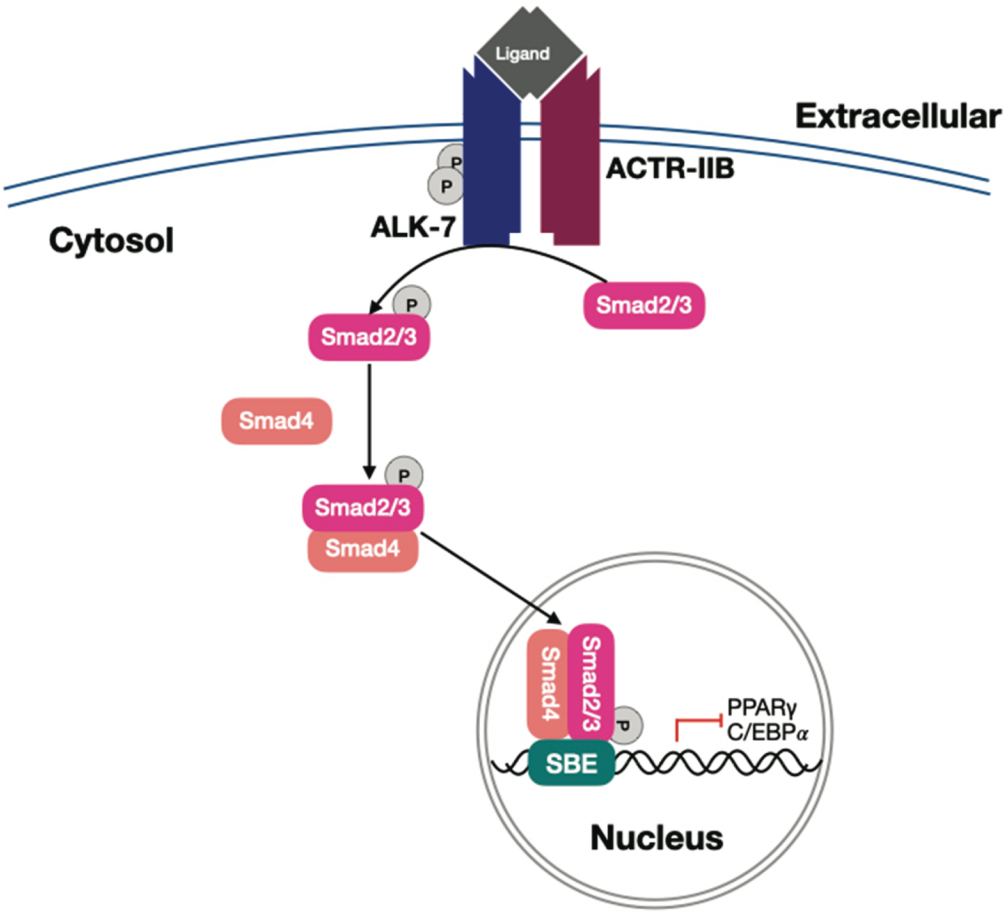

Figure 4.2 The Smad-dependent signalling pathway mediated through ALK-7. An active ligand/receptor complex is composed of two ALK-7, two ACTR-IIB and a dimeric ligand. Ligands, such as Nodal, bind to ACTR-IIB, which phosphorylates the GS domain of ALK-7. ALK-7 is then activated and phosphorylates Smad2/3. Phosphorylated Smad2/3 recruits Smad4 to form a Smad complex, which subsequently translocates to the nucleus and binds with SBEs to regulate downstream gene transcription. In the setting of an adipocyte, the ALK-7 mediated Smad signalling pathway has been implicated in the downregulation of PPARγ and C/EBPα expression.

The Smad signalling pathway is ubiquitous and functions universally in response to the TGF-β superfamily (*242*). However, several alternative signalling pathways independent of Smads have been elucidated in a cell type-specific manner (*242*, *246*). Studies have reported that ALK-7 activation can initiate several different non-Smad signalling pathways, for example via MEK (mitogen-activated protein kinase kinase)-ERK1/2 in the murine heart, or via MAPK-ERK and JNK in a rat pheochromocytoma cell line (*281*, *445*). In addition, some Smad-independent pathways function in concert with the canonical Smad signalling pathways to promote TGF-β

superfamily responses (*242*). For example, ALK-7 induced apoptosis through the activation of MAPK and JNK via a Smad-dependent mechanism in hepatoma cell lines (*446*).

4.2.4 Predicted functional impact of ALK-7 variants

In agreement with our findings, two separate groups have identified the same variants in the *ALK7* gene which are associated with reduced WHR and a lower risk of T2D (*1*, *18*, *451*). *In silico* software analysis and structural modelling predict that both variants p.I195T and p.N150H would impair the function of the gene (*1*, *18*). Particularly the p.I195T variant, which shows a more deleterious functional consequence than p.N150H, appears to have a greater phenotypic impact on WHR and risk of T2D than p.N150H, indicating that the severity of the loss of ALK-7 function could potentially influence the magnitude of the alteration of body fat distribution and the protection from T2D (*1*, *18*).

The isoleucine at position 195 lies within a "hinge" between the GS and kinase domains (Figure 4.3 A). This residue is also tightly packed against both domains and is expected to be involved in the movement of the GS and kinase domain once ALK-7 is phosphorylated and activated (*1*). Since the side chain of I195 is buried in a hydrophobic environment, the effect of the change from a hydrophobic non-polar amino acid to a smaller polar residue could be striking. Besides, I195 is only occasionally replaced with another hydrophobic amino acid valine in the whole family of type I receptor kinases, indicating that this residue is highly conserved (Figure 4.3 B) (*1*). Replacement with threonine could ultimately disturb the kinase domain and affect the interaction with Smads, thereby abolishing its function as a receptor for extracellular signal transduction. On the contrary, the asparagine at position 150 resides in the linker region between the transmembrane and the GS domain (Figure 4.3 A). This residue, as well as this region, is poorly conserved among the members of the type I receptor kinase family, where other types of amino acids with hydrophobic side chains or electrically charged residues are observed (Figure 4.3 C). The substitution with histidine results in a bigger positively charged residue, hence the local conformation might be slightly destabilised. However, due to the lack of a modelling template, no definite prediction could be made regarding the functional impact of the p.N150H variant (*1*).

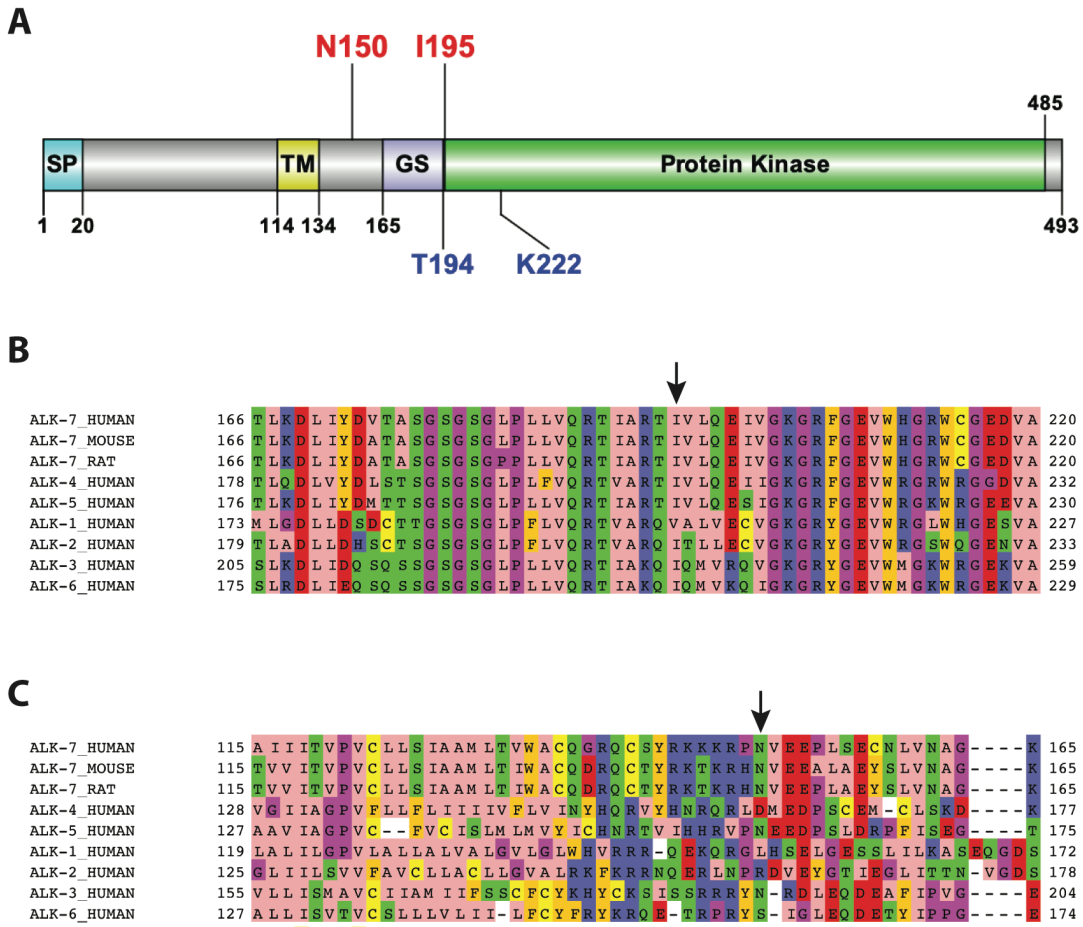

Figure 4.3 Location of the human ALK-7 p.I195T and N150H variants. (A) Domain organisation of human ALK-7. Human ALK-7 is composed of a signal peptide (SP), a ligand binding domain, a transmembrane domain (TM), a GS domain followed by a protein kinase domain. Residues T194 in the GS domain and K222 in the protein kinase domain are indicated. The location of the two missense variants at position 150 and 195 are labelled in red. (B, C) Alignment of ALK-7 sequence segments from selected species and human paralogues. The mutated residues I195 (B) and N150 (C) are indicated with arrows. The domain graph was generated by GPS (*249*) and sequence alignment was performed with Jalview (*468*).

4.3 Materials and Methods

4.3.1 Cloning strategy

The pEYFP-C1 plasmids containing the sequence of wild type (WT) human PNPLA2 or the N252K variant were gifts from Prof Rudolf Zechner (University of Graz, Austria). Catalytically inactive mutants S47A with either WT or N252K background were generated by site-directed mutagenesis as described in 2.1.10. The set of primers are listed in Appendix 2. Sequences of all constructs were verified by Sanger sequencing as described in 2.1.11. Sequences were analysed against the *PNPLA2* reference sequence (Transcript ID: ENST00000336615.9) obtained from Ensembl.

ALK-7 constructs cloned in a pcDNA3.1 vector backbone, including WT, I195T, N150H, K222R (kinase defective mutant) and T194D (constitutively active mutant), were kind gifts from Dr Nuno Rocha (*248*, *260*). The kinase defective mutant K222R has been shown to inhibit the kinase activity previously, while the constitutively active mutant T194D was able to enhance the transduction signalling activity without any ligand stimulation (*248*). Other ALK-7 associated constructs, ACVR-IIB and CRIPTO, were also shared by Dr Nuno Rocha. The pGL4.48[*luc2P*/SBE/Hygro] vector and *Renilla* luciferase control reporter vector pRL-SV40 vectors were purchased from Promega (USA). The empty pcDNA3.1 vector was used as a negative control compared to the ALK-7 constructs.

4.3.2 Cell culture

COS-7 and HEK293 cells were maintained as described in 2.2.1 to study the intracellular localisation of PNPLA2 constructs, and Smad signalling transduction activity via ALK-7, respectively.

4.3.3 Transient transfection

COS-7 cells were seeded in 12-well tissue culture plates at a density of 60,000 cells per well and were transfected with 300 ng of plasmid DNA containing the PNPLA2 constructs using Lipofectamine LTX with PLUS Reagent according to the manufacturer's manual the following day. After 4 hours of transfection, 400 µM oleic acid (BSA-conjugated) was added to the media for 20 hours to promote lipid droplet formation.

HEK293 cells were seeded at a density 150,000 cells per well in a 24-well tissue culture plates pre-treated with poly-D-lysine. On the following day, medium was replaced with Opti-MEM I Reduced Serum medium and a total amount of 550 ng of plasmid DNA were used to transfect HEK293 cells using Lipofectamine 3000 Reagent following the manufacturer's protocol. Opti-MEM I Reduced Serum medium was then replaced with DMEM growth medium 6 hours post transfection. At 24 hours post transfection, cells were serum starved in serum-free DMEM medium for another 24 hours prior to Nodal stimulation. Recombinant human Nodal protein (R&D Systems, USA) was supplemented in the media to stimulate the cells at a concentration of 200 ng/ml for 24 hours.

Stock solution of recombinant human Nodal protein (100 µg/ml) was prepared by reconstituting in 4 mM HCl containing 0.1% BSA according to the product datasheet.

4.3.4 Dual-luciferase reporter assay

Nodal stimulated, as well as non-stimulated HEK293 cells were washed once with DPBS, followed by an active lysis procedure, according to the manufacturer's manual. Briefly, 125 µl of passive lysis buffer was added in each well and the cells were subjected to one cycle of a freeze-thaw process. Cell lysates were cleared of cell debris by centrifugation at 21,130 *x g* for one minute.

The dual-luciferase reporter assay was performed following the manufacturer's protocol. The assay was conducted in a 96-well plate format. In each assay, 20 µl of cleared supernatant was pre-dispensed, followed by sequential measurement of firefly and *Renilla* luciferase using a Tecan Spark 10M plate reader (Tecan, Switzerland). Firefly luciferase activity was

normalised for *Renilla* luciferase activity, and then further normalised with values from non-stimulated cells transfected with empty pcDNA3.1 vector (EV).

4.3.5 Real-time quantitative PCR (qPCR)

Isolated PBMCs from participants in the Fenland study were used for *PNPLA2* mRNA analysis, including 106 randomly selected homozygous WT C allele carriers and 26 heterozygous G allele carriers. The Fenland study is a population-based cohort study with more than 10,000 participants recruited across Cambridgeshire in the UK at the beginning of 2005 (https://www.mrc-epid.cam.ac.uk/research/studies/fenland/). PBMCs were isolated from these participants using Ficoll-Paque (VWR International, USA) density gradient centrifugation from 20 ml aliquots of whole blood with sodium citrate as an anticoagulant (*1*). Cells were then resuspended in 1 ml of KnockOut Serum Replacement media (Sigma-Aldrich, USA) in the presence of DMSO at a concentration of $1x10^7$ cells per ml after a brief PBS wash (*1*). These cells were frozen in cryovials at -80°C and then transferred to liquid nitrogen for storage (*1*).

Frozen PBMCs obtained from the MRC Epidemiology Unit were thawed rapidly by placing the cryovials in a 37°C water bath, and then transferred dropwise to a centrifuge tube containing 9 ml of Roswell Park Memorial Institute 1640 medium (Sigma-Aldrich, USA) supplemented with 10% (v/v) FBS, 100 units/ml penicillin and 100 µg/ml streptomycin. The cell suspensions were spun down at 200 *x g* for 10 minutes at RT to remove DMSO. The PBMC pellets were lysed in 100 µl RLT Plus supplemented with 1% (v/v) β-mercaptoethanol and kept at -80°C until all samples were collected for RNA extraction. Isolation of RNA and cDNA synthesis was performed as described in 2.3.1 and 2.3.2, respectively. A total amount of 0.1 µg of RNA was reverse transcribed to cDNA and used as a template for qPCR to determine *PNPLA2* gene expression as described in 2.3.3. The TaqMan gene expression assays used in this study have been listed in Appendix 4. The mRNA expression of *PNPLA2* was normalised to expression of hypoxanthine-guanine phosphoribosyltransferase (*HPRT1*), a housekeeping gene, and then further normalised to WT controls.

4.3.6 Western blotting

Protein samples were prepared as described in 2.4.1 and were subjected to SDS-PAGE followed by western blotting as described in 2.4.2. Details of antibodies used in this study are included in Appendix 5.

4.3.7 Confocal microscopy

Transfected COS-7 cells were fixed and stained with the HCS LipidTOX Deep Red Neutral Lipid Stain for lipid droplet staining and mounted with ProLong Gold Antifade Mountant with DAPI as described in 2.5.1. The intracellular localisation of PNPLA2 was determined using confocal microscopy as described in 2.6. In this study, DAPI was excited with a 405 nm laser and emission was detected between 420 and 460 nm. The fluorescence of YFP-tagged PNPLA2 was excited with a 514 nm laser and emission was detected between 520 and 545 nm. LipidTOX Deep Red was excited with 633 nm and emission was detected between 640 and 680 nm. Antibodies and fluorescent dyes used for immunofluorescence in this study are provided in Appendix 5.

4.4 Results

4.4.1 Functional analysis of PNPLA2 p.N252K

4.4.1.1 Gene expression of human PNPLA2 variant

Given the possibility that the PNPLA2 p.N252K variant might affect splicing and thus trigger nonsense mediated mRNA decay, we began by checking the expression of *PNPLA2* mRNA in human PBMCs.

PBMCs taken from 106 homozygous carriers of WT C allele and 26 heterozygous carriers of variant G allele from the Fenland study were used to analyse the association between genotype and *PNPLA2* gene expression. Total mRNA from PBMCs was extracted and qPCR analysis was performed. Figure 4.4 A shows that the overall expression level of *PNPLA2* mRNA was approximately 20% lower in heterozygous carriers of the G allele (0.81±0.23) compared with individuals homozygous for the WT C allele (1.00±0.54). Comparison between the overall expression of *PNPLA2* mRNA was also conducted after 4 sample outliers (2.479, 2.332, 2.590, and 5.081) were excluded from the WT group. Consequently, the overall expression level of *PNPLA2* mRNA was only approximately 12% lower in heterozygous carriers of the G allele (0.88±0.25) than that in homozygous for the WT C allele (1.00±0.29), resulting in no statistical difference between the two groups (P = 0.0598) (data not shown).

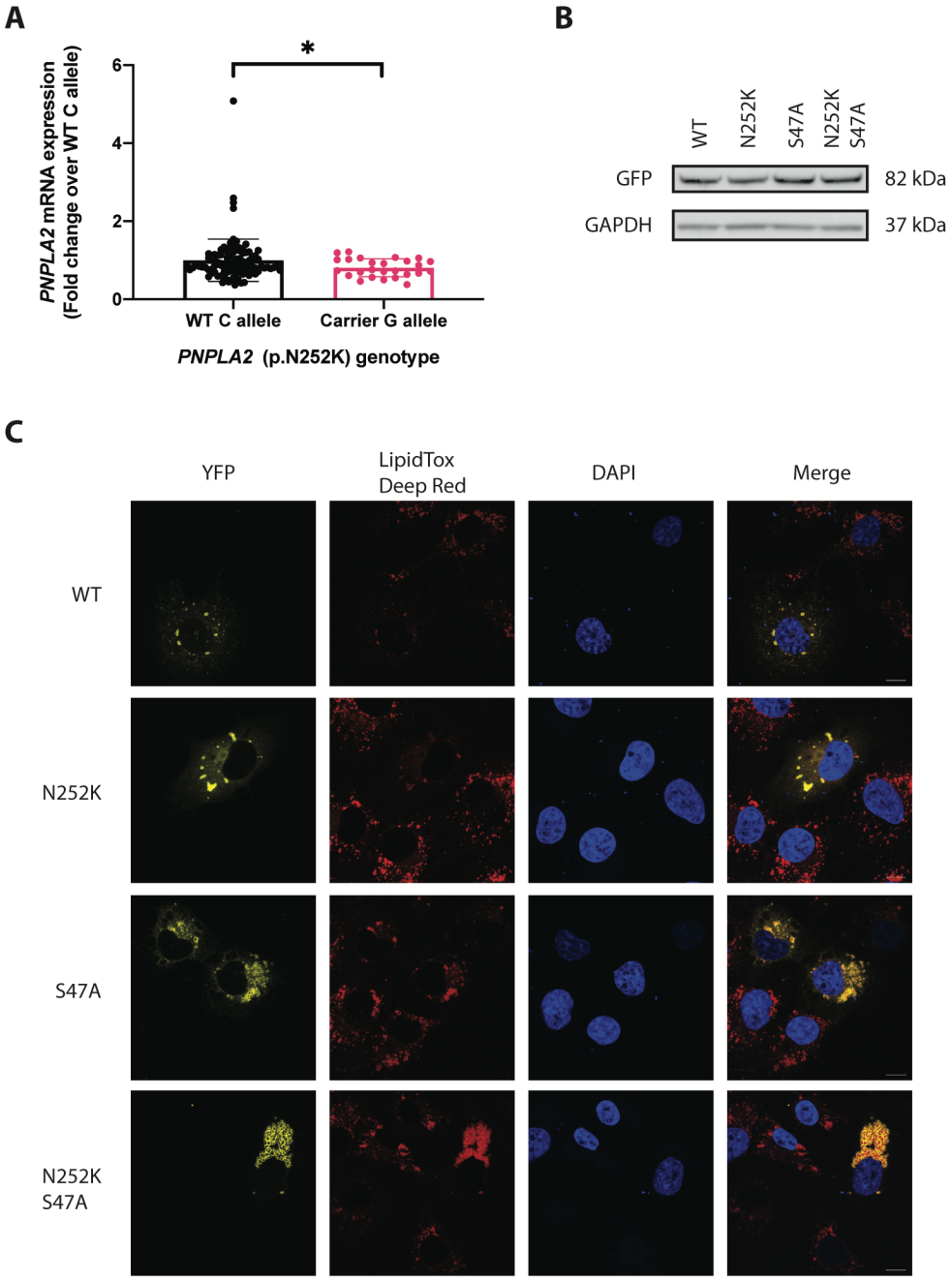

Figure 4.4 Characterisation of PNPLA2 N252K on gene expression and intracellular localisation. (A) Overall mRNA expression of *PNPLA2* in PBMCs obtained from 106 random selected WT homozygous C allele and 26 mutant heterozygous G allele carriers. The level of *PNPLA2* expression was normalised to *HPRT1* and further normalised to WT and presented as fold change. Data presented as mean ± SD. Statistical significance was evaluated by Mann-Whitney test. * $P < 0.05$. (B, C) PNPLA2 constructs tagged with YFP were transfected in COS-7 cells followed by oleic acid loading. (B) The expression of YFP-tagged WT, N252K, S47A and N252K S47A was assessed by western blotting using anti-GFP antibodies, while GAPDH was used as a loading control. Blots are representative of three independent experiments. (C) The intracellular localisation of PNPLA2 constructs was examined by immunofluorescence. Images are representative of three independent experiments. Scale bars, 10 μm.

4.4.1.2 The PNPLA2 variant is able to target lipid droplets

To determine the intracellular localisation of the PNPLA2 variant, both YFP-tagged PNPLA2 WT and N252K constructs were overexpressed in COS-7 cells loaded with oleic acid. Both constructs were found to be localised on lipid droplets by immunofluorescence microscopy (Figure 4.4 C). Although not formally quantified, the size of lipid droplets in cells positively transfected with either WT or N252K cells appeared to be smaller than in untransfected cells, suggesting that they were undergoing active lipolysis mediated by PNPLA2 (Figure 4.4 C). When S47A, a catalytically inactivating mutation was introduced to both WT and N252K PNPLA2 constructs, the size of lipid droplets was visually comparable to that of untransfected cells, suggesting that the alteration seen in lipid droplet size is likely related to the enzymatic activity of PNPLA2 (Figure 4.4 C). The expression levels of all PNPLA2 constructs were validated by western blotting analysis (Figure 4.4 B).

4.4.1.3 Activity of the PNPLA2 variant

Enzyme activity of the N252K variant was assessed in collaboration with the Zechner laboratory. The results are reviewed in the discussion section of this chapter.

4.4.2 ALK-7 mediated Smad signalling

In order to reconstitute ALK-7 signalling in HEK293 cells, different pcDNA3.1 based ALK-7 constructs listed in Table 4.1 were co-transfected into HEK293 cells with constructs encoding receptor components (ACVR-IIB and CRIPTO) along with firefly and *Renilla* luciferase reporter plasmids. After 48 hours of transfection, cells were stimulated with Nodal, a known ligand of ALK-7, for the dual-luciferase reporter assay.

Table 4.1 Overview of ALK-7 co-transfection conditions.

pcDNA3.1 construct	Receptor components
WT	ACVR-IIB, CRIPTO, pGL4.48[*luc2P*/SBE/Hygro], pRL-SV40
I195T	ACVR-IIB, CRIPTO, pGL4.48[*luc2P*/SBE/Hygro], pRL-SV40
N150H	ACVR-IIB, CRIPTO, pGL4.48[*luc2P*/SBE/Hygro], pRL-SV40
K222R	ACVR-IIB, CRIPTO, pGL4.48[*luc2P*/SBE/Hygro], pRL-SV40
T194D	ACVR-IIB, CRIPTO, pGL4.48[*luc2P*/SBE/Hygro], pRL-SV40
EV (empty vector)	ACVR-IIB, CRIPTO, pGL4.48[*luc2P*/SBE/Hygro], pRL-SV40

Overall, Nodal stimulation failed to induce luciferase activity compared to the basal state (Figure 4.5 A). As illustrated in Figure 4.5 A, HEK293 cells that were transfected with WT ALK-7 and its receptor complex showed high basal luciferase activity (8.48±1.54), although this was comparable to the levels observed after stimulation with Nodal (8.25±1.62). However, luciferase activity in cells transfected with the EV construct showed much lower levels of luciferase activity, suggesting that activation was indeed due to the exogeneous expression of ALK-7 (1.00±0.86 at basal and 1.59±0.82 with Nodal) (Figure 4.5 A and B). As expected, the kinase defective construct K222R showed a substantial decrease in luciferase activity compared to the WT regardless of Nodal stimulation (basal 1.97±0.62 and stimulated 3.16±0.35) (Figure 4.5 A). Due to the unexpected high basal luciferase activity observed in WT expressing cells, the constitutively active construct T194D did not appear to have significantly different activities compared to WT in both the basal (6.87±1.83) and Nodal-stimulated conditions (5.99±1.07) (Figure 4.5 A). Similarly to what was observed for T194D, basal

(9.91±1.45) as well as Nodal stimulated (10.06±2.23) luciferase activity was high in N150H expressing cells but not significantly different from that in the WT cells (Figure 4.5 A). On the other hand, I195T expressing cells showed substantially diminished luciferase activity compared to WT cells in both the non-stimulated (1.24±0.50) and Nodal stimulated (2.22±0.48) conditions (Figure 4.5 A).

Interestingly, the expression levels of the various ALK-7 constructs were consistently different (n=3) (Figure 4.5 B). Western blotting against ALK-7 showed that the expression of WT ALK-7 was lower than the constitutively active construct T194D, which had the highest expression level among all the constructs, while protein expression of the kinase defective construct, K222R, was barely detectable (Figure 4.5 B). Meanwhile, similar protein expression was observed between the two variants I195T and N150H (Figure 4.5 B). However, ALK-7 protein expression for individual constructs did not seem to differ between the non-stimulated and stimulated cells (Figure 4.5 B).

As shown in Figure 4.5 B, the expression of total Smad2 appears to be comparable in all conditions. Moreover, phosphorylation of Smad2 was in general elevated upon Nodal stimulation in all genotypes, based on protein densitometric calculation of the p-Smad2 to total Smad2 ratio (p-Smad2/Smad2) (Figure 4.5 B and C). In fact, there was a two-fold induction of p-Smad2/Smad2 in EV expressing cells upon Nodal stimulation (2.00±0.48) compared to the basal state (1.00±0.40) (Figure 4.5 C). Overexpression of WT ALK-7 increased the level of p-Smad2/Smad2 even when cells were not stimulated (1.96±0.75), while treatment with Nodal further induced the p-Smad2/Smad2 levels by approximately 2.3-fold (4.50±2.16) (Figure 4.5 C). However, the differences between WT and EV in both conditions were not significant. The level of p-Smad2/Smad2 in K222R expressing cells exhibited a similar pattern to that seen in EV expressing cells (1.00±0.75 at basal and 2.22±0.73 when stimulated), which did not reach statistically significant difference either when compared with WT (Figure 4.5 C). The constitutively active mutant T194D showed the highest p-Smad2/Smad2 levels in the absence (4.84±0.99), as well as in the presence of Nodal (6.86±2.48) (Figure 4.5 C). A slight but not significant increase of p-Smad2/Smad2 was observed in N150H expressing cells in the non-stimulated condition (3.22±0.70) compared to WT (Figure 4.5 C). However, the p-Smad2/Smad2 levels in these cells upon Nodal stimulation (4.68±0.95) was comparable with

that in WT transfected cells (Figure 4.5 C). In contrast, p-Smad2/Smad2 in cells expressing I195T tended to be lower than WT in both non-stimulated (1.38±1.03) and stimulated (2.12±0.52) conditions, although the differences were not significant (Figure 4.5 C).

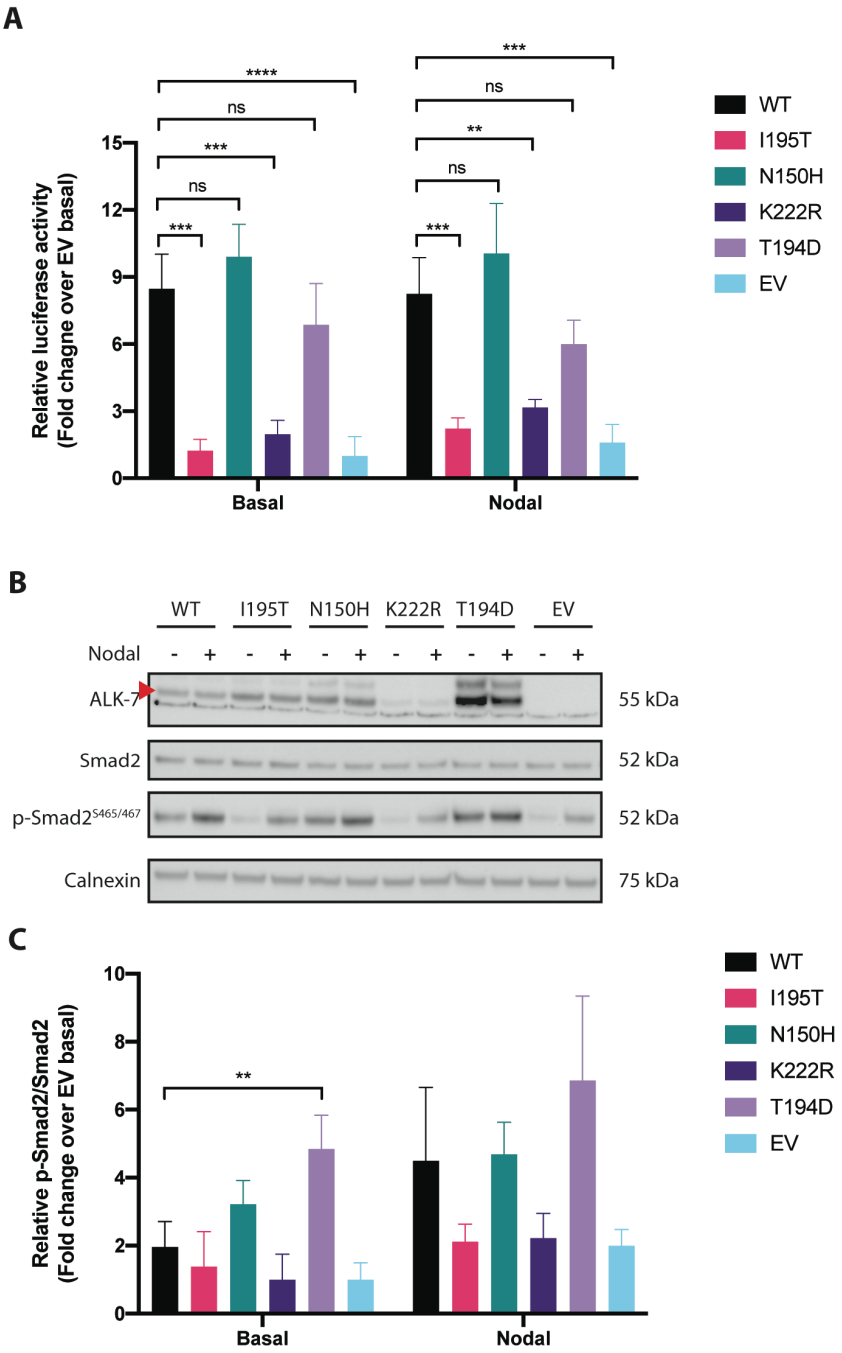

Figure 4.5 Functional impact of ALK-7 variants on Smad signalling. HEK293 cells were transiently transfected with ALK-7 constructs and their receptor components, along with firefly and *Renilla* luciferase expression plasmids. Cells were treated with or without Nodal 48 hours post transfection. (A) Firefly luciferase activity was normalised to *Renilla* activity, the luciferase activity in non-stimulated cells transfected with EV was set to 1. Results from three independent experiments are presented as mean ± SD. (B) Expression of ALK-7 constructs, as well as phosphorylated and total Smad2 levels, were assessed by western blotting. Calnexin was served as a loading control. Blots are representative of three independent experiments. The red arrowhead denotes the correct ALK-7 band. (C) Densitometric analysis was performed by taking the ratio of p-Smad2 to total Smad2 and further normalised to EV basal. Results from three independent experiments are presented as mean ± SD. In A and C, statistical significance was evaluated by one-way ANOVA with Tukey's post hoc test for multiple comparisons between pairs in either basal or Nodal group. **** $P < 0.0001$, *** $P < 0.001$, ** $P < 0.01$, ns not significant.

4.5 Discussion

4.5.1 Reduced expression of PNPLA2 mRNA in carriers

As described previously in the introduction, the nucleotide change from C to G at position 756 occurs at position -2 near the 5' donor splice site in exon 6 of the human *PNPLA2* gene (Figure 4.1 B) (*1*). This substitution is predicted to have a high likelihood of resulting in exon skipping (*1*). This *in silico* analysis led to the hypothesis that expression levels of *PNPLA2* could potentially be affected in p.N252K carriers (*1*).

PBMCs represent a set of blood cells, including lymphocytes and monocytes, with unique features that render them useful in disease prognosis and diagnosis (*569*, *570*). Firstly, PBMCs carry distinctive transcriptomic signatures amongst individuals, which may function as biomarkers for diseases such as cancer (*570*, *571*). It has been reported that on average more than 80% of genes expressed in a range of tissues, such as brain, heart and liver, are also expressed in the blood cells (*570*). These overlapping genes found in peripheral blood cells as well as in other tissues are not limited to housekeeping genes, but also include tissue-specific genes (*570*). In addition, some studies have demonstrated that alterations in gene expression patterns from PBMCs reflect changes in response to physiological and environmental cues, as well as dietary status (*569*, *570*). It is also evident that there is a relationship between gene expression levels in PBMCs and the metabolic syndrome (*572–574*). Last but not least, peripheral blood can be collected easily and repeatedly with minimal discomfort or risk compared to other tissue biopsies, which are sometimes impractical to obtain (*569–571*). Considering that the MAF of *PNPLA2* p.N252K is only 1.4%, PBMCs were therefore chosen to be utilised as a source to analyse overall *PNPLA2* mRNA expression. qPCR data suggested that heterozygous G allele carriers indeed had approximately 20% lower mRNA expression of *PNPLA2* on average compared to homozygous WT C allele participants. However, the difference in the overall expression of *PNPLA2* mRNA between the two groups failed to remain significant after removing the outliers in the WT group (data not shown). Since the primers used in this assay were not designed to detect the G allele-specific mRNA expression in the carriers, the overall expression of *PNPLA2* mRNA detected in the carriers could therefore potentially be driven by the WT C allele. A more relevant approach for quantitative

allele-specific expression analysis would be to amplify the region containing the mutated nucleotide with an allele-specific primer using PCR or qPCR (*575*, *576*).

Although reduced overall expression of *PNPLA2* was observed in PBMCs obtained from carriers with the heterozygous G allele, it would still be interesting to investigate the association between *PNPLA2* genotypes and expression levels specifically in adipose tissue where PNPLA2 is highly enriched. Lotta et al. analysed *PNPLA2* mRNA expression in RNAseq data obtained from SAT of four unrelated female heterozygous G allele carriers recruited for the TwinsUK study (*1*). Interestingly the number of mutant reads was 21% lower than that of WT reads, and statistical analysis indicated a significant difference within three out of four individuals (*1*). To summarise, mutant G allele specific expression was indeed reduced in heterozygous carriers, this could potentially lead to lower PNPLA2 protein expression, and ultimately less LD-associated PNPLA2 to catalyse TG hydrolysis. Whether this phenotype is necessarily caused by alternative splicing will be discussed in the next section.

4.5.2 The impact of substitution at PNPLA2 c.756C>G on RNA splicing

So far it has been established that the overall expression of *PNPLA2* mRNA is on average lower in carriers with a heterozygous G allele than homozygous C allele. The reduced expression level may be driven by alternative splicing due to its position near the splice junction in exon 6 (*1*). Computational algorithms suggest that the mutation at c.756C>G may create a new exonic splicing silencer (ESS) motif and break an existing exonic splicing enhancer (ESE) motif (Figure 4.6) (*577*).

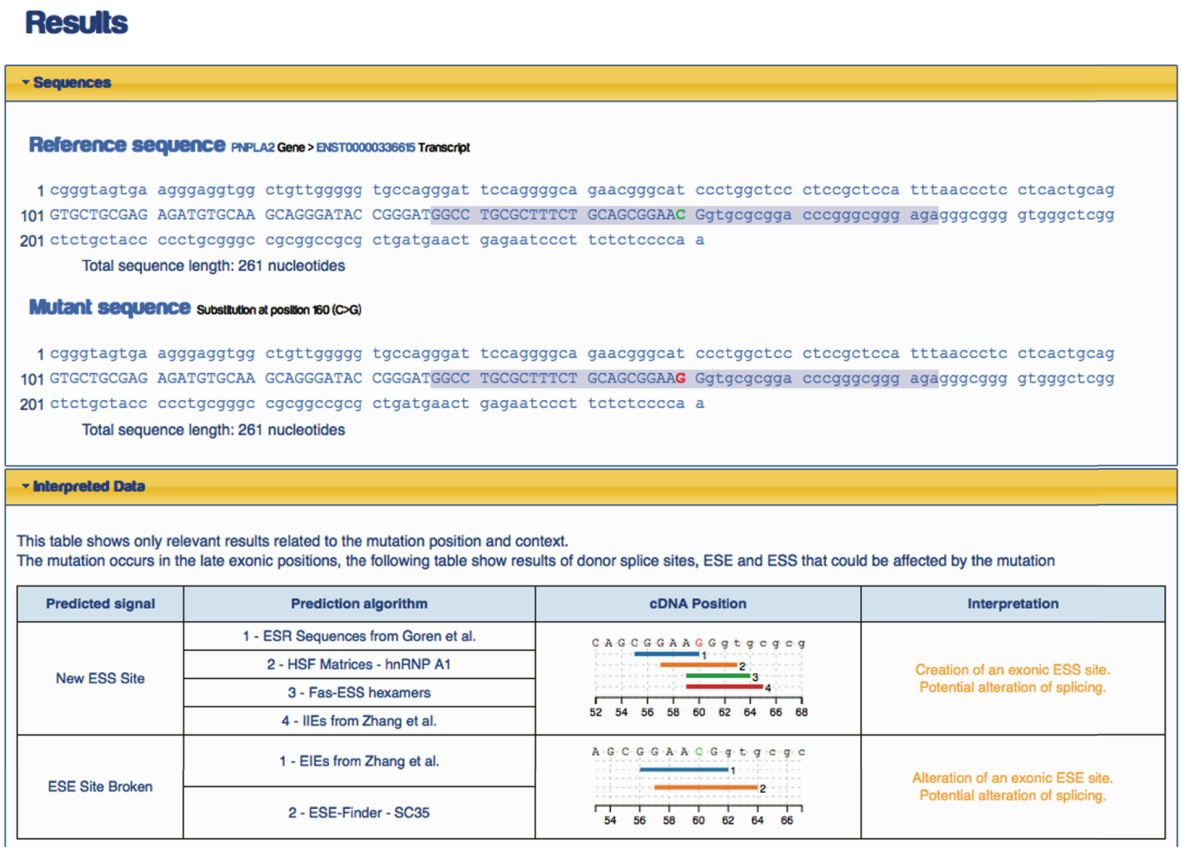

Figure 4.6 The predicted effect of the *PNPLA2* c.756C>G on splicing signals. *In silico* prediction shows that the mutation c.756C>G could result in exon skipping by creating a new ESS site and breaking an existing ESE site. The analysis was performed using Human Splicing Finder (*570*).

RNA splicing is a process that removes introns and ligates exons together from pre-mRNA to form mature mRNA. This process is involved in the assembly of a highly dynamic ribonucleoprotein complex termed the spliceosome, which consists of five small nuclear RNAs and a range of protein factors (*578*). It is a fundamental step in the post-transcriptional regulation of gene expression (*578*). Mutations that occur in or near splice sites can affect the pre-mRNA splicing pattern through *cis*-acting elements or *trans*-acting factors, resulting in alternative splicing (*578*, *579*). The ESS and ESE are such regulatory sites located in the exons and function to suppress or promote splicing activity by binding with negatively or positively acting factors, respectively (*578*, *579*). Taking *PNPLA2* c.756C>G as an example, it is predicted to inhibit splicing activity leading to a higher probability of exon skipping (Figure 4.6).

To identify any alternative transcripts caused by the *PNPLA2* c.756C>G variant, 3' RACE (abbreviated for rapid amplification of cDNA ends) followed by Sanger sequencing was

performed by Dr Koi Ni Lim, a postdoctoral fellow in our laboratory. Briefly, total mRNA was extracted from PBMCs obtained from carriers with both the homozygous C allele and the heterozygous G allele, and then reverse transcribed to cDNA using an oligo(dT) primer. Two rounds of nested PCR were conducted using gene-specific primers to amplify the 3' end flanking the exons and the poly(A) tail (*580*). A final round of PCR was performed to amplify the fragment between exon 4 and 8 in order to capture all possible transcripts. These PCR products were then cloned into a TOPO cloning vector for propagation, and subsequently sequenced by Sanger sequencing. No evidence of exon skipping was observed in heterozygous G allele carriers (unpublished data).

There are two conserved splice sites located in the 5' (donor, GU) and 3' (acceptor, AG) ends of the intron region, which are required for constitutive splicing (*581*). Any variations in these four splice sites would cause disruption to normal splicing (*582*). However, studies have suggested that sequences ±25bp from both splice junctions are also important, and single nucleotide substitutions associated with human genetic diseases occur more frequently near donor than acceptor splice sites (*582–584*). One study particularly focusing on the quantification of mutational intolerance for bases at ±10bp around splice sites has shown that nucleotide change at donor position -2 is tolerable, although A and C are preferred (*581*). This could possibly explain the absence of any detectable splicing defects in the heterozygous mutant carriers.

So, for now the data does suggest that the *PNPLA2* p.N252K variant reduces *PNPLA2* mRNA expression in PBMCs and possibly in adipose tissue too, but the underlying mechanism as well as the impact on protein expression remain unknown.

4.5.3 Localisation and enzymatic activity of the PNPLA2 N252K variant

The intracellular localisation of the mutant PNPLA2 appeared to be unaffected. This is not surprising as the C-terminus, particularly the hydrophobic stretch, which is involved in LD targeting, is still intact in the N252K mutant. However, visualisation of LDs by lipid staining was limited by the enzymatic nature of PNPLA2, resulting in a reduction in the size of LDs in transfected cells. Therefore, a catalytically defective mutation, S47A, was introduced into

both WT and N252K constructs for better visualisation of PNPLA2 targeting on LDs. Indeed, they were both still found to be associated with LDs when overexpressed in COS-7 cells supplemented with oleic acid. The subcellular localisation of WT and S47A observed in this study is in agreement with previous findings from various cell lines (*403*, *410*, *416*, *585*).

As demonstrated in the work from Lotta et al., the *PNPLA2* p.N252K variant is associated with higher TG and low-density lipoprotein-cholesterol levels, leading to an increased cardiometabolic risk in the general population (*1*). Although the mutation occurs immediately downstream of the three-layer α/β/α sandwich fold, the patatin domain which contains the catalytic dyad for its lipase activity, as well as its binding with co-factors, is not affected. Additionally, computational modelling has indicated that the amino acid change does not seem to cause destabilisation of the quaternary structure of the α/β/α sandwich fold (*1*). Therefore, the hypothesis is that the enzymatic activity may not be distinguishable between WT and N252K. Nevertheless, efforts were made to evaluate the impact of this variant on TG hydrolase activity in collaboration with Prof Rudolf Zechner. In brief, COS-7 cells overexpressing PNPLA2 constructs, both WT and N252K, were collected and incubated with either purified human ABHD5 or G0S2, in the presence of radiolabelled triolein as substrate (*1*, *586*). Fatty acids were then extracted, and radioactivity was detected by a liquid scintillation counter (*1*, *586*). As expected, radioactivity was greatly elevated when PNPLA2 was incubated with ABHD5, and markedly suppressed by G0S2 (*1*). However, TG hydrolase activity of PNPLA2 did not show any differences between the WT and the N252K variant, regardless of the presence of its co-factors (*1*). This is consistent with what has been reported for this variant previously by Coassin et al. (*521*).

4.5.4 ALK-7 and Smad signalling

ALK-7 has been implicated in a number of studies for its role as a type I receptor kinase for extracellular ligands, such as Nodal, activin B and GDF-3 (*267–270*). The design of my study was to use a firefly luciferase reporter gene activated by SBEs upon treatment with ligand as a readout to determine the functional consequences of the ALK-7 variants. Such bioassays using reporter genes, including luciferase and β-galactosidase, have been widely used to study signally pathways mediated by ALK-7 and its family members in diverse cell types (*248*, *250*, *268*, *274*, *445*, *552*). As set out in this experiment, a second reporter vector constitutively expressing *Renilla* was co-transfected with the firefly luciferase vector into HEK293 cells to serve as an internal control for any variations in transfection efficiency or cell viability (*587*).

Importantly, it seems as if ALK-7 WT activates luciferase activity without any additional ligand stimulation, and treatment with Nodal did not further enhance the transcription driven by the activation of the SBEs. This mirrors the reporter activity in cells expressing the constitutively active ALK-7 mutant T194D. Theoretically, ligand binding is a prerequisite for activation of ALK-7 through phosphorylation by ACVR-IIB, the type II receptor kinase, thereby initiating downstream signalling. Therefore, we did not expect to observe such a high basal luciferase activity for WT compared to EV and K222R, the catalytically defective mutant. A similar phenomenon was also noticed by another PhD student in Prof Sir Stephen O'Rahilly's laboratory. In their experiments in HepG2 cells, the luciferase activity of WT ALK-7 did not appear to respond to ligand stimulation due to high levels of luciferase activity in the non-stimulated (basal) condition; a slight but statistically non-significant increase in luciferase activity was observed in WT cells treated with Nodal or GDF-3 (unpublished data). Both results contradict the findings from the majority of previous studies where luciferase activity in stimulated cells was induced by two- to six-fold, depending on the experimental cell type, compared to unstimulated cells (*250*, *268*). However, the observed activation of WT ALK-7 in the basal state could be possibly explained by the co-transfection of CRIPTO, a coreceptor for Nodal. It has been suggested that CRIPTO potentiates ALK-7 and ALK-4 activation by Nodal, albeit it is prerequisite for signalling only in the latter case (*274*). However, in addition to its role as a coreceptor, other studies have suggested that CRIPTO itself can also function as a

secreted growth factor-like ligand and interact directly with ALK-7 (*274*, *588*). Therefore, it is possible that the co-expression of CRIPTO might be enough to activate ALK-7 without any ligand stimulation, hence explaining the high level of luciferase activity obtained even when WT expressing cells were not stimulated. Another possibility for the unexpected high basal reporter activity is that HEK293 could be secreting other ligands that share the same ALK-7 signalling pathways, such as activin B.

Despite the unusual observation for HEK293 cells transfected with ALK-7 WT together with its signalling complex, luciferase activities for all relevant control constructs, such as K222R, T194D and EV, showed the expected signalling patterns, in line with previous studies (*248*, *250*). Interestingly, the luciferase activity data for the two ALK-7 variants, I195T and N150H, indicated very different effects on Nodal signalling. Consistent with *in silico* structural modelling predictions, I195T appeared to be a complete loss-of-function mutant following a similar signalling pattern to that of the catalytically defective K222R variant (*1*). On the other hand, the luciferase activity of N150H expressing cells was high regardless of Nodal stimulation and significantly increased compared to that of the constitutively active T194D expressing cells when stimulated, indicating a hyperactive kinase activity. As described previously, ALK-7 signalling has been implicated in lipid remodelling mediated by PPARγ and C/EBPα in mature adipocytes, as loss of ALK-7 function results in elevated lipase levels (*448*). At least in an adipocyte cell line, data from my bioassays suggests that the loss-of-function variant I195T could potentially upregulate lipolysis, while lipolysis might be downregulated by the N150H variant. However, it is interesting to note that both variants have been shown to be associated with greater gluteo-femoral fat with protection from cardiometabolic disease in the general population (*1*). At this point, we do not have a clear explanation for these findings.

Although the reporter assay conducted in this study utilised an internal control for normalisation, one can still argue that any differences observed in luciferase activity could result from differences in the protein expression levels of the ALK-7 constructs. It is true that T194D expression was substantially higher than K222R, which might explain the difference in luciferase activity. Indeed, missense mutations can sometimes alter the expression of the corresponding protein, resulting in the disruption of the protein function which may in turn

cause diseases. For example, a selection of missense mutations associated with chronic pancreatitis in the pancreatic secretory trypsin inhibitor (*SPINK1*) gene have been shown to cause significantly reduced or complete loss of protein expression (*589*). Nevertheless, comparable expression levels of I195T and N150H were observed, and yet signalling transduction activity was significantly different between the two. Therefore, the observed receptor activity of ALK-7 constructs is not solely determined by protein expression levels. Another factor to consider is post-translational modification of ALK-7 as phosphorylation in the GS domain is key for its activation upon ligand stimulation, although deactivation of ALK-7 by dephosphorylation has never been described. However, dephosphorylation of ALK-5 has been reported to be mediated by Smad7, an inhibitory Smad, which recruits the catalytic subunit of protein phosphatase 1 and forms a complex in order to antagonize TGF-β signalling (*590–592*). Another consideration is the regulation of receptor stability, especially the internalisation of receptor complexes (*593*). Studies on TGF-β receptors have shown that the receptor complex can be internalised via clathrin-mediated endocytosis for sustained signalling and receptor complex recycling, or caveolin-positive lipid rafts for degradation via proteasomal and lysosomal pathways (*591–593*). Degradation of ALK-4 receptor complex through the lysosomal pathway to downregulate Nodal signalling has been reported, but it is still unclear whether ALK-7 activity is also modulated in a similar manner (*594*).

Signalling through Nodal activates the receptor complex, which in turn triggers the phosphorylation of intracellular Smad proteins to relay the signals to the nucleus to control gene transcription (*592*). As a result, phosphorylation of Smad2 was examined as a downstream target of ALK-7 mediated Nodal signalling in this study. All ALK-7 constructs tested in the study displayed varying levels of basal Smad2 phosphorylation, the trend of which mirrored the observed luciferase activity in unstimulated cells. Treatment with Nodal increased the phosphorylation of Smad2 to various degrees, indicating that the intracellular signalling cascade was indeed initiated by extracellular ligand binding. However, it should be highlighted that p-Smad2 was also detected in negative control cells, which were only transfected with empty pcDNA3.1 vector along with other ALK-7 associated components. Furthermore, p-Smad2 in EV expressing cells was also further induced by Nodal stimulation, suggesting that there might be some other endogenous receptor complex present on the cell membrane for Nodal signal transduction. Currently the other known type I receptor for Nodal

is ALK-4, which interacts with CRIPTO and also pairs with ACVR-IIB upon Nodal binding to activate R-Smads (*595*). Additional experiments need to be performed to validate this hypothesis.

4.6 Conclusion

In conclusion, the PNPLA2 N252K variant did not alter LD-targeting properties, or have any impact on the ability to hydrolyse TG *in vitro* compared to WT when overexpressed. It should be noted that these findings were obtained *in vitro* where the expression levels between WT and N252K variant were designed to be comparable, which may not be the case *in vivo*. Indeed, reduced mRNA expression of *PNPLA2* was observed in carriers with the heterozygous G allele. As presented in the previous chapter, silencing endogenous *Pnpla2* gene expression in 3T3-L1 adipocytes diminished basal and stimulated lipolysis. Taken together, these observations indicate that reduced *PNPLA2* expression could potentially lead to impaired lipolytic activity in carriers with N252K. It is yet to be elucidated why reduced *PNPLA2* mRNA expression was observed in carriers, if it did not result from exon skipping.

To summarise the data generated from the dual-luciferase reporter assay for Nodal signalling mediated by ALK-7, it demonstrated that I195T impairs Smad signalling, while N150H possibly enhances it regardless of Nodal stimulation, when overexpressed with its associated receptor components in HEK293 cells. Additional work is required to improve the current experimental settings by identifying whether CRIPTO is the cause for the unexpected high basal luciferase activity, as well as verifying possible endogenous signalling pathways. Although this study provides some insight into the functional consequences of the ALK-7 variants, their association with the observed phenotypes in the general population requires further work. As carriers with either variant seem to present similar phenotypes such as larger hip circumference, future studies should perhaps focus on human cellular studies to investigate the depot-specific effects of ALK-7 mutations in the regulation of adipocyte biology (*1*).

5 Functional characterisation of a PLIN1 missense variant associated with altered body fat distribution

5.1 Abstract

The impact of *Plin1* depletion in 3T3-L1 adipocytes on both adipogenesis and lipolysis has been described previously in Chapter 3. This chapter will focus on the functional analysis of the p.L90P PLIN1 variant. This variant is predicted to alter the interaction of PLIN1 with HSL, thus potentially affecting the regulation of lipolysis. Therefore, BiFC was performed to study the PLIN1-HSL interaction. The data suggested that the interaction of the variant L90P with HSL was enhanced compared to that of WT in the non-stimulated (basal) state. In order to further investigate the impact of L90P on adipocyte biology, MEFs derived from *Plin1* null mice were stably transduced with lentiviruses expressing the PLIN1 WT and mutant. Lipid accumulation assessed by Oil Red O staining did not show any differences between WT and L90P expressing MEFs. However, glycerol and FFA release assays demonstrated a reduced lipolytic response to isoproterenol and IBMX stimulation in MEFs expressing the L90P mutant compared with the WT.

5.2 Introduction

5.2.1 The Tet-On system

To study the adipogenic and lipogenic responses of the PLIN1 variant, either the WT or the L90P mutant were ectopically expressed in *Plin1* KO MEFs which lack endogenous *Plin1* expression. In order to generate stable expression, an inducible lentiviral delivery system (pSLIK vector) was used (Figure 5.1) (*596–599*). It is a conditional tetracycline-based system where the tetracycline-response element (TRE) is only activated through binding with the reverse Tet transactivator (rtTA) in the presence of tetracycline, or its derivative doxycycline (Dox), to drive the expression of the gene of interest (Figure 5.1) (*596*, *600*). Therefore, the activation and expression of the gene of interest can be tightly controlled by the concentration of Dox in the culture medium (*601*).

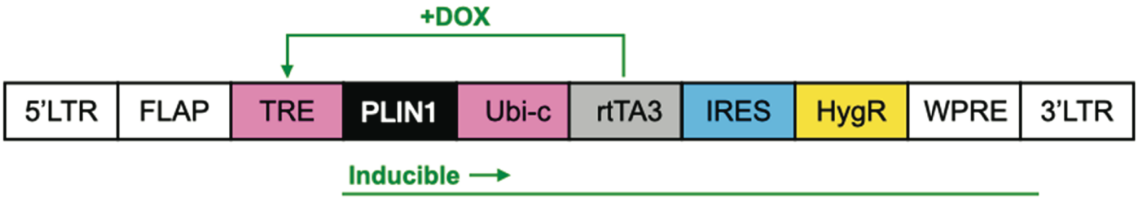

Figure 5.1 Schematic diagram showing the key elements flanking the transgene sequence (PLIN1) in the inducible lentiviral vector. The pSLIK vector includes long terminal repeat (LTR) sequences that facilitate the integration of the target gene into the host cell genome, a DNA FLAP that stimulates the nuclear importation of the viral genome, and a woodchuck hepatitis virus post-transcriptional regulatory element (WPRE) that increases transgene expression (*590*, *591*, *593*). The addition of Dox, indicated in green, allows the rtTA3 (rtTA with three amino acid changes) to bind with TRE and drive the expression of PLIN1 (*592*). Meanwhile, the internal ribosome entry site (IRES) allows the co-expression of the hygromycin resistance marker (HygR) from the same transcript (*593*).

5.2.2 Lipid droplet targeting of PLIN1

PLIN1 is a lipid droplet coat protein but the exact mechanism for PLIN1 to target LDs is not fully understood. As described in Chapter 1, it has been proposed that the N-terminal 11-mer repeat region of PLIN1 folds into amphipathic helices to position PLIN1 onto the surface of LDs (*179*). In addition to the initial LD sensing by the 11-mer repeat region, a more recent study suggests that the C-terminal 4-helix bundle domain unfolds and stabilises PLIN1 association with LDs (*602*).

5.2.3 PLIN1 as a gatekeeper for intracellular lipolysis

As a key regulator of lipid metabolism in adipocytes, PLIN1 resides on the surface of LDs to serve as a protective barrier restricting the access of lipases to suppress basal lipolysis, as well as a recruitment site for lipases to augment stimulated lipolysis (*603*). The switch between its dual roles is mediated by cAMP-dependent PKA phosphorylation (Figure 5.2). In the "basal" or "fed" state, the C-terminus of unphosphorylated PLIN1 sequesters the key lipolysis regulator ABHD5, so that it cannot interact with or activate ATGL (*349*, *350*, *604*). Upon β-adrenergic stimulation or in a "fasted" state, PKA phosphorylates PLIN1 at S492 (S517 in murine PLIN1), which in turn rapidly releases ABHD5 to activate ATGL and initiate lipolysis to

convert TG into DG (*351*). Meanwhile, the phosphorylation of murine ABHD5 at S239 (S237 in human) by PKA facilitates the dispersion of ABHD5 from PLIN1 and increases the availability of ABHD5 for ATGL activation (*604*). On the other hand, phosphorylation of PLIN1 in the N-terminus PAT domain is essential for HSL binding and the conversion of ATGL-derived DGs into MGs (*185*, *342*). Furthermore, PKA also phosphorylates HSL at S563 in rats (corresponding to human S552) which promotes the translocation of HSL from the cytosol to the surface of PLIN1-coated LDs, while phosphorylation at S659 and S660 (equivalent to human S649 and S650) of HSL are involved in the activation of its enzymatic activity (*605*–*607*).

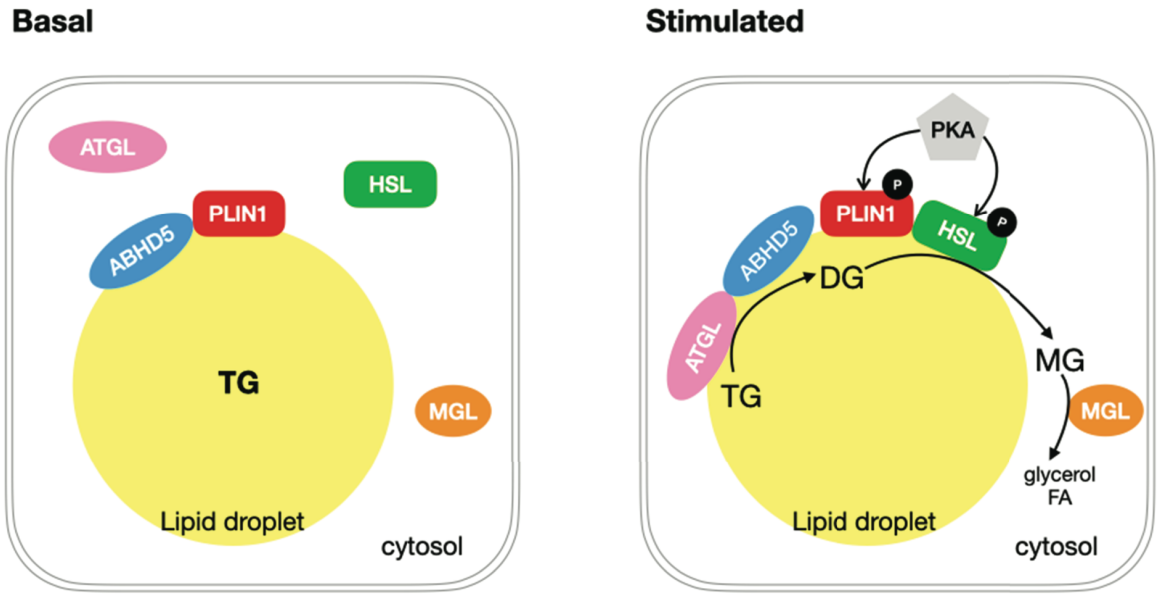

Figure 5.2 PLIN1-mediated intracellular lipolysis in adipocytes. In the basal state (left), PLIN1 is found on the surface of lipid droplets, stabilising ABHD5. However, lipases such as ATGL and HSL, are inactive in the cytosol. Upon lipolytic stimulation (right), PKA is activated and phosphorylates both PLIN1 and HSL. Phosphorylation of PLIN1 results in the dissociation of ABHD5, which subsequently binds to ATGL in order to initiate lipolysis. Meanwhile phosphorylated HSL translocates from the cytosol to the surface of LDs and interacts with phosphorylated PLIN1, leading to the hydrolysis of DG into MG. MGL catalyses the hydrolysis of MG to release glycerol and FA.

5.2.4 Predicted functional impact of the PLIN1 variant

The mutated leucine residue (L90) lies in the highly conserved PAT domain of PLIN1, which provides a binding site for HSL (Figure 5.3 A). Sequence alignment shows that leucine at position 90 is conserved in mammals but can occasionally be replaced by tyrosine in other perilipin proteins (Figure 5.3 B). Since the leucine residue is located within a predicted α-helix, the substitution with proline could introduce a sharp bend due to the missing hydrogen bond, thus disturbing the helix (Figure 5.3 C) (*1*, *608*). Furthermore, as this residue lies in the vicinity of the conserved S81, which is phosphorylated in order to interact with HSL, this mutation could potentially affect intracellular lipolysis by altering the interaction of PLIN1 and HSL (*1*).

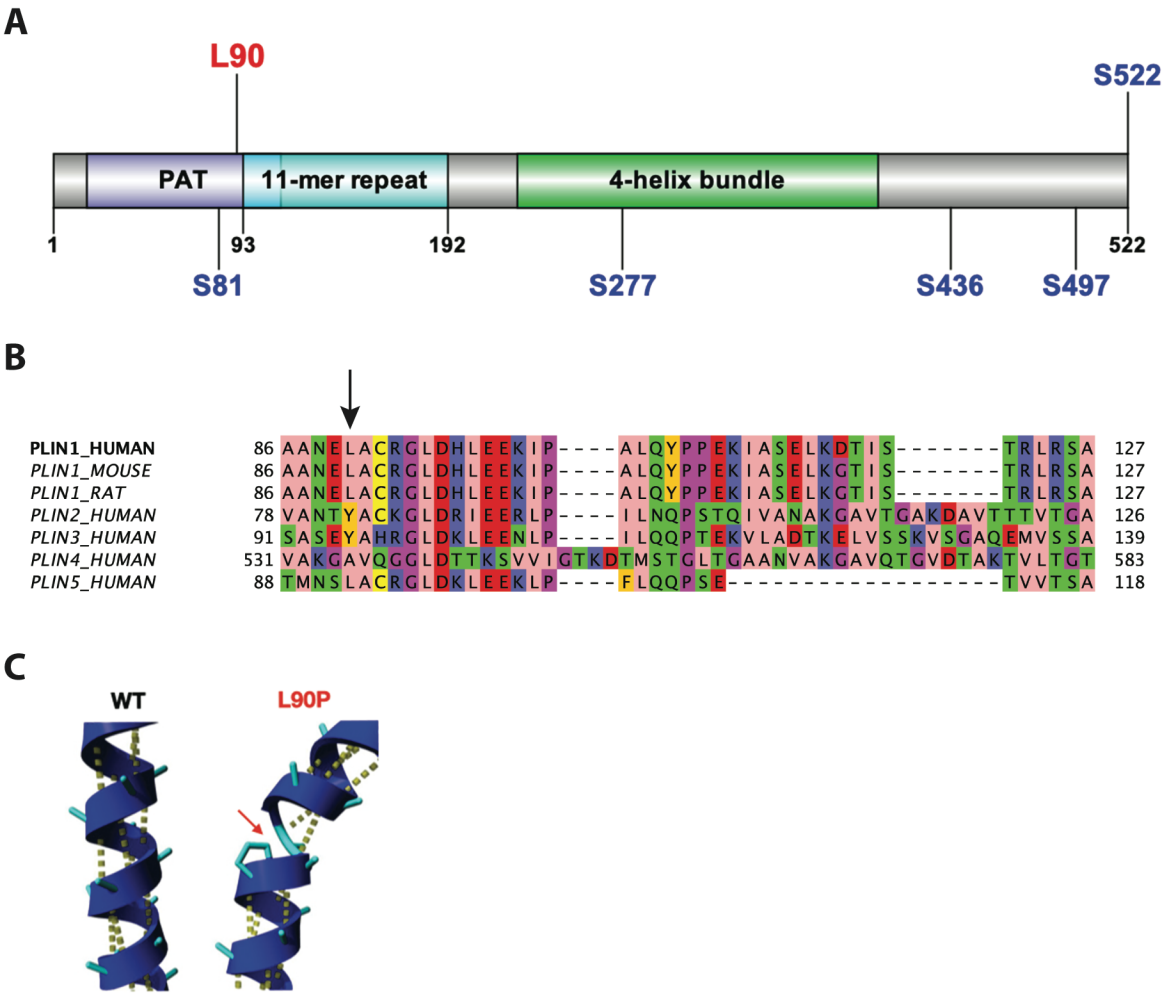

Figure 5.3 Location of human PLIN1 p.L90P variant. (A) Domain organisation of the human PLIN1. Human PLIN1 consists of 522 amino acid residues. The missense variant at residue position 90, labelled in red, is located in the PAT domain and is close to phosphorylation site, S81, indicated in blue. Other putative phosphorylation sites S277, S436, S497 and S522 are also labelled in blue. The 11-mer repeat and 4-helix bundle domains are also indicated. (B) Sequence alignment of PLIN1 segments from selected species and the human paralogues. The mutated residue L90 is indicated by an arrow. (C) Structural impact of the missense mutation L90P of human PLIN1. The residue is predicted to be located in an α-helix with the WT fragment shown on the left, and the mutant helix on the right. The side chain of the mutated proline residue resulting in a missing hydrogen bond is indicated by a red arrow. The domain structure was generated by GPS (*249*), sequence alignment was performed with Jalview (*468*), and the structural difference between WT and L90P was analysed by HOPE (*601*).

5.3 Materials and Methods

5.3.1 Cloning strategy

To study the protein-protein interaction between PLIN1 and HSL by bimolecular fluorescence complementation (BiFC), full length YFP was split into two fragments, Yc and Yn, which were tagged to produce pcDNA3.1-myc-PLIN1-Yc and pcDNA3.1-Yn-HSL, respectively. Both constructs were generated by Dr Wei Yang, a previous PhD student in the laboratory. The L90P variant was introduced by site-directed mutagenesis as described in 2.1.10, the construct was then subcloned into the same vector backbone using EcoRV and NotI restriction sites. The set of primers used is listed in Appendix 2.

For generation of the inducible *Plin1* KO MEF stable cell line, both WT and L90P versions of myc-PLIN1 were amplified by PCR from pcDNA3.1-myc-PLIN1-Yc and pcDNA3.1-myc-PLIN1-L90P-Yc, respectively. The sequences of the primers are provided in Appendix 1. The sequences were cloned into the entry vector pEN-Tmcs using BcuI and NotI restriction sites. The expression cassettes were then subcloned into the pSLIK-Hygro lentiviral vector by site-specific recombination using Gateway LR Clonase II Enzyme mix (Thermo Fisher Scientific, USA) according to the guide from the manufacturer. Lentiviruses stably expressing EGFP were also transduced in *Plin1* KO MEFs and served as a negative control.

All clones were confirmed by Sanger sequencing against the *PLIN1* reference sequence (Transcript ID: ENST00000300055.10) obtained from Ensembl.

5.3.2 Cell culture

The 3T3-L1 preadipocytes were maintained as described in 2.2.1. MEF cells were cultured and differentiated into mature adipocytes as described in 2.2.1 and 2.2.3, respectively.

5.3.3 Transient transfection

As described in 2.5.2, 3T3-L1 preadipocytes were seeded in 12-well tissue culture plates at a density of 50,000 cells per well. The following day, cells were transfected with 1 µg of plasmid DNA in total containing equal amounts of pcDNA3.1-myc-PLIN1-Yc (WT or L90P) and pcDNA3.1-Yn-HSL, using Lipofectamine LTX with PLUS Reagent according to the manufacturer's manual.

5.3.4 MEF stable cell line generation

To characterise the adipogenic and lipolytic functions of the PLIN1 variant, the *Plin1* KO MEF cell line was employed to generate PLIN1 WT and L90P overexpressing stable cell lines as described in 2.2.6. Positively transduced MEF cells were selected using 200 µg/ml hygromycin. The expression of the gene of interest was induced by Dox administration. To determine the final concentration of Dox required in the media in order to achieve a comparable expression level between WT and L90P, a range of Dox concentrations was tested. Both mRNA and protein expression of PLIN1 were assessed. Dox at a concentration of 150 ng/ml was selected for WT, and 1000 ng/ml for L90P or EGFP.

5.3.5 Oil Red O assay

Stably transduced *Plin1* KO MEF cells were differentiated into mature adipocytes and subjected to Oil Red O staining to quantify intracellular lipid accumulation as described in 2.2.10. The whole wells were scanned by an Epson V550 scanner and individual images were taken by a DP20 digital camera connected to an Olympus CKX41 inverted microscope.

5.3.6 Glycerol release assay

MEF cells stably expressing EGFP, PLIN1 WT or L90P were differentiated into mature adipocytes until day 9. Protein expression was induced from day 3 onwards by adding Dox, which was then replaced every 24 hours. Cells were serum starved and treated with either

basal or lipolytic medium as described in 2.9.1. Medium was collected for the glycerol release assay as described in 2.9.2. Meanwhile, 50 µl of medium from each stable cell line under both non-stimulated and stimulated conditions was sent to the Core Biochemical Assay Laboratory (Cambridge, UK) for a FFA assay. Glycerol or FFA release was normalised to the total protein amount or lipid content and then further normalised from non-stimulated WT cells.

5.3.7 Real-time quantitative PCR (qPCR)

Differentiated MEF adipocytes were lysed in 350 µl RLT supplemented with 1% (v/v) β-mercaptoethanol and kept at -80°C until RNA extraction commenced. Isolation of RNA and cDNA synthesis were performed as described in 2.3.1 and 2.3.2, respectively. cDNA was diluted and used as the template for qPCR to determine gene expression at a transcription level as described in 2.3.3. The primers used in this study are listed in the Appendix 4. The mRNA expression of *PLIN1* was normalised to beta-2-microglobulin (*B2m*) housekeeping gene expression level, and further normalised to WT plus Dox.

5.3.8 Western blotting

Protein samples were prepared as described in 2.4.1 and were subjected to SDS-PAGE followed by transfer onto a nitrocellulose membrane as described in 2.4.2. Western blotting was performed as described in 2.4.2. Details of antibodies used in this study are listed in the Appendix 5.

5.3.9 Biomolecular fluorescence complementation (BiFC)

BiFC experiments were performed in 3T3-L1 preadipocytes as described in 2.5.2 and 5.2.3. Fluorescence intensities were quantified as described in 2.7. The total intensity of YFP fluorescence was normalised to the total myc intensity and then further normalised to non-stimulated PLIN1 WT control cells. To establish the specificity of the observed BiFC signals, a negative control was included in each experiment. This was achieved by mutating both serine

residues in human PLIN1 (S81 and S277) to alanine (S81/277A, generated by Dr Wei Yang) to abolish the phosphorylation at these sites, thus eliminating the interaction with HSL.

5.3.10 Confocal microscopy

For BiFC, transfected 3T3-L1 preadipocytes were fixed and permeabilised as described in 2.5.1. Cells were then stained with an anti-myc antibody (Millipore, USA), followed by secondary antibody incubation with goat anti-mouse Alexa Fluor 405 (Thermo Fisher Scientific, USA). Lipid droplets were stained with the HCS LipidTOX Deep Red Neutral Lipid Stain as described in 2.5.1. Fluorescence of myc-tagged PLIN1 was excited at 405 nm and emission was detected between 420 and 460 nm. The yellow fluorescence for BiFC signal was excited at 514 nm and emission was detected between 520 and 560 nm.

To characterise *Plin1* KO MEF cells, WT MEFs were cultured alongside KO MEFs and seeded in 12-well tissue culture plates. MEFs were differentiated, fixed and permeabilised on day 9 as described previously in section 2.2.3. Cells were then incubated with an anti-PLIN1 primary antibody (Cell Signalling Technology, USA), followed by incubation with goat anti-mouse Alexa Fluro 647 on the following day. Lipid droplets were stained by BODIPY 493/503 (Thermo Fisher Scientific, USA) before mounting. PLIN1 was detected by excitation at 647 nm and emission detected between 650 and 690 nm. BODIPY 493/503 was excited at 493 nm and detected between 505 and 525 nm.

Plin1 KO MEFs overexpressing EGFP, PLIN1 WT or L90P following Dox induction were either differentiated into adipocytes or loaded with 400 µM oleic acid as preadipocytes. EGFP expressing stable MEF cells were then fixed, while MEFs stably overexpressing either PLIN1 WT or L90P were fixed and permeabilised, as described in 2.5.1. PLIN1 overexpressing cells were then stained with an anti-myc antibody (Millipore, USA), followed by goat anti-mouse Alexa Fluor 488 antibody (Thermo Fisher Scientific, USA). Lipid droplets in all MEF cells were stained with HCS LipidTOX Deep Red Neutral Lipid Stain and mounted as described in 2.5.1. EGFP and myc-tagged PLIN1 were detected by excitation at 488 nm; emission of the former was detected between 490 and 530 nm, and the latter was between 510 and 530 nm. 3D images were acquired as described in 2.6.

In all cases, DAPI was excited at 405 nm with emission detected between 420 and 460 nm and LipidTox Deep Red Neutral Lipid Stain was excited at 633 nm with emission detected between 640 and 680 nm.

Antibodies and fluorescent dyes used for immunofluorescence in this study are listed in Appendix 5.

5.3.11 Lipid droplet size measurement

The size of lipid droplets in stably transduced *Plin1* KO MEF preadipocytes was measured. Cells were seeded into 12-well tissue culture plates and cultured until they have reached approximately 70% confluency. Cells were then loaded with 400 µM oleic acid, followed by treatment with or without Dox for 24 hours. On the following day, cells were fixed and stained for confocal microscopy as described previously. 3D images were taken, and the volume of LDs was measured using Imaris x64 9.2.1 software as described in 2.7. An average of 400 LDs from WT or L90P cells were measured in each experiment.

5.4 Results

5.4.1 Interaction of PLIN1 and HSL

As described in the introduction, the mutation site L90 is located close to a conserved phosphorylation site S81, which is believed to be involved in the interaction with HSL. Therefore, to assess the interaction between PLIN1 and HSL under both non-stimulated and stimulated conditions, PLIN1 and HSL were fused with non-fluorescent split fragments of YFP and co-transfected into 3T3-L1 preadipocytes. Their interaction would facilitate the association of the YFP fragments to form a functional YFP, which could be visualised by confocal microscopy.

Firstly, Figure 5.4 A shows that both WT and L90P were localised on the surface of LDs, based on the staining of myc tag of PLIN1 constructs. Secondly, BiFC signals were also detected, indicating that both constructs were able to interact with HSL on the surface of LDs (Figure 5.4 A). The intensity of BiFC signals was quantified and normalised to PLIN1 expression, which was assessed by myc intensity. Figure 5.4 B demonstrates that detected BiFC signals were induced by approximately two-fold when Yn-HSL was co-expressed with myc-PLIN1-L90P-Yc than with WT myc-PLIN1-Yc in the basal state. However, this difference in BiFC intensity in L90P compared to WT was smaller when cells were stimulated with isoproterenol and IBMX (Figure 5.4 B). In fact, stimulation tended to reduce, rather than enhance, the BiFC signals in both genotypes by approximately 50% (Figure 5.4 B). The protein expression of PLIN1 was validated by probing the immunoblot with an anti-myc antibody, which does not show any differences in the level of expression between WT and L90P (Figure 5.4 C). Similar expression levels of HSL were also observed, and phosphorylation of PLIN1 and HSL were both upregulated following lipolytic stimulation (Figure 5.4 C).

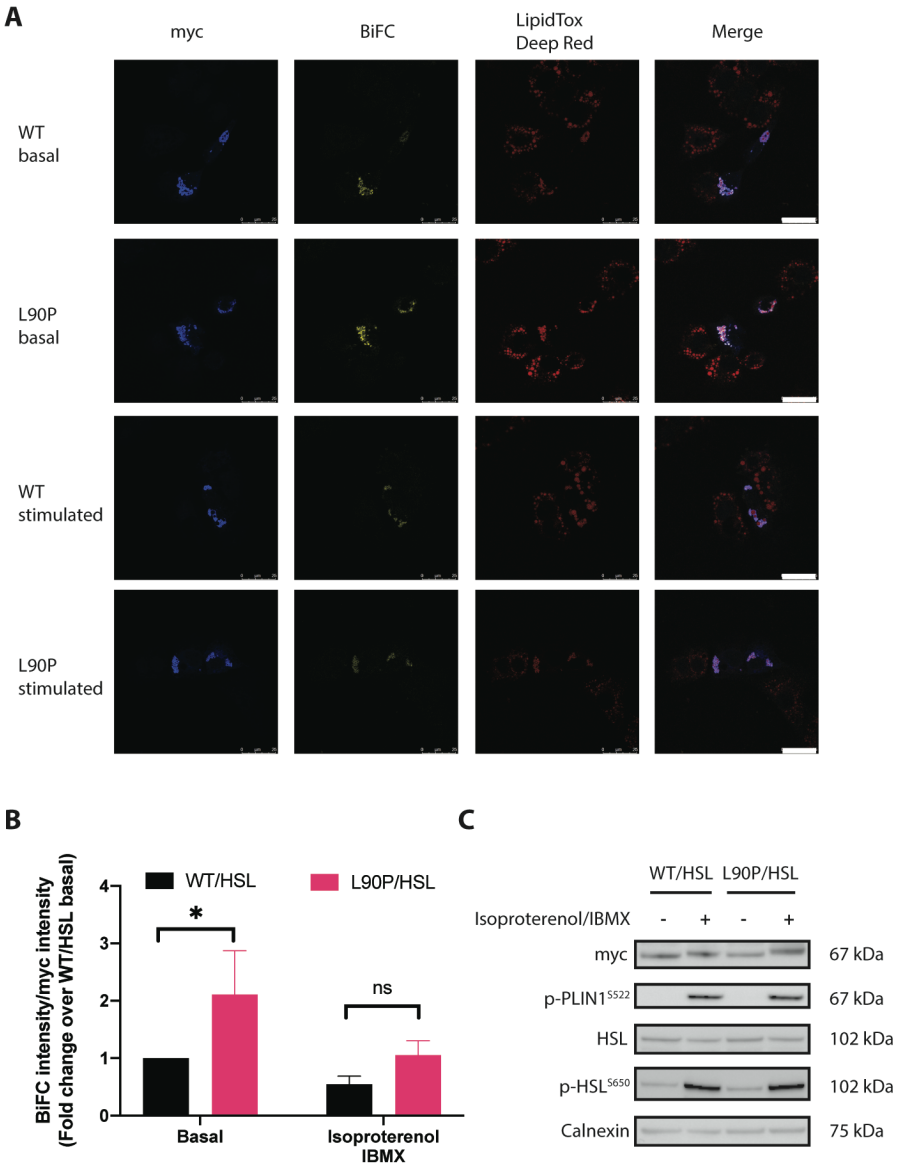

Figure 5.4 Characterisation of the PLIN1 p.L90P variant on the interaction with HSL. (A) The interaction between PLIN1 and HSL was assessed by a BiFC assay. Myc-PLIN1-Yc (WT or L90P) and Yn-HSL were co-transfected in 3T3-L1 preadipocytes and treated with either basal or "stimulated" media. The presence of a BiFC signal indicates a direct interaction between PLIN1 and HSL forming YFP fluorescence. Images are representative of three independent experiments. Scale bars, 25 µm. (B) The BiFC signal was quantified and normalised to myc signal, the latter serves as an indication for PLIN1 expression. Normalised BiFC signal was further normalised to WT/HSL basal results. Results from three independent experiments are expressed as mean ± SD. Statistical significance was evaluated by two-way ANOVA with Tukey's post hoc test for multiple comparisons. * $P < 0.05$. (C) Expression of BiFC constructs myc-PLIN1, HSL, as well as phosphorylated PLIN1 (S522) and HSL (S650), was assessed by western blotting. Calnexin served as a loading control. Blots are representative of three independent experiments.

5.4.2 Characterisation of the Plin1 KO MEF cell line

To determine the differentiation potential of *Plin1* KO MEFs, cells were seeded into 12-well tissue culture plate for differentiation as described previously. As a positive control, WT MEFs frozen by Dr Kristina Kozusko, a former PhD student in the laboratory, were thawed and cultured at the same time.

Both WT and KO MEFs were able to accumulate lipids when cells were differentiated, despite the fact that *Plin1* had been depleted in the KO MEFs (Figure 5.5 A). This is because the KO MEF cell line has been stably transfected with retrovirus expressing mouse PPARγ to drive adipogenesis (Figure 5.5 B) (*435*). The absence of PLIN1 in KO MEFs was verified by immunofluorescence microscopy (Figure 5.5 A). In WT MEFs, PLIN1 was observed coating the surface of LDs, while no fluorescent signal corresponding to PLIN1 was detected in *Plin1* KO MEFs (Figure 5.5 A). Western blotting against PLIN1 further confirmed that the KO MEF cell line was indeed lacking endogenous PLIN1 expression (Figure 5.5 B).

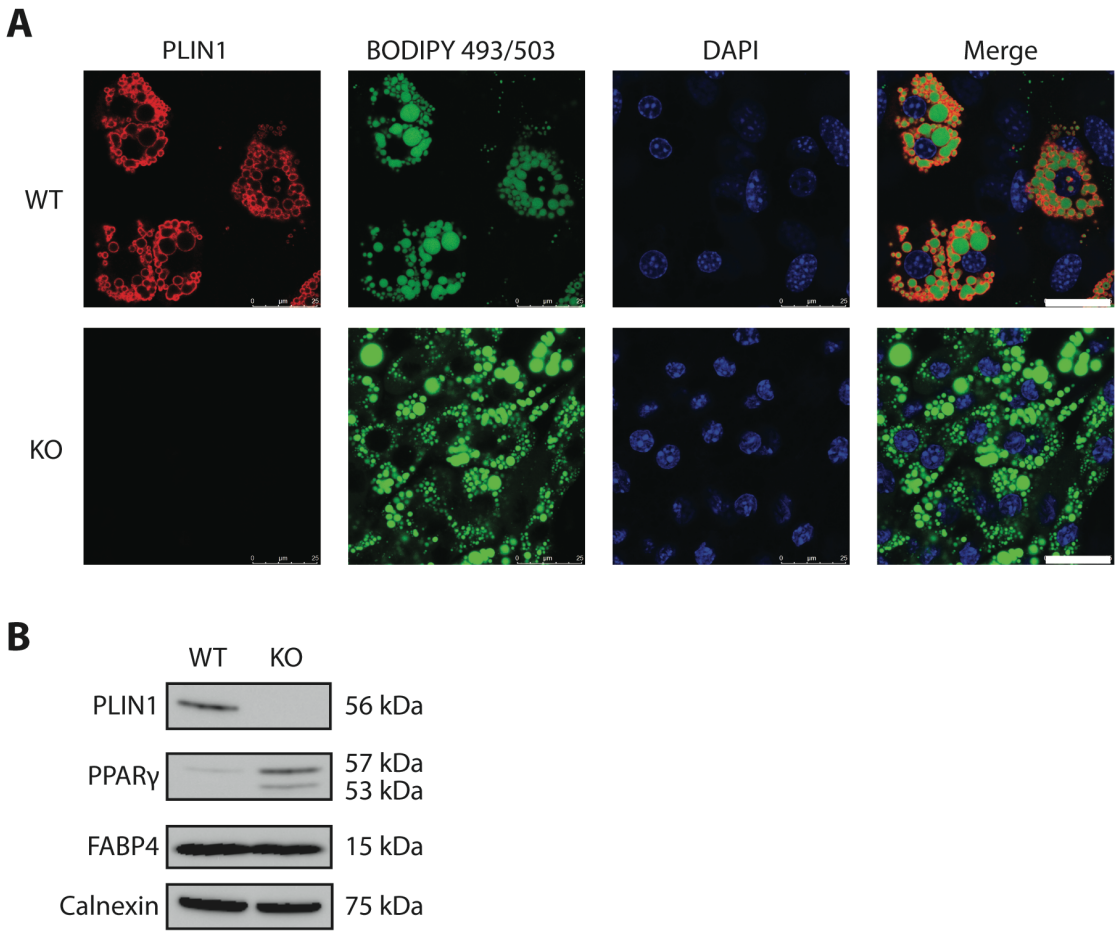

Figure 5.5 Characterisation of *Plin1* KO MEFs. (A) Visualisation of lipid accumulation and endogenous PLIN1 expression by confocal microscopy of differentiated MEFs (WT and KO). Images are representative of two independent experiments. Scale bars, 25 µm. (B) Western blotting analysis of the expression of PLIN1, PPARγ and FABP4 in both WT and KO MEFs harvested on day 9. Calnexin served as a loading control. Blots are representative of two independent experiments.

5.4.3 Generation of Plin1 KO MEFs stably expressing the PLIN1 variant

Having established the differentiation capacity of MEFs derived from *Plin1* null mice, stable cell lines expressing PLIN1 constructs were generated. In order to study the function of the PLIN1 L90P variant in adipocyte biology, *Plin1* KO MEFs were lentivirally transduced with EGFP or PLIN1 constructs and then differentiated into mature adipocytes. Dox was added from the third day throughout the course of differentiation to maintain a sustained expression of EGFP, PLIN1 WT or L90P (Figure 5.6 A). The expression of PLIN1 induced by Dox addition was confirmed by qPCR and western blotting as indicated in Figure 5.6 B and D, respectively. Compared to cells without Dox addition, *PLIN1* expression was significantly induced in the

presence of Dox (Figure 5.6 B). However notably, MEFs stably transduced with L90P seemed to have significantly higher mRNA expression of *PLIN1* than that from WT expressing cells (Figure 5.6 B). In contrast, protein expression of the L90P mutant was reduced to approximately 80% of what was detected in WT expressing cells quantified by protein densitometry (Figure 5.6 D and E). However, this finding did not reach statistical significance. As expected, mRNA expression of *PLIN1* was undetectable in control MEFs stably expressing EGFP regardless of Dox administration (Figure 5.6 B).

Historically, MEFs lacking *Plin1* have been transduced with PPARγ by retroviruses to drive the progression of adipogenesis (*435*). The differentiation potential of *Plin1* KO MEFs was validated in the previous section. MEFs stably expressing EGFP, PLIN1 WT or L90P retained differentiation potential, as shown by *Pparg2* mRNA expression by qPCR in Figure 5.6 C, as well as protein expression by western blotting in Figure 5.6 D.

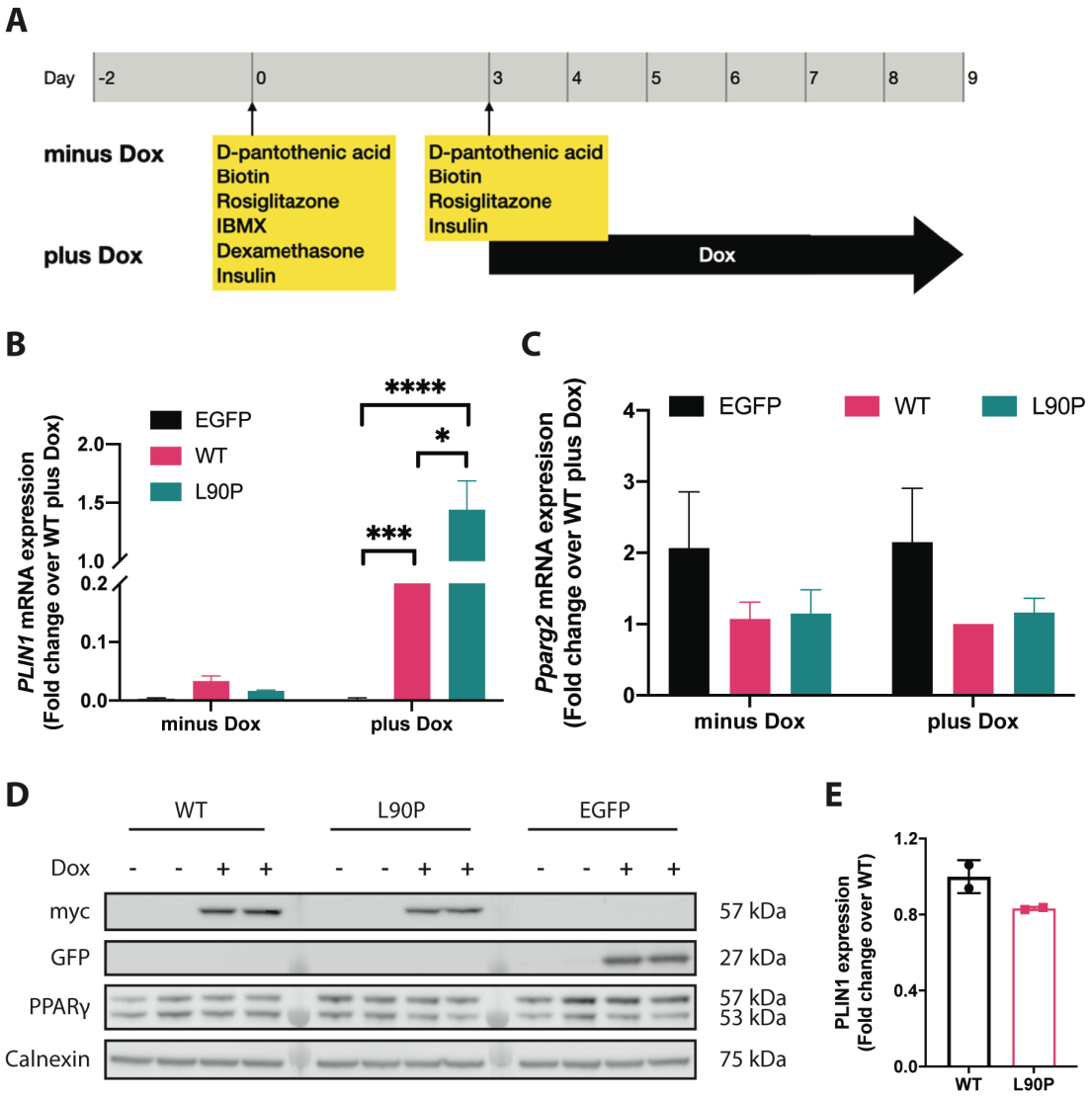

Figure 5.6 Characterisation of *Plin1* KO MEFs stably expressing EGFP, PLIN1 WT or L90P mutant by Dox induction. (A) Schematic diagram showing the protocol for differentiating *Plin1* KO MEF stable cell lines in the absence (minus Dox) or presence (plus Dox) of Dox. Cells were differentiated until day 9 in both conditions, adipogenic cocktail was added two days post-confluency (day 0) as well as on day 3. Protein expression was induced by adding Dox from day 3, which was then replaced every 24 hours until day 9. (B) The mRNA expression of *PLIN1* was assessed by qPCR. The expression in WT stable cell lines in the presence of Dox was set to 1. Results from three independent experiments are presented as mean ± SD. (C) *Pparg2* mRNA expression was determined by qPCR and further normalised to WT plus Dox. Results from three independent experiments are presented as mean ± SD. (D) Immunoblot analysis of PLIN1, EGFP and PPARγ expression in *Plin1* KO MEF stable cell lines. PLIN1 was detected by probing against the myc tag, while PPARγ2 expression was detected as the top band in the PPARγ blot. Calnexin served as a loading control. Blots are representative of two independent experiments. (E) Protein densitometry analysis of the anti-myc blot in D. Results from two independent experiments are presented as mean ± SD. In B and C, statistical significance was evaluated by one-way ANOVA with Tukey's post hoc test for multiple comparisons within the minus Dox or the plus Dox group. In E, statistical significance was evaluated with an unpaired t test. **** $P < 0.0001$, *** $P < 0.001$, * $P < 0.05$.

5.4.4 Intracellular localisation of PLIN1 variant

As described previously, the PLIN1 constructs overexpressed in oleic acid-loaded 3T3-L1 preadipocytes were localised on the surface of LDs. To determine whether a similar localisation can be observed in lentiviral transduced MEF stable cell lines, these cells were differentiated using the same protocol as illustrated in Figure 5.6 A, fixed and stained for immunofluorescence microscopy. As shown in Figure 5.7, all stable MEF lines were able to differentiate and accumulate lipids irrespective of Dox conditions. The expression of PLIN1 or EGFP was evidently induced by Dox addition (Figure 5.7). Both WT and the L90P variant were able to localise to LDs, while EGFP appeared to be diffused in cells (Figure 5.7).

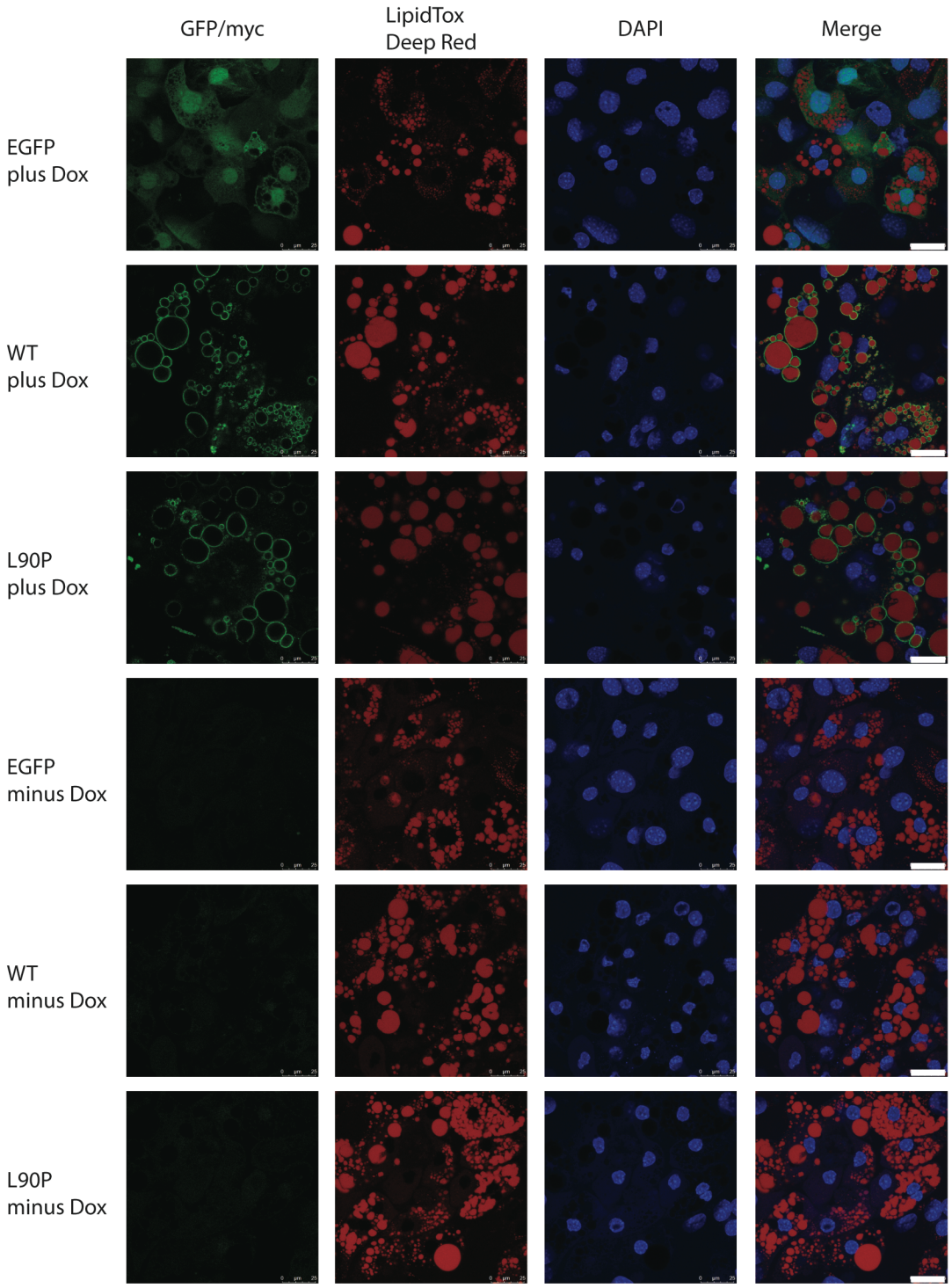

Figure 5.7 Intracellular localisation of EGFP, PLIN1 WT or L90P variant in differentiated *Plin1* KO MEFs stable cell lines. Differentiated cells under both minus and plus Dox conditions were fixed and stained with anti-myc antibody except for the EGFP stable cell line. Lipid droplets were stained with LipidTox DeepRed while DAPI was used for nuclear stain. Images are representative of three independent experiments. Scale bars, 25 μm.

5.4.5 Adipogenesis of Plin1 KO MEFs stably expressing PLIN1 variant

To investigate the impact of PLIN1 WT and the L90P variant on adipogenesis, all *Plin1* KO MEF stable cell lines were differentiated in the absence or presence of Dox from day 3 as described previously. Lipid accumulation was assessed by Oil Red O staining (Figure 5.8 A and B). Quantification of Oil Red O staining suggests the induction of PLIN1 expression by Dox, regardless of its genotype, markedly promoted lipid accumulation compared to EGFP (Figure 5.8 C). Lipid accumulation was not significantly different between WT and L90P in this condition (Figure 5.8 C). While a significant increase in lipid accumulation was observed in PLIN1 expressing MEFs induced by Dox compared to minus Dox, this phenomenon was however not observed in EGFP stable cell lines (Figure 5.8 D).

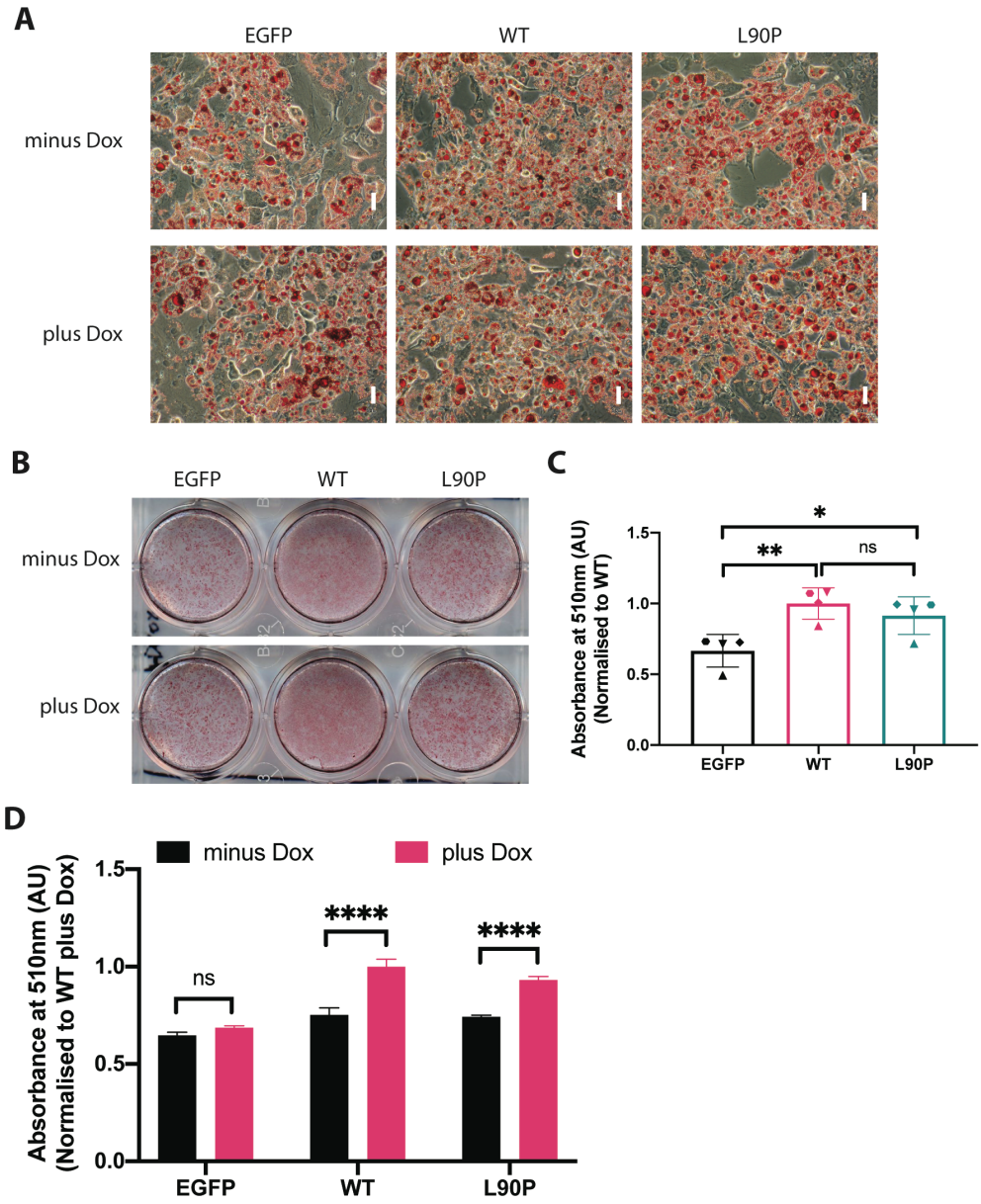

Figure 5.8 Lipid accumulation in *Plin1* KO MEFs stably expressing EGFP, PLIN1 WT or the L90P mutant by Oil Red O staining. (A) Microscopic images showing the accumulation of lipids stained by Oil Red O. Images are representative of three independent experiments. Scale bars, 50 mm. (B) Differentiated MEFs in the absence (minus Dox) or presence (plus Dox) of Dox were harvested on day 9, stained with Oil Red O and photographed. Images are representative of three independent experiments. (C) Quantification of Oil Red O staining in MEFs differentiated in the presence of Dox. Results from four independent experiments are presented as mean ± SD. Statistical significance was evaluated by one-way ANOVA with Tukey's post hoc test for multiple comparisons. (D) Quantification of Oil Red O staining in MEFs under both minus and plus Dox conditions. Results from three independent experiments are presented as mean ± SD. Statistical significance was evaluated by two-way ANOVA with Bonferroni's post hoc test for multiple comparisons. **** $P < 0.0001$, ** $P < 0.01$, * $P < 0.05$, ns not significant.

5.4.6 Lipid droplet size in Plin1 KO MEFs stably expressing PLIN1 variant

To investigate the impact of the L90P mutation on the regulation of LD size, undifferentiated MEFs were loaded with oleic acid prior to the induction of protein expression by Dox. Quantification of lipid droplet size was performed in preadipocytes 24 hours post Dox induction. As demonstrated in Figure 5.9 A, both WT and L90P specifically targeted LDs, while EGFP did not. Analysis of lipid droplet size distribution showed no difference between WT and L90P expressing preadipocytes (Figure 5.9 B). However, a statistically significant larger proportion of small LDs with a volume less than 1 μm^3 was observed in EGFP positive preadipocytes, indicating that EGFP failed to promote lipid accumulation (Figure 5.9 B). At the same timepoint, western blotting showed an increase in protein expression when PLIN1-expressing preadipocytes were exposed to media containing oleic acid (Figure 5.9 C).

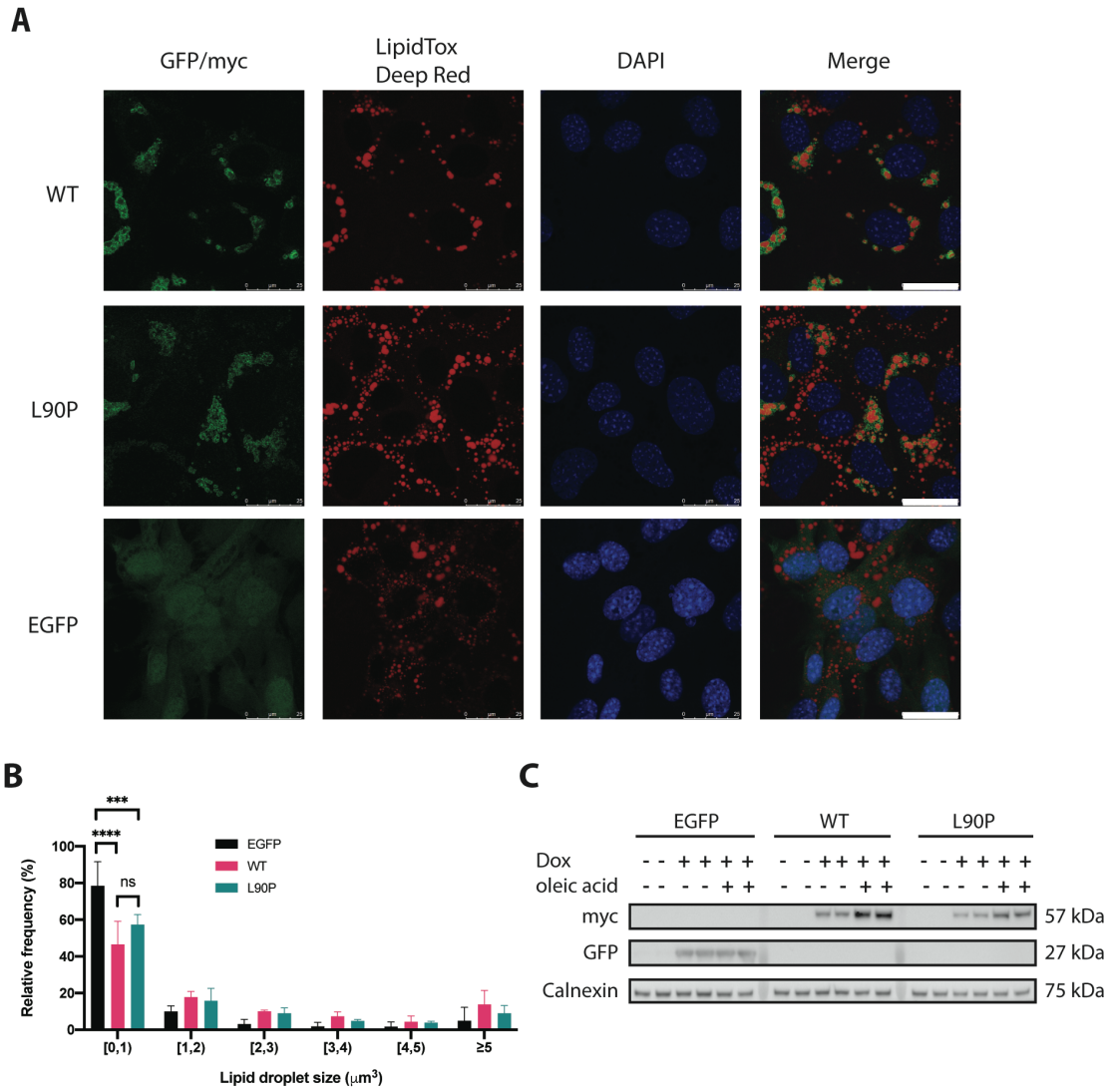

Figure 5.9 Characterisation of undifferentiated *Plin1* KO MEFs stably expressing EGFP, PLIN1 WT or L90P mutant. Cells were seeded and loaded with oleic acid prior to the induction of protein expression by Dox. (A) Intracellular localisation of PLIN1 WT, L90P and EGFP in MEF preadipocytes. (B) Lipid droplet size distribution in MEF preadipocytes stably expressing EGFP, PLIN1 WT or L90P. Lipid droplet volumes were clustered in ascending 1 μm^3 intervals; the last bin contains all volumes greater than 5 μm^3. Results from three independent experiments are presented as mean ± SD. Statistical significance was evaluated by two-way ANOVA with Tukey's post hoc test for multiple comparisons. **** $P < 0.0001$, *** $P < 0.001$, ns not significant. (C) Western blot analysis of PLIN1 and EGFP expression in preadipocytes from MEF stable cell lines. PLIN1 was detected by probing against myc tag. Calnexin served as a loading control. Blots are representative of three independent experiments.

5.4.7 Lipolysis of Plin1 KO MEFs stably expressing PLIN1 variant

To determine the impact of the L90P mutant on intracellular lipolysis, the rate of lipolysis was assessed by the quantification of glycerol as well as FFA released into the medium from differentiated MEF stable cell lines. When normalised to total protein amount, MEFs stably expressing WT and L90P showed elevated basal lipolysis, measured by glycerol and FFA, compared to EGFP, which is unexpected as introducing PLIN1 to *Plin1* KO MEFs should inhibit basal lipolysis (Figure 5.10 A and C) (*435*). Isoproterenol and IBMX stimulated glycerol release was markedly induced in WT expressing MEFs, but tended to be lower in L90P (Figure 5.10 A). This difference between WT and L90P expressing MEFs was significant when expressed as fold change of the 'stimulated' versus 'basal' states (Figure 5.10 B). The data from FFA analysis showed a substantial increase of FFA release from PLIN1 expressing MEFs upon lipolytic stimulation, although significantly less FFA was released from L90P than that from WT expressing MEFs (Figure 5.10 C). With regard to the ability of stable MEFs to respond to isoproterenol and IBMX stimulation, both datasets indicated a potent response in PLIN1 expressing MEFs, while L90P showed less fold induction than WT (Figure 5.10 B and D).

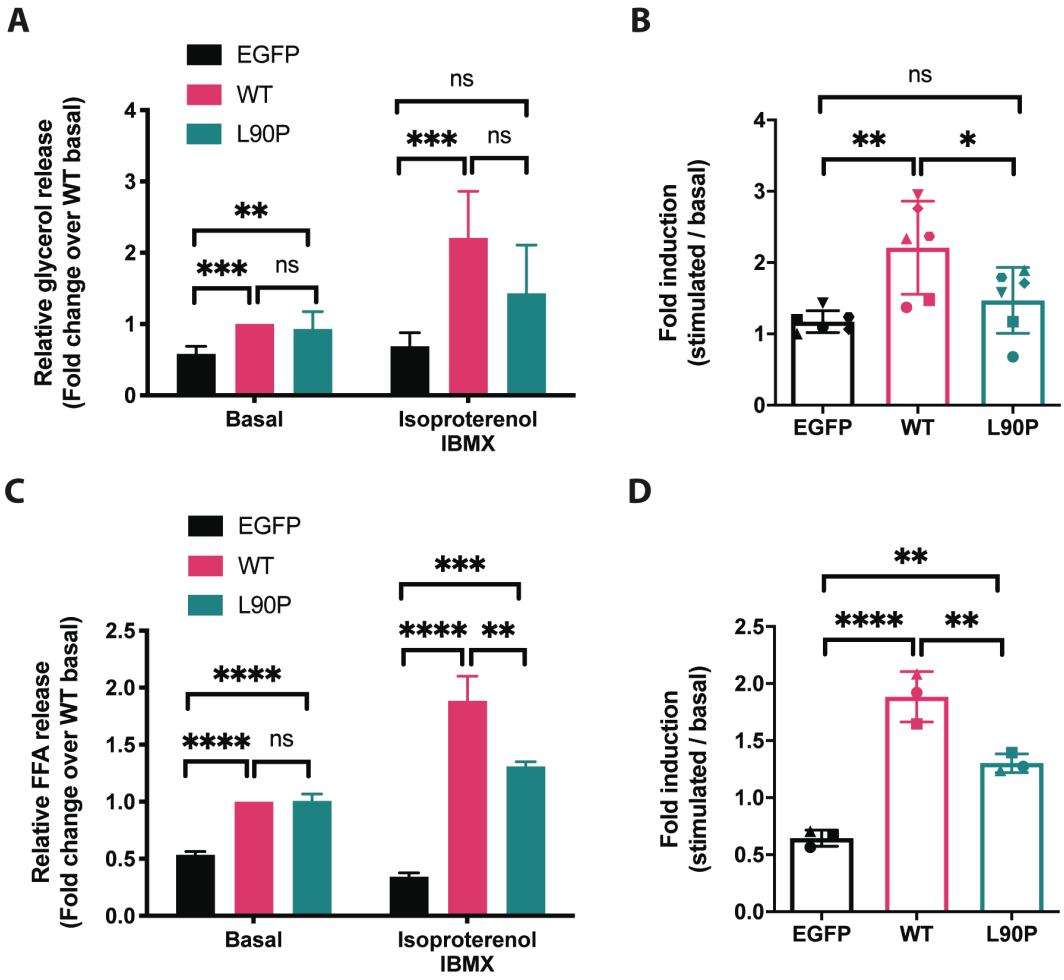

Figure 5.10 Lipolysis in *Plin1* KO MEFs stably expressing EGFP, PLIN1 WT or L90P mutant using protein amount as the normalisation method. Cells were differentiated in the presence of Dox and harvested after treatment with either basal or stimulated (isoproterenol and IBMX) medium on day 9. Glycerol or FFA release assays were performed and normalised to total protein amount. (A) The rate of lipolysis was assessed by glycerol release assay and further normalised to the WT basal state data. (B) Fold inductions of induced lipolysis by isoproterenol and IBMX are calculated as the ratio between stimulated and basal glycerol release. (C) Rate of lipolysis was analysed by a FFA assay and further normalised to WT basal. (D) Fold inductions of induced lipolysis by isoproterenol and IBMX are calculated as the ratio between stimulated and basal FFA release. Results from six in A and B, or three in C and D independent experiments are presented as mean ± SD. Statistical significance was evaluated by one-way ANOVA with Tukey's post hoc test for multiple comparisons within the group. **** $P < 0.0001$, *** $P < 0.001$, ** $P < 0.01$, * $P < 0.05$, ns not significant.

As described in the previous section, ectopic expression of PLIN1 (WT and L90P) in KO MEFs enhanced differentiation potential compared to EGFP expressing MEFs when protein expression was induced by Dox addition, at least in terms of lipid accumulation in the adipocytes (Figure 5.8 C). This could explain the apparently higher basal lipolysis rate in cells expressing WT or L90P PLIN1. Therefore, glycerol or FFA released from each cell line was also normalised to the Oil Red O quantification data, which was used as an indicator of lipid content. In the non-stimulated state, no difference in glycerol release was observed between the cell lines (Figure 5.11 A). However, in contrast to basal glycerol release, FFAs released in the basal state from MEF adipocytes stably expressing WT PLIN1 was still significantly increased compared with the other two stable cell lines (Figure 5.11 C). The results for stimulated lipolysis assessed by both the glycerol and FFA assay were in agreement with data obtained using total protein content as the normalisation method (Figure 5.11 A and C). Consistent with previous observations, introducing PLIN1 into *Plin1* KO MEFs restored the ability to respond to stimulation, with WT PLIN1 expressing MEFs displaying a significantly higher fold induction of isoproterenol and IBMX stimulated lipolysis than that of L90P cells (Figure 5.11 B and D).

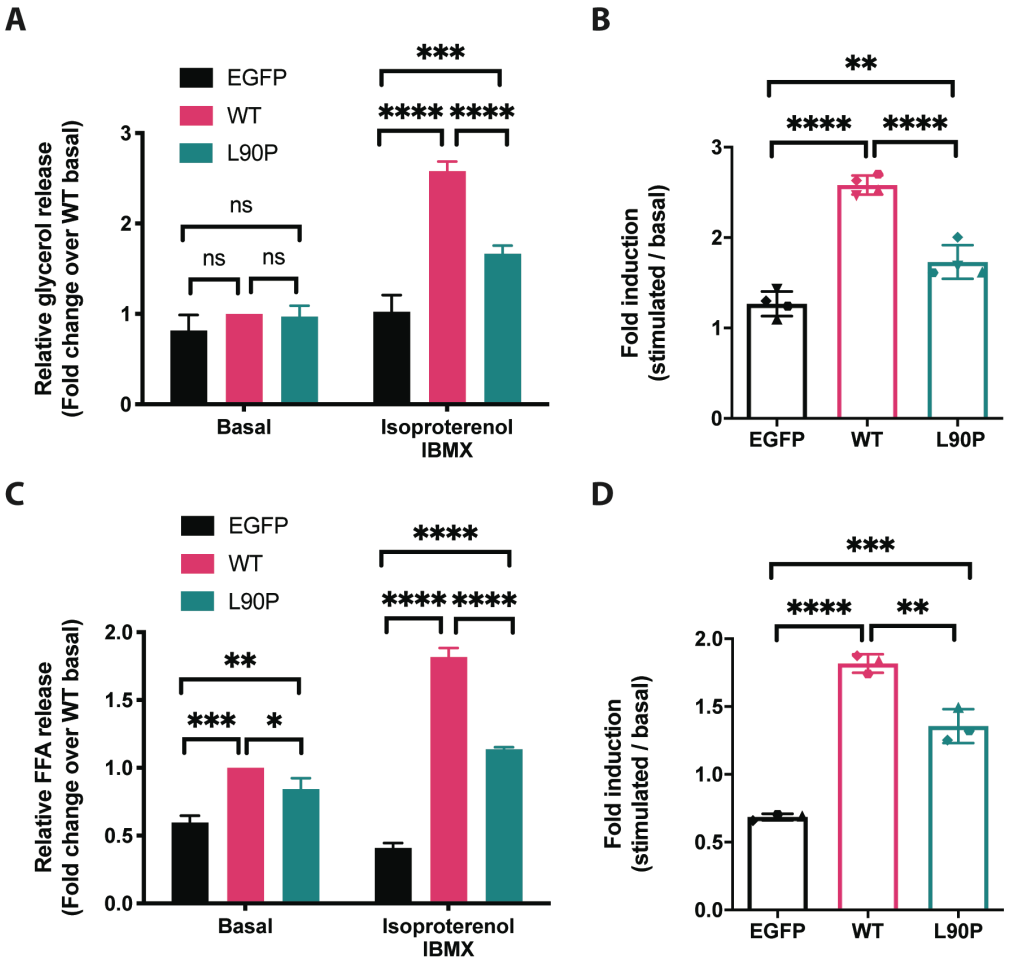

Figure 5.11 Lipolysis in *Plin1* KO MEFs stably expressing EGFP, PLIN1 WT or L90P mutant using lipid content as the normalisation method. Cells were differentiated in the presence of Dox and harvested after treatment with either basal or stimulated (isoproterenol and IBMX) medium on day 9. Glycerol or FFA release assays were performed and normalised to total lipid content. (A) Rate of lipolysis was assessed by glycerol release assay and further normalised to the WT basal state data. (B) Fold inductions of induced lipolysis by isoproterenol and IBMX are calculated as the ratio between stimulated and basal glycerol release. (C) Rate of lipolysis was analysed by a FFA assay and further normalised to WT basal. (D) Fold inductions of induced lipolysis by isoproterenol and IBMX are calculated as the ratio between stimulated and basal FFA release. Results from four in A and B, or three in C and D independent experiments are presented as mean ± SD. Statistical significance was evaluated by one-way ANOVA with Tukey's post hoc test for multiple comparisons within the group. **** $P < 0.0001$, *** $P < 0.001$, ** $P < 0.01$, * $P < 0.05$, ns not significant.

Western blot analysis showed that the expression of PLIN1 was consistently lower in L90P cells compared to WT cells regardless of which antibody was used for PLIN1 detection (Figure 5.12 A). In addition, a significantly lower degree of PLIN1 phosphorylation was also observed in L90P expressing cells than that from WT when stimulated, which was quantified by protein densitometry (Figure 5.12 A and B). Total HSL expression appeared to be higher in MEFs stably expressing WT than other genotypes, while the phosphorylated HSL levels did not seem to differ (Figure 5.12 A). The expression of ABHD5 was significantly upregulated alongside the induction of PLIN1 WT expression by Dox addition, but no statistically significant difference was observed in MEFs stably expressing L90P and EGFP (Figure 5.12 A and C). Although there was a significant reduction of ABHD5 expression in L90P compared to WT cells in the basal state, this reduction was not significant in cells in the stimulated state (Figure 5.12 C). Furthermore, the expression of ATGL seemed to be comparable between cell lines under both basal and stimulated conditions regardless of Dox addition, except for L90P which seemed to have lower ATGL expression when treated with Dox (Figure 5.12 A and D).

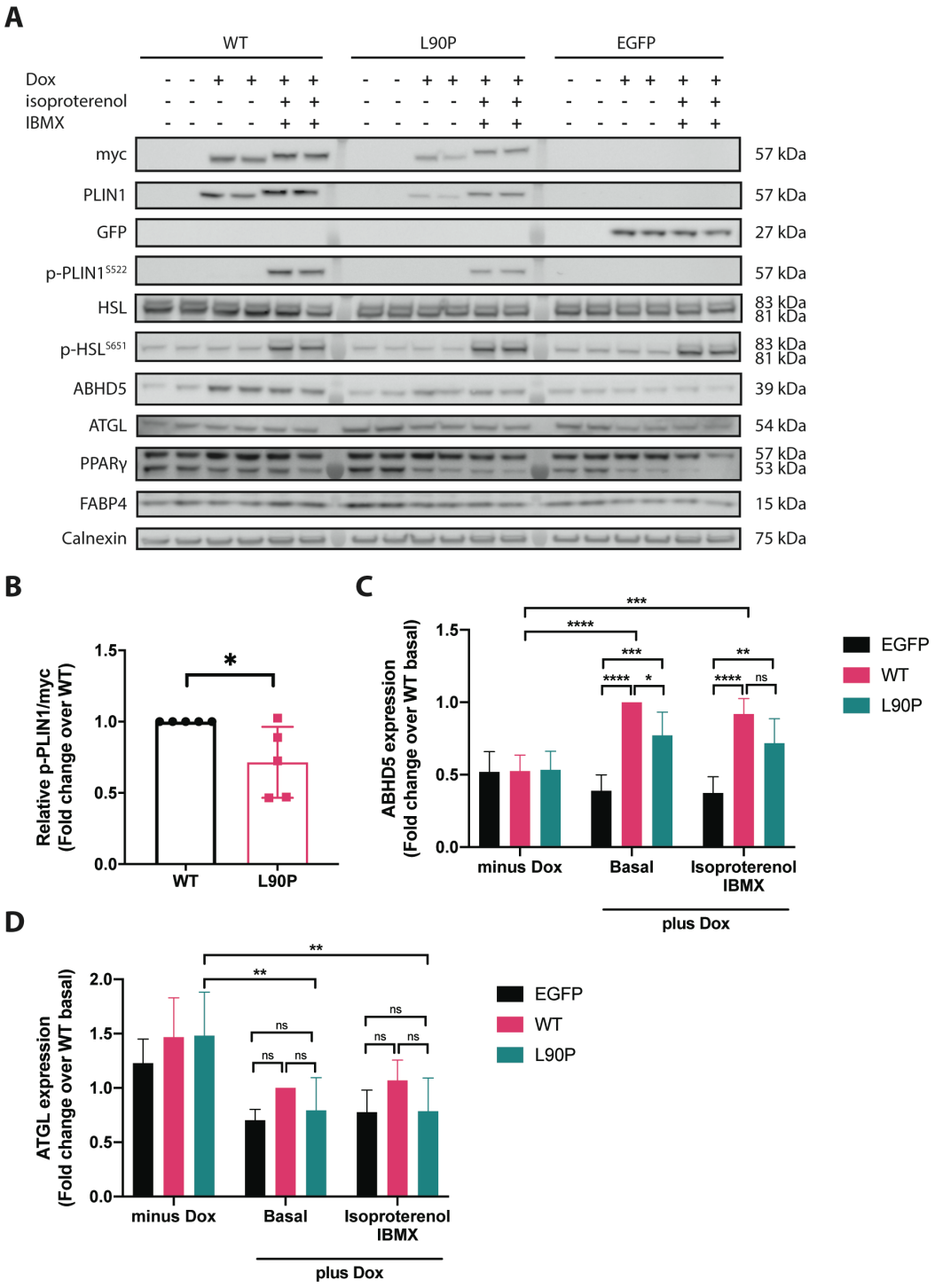

Figure 5.12 Western blot analysis of *Plin1* KO MEFs stably expressing EGFP, PLIN1 WT or the L90P mutant. Cells were differentiated with or without Dox addition until day 9. The resulting MEF adipocytes with Dox addition were subjected to lipolytic treatment and harvested for western blotting. (A) Immunoblot analysis showing the expression level of PLIN1 or EGFP from stable cell lines after treatment in either basal or the stimulated state. Detection of PLIN1 was performed using either a myc or PLIN1 antibody. The expression of phosphorylated PLIN1 and HSL, total HSL, ABHD5 and ATGL were also assessed by western blotting. PPARγ and FABP4 were used as markers for mature adipocytes. Calnexin served as a loading control. Blots are representative of five independent experiments. (B) Densitometric analysis of p-PLIN1 upon lipolytic stimulation by isoproterenol and IBMX. (C) Densitometric analysis of ABHD5 expression in all conditions. (D) Densitometric analysis of ATGL expression in all conditions. In B, C and D, results from five independent experiments are presented as mean ± SD. Statistical significance was evaluated by unpaired t test in B, and by two-way ANOVA with Tukey's post hoc test for multiple comparisons in C and D. **** $P < 0.0001$, *** $P < 0.001$, ** $P < 0.01$, * $P < 0.05$, ns not significant.

5.5 Discussion

Data presented in this chapter suggests that the interaction between the PLIN1 L90P mutant and HSL was more intense than that of WT with HSL when overexpressed in 3T3-L1 preadipocytes under basal conditions of the BiFC assay. Functional studies were also conducted to characterise the impact of L90P on adipose biology by generating stable lines of *Plin1* KO MEFs expressing PLIN1 WT or L90P. In these stably transfected MEF adipocytes, L90P was able to localise on the surface of LDs as does WT PLIN1. Adipogenesis measured by Oil Red O staining in PLIN1 expressing MEF adipocytes was not affected by the L90P mutation. Although basal lipolysis was observed to be similar in WT and L90P expressing MEFs, stimulated lipolysis was significantly impaired in cells expressing L90P, indicating that the cells were less responsive to lipolytic stimulation.

5.5.1 The impact of L90P on the interaction with HSL

The L90P site lies in the highly conserved PAT domain in PLIN1 which has been shown to be involved in the interaction with HSL (*342*). Therefore, a BiFC assay was performed to visualise and compare the interaction of WT and L90P PLIN1 with HSL. Both PLIN1 and HSL were fused with non-fluorescent fragments of YFP (Yc and Yn, respectively), followed by co-transfection into 3T3-L1 preadipocytes treated with oleic acid to promote LD formation. Theoretically the interaction between the two proteins would bring the split YFP fragments into close proximity and facilitate the formation of a functional YFP complex. The detection of a YFP signal, as an indicator for BiFC, using fluorescence microscopy confirmed that the interaction between PLIN1 and HSL takes place on the surface of LDs. Previous reports have suggested that phosphorylation of the first three PKA sites at the N-terminus of mouse PLIN1, which are equivalent to S81 and S277 in human PLIN1, controls the dynamic PLIN1-HSL interaction (*342*). Thus, a PLIN1 mutant harbouring replacements of both serine residues with alanine was included in this experiment and served as a negative control. The PLIN1 S81/227A mutant indeed lost the ability to interact with HSL regardless of stimulation, indicating that the signal detected in this assay reflects a specific protein-protein interaction (data not shown). In fact,

the same method has been utilised previously to demonstrate the interaction between PLIN1 and HSL, which were cloned from other species such as rat and mouse (*605*, *609*). Both groups observed a physical interaction of PLIN1 with HSL under basal conditions, which was visualised by the BiFC assay (*605*, *609*). However, whether there are any changes in the intensity of BiFC signals upon lipolytic stimulation has not been reported (*605*, *609*).

Although the subcellular localisation of HSL in adipocyte is mainly cytosolic, there is evidence suggesting that up to 60% of HSL can be associated with LDs under non-stimulated conditions (*345*, *435*, *610*, *611*). Moreover, low levels of phosphorylated PLIN1 and HSL were detected by western blotting under basal conditions. Thus, it is not surprising to observe BiFC signals in the basal state where it also shows a significantly higher BiFC intensity in cells co-transfected with L90P and HSL than that with WT and HSL. It has been shown that the fluorescence intensity is positively correlated with the strength of the interaction between two interaction partners (*612*). Therefore, considering that the L90P mutation did not alter the protein expression, nor the intracellular localisation of PLIN1, it is concluded that L90P presents a relatively higher efficiency of complex formation than WT when co-expressed with HSL. This suggests that HSL binds more strongly with L90P than WT PLIN1 under basal condition.

Following lipolytic stimulation, cAMP-dependent PKA is activated which subsequently phosphorylates both PLIN1 and HSL in adipocytes. Although it is still debatable whether the translocation of phosphorylated HSL from the cytosol to the surface of LDs requires PKA-dependent phosphorylation of PLIN1, it is undoubtedly true that stimulation triggers HSL translocation specifically to PLIN1 containing LDs in adipocytes (*345*, *435*, *605*). In addition to colocalization of PLIN1 and HSL detected by fluorescence microscopy, studies using various techniques including Förster resonance energy transfer (FRET) and co-immunoprecipitation have showed enhanced PLIN1-HSL interaction after PKA stimulation (*342*, *343*, *435*, *603*). Therefore, the formation of YFP complex assessed by the BiFC assay in the current study was hypothesised to be more efficient under lipolytic conditions. Surprisingly, when transfected cells were stimulated with isoproterenol and IBMX, the BiFC intensity was not induced as expected compared to the basal state, regardless of genotype. This is probably due to at least one limitation of the BiFC assay, namely the slow maturation time of the fluorophore, which

can take hours until fluorescence is detected (*437*). This could potentially prevent the accurate detection of a rapid rise in PLIN1-HSL interaction caused by lipolytic stimulation, which occurs in minutes *in vitro* (*435*, *605*, *613*). Therefore, newly formed interactions between PLIN1 and HSL might not be given enough time to produce the fluorescent BiFC complex in the current experimental setting (two-hour stimulation), especially when comparing BiFC efficiencies between WT and the mutant for quantitative analysis. However, one advantage of the BiFC analysis is that the formation of a BiFC complex is essentially irreversible after the association of the split fragments (*437*, *614*). Thus, the BiFC signals detected after stimulation include the interaction between PLIN1 and the pool of HSL which has pre-positioned to LDs under basal conditions. Moreover, PKA-mediated phosphorylation of PLIN1 following chronic lipolytic stimulation is known to direct LD remodelling such as fragmentation and dispersion (*353*). It has been proposed that PLIN1 slowly departs from the large LDs where HSL remains and continues with lipolysis, which might be another possible explanation for not observing increased BiFC signals in the present study (*345*).

In order to detect the rapid association between PLIN1 and HSL in real-time upon lipolytic stimulation, efforts have been made to monitor their interaction in live cells using the NanoBiT protein-protein interaction assay (*615*). The assay is based on a two-subunit system which are fused to the proteins of interest. The interaction of the two proteins would bring the subunits into close proximity and form a functional enzyme to produce a luminescent signal (*615*). Unlike the BiFC assay, it offers real-time measurement and allows kinetic analysis which makes it a valuable tool when comparing binding efficiencies with HSL between WT and L90P in the current study. Initial experiments were focused on the optimisation of the expression constructs to determine the orientation for fusing to the subunits, as well as the length of linker sequence to allow optimal space for contact between the subunits. No further attempts were possible to assess whether there is any difference in the binding efficiency with HSL between WT and L90P because of time constraints and the COVID pandemic, but this approach is worth pursuing.

The advantage of using the 3T3-L1 preadipocytes to study the interaction of PLIN1 with HSL is that the cells normally lack endogenous expression of these proteins of interest (*354*, *616*). However, the BiFC signals detected could be artefactual due to the abundance of each

interaction partner by overexpression. In addition, the split fragments of the fluorescent protein do have limited ability to associate with each other independent of an interaction between the proteins that are fused to them (*437*). Therefore, it is possible that a false positive interaction may be detected in the BiFC assay. Consequently, alternative approaches to study PLIN1-HSL interaction need to be carried out to validate the findings presented in the current study. For example, FRET experiments can be performed to detect and track the interaction between PLIN1 and HSL in live cells, thus changes in the protein interactions upon lipolytic stimulation can be analysed (*342*, *605*). Other methods such as pull-down assays or co-immunoprecipitation could also be utilised to verify the findings (*342*, *343*, *435*).

5.5.2 Ectopic PLIN1 expression in Plin1 KO MEFs

As indicated in the BiFC analysis, a stronger interaction between PLIN1 L90P and HSL was observed when overexpressed in non-stimulated 3T3-L1 preadipocytes, which led to the investigation of the function of the mutation in regulating lipolysis using the *Plin1* KO MEF system.

The MEFs were originally generated from 12.5 – 14.5 day embryos of *Plin1* KO mice (*435*). Additionally, the *Plin1* KO MEFs have been transduced with retrovirus expressing PPARγ to allow the cells to differentiate into adipocytes (*435*). This has been confirmed in the current study which shows the overexpression of PPARγ in the KO cell line. Furthermore, the adipogenic potential of these cells was intact as shown by immunofluorescence and western blotting analysis, in line with a previous report (*435*).

To establish comparable levels of Dox induced expression of PLIN1 constructs in the stable cell lines, different viral titres of lentiviral constructs and doses of Dox ranging from 0 to 2000 ng/ml were tested and analysed using qPCR and western blot analysis (data not shown). Eventually two concentrations of Dox were selected based on the minimum difference observed on both transcriptional and post-transcriptional levels between the WT and L90P expressing MEFs. As indicated in the results, at 1000 ng/ml Dox the protein expression level of PLIN1 in L90P expressing MEF adipocytes was comparable with WT expression induced by

150 ng/ml Dox administration. However, it should be noted that on average the *PLIN1* mRNA expression level of L90P was approximately 1.4-fold higher than that of WT. It might be due to the instability or relatively rapid degradation of the mutated L90P protein, as such a substitution might destabilise the protein. Although the mechanisms for controlling PLIN1 degradation in adipocytes are largely unknown, previous studies have shown that it is mediated via the ubiquitin-proteasome pathway, as well as lysosomal proteolysis (*617–619*). In addition, WT PLIN1 has been shown to be highly stable with an estimated half-life of 40 to over 70 hours when associated with LDs (*556*, *618*). The impact of the L90P on PLIN1 protein stability could be assessed by performing a cycloheximide chase assay, which functions through the inhibition of translation elongation (*620*).

As the L90P containing N-terminal PAT domain is close to the 11-mer repeat region which has been shown to be essential for LD targeting of PLIN1, we also sought to inspect whether this mutation has any effect on LD targeting (*179*). The results showed that in both 3T3-L1 and *Plin1* KO MEF cell lines, the L90P mutant is able to target LDs. Ectopic expression of PLIN1, either the WT or the L90P mutant, has been proven to promote lipid accumulation compared to that of EGFP. Moreover, no significant changes in LD size distribution were observed in MEF preadipocytes expressing L90P compared with that of cells expressing WT, indicating that this mutation does not alter lipid accumulation. A similar observation was also made for lipid accumulation in differentiated MEF adipocytes determined by Oil Red O staining. This is in agreement with a previous report which demonstrated that the C-terminus of PLIN1 is critical in promoting TG storage, while the PAT domain does not seem to affect this aspect of PLIN1 function (*340*).

The lack of endogenous *Plin1* expression in *Plin1* null cells makes them suitable for the characterisation of specific functions of PLIN1 mutants as presented in previous studies, including the role of multiple PLIN1 phosphorylation sites in PKA-stimulated lipolysis (*352*, *435*, *618*). As described previously, PLIN1 is a key regulator of lipolysis as the absence of *Plin1* results in elevated basal lipolysis and attenuated stimulated lipolysis *in vivo* (*358*, *359*). By introducing PLIN1 WT into the *Plin1* KO MEFs, it was anticipated that the KO phenotype could be rescued so that basal lipolysis would be repressed, while stimulated lipolysis would be enhanced, comparing with KO MEFs expressing EGFP. The results presented in this chapter

suggest that ectopic expression of PLIN1 WT indeed had the ability to increase lipolysis following isoproterenol and IBMX treatment but failed to block basal lipolysis as expected. Unlike previously published studies where reduced basal lipolysis, as measured by glycerol release, was observed in MEFs expressing PLIN1, this phenomenon never occurred in my experiments despite the assessment of both lipolytic products (glycerol and FAs) using multiple normalisation methods (*352*, *435*, *618*).

One major concern in the current experimental design is the lack of an appropriate positive control, which ideally would be the WT MEFs isolated from littermates. Thus, it is unclear whether the level of PLIN1 expression achieved in the stable cell lines is comparable with endogenous PLIN1 expression in the WT MEFs and it is known that the modulation of PLIN1 protein expression regulates lipolytic rates (*618*, *621*). It is possible that the PLIN1 expression in *Plin1* KO MEF adipocytes stably expressing PLIN1 WT may be lower than endogenous levels and hence not sufficient to inhibit basal lipolysis. Similarly, as the protein expression of PLIN1 L90P was comparable or even less than WT, it was not too surprising to learn that L90P also failed to block basal lipolysis in MEF adipocytes. On the other hand, phosphorylation of PLIN1 was unaffected in WT expressing stable MEFs since all putative PKA phosphorylation sites were intact, resulting in increased stimulated lipolysis, although the magnitude of the fold induction was not as substantial as previously reported (approximately 12 folds) (*435*). Immunoblot data seemed to suggest that the phosphorylation of PLIN1 L90P at S522 was significantly reduced compared to WT, which may contribute to the impaired stimulated lipolysis and limited fold induction upon stimulation. While we currently cannot offer any explanation as to how the L90P mutant affects PLIN1 S522 phosphorylation, the result is in agreement with previous studies which suggest that the phosphorylation of S517 of mouse PLIN1 (equivalent to human S522) is the master regulator of PKA stimulated lipolysis mainly by regulating the lipolytic action of ATGL (*352*). Previous studies revealed that the mutation of all three PKA sites at the N-terminus of mouse PLIN1 (corresponding to two of human PLIN1) partially blocked stimulated lipolysis since phosphorylation of these sites is required for HSL translocation (*341*, *345*, *352*, *622*, *623*). Moreover, replacement of serine at 81 alone with alanine in mouse PLIN1 has been shown to be sufficient to reduce HSL translocation following PKA activation, although it does not have any effect on lipolysis (*342*, *352*). However, the possibility that a malfunction of S81 of human PLIN1 in the control of HSL activity upon

lipolytic stimulation due to this point mutation L90P cannot be ruled out. Therefore, a customised phospho-specific antibody alongside co-immunoprecipitation could help to assess the effect of the L90P mutation on S81 phosphorylation, as well as the interaction with HSL under stimulated conditions.

One technical difference in the choice of viral gene delivery system, which could perhaps account for the discrepancies between the phenotype described in previous reports and what was observed in the current data. Firstly, an adenoviral transduction system was applied in the previous studies, the advantage of which is high transduction efficiency to achieve high levels of protein expression transiently (*435*, *624*). In contrast, the lentiviral system employed in this work allows stable gene expression, although the level of protein expression may not be as high as in the adenoviral system. The intention for adopting this approach was to take advantage of the conditional Tet-On system in order to assure comparable expression levels between PLIN1 WT and L90P by adjusting the concentration of Dox in the media. Secondly, while adenoviruses remain episomal, lentiviruses integrate into the host genome randomly which is known to cause potential insertional mutagenesis (*600*, *625*). It should be noted that although the effect of random insertion was mitigated by including uninduced cells (minus Dox) within individual stable cell lines, a limitation of the current study is that the sites of insertion are not necessarily identical for all stable cell lines. Therefore, an inducible adenoviral system might be a better strategy to study the role of the PLIN1 mutant using the *Plin1* KO MEF model.

5.6 Conclusion

In summary, the experiments outlined in this chapter suggest that the substitution from leucine to proline at residue position 90 in PLIN1 may enhance its interaction with HSL under non-stimulated conditions, assessed by BiFC assay. In addition, this point mutation may also interfere with lipolysis in response to isoproterenol and IBMX stimulation. However, whether this effect is modulated through the interaction with HSL upon lipolytic stimulation still requires further work.

The L90P variant is associated with overall adiposity but lower WHR owing primarily to larger hip circumferences, suggesting that the variant may enhance the storage of gluoteo-femoral adipose tissue (*1*). This variant is also associated with lower levels of TG, as well as other beneficial lipid profiles with protection from cardiometabolic disease, implying that it may also affect intracellular lipolysis (*1*). Therefore, human genetic studies implicate regional differences in response to biological cues with this variant, which may be involved in the PLIN1-HSL interaction. Further characterisation of the function of L90P in depot-specific adipocyte biology with human cellular studies ought to be considered though these may prove to be technically challenging.

6 General Discussion

Body fat distribution is an independent predictor of metabolic and cardiovascular disease and is heritable (*626*). As a surrogate for the measurement of body fat distribution, BMI adjusted WHR shows a heritability of up to approximately 60% (*626*). Previous studies also indicate that genetic factors seem to have a greater effect on abdominal VAT than abdominal SAT (*216*, *217*, *626*). Therefore, it is postulated that the heterogeneity of adipose tissue, in terms of differential gene expression profiles between VAT and SAT, as well as polymorphisms in genes leading to functional changes, could potentially regulate body fat distribution.

A plethora of novel genes/loci that are associated with WHR have been identified using GWAS in recent years. It is also noteworthy that many WHR associated loci have also shown associations for cardiometabolic traits (*626*). As mentioned in Chapter 1, the vast majority of the identified variants are predominantly located in the non-coding regions of the genome. Hence, it is difficult to establish the functionality of these SNPs and disease causality (*219*). In contrast, low frequency nonsynonymous variants often offer strong link between gene and phenotype since the functional effect is mostly due to the variant itself (*239*). Most importantly, the study of low frequency nonsynonymous alleles has also catalysed the translation from gene identification to therapeutic drug development (*1*, *627*). Therefore, a better knowledge of the functional consequences caused by these coding genetic variants leading to altered body shape and cardiometabolic risk is crucial for understanding the underlying mechanisms of association. Prompted by the initial GWAS conducted by Lotta et al., the aim of this thesis was to investigate the role of *ALK7*, *CALCRL*, *PLIN1*, *PDE3B* and *PNPLA2* in adipocyte biology and to characterise the molecular and cellular effects of the nonsynonymous alleles at *ALK7*, *PLIN1* and *PNPLA2* that are associated with altered body fat distribution (*1*).

6.1 Loss-of-function studies by gene knockdown

Lotta et al. have conducted detailed *in silico* analyses using a variety of online algorithms such as SIFT and Polyphen, to predict the possible functional impact of the identified variants (*1*).

As the *PDE3B* p.R783X variant is expected to truncate the protein within its catalytic domain (as illustrated in Figure 3.2), the evidence for a deleterious impact was very strong (*1*). Prediction of the functional impact on *CALCRL* p.L87P was mild, while a likely deleterious impact was predicted for the *PLIN1* p.L90P variant (*1*). Between the two variants at the *ALK7* locus, p.I195T was predicted to have a more deleterious functional impact than the p.N150H variant (*1*). Similarly, the overall predication of the *PNPLA2* p.N252K was also to be likely deleterious (*1*). Since all genes of interest are expressed in adipose tissue and the bioinformatic annotation of the variants was all likely to be deleterious, a loss-of-function study was therefore conducted aiming to highlight the physiological significance of *Alk7*, *Calcrl*, *Plin1*, *Pde3b* and *Pnpla2* in adipocyte biology using the 3T3-L1 cell model (*1*).

Repeated siRNA mediated gene knockdown was performed in 3T3-L1 (pre)adipocytes, which were then analysed for adipogenesis and intracellular lipolysis. The 3T3-L1 cell model has been used extensively in the research of lipogenesis and lipolysis as they offer an abundant supply of homogeneous cells that responded reliably and predictably to treatments, which makes them suitable for studying molecular mechanisms that are involved in adipocyte biology (*444*, *628*, *629*). By combining with gene silencing techniques such as siRNA transfection, it allows the study of the function of a specific gene associated with adipogenesis and lipolysis (*444*). However, there are a few limitations using the 3T3-L1 cell model. Firstly, the differentiation capacity decreases when passaged extensively (*444*, *628*). Secondly, as the 3T3-L1 cell line is originated from one single clone, it may fail to recapitulate the characteristics of the primary cells it models (*444*, *548*). Thirdly, differentiated 3T3-L1 adipocytes which display features of multiple adipocytes lineages, are phenotypically and metabolically different from white adipocytes (*630*). Lastly, they are relatively difficult to transfect as transient transfection normally requires subconfluent cells (*444*, *548*). Therefore, to ensure a proper suppression of gene expression, several rounds of siRNA transfection were performed prior to and during the course of 3T3-L1 differentiation. It should be noted that the block of gene expression is rarely complete, thus some protein function may be retained due to incomplete knockdown by this approach (*631*, *632*).

6.1.1 ALK-7

The loss-of-function study by knocking down *Alk7* in 3T3-L1 cells was performed twice in this thesis. While lipolysis was consistently reduced in both sets of studies, the impact of ALK-7 knockdown on 3T3-L1 adipogenesis was conflicting. In the first set of experiments, siRNA of *Alk7* had no impact on adipogenesis, while in the second set of experiments where the knockdown efficiency of *Alk7* siRNA reached 90%, adipogenesis was impaired. As detailed in Chapter 3, this discrepancy might be due to differences in the passage number of cells between experiments as well as the variable knockdown efficacy. However, previously published work argues against a role of ALK-7 in adipogenesis. Firstly, *Alk7* KO mice show apparently normal development of adipose tissue (*268*). Secondly, ALK-7 expression is only induced during the late phases of adipocyte differentiation (*267*, *542*). At present, there is no publicly available data demonstrating the impact of knocking down *Alk7* in *in vitro* cell models and its role in adipogenesis. While the data in this thesis (due to technical challenges) does not provide a definitive conclusion for a role of ALK-7 in adipogenesis, further investigations are warranted.

Further clarification is also required for ALK-7 regulation of lipolysis. All previously published data suggest that ALK-7 is a negative regulator of lipolysis since depletion of *Alk7* in mice results in increased lipolysis (*277*, *448*). On the contrary, knocking down *Alk7* in 3T3-L1 adipocytes led to reduced basal and catecholamine stimulated lipolysis in this thesis. At present, we hypothesise that this might be a reflection of the impaired adipogenesis that is concurrently observed with *Alk7* knockdown. It is worth noting that *in vivo* analysis is a complex phenotype to analyse with cross communication from multiple tissues and cell types as ALK-7 serves as a receptor for multiple ligands in the TGF-β family that are not only expressed in mature adipocytes, but also secreted from cells in the SVF, *in vitro* cellular model thus may not replicate the *in vivo* findings (*270*). Therefore, it is necessary to confirm the findings in this thesis with alternative approaches in order to fully reveal the physiological function of ALK-7 in adipocyte biology. For example, the use of CRISPR could potentially improve *Alk7* targeting and the study of differentiated SVF adipocytes from *Alk7* KO mice could also be informative.

6.1.2 CALCRL

Deletion of *Calcrl expression* globally, or, specifically within lymphatic endothelium during adulthood results in reduced body weight. This phenotype was shown to be due to impaired lipid absorption in the intestine in mice, highlighting its role in maintaining lymphatic function in intestines (*459*, *460*). However, the exact role of CALCRL in adipocyte biology has not been fully investigated. In fact, *in vitro* loss-of-function studies of CALCRL in adipocytes or adipose tissue has not been done to my knowledge. Findings from this thesis support a potential role of CALCRL in lipolysis. The data presented in Chapter 3 indicated that knocking down *Calcrl* in two independent sets of experiments suppresses lipolysis in 3T3-L1 adipocytes. As the receptor for ligands ADM and CGRP, which are known to induce lipolysis, the loss of CALCRL could impair the signal transduction pathway (*322*, *554*). However, previous reports also show that ADM inhibits stimulated lipolysis via oxidation of isoproterenol by NO, suggesting that the absence of CALCRL could potentially result in elevated stimulated lipolysis, which however was not seen in this thesis (*314*). This might suggest different signalling pathways of ADM and isoproterenol in the regulation of lipolysis. Therefore, the question as to which signalling axis is predominant due to the silencing of *Calcrl* expression still needs to be answered.

We have hypothesised that the impaired differentiation due to the knockdown of *Calcrl* in the second set of experiments might also contribute to the observed reduced lipolysis. Therefore, a knockdown experiment at a later stage of differentiation could be performed to validate this possibility. The inconsistent results for CALCRL on adipogenesis could be affected by the difference in knockdown efficiency as well as the passage number of the cells, as discussed in Chapter 3. The limitation of this particular experiment that cannot be overlooked is the lack of a suitable antibody to test the knockdown efficacy of CALCRL at the protein level. Therefore, any residual CALCRL protein remaining could be sufficient in transducing signals in response to ligand. The possible mechanism for the observed impaired adipogenesis in the current study could be related to the inability to elevate cAMP levels due to the lack of CALCRL in 3T3-L1 preadipocytes. As a result, failing to activate PKA by cAMP would inhibit downstream CREB activity, which may affect transcription of early adipogenic markers such as C/EBPβ, thus blocking adipogenesis (*633*). This hypothesis does not rule out other mechanisms as CALCRL mediated cAMP/PKA pathway regulates multiple downstream targets (Figure 1.9). Significant

investigation will be required to uncover which mechanisms are actually altered in the absence of CALCRL.

As described in Chapter 1, CALCRL can bind with different RAMPs to form different receptor complexes for CGRP, ADM and ADM2. These peptides are potentially involved in the pathophysiology of the metabolic syndrome, although much remains unclear (*291*, *634*, *635*). Some correlation between the expression levels of these peptides and obesity or diabetes mellitus has been reported (*462*, *467*, *468*, *470*, *636–638*). However, only a few determined the association with the expression level of the corresponding receptor components. For example, recently it has been shown that obese rats had increased endogenous protein expression of ADM, CALCRL, RAMP2 and RAMP3 in VAT (*638*). Similar observations were made in mRNA expression level from human omental adipose tissue isolated from gestational diabetes mellitus pregnancies (*468*). Taken together, elevations in the peptides and the receptor complexes in adipose tissue locally could potentially alter lipid metabolism. In addition, CGRP released from sensory nerves could modulate the innervated WAT to initiate lipolysis, indicating a dynamic crosstalk between the CNS and WAT (*639*). Therefore, the impact of its receptor CALCRL on the control of lipid mobilisation could also be related to sympathetic activation rather than intrinsic regulation within adipose tissue (*640*, *641*).

While the functional characterisation of the CALCRL variant was not investigated in this thesis, the L87P mutation is predicted to be deleterious to downstream signalling (*1*). The mutation is located in the ECD where it interacts with RAMPs, which could potentially result in a readjustment of the secondary structure, thereby affecting ligand binding and signal transduction (*1*). Based on the findings from Chapter 3 where the loss of *Caclrl* expression impairs lipolysis and possibly signalling, one therefore could infer that carriers with the p.L87P variant could benefit from the reduced FA thus leading to the protective role of this variant from cardiometabolic diseases. Given this notion, external collaborations to study the signal transduction of this particular variant have been initiated.

6.1.3 PLIN1

Data presented in this thesis suggests that cells lacking *Plin1* failed to block basal lipolysis, while stimulated lipolysis was attenuated. This is in line with the established role of PLIN1 as the gatekeeper of intracellular lipolysis, as it is critical in restricting basal lipolysis and facilitating stimulated lipolysis at the lipid droplet within adipocytes (*331*). The results were also verified by previous knockdown studies carried out in 3T3-L1 adipocytes and a similar phenotype was observed in *Plin1* null mice (*349*, *351*, *358*, *359*). As opposed to previous knockdown assays that were performed in differentiated 3T3-L1 adipocytes, the current experiment was conducted before the initiation of differentiation with impaired adipogenesis observed (*349*, *351*). This was accompanied by a significant reduction in the expression of a few key adipogenic markers. The finding of impaired adipogenesis was unexpected since adipocyte differentiation appeared to be normal in white adipocytes isolated from the KO mice as well as exhibit normal mRNA expression of *Pparg* and *Cebpa* (*359*). However, as discussed in Chapter 3, there is evidence to suggest a role of *Plin1* in adipogenesis, as *Plin1* KO SVC showed defective adipocyte differentiation (*485*). Furthermore, within the same study an impairment of SREBP1c function was observed and implicated in adipogenesis due to the reduction of target genes, TG synthesis and LD formation (*484*, *485*). SREBP1 regulation was not examined in this thesis, therefore the contribution of this axis in siPlin1 regulation of adipogenesis remains unknown. Rather, the more definitive role of *Plin1* in lipolysis may underlie the reduction in LD accumulation seen in the knockdown cells. Collectively, the loss-of-function study has emphasized the role of PLIN1 in the regulation of lipolysis, although the exact mechanism as to how PLIN1 affects adipogenesis requires further studies.

6.1.4 PDE3B

PDE3B is known for its role in hydrolysing cAMP in response to insulin in adipocytes. As cAMP levels decrease, PKA action reduces which prevents HSL activation thereby inhibiting lipolysis. Furthermore, *in vivo* studies indicate that stimulated lipolysis was enhanced in *Pde3b* null mice, while basal lipolysis was not affected (*509*). Therefore, knocking down *Pde3b* should theoretically result in elevated lipolysis. However, data presented in Chapter 3 showed that silencing *Pde3b* expression in 3T3-L1 adipocytes did not have any impact on lipolysis. The discrepancy between the observed phenotypes could be due to two reasons. Firstly, the *in vivo* lipolysis was measured systemically where lipolysis is also influenced by other systems

(*509*). Secondly, differentiated 3T3-L1 adipocytes are morphologically different as they remain multilocular compared to unilocular white adipocytes. Nonetheless, previous *in vitro* studies suggest that insulin-mediated regulation of lipolysis is partly dependent on the ability of PDE3B to catalyse the breakdown of cAMP (*558*, *559*). In the few attempts made here in this thesis, the role of PDE3B in insulin mediated suppression of lipolysis proved to be inconclusive. This was mainly due to the lack of an observable inhibition of lipolysis by insulin in control cells and also a lack of effect with siPde3b. Due to the lack of a suitable PDE3B antibody, the evaluation of knockdown efficacy at the protein level is not available. Hence, the possibility of a partial loss-of-function of PDE3B protein also needs to be taken into consideration when interpreting these results. The same applies for not observing any impact on adipogenesis following *Pde3b* knockdown as it has been reported that the mRNA expression of a subset of adipogenic transcription factors such as *Cepba* and *Cebpb* were upregulated in the WAT of *Pde3b* KO mice compared with WT counterparts (*510*). As discussed in Chapter 3, knocking down the *PDE3B* gene in human preadipocytes led to increased lipid accumulation which was explained by a higher lipogenesis/lipolysis ratio (*512*). Therefore, since basal lipolysis was not affected by *Pde3b* knockdown in this study, it seems plausible for not visually observing any difference in lipid accumulation. Future work is required to verify the findings as to whether PDE3B is dispensable in adipogenesis.

Functional studies for the variant R783X are being carried out by other members of the laboratory and are ongoing. As mentioned previously in Chapter 3, this nonsense mutation occurs in the catalytic domain and the product of which is predicted to result in a loss of function of PDE3B (*1*). Studies from the KO mice have revealed different responses in different tissues (Table 3.4) with beneficial effects mainly include lower fat mass, enhanced lipolysis and energy expenditure, linking the association of this predicted loss-of-function variant with lower levels of TG in carriers (*1*, *367*, *377*, *384*, *398*, *509*). However, *Pde3b* null mice are known to develop insulin resistance as evidenced by the impaired suppression of glucose production in liver (*398*, *509*). Therefore, as tempting as it sounds, the outcome of inhibiting PDE3B activity is rather difficult to predict.

6.1.5 PNPLA2

Depletion of *Pnpla2* in 3T3-L1 cells had no visible effect on lipid accumulation when differentiated into mature adipocytes. However, both basal and stimulated lipolysis were severely impaired due to the loss of expression of PNPLA2. This is in line with previous reports showing the reduction in lipolytic products in 3T3-L1 adipocytes treated with *Pnpla2* siRNA (*407*). Similarly, the decreased TG turnover rate was also observed in both global and adipose tissue specific *Pnpla2* KO mice (*422*, *523*). The results presented in this thesis corroborate the role of PNPLA2 in the regulation of TG hydrolysis. Although impaired TG mobilisation in *Pnpla2* deficient mice led to increased fat mass and massive accumulation of TG in multiple non-adipose tissues which ultimately caused premature death, the glucose tolerance and insulin sensitivity were in fact improved (*523*, *525*, *529*, *530*). Moreover, increased glucose uptake and enhanced insulin signalling were observed in skeletal muscle and liver of these mice, indicating that PNPLA2 affects whole-body glucose homeostasis (*523*, *525*, *530*). Similar improvement in glucose and insulin tolerance was observed in adipocyte-specific *Pnpla2* KO mice, primarily due to enhanced hepatic insulin signalling (*422*, *530*). It is worth noting that these mice exhibited BAT expansion resulting from impaired lipolysis and/or lipid oxidation (*530*). However, the contribution of PNPLA2 mediated lipolysis to whole-body energy metabolism still needs to be validated in human (*431*).

6.2 Functional consequences of the rare nonsynonymous variants and translation to human body fat distribution and cardiometabolic risk

The functional consequences of the selected genetic variants were evaluated using *in vitro* cell models in the experiments, which mainly involve the overexpression and ectopic expression of the constructs into the host cell line. This allows the study of the biological function of target gene products under controlled conditions, thus providing insights into the possible effect of the mutations. However, not only could overexpression studies give rise to false positive results in the functional analyses, but the scope provided by the *in vitro* cell line itself is also limited, thus may not be representative of the *in vivo* conditions (*642*). Furthermore, the functional effects of rare nonsynonymous variants could be expected to be mild since the change of amino acid mostly affects protein expression or stability, or protein-protein interaction, which will be discussed in the sections below. My own studies reported

in this thesis highlight how difficult it can be to generate definitive data on the functional impact of many variants identified in GWAS, even when these focus on coding variants. This is perhaps not too surprising as these variants have very modest phenotypic consequences on their own. Hence a robust assay system is vital for detection of subtle difference of variants in functional analysis.

6.2.1 PNPLA2 (p.N252K)

An association of a higher BMI adjusted WHR and a higher cardiometabolic risk was identified in participants carrying the PNPLA2 p.N252K mutation (*1*). Initial characterisation of this particular variant showed a reduced overall mRNA expression in the heterozygous carriers with the mutant allele compared with homozygous carriers of the WT allele. Depot-specific differences in *PNPLA2* mRNA expression have been reported though this has not always led to changes in protein expression (*643*). Therefore, a comparison of the protein expression between WT and N252K in various adipose tissue depots would provide more information as to how PNPLA2 expression contributes to altered body shape. Furthermore, the exact mechanisms by which the mutant reduces overall mRNA expression is still missing since this particular nucleotide substitution did not seem to affect splicing. Other factors that may affect mRNA stability such as codon usage or RNA modification might be interesting to explore (*644*–*646*).

Previous studies have described loss-of-function mutations in *PNPLA2* causing a rare autosomal recessive disorder known as NLSDM (*428*–*430*, *647*). The disease is characterised by ectopic fat deposition and has been reported to be associated with dyslipidaemia and diabetes in some cases (*1*, *428*, *429*). Patients carrying *PNPLA2* missense mutations disrupting the catalytic site manifest a rather severe disease phenotype, indicating that there is a link between lipolytic activity and disease severity (*648*). As indicated in Chapter 4, this mutant retained its ability to target LD and possessed normal lipase activity at least *in vitro*, hence how this then leads to differences in lipolysis is still unclear. As described above and elsewhere, it could simply be surmised that the reduced mRNA observed (and subsequent protein expression) in the p.N252K carriers results in a reduced lipolytic rate, which might

explain the shift towards lower FFA levels (*521*). Further analyses of this N252K variant will be needed to explain the association between lipolytic activity and increased metabolic risk.

6.2.2 ALK7 (p.I195T and N150H)

The data presented in Chapter 4 aimed to shed some lights on the functional impact of the two variants p.I195T and N150H at the *ALK7* locus on Smad signalling transduction. The I195T, is predicted to have a deleterious functional consequence as it lies between the GS and the kinase domain that would impact on the activation of ALK-7, as well as the interaction with downstream Smads (*1*). It is therefore possible that this loss-of-function mutation I195T may act in a dominant negative manner, which then subsequently impedes Smad signalling in the carriers. In agreement with the *in silico* analysis where N150H is predicted to have a rather mild impact, N150H mediated Smad signalling transduction did seem to be normal compared with the WT. However, this does not exclude the possibility that other Smad-independent pathways might be affected. Future work will be required to test these hypotheses.

The findings that the I195T and N150H variants lead to the loss of ALK-7 function are in agreement with other studies (*18*, *451*). Emdin et al. further demonstrated another two damaging variants are also associated with lower WHR and protected against T2D in human (*18*). Particularly the non-coding variant in *ALK7* (rs72927479) has been shown to be associated with reduced expression in SAT and pancreas, indicating that a depot-specific model may be required to understand the relationship between these genetic variants and body fat distribution (*18*). Similarly, *Alk7* deficient mice and mice treated with chemical inhibitors of *Alk7* have been reported to have reduced lipid accumulation and enhanced lipolysis, suggesting that reduced ALK-7 receptor function in carriers with ALK-7 variants alters body fat (*277*, *280*, *448*). However, enhanced lipolysis can be a contributor to insulin resistance in humans, which consequently contradicts the protective effect that reported in human genetic studies (*1*, *18*). Although data generated from Chapter 3 demonstrated reduced lipolysis supporting a protective role for reduced ALK-7 function, further characterisation of these variants is necessary to more convincingly provide a molecular mechanism for the observed protective association.

6.2.3 PLIN1 (p.L90P)

Frameshift mutations of human PLIN1 have been associated with FPLD4, which is characterised by the loss of gluteo-femoral adipose tissue, dyslipidaemia and insulin resistance (*361*, *362*). Functional analysis showed that these mutations failed to suppress basal lipolysis, leading to the lipodystrophic phenotype (*360*–*362*). In this study, carriers with the L90P variant in *PLIN1* manifest enhanced lipid storage in the gluteo-femoral adipose tissue which might offer protection against cardiometabolic risk (*1*). This prompted the characterisation of this mutant to investigate the impact on lipid storage and mobilisation in various adipocyte models. As the mutated residue is located in the vicinity of a conserved phosphorylation site (S81) which is believed to be involved in the interaction with HSL, a protein-protein interaction assay was performed for an initial characterisation. The BiFC assay showed enhanced interaction with HSL compared with the WT although no difference was observed in the BiFC signals upon lipolytic stimulation. Based on this observation, elevated basal lipolysis might be predicted, although ectopic expression of L90P in *Plin1* null MEFs did not seem to enhance basal lipolysis compared to WT. Indeed, enhanced interaction between L90P and HSL in the basal state does not necessarily elevate basal lipolysis which is mainly influenced by the expression of PNPLA2 (*649*). Further work with other methods therefore should be explored to verify the findings presented in this thesis.

Although the possibility that decreased protein stability of L90P could result in reduced lipolysis and subsequently reduced FA levels, thus explaining the apparently protective role in carriers with this variant was proposed according to the findings presented in Chapter 5, the molecular explanation as to how this variant affects body fat distribution remains largely unknown. A good starting point would be examination of the expression profiles from different adipose tissue depots in both WT and L90P carriers. Previous studies have shown that the mRNA expression of PLIN1 was significantly reduced in abdominal omental compared with the subcutaneous adipose tissue in obese subjects, although no significant difference was observed in the protein levels, suggesting that PLIN1 may be regulated at a post-transcriptional level (*487*, *650*). In non-obese subjects, no difference was observed in the mRNA expression level between abdominal and gluteal SAT although whether there is any difference on the protein level has not yet been reported (*643*). Therefore, future work that

involves the investigation of depot-specific expression of PLIN1, particularly in the abdominal versus the gluteo-femoral regions, would be useful to reveal the underlying mechanisms linking the PLIN1 variant to altered body fat distribution.

6.3 Implications in drug discovery and development

Based on human genetic findings, genes that influence human health and disease can potentially transform the process of the selection of drug targets (*651*). Identification of rare missense variants has led to therapeutic drug development, particularly since the ones that offer protection against disease risk mimic the effect of modulating drug target genes (*652*, *653*). The most successful example being the discovery of the loss-of-function low-frequency coding variants in *PCSK9* (proprotein convertase subtilisin/kexin type 9) which led to the development of a monoclonal antibody evolocumab, resulting in lower levels of low-density lipoprotein (LDL) cholesterol with a reduced risk of coronary heart disease on a background of statin therapy (*654–656*).

As for the alleles that have been associated with greater disease risk, they can potentially be used as biomarkers for personalised medicine (*652*). However, cautions must be taken to determine whether the detected variant is truly a pathogenic variant in order to deliver a genotype-based prediction in a safe and effective manner (*652*, *657*).

In addition, as presented in this thesis as well as previous literature, all the genes we focussed on are potentially implicated in the regulation of intracellular lipolysis. This pathway is pharmacologically modifiable (*1*). As summarised in Chapter 1, ALK-7 has become an interesting target for obesity, while PDE3B inhibitors have been utilised in cardiovascular therapies (*658*). Similarly, pharmacological inhibition of PNPLA2 is also considered as a potential therapeutic strategy to treat obesity and its associated metabolic complications, although it is only effective in mouse models (*433*, *434*, *659*). Therefore, validating the biological consequences of these gene variants for correct annotation may offer new opportunities in modulating intracellular lipolysis, leading to progress in the prevention and treatment of cardiometabolic diseases.

6.4 Future directions

The investigation of the roles of the selected genes/variants could benefit from another approach by employing a more powerful gene editing tool, the CRISPR/Cas method, in order to improve the current cellular models. Firstly, the outcome of the loss-of-function studies presented in Chapter 3 was limited by the knockdown efficacy where the expression of the target gene was not blocked completely. Implementation of CRISPR KO methodology could more efficiently silence endogenous expression of selected genes which would probably give clearer insights into the gene functions in the regulation of adipogenesis and lipolysis, particularly in the case where the precise roles of ALK-7 and CALCRL are unknown. Secondly, a single nucleotide change can also be introduced by CRISPR, which could be a more suitable approach, compared to overexpression, to study the functional consequences of a genetic variant.

The functional characterisation of the genetic variants was performed with *in vitro* cell models, but the mechanisms by which genetic variants alter body fat distribution has yet to be delineated in this thesis as it cannot not fully reflect the physiological responses in a whole organism (*660*). Therefore, transgenic mouse models could be useful to identify the molecular mechanisms in relation to altered body fat distribution, especially if the mouse model can be genetically manipulated in a depot-specific manner (*661*, *662*). As discussed in Chapter 1, depot-specific transcriptomic and proteomic profiles may be involved in the cardiometabolic disease risk associated with body shape, thus it would be beneficial to examine the expression levels of the genes of interest in the abdominal and gluteo-femoral adipose tissue from the 'affected' study participants, while comparing with the WT allele carriers. Recently a GWAS of human SAT has revealed a genetic locus on *HIF3A* (hypoxia-inducible factor 3α) that is associated with lipolysis, indicating that local oxygen tension could potentially be an interesting parameter to compare in various fat depots (*663*). Furthermore, the impact of these gene variants on adipocyte biology could also be investigated directly using human primary preadipocytes. Although the 3T3-L1 cell model is the most commonly used cell model to study adipocyte function, an important limitation is that multiple cytosolic lipid droplets

are normally formed when differentiated into mature adipocytes. This presents a distinct morphological difference from human adipocytes with a single large lipid droplet (*603*). Additionally, whether 3T3-L1 adipocytes resemble any particular depot-specific adipocytes found *in vivo* is still unclear (*662*). Human primary preadipocytes, on the other hand, possibly represent more closely to the context of adipose function *in vivo* with depot-specific properties when differentiated into adipocytes (*629*, *642*, *662*). Although it is technically challenging to isolate preadipocytes from other fibroblast-like cells, the proliferation, differentiation and responsiveness to treatment of primary preadipocytes are influenced by anatomic site of the depots, which may make them an improved model to address the underlying mechanisms affecting body fat distribution (*629*, *664*).

6.5 Concluding remarks

In conclusion, this work reinforces the crucial roles of PLIN1 and PNPLA2, as well as the potential roles of ALK-7 and CALCRL in the regulation of lipid metabolism. The effects of all genes of interest on lipid homeostasis are potentially interesting fields of investigation. The work described in this thesis extends GWAS findings by demonstrating functional characterisations of ALK-7, PNPLA2 and PLIN1 variants *in vitro*. These findings provide some early insights into the potential impact of these genetic variants on altered body fat distribution and cardiometabolic risk.

References

1. L. A. Lotta *et al.*, “Genome-wide scan and fine-mapping of rare nonsynonymous associations implicates intracellular lipolysis genes in fat distribution and cardio-metabolic risk” (2018), (available at http://biorxiv.org/content/early/2018/07/18/372128.abstract).
2. D. R. Meldrum, M. A. Morris, J. C. Gambone, Obesity pandemic: causes, consequences, and solutions—but do we have the will? *Fertil. Steril.* **107**, 833–839 (2017).
3. M. Blüher, Obesity: global epidemiology and pathogenesis. *Nat. Rev. Endocrinol.* **15** (2019), doi:10.1038/s41574-019-0176-8.
4. K. McPherson, T. Marsh, M. Brown, Foresight: Tackling Obesities: Future Choices – Modelling Future Trends in Obesity and the Impact on Health. *Gov. Off. Sci.*, 76 (2007).
5. E. A. Finkelstein *et al.*, Obesity and severe obesity forecasts through 2030. *Am. J. Prev. Med.* **42**, 563–570 (2012).
6. J. Cawley, An economy of scales: A selective review of obesity’s economic causes, consequences, and solutions. *J. Health Econ.* **43**, 244–268 (2015).
7. S. Averett, Obesity and labor market outcomes. *IZA World Labor*. **32**, 1–10 (2014).
8. A. Booth, A. Magnuson, M. Foster, Detrimental and protective fat: Body fat distribution and its relation to metabolic disease. *Horm. Mol. Biol. Clin. Investig.* **17**, 13–27 (2014).
9. B. Bjørndal, L. Burri, V. Staalesen, J. Skorve, R. K. Berge, Different adipose depots: Their role in the development of metabolic syndrome and mitochondrial response to hypolipidemic agents. *J. Obes.* **2011** (2011), doi:10.1155/2011/490650.
10. M. G. Saklayen, The epidemic of the metabolic syndrome. *Curr. Hypertens. Rep.* **20**, 1–8 (2018).
11. T. L. S. Visscher, M. B. Snijder, J. C. Seidell, in *Clinical Obesity in Adults and Children* (2009; https://doi.org/10.1002/9781444307627.ch1), *Wiley Online Books*, pp. 1–14.
12. J. Q. Purnell, in *Endotext [Internet]*, K. R. Feingold et al., Eds. (MDText.com, Inc., South Dartmouth (MA), 2000; https://www.ncbi.nlm.nih.gov/books/NBK279167/).

13. M. A. Staten, W. G. Totty, W. M. Kohrt, Measurement of fat distribution by Magnetic Resonance Imaging. *Invest Radiol*. **24**, 345–9 (1989).
14. J. VAGUE, The degree of masculine differentiation of obesities: a factor determining predisposition to diabetes, atherosclerosis, gout, and uric calculous disease. *Am. J. Clin. Nutr.* **4**, 20–34 (1956).
15. C. T. Montague, S. O'Rahilly, The Perils of Portliness Causes and Consequences of Visceral Adiposity. *Diabetes*. **49**, 883–888 (2000).
16. M. B. Snijder, R. M. van Dam, M. Visser, J. C. Seidell, What aspects of body fat are particularly hazardous and how do we measure them? *Int. J. Epidemiol.* **35**, 83–92 (2006).
17. C. E. Dale *et al.*, Causal Associations of Adiposity and Body Fat Distribution with Coronary Heart Disease, Stroke Subtypes, and Type 2 Diabetes Mellitus: A Mendelian Randomization Analysis. *Circulation*. **135**, 2373–2388 (2017).
18. C. A. Emdin *et al.*, DNA sequence variation in ACVR1C encoding the activin receptor-like kinase 7 influences body fat distribution and protects against type 2 diabetes. *Diabetes*. **68**, 226–234 (2019).
19. T. Pischon *et al.*, General and Abdominal Adiposity and Risk of Death in Europe. *N. Engl. J. Med.* **359**, 2105–2120 (2008).
20. S. Yusuf *et al.*, Obesity and the risk of myocardial infarction in 27,000 participants from 52 countries: a case-control study. *Lancet*. **366**, 1640–1649 (2005).
21. L. Lapidus *et al.*, Distribution of adipose tissue and risk of cardiovascular disease and death: a 12 year follow up of participants in the population study of women in Gothenburg, Sweden. *Br. Med. J. (Clin. Res. Ed).* **289**, 1257–1261 (1984).
22. B. Larsson, K. Svardsudd, L. Welin, Abdominal adipose tissue distribution, obesity, and risk of cardiovascular disease and death: 13 year follow up of participants in the study of men born in 1913. *Br. Med. J.* **288**, 1401–1404 (1984).
23. K. Silventoinen, P. Jousilahti, E. Vartiainen, J. Tuomilehto, Appropriateness of anthropometric obesity indicators in assessment of coronary heart disease risk among Finnish men and women. *Scand. J. Public Health*. **31**, 283–290 (2003).
24. M. B. Snijder *et al.*, Associations of hip and thigh circumferences independent of waist circumference with the incidence of type 2 diabetes: The Hoorn Study. *Am. J. Clin. Nutr.* **77**, 1192–1197 (2003).

25. S. Gesta, Y. H. Tseng, C. R. Kahn, Developmental Origin of Fat: Tracking Obesity to Its Source. *Cell*. **131**, 242–256 (2007).
26. M. M. Ibrahim, Subcutaneous and visceral adipose tissue: Structural and functional differences. *Obes. Rev.* **11**, 11–18 (2010).
27. E. K. Oikonomou, C. Antoniades, The role of adipose tissue in cardiovascular health and disease. *Nat. Rev. Cardiol.* (2018), doi:10.1038/s41569-018-0097-6.
28. E. E. Kershaw, J. S. Flier, Adipose tissue as an endocrine organ. *J. Clin. Endocrinol. Metab.* **89**, 2548–2556 (2004).
29. L. Luo, M. Liu, Adipose tissue in control of metabolism. *J. Endocrinol.* **231**, R77–R99 (2016).
30. P. Cohen, B. M. Spiegelman, Cell biology of fat storage. *Mol. Biol. Cell*. **27**, 2523–2527 (2016).
31. A. Wronska, Z. Kmiec, Structural and biochemical characteristics of various white adipose tissue depots. *Acta Physiol.* **205**, 194–208 (2012).
32. A. Garg, Adipose Tissue Dysfunction in Obesity and Lipodystrophy. *Clin. Cornerstone*. **8**, S7–S13 (2006).
33. C. R. Kahn, G. Wang, K. Y. Lee, Altered adipose tissue and adipocyte function in the pathogenesis of metabolic syndrome. *J. Clin. Invest.* **129**, 3990–4000 (2019).
34. L. Sidossis, S. Kajimura, Brown and beige fat in humans: Thermogenic adipocytes that control energy and glucose homeostasis. *J. Clin. Invest.* **125**, 478–486 (2015).
35. X. Liu, C. Cervantes, F. Liu, Common and distinct regulation of human and mouse brown and beige adipose tissues: a promising therapeutic target for obesity. *Protein Cell*. **8**, 446–454 (2017).
36. X. Ma, P. Lee, D. J. Chisholm, D. E. James, Control of adipocyte differentiation in different fat depots; Implications for pathophysiology or therapy. *Front. Endocrinol. (Lausanne).* **6**, 1–8 (2015).
37. J. Wu *et al.*, Beige adipocytes are a distinct type of thermogenic fat cell in mouse and human. *Cell*. **150**, 366–376 (2012).
38. L. Z. Sharp *et al.*, Human BAT Possesses Molecular Signatures That Resemble Beige/Brite Cells. *PLoS One*. **7** (2012), doi:10.1371/journal.pone.0049452.
39. A. P. Frank, R. De Souza Santos, B. F. Palmer, D. J. Clegg, Determinants of body fat distribution in humans may provide insight about obesity-related health risks. *J. Lipid*

Res. **60**, 1710–1719 (2019).

40. S. X. Chen, L. J. Zhang, R. L. Gallo, Dermal White Adipose Tissue: A Newly Recognized Layer of Skin Innate Defense. *J. Invest. Dermatol.* **139**, 1002–1009 (2019).
41. Q. Luong, K. Y. Lee, in *Adipose Tissue* (2018; https://www.intechopen.com/books/adipose-tissue/the-heterogeneity-of-white-adipose-tissue), pp. 177–206.
42. A. Chait, L. J. den Hartigh, Adipose Tissue Distribution, Inflammation and Its Metabolic Consequences, Including Diabetes and Cardiovascular Disease. *Front. Cardiovasc. Med.* **7**, 1–41 (2020).
43. J. J. Lee *et al.*, Upper Body Subcutaneous Fat Is Associated with Cardiometabolic Risk Factors. *Am. J. Med.* **130**, 958-966.e1 (2017).
44. K. A. Britton *et al.*, Body fat distribution, incident cardiovascular disease, cancer, and all-cause mortality. *J. Am. Coll. Cardiol.* **62**, 921–925 (2013).
45. S. Klein *et al.*, Absence of an Effect of Liposuction on Insulin Action and Risk Factors for Coronary Heart Disease. *N. Engl. J. Med.* **350**, 2549–2557 (2004).
46. A. Thörne, F. Lönnqvist, J. Apelman, G. Hellers, P. Arner, A pilot study of long-term effects of a novel obesity treatment: Omentectomy in connection with adjustable gastric banding. *Int. J. Obes.* **26**, 193–199 (2002).
47. T. T. Tran, Y. Yamamoto, S. Gesta, C. R. Kahn, Beneficial Effects of Subcutaneous Fat Transplantation on Metabolism. *Cell Metab.* **7**, 410–420 (2008).
48. C. M. Poissonnet, A. R. Burdi, S. M. Garn, The chronology of adipose tissue appearance and distribution in the human fetus. *Early Hum. Dev.* **10**, 1–11 (1984).
49. C. M. Poissonnet, M. LaVelle, A. R. Burdi, Growth and development of adipose tissue. *J. Pediatr.* **113**, 1–9 (1988).
50. Z. L. Sebo, M. S. Rodeheffer, Assembling the adipose organ: Adipocyte lineage segregation and adipogenesis in vivo. *Dev.* **146** (2019), doi:10.1242/dev.172098.
51. K. Y. Lee *et al.*, Developmental and functional heterogeneity of white adipocytes within a single fat depot. *EMBO J.* **38**, 1–19 (2019).
52. S. Gesta *et al.*, Evidence for a role of developmental genes in the origin of obesity and body fat distribution. *Proc. Natl. Acad. Sci. U. S. A.* **103**, 6676–6681 (2006).
53. T. Tchkonia *et al.*, Identification of depot-specific human fat cell progenitors through distinct expression profiles and developmental gene patterns. *Am. J. Physiol.* -

Endocrinol. Metab. **292**, 298–307 (2007).

54. S. Y. Min *et al.*, Diverse repertoire of human adipocyte subtypes develops from transcriptionally distinct mesenchymal progenitor cells. *Proc. Natl. Acad. Sci. U. S. A.* **116**, 17970–17979 (2019).
55. N. Billon, C. Dani, Developmental Origins of the Adipocyte Lineage: New Insights from Genetics and Genomics Studies. *Stem Cell Rev. Reports*. **8**, 55–66 (2012).
56. M. Coelho, T. Oliveira, R. Fernandes, Biochemistry of adipose tissue: An endocrine organ. *Arch. Med. Sci.* **9**, 191–200 (2013).
57. A. T. Ali, W. E. Hochfeld, R. Myburgh, M. S. Pepper, Adipocyte and adipogenesis. *Eur. J. Cell Biol.* **92**, 229–236 (2013).
58. M. J. Lee, Y. Wu, S. K. Fried, Adipose tissue heterogeneity: Implication of depot differences in adipose tissue for obesity complications. *Mol. Aspects Med.* **34**, 1–11 (2013).
59. C. Hilton, F. Karpe, K. E. Pinnick, Role of developmental transcription factors in white, brown and beige adipose tissues. *Biochim. Biophys. Acta - Mol. Cell Biol. Lipids*. **1851**, 686–696 (2015).
60. M. D. Jensen, M. G. Sarr, D. A. Dumesic, P. A. Southorn, J. A. Levine, Regional uptake of meal fatty acids in humans. *Am. J. Physiol. - Endocrinol. Metab.* **285**, 1282–1288 (2003).
61. T. Tchkonia *et al.*, Mechanisms and metabolic implications of regional differences among fat depots. *Cell Metab.* **17**, 644–656 (2013).
62. S. A. Romanski, R. M. Nelson, M. D. Jensen, Meal fatty acid uptake in adipose tissue: Gender effects in nonobese humans. *Am. J. Physiol. - Endocrinol. Metab.* **279**, 455–462 (2000).
63. A. L. Ghaben, P. E. Scherer, Adipogenesis and metabolic health. *Nat. Rev. Mol. Cell Biol.* **20**, 242–258 (2019).
64. C. M. Kusminski, P. E. Bickel, P. E. Scherer, Targeting adipose tissue in the treatment of obesity-associated diabetes. *Nat. Rev. Drug Discov.* **15**, 639–660 (2016).
65. M. I. Lefterova, M. A. Lazar, New developments in adipogenesis. *Trends Endocrinol. Metab.* **20**, 107–114 (2009).
66. C. E. Lowe, S. O'Rahilly, J. J. Rochford, Adipogenesis at a glance. *J. Cell Sci.* **124**, 2681–2686 (2011).

67. M. Lundgren *et al.*, Fat cell enlargement is an independent marker of insulin resistance and “hyperleptinaemia.” *Diabetologia*. **50**, 625–633 (2007).
68. R. K. Gupta, Adipocytes. *Curr. Biol.* **24**, R988–R993 (2014).
69. P. Trayhurn, Hypoxia and adipose tissue function and dysfunction in obesity. *Physiol. Rev.* **93**, 1–21 (2013).
70. L. B. Salans, J. L. Knittle, J. Hirsch, The role of adipose cell size and adipose tissue insulin sensitivity in the carbohydrate intolerance of human obesity. *J. Clin. Invest.* **47**, 153–165 (1968).
71. M. Lönn, K. Mehlig, C. Bengtsson, L. Lissner, Adipocyte size predicts incidence of type 2 diabetes in women. *FASEB J.* **24**, 326–331 (2010).
72. N. K. Edens, S. K. Fried, J. G. Kral, J. Hirsch, R. L. Leibel, In vitro lipid synthesis in human adipose tissue from three abdominal sites. *Am. J. Physiol. - Endocrinol. Metab.* **265** (1993), doi:10.1152/ajpendo.1993.265.3.e374.
73. K. L. Spalding *et al.*, Dynamics of fat cell turnover in humans. *Nature*. **453**, 783–787 (2008).
74. A. Hammarstedt, S. Gogg, S. Hedjazifar, A. Nerstedt, U. Smith, Impaired adipogenesis and dysfunctional adipose tissue in human hypertrophic obesity. *Physiol. Rev.* **98**, 1911–1941 (2018).
75. V. Van Harmelen, K. Röhrig, H. Hauner, Comparison of Proliferation and Differentiation Capacity of Human Adipocyte Precursor Cells from the Omental and Subcutaneous Adipose Tissue Depot of Obese Subjects. *Metabolism.* **53**, 632–637 (2004).
76. U. Smith, B. B. Kahn, Adipose tissue regulates insulin sensitivity: role of adipogenesis, de novo lipogenesis and novel lipids. *J. Intern. Med.* **280**, 465–475 (2016).
77. T. McLaughlin *et al.*, Enhanced proportion of small adipose cells in insulin-resistant vs insulin-sensitive obese individuals implicates impaired adipogenesis. *Diabetologia*. **50**, 1707–1715 (2007).
78. M. Adams *et al.*, Activators of Peroxisome Proliferator–activated Receptor ⁄ Have Depot-specific Effects on Human Preadipocyte Differentiation. *J. Clin. Invest.* **100**, 3149–3153 (1997).
79. D. G. Carey *et al.*, Sensitivity effect of rosiglitazone on insulin and body composition in type 2 diabetic patients. *Obes. Res.* **10**, 1008–1015 (2002).

80. The DREAM, Effect of rosiglitazone on the frequency of diabetes in patients with impaired glucose tolerance or impaired fasting glucose: a randomised controlled trial. *Lancet*. **368**, 1096–1105 (2006).
81. X. Su, N. A. Abumrad, Cellular Fatty Acid Uptake: A Pathway Under Construction. *Trends Endocrinol. Metab.* **20**, 72–77 (2009).
82. S. Lobo, B. M. Wiczer, A. J. Smith, A. M. Hall, D. A. Bernlohr, Fatty acid metabolism in adipocytes: Functional analysis of fatty acid transport proteins 1 and 4. *J. Lipid Res.* **48**, 609–620 (2007).
83. M. Furuhashi, S. Saitoh, K. Shimamoto, T. Miura, Fatty acid-binding protein 4 (FABP4): Pathophysiological insights and potent clinical biomarker of metabolic and cardiovascular diseases. *Clin. Med. Insights Cardiol.* **2014**, 23–33 (2014).
84. J. M. Muretta, C. C. Mastick, *Chapter 10 How Insulin Regulates Glucose Transport in Adipocytes* (Elsevier Inc., ed. 1, 2009; http://dx.doi.org/10.1016/S0083-6729(08)00610-9), vol. 80.
85. C. K. Nye, R. W. Hanson, S. C. Kalhan, Glyceroneogenesis is the dominant pathway for triglyceride glycerol synthesis in vivo in the rat. *J. Biol. Chem.* **283**, 27565–27574 (2008).
86. F. Rotondo *et al.*, Glycerol is synthesized and secreted by adipocytes to dispose of excess glucose, via glycerogenesis and increased acyl-glycerol turnover. *Sci. Rep.* **7**, 1–14 (2017).
87. M. El Hafidi, M. Buelna-Chontal, F. Sánchez-Muñoz, R. Carbó, Adipogenesis: A Necessary but Harmful Strategy. *Int. J. Mol. Sci.* **20**, 3657 (2019).
88. M. Ahmadian, R. E. Duncan, K. Jaworski, E. Sarkadi-Nagy, H. S. Sul, Triacylglycerol metabolism in adipose tissue. *Future Lipidol.* **2**, 229–237 (2007).
89. K. Bódis, M. Roden, Energy metabolism of white adipose tissue and insulin resistance in humans. *Eur. J. Clin. Invest.* **48** (2018), doi:10.1111/eci.13017.
90. B. Peck, A. Schulze, Lipid desaturation – the next step in targeting lipogenesis in cancer? *FEBS J.* **283**, 2767–2778 (2016).
91. S. Kersten, Mechanisms of nutritional and hormonal regulation of lipogenesis. *EMBO Rep.* **2**, 282–286 (2001).
92. K. A. Virtanen *et al.*, Glucose uptake and perfusion in subcutaneous and visceral adipose tissue during insulin stimulation in nonobese and obese humans. *J. Clin.*

Endocrinol. Metab. **87**, 3902–3910 (2002).

93. M. Stolic *et al.*, Glucose uptake and insulin action in human adipose tissue- Influence of BMI, anatomical depot and body fat distribution. *Int. J. Obes.* **26**, 17–23 (2002).
94. A. Veilleux *et al.*, Glucose transporter 4 and insulin receptor substrate-1 messenger RNA expression in omental and subcutaneous adipose tissue in women. *Metabolism.* **58**, 624–631 (2009).
95. S. Shadid, C. Koutsari, M. D. Jensen, Direct Free Fatty Acid Uptake Into Human Adipocytes In Vivo. *Diabetes*. **56**, 1369–1375 (2007).
96. M. C. Serra, A. S. Ryan, J. D. Sorkin, K. H. Favor, A. P. Goldberg, High adipose LPL activity and adipocyte hypertrophy reduce visceral fat and metabolic risk in obese, older women. *Obesity*. **23**, 602–607 (2015).
97. M. C. Serra, A. S. Ryan, A. P. Goldberg, Reduced LPL and subcutaneous lipid storage capacity are associated with metabolic syndrome in postmenopausal women with obesity. *Obes. Sci. Pract.* **3**, 106–114 (2017).
98. G. Frühbeck, L. Méndez-Giménez, J. A. Fernández-Formoso, S. Fernández, A. Rodríguez, *Regulation of adipocyte lipolysis* (2014), vol. 27.
99. R. Zechner *et al.*, FAT SIGNALS - Lipases and lipolysis in lipid metabolism and signaling. *Cell Metab.* **15**, 279–291 (2012).
100. S. G. Young, R. Zechner, Biochemistry and pathophysiology of intravascular and intracellular lipolysis. *Genes Dev.* **27**, 459–484 (2013).
101. A. Lass, R. Zimmermann, M. Oberer, R. Zechner, Lipolysis - A highly regulated multi-enzyme complex mediates the catabolism of cellular fat stores. *Prog. Lipid Res.* **50**, 14–27 (2011).
102. A. Yang, E. P. Mottillo, Adipocyte lipolysis: from molecular mechanisms of regulation to disease and therapeutics. *Biochem. J.* **477**, 985–1008 (2020).
103. G. Y. Carmen, S. M. Víctor, Signalling mechanisms regulating lipolysis. *Cell. Signal.* **18**, 401–408 (2006).
104. S. Naghshineh, M. Noguchi, K. P. Huang, C. Londos, Activation of adipocyte adenylate cyclase by protein kinase C. *J. Biol. Chem.* **261**, 14534–14538 (1986).
105. V. E. Chaves, D. Frasson, N. H. Kawashita, Several agents and pathways regulate lipolysis in adipocytes. *Biochimie*. **93**, 1631–1640 (2011).
106. A. S. Greenberg *et al.*, Stimulation of Lipolysis and Hormone-sensitive Lipase via the

Extracellular Signal-regulated Kinase Pathway. *J. Biol. Chem.* **276**, 45456–45461 (2001).

107. C. Sengenès *et al.*, Involvement of a cGMP-dependent pathway in the natriuretic peptide-mediated hormone-sensitive lipase phosphorylation in human adipocytes. *J. Biol. Chem.* **278**, 48617–48626 (2003).
108. M. Ahmadian, Y. Wang, H. S. Sul, Lipolysis in adipocytes. *Int. J. Biochem. Cell Biol.* **42**, 555–559 (2010).
109. C. Berggreen, A. Gormand, B. Omar, E. Degerman, O. Göransson, Protein kinase B activity is required for the effects of insulin on lipid metabolism in adipocytes. *Am. J. Physiol. - Endocrinol. Metab.* **296** (2009), doi:10.1152/ajpendo.90596.2008.
110. R. E. Duncan, M. Ahmadian, K. Jaworski, E. Sarkadi-Nagy, H. S. Sul, Regulation of Lipolysis in Adipocytes. *Annu. Rev. Nutr.* **27**, 79–101 (2007).
111. P. Morigny, M. Houssier, E. Mouisel, D. Langin, Adipocyte lipolysis and insulin resistance. *Biochimie*. **125**, 259–266 (2016).
112. K. Ahmed *et al.*, An Autocrine Lactate Loop Mediates Insulin-Dependent Inhibition of Lipolysis through GPR81. *Cell Metab.* **11**, 311–319 (2010).
113. S. M. Jeon, Regulation and function of AMPK in physiology and diseases. *Exp. Mol. Med.* **48**, e245 (2016).
114. S. Kim *et al.*, AMPK Phosphorylates Desnutrin/ATGL and Hormone-Sensitive Lipase To Regulate Lipolysis and Fatty Acid Oxidation within Adipose Tissue. *Mol. Cell. Biol.* **36**, 1961–1976 (2016).
115. M. P. Gaidhu, R. B. Ceddia, Remodeling glucose and lipid metabolism through AMPK activation: Relevance for treating obesity and Type 2 diabetes. *Future Lipidol.* **4**, 465–477 (2009).
116. W. Yin, J. Mu, M. J. Birnbaum, Role of AMP-activated Protein Kinase in Cyclic AMP-dependent Lipolysis in 3T3-L1 Adipocytes. *J. Biol. Chem.* **278**, 43074–43080 (2003).
117. P. Arner, Differences in lipolysis between human subcutaneous and omental adipose tissues. *Ann. Med.* **27**, 435–438 (1995).
118. S. E. Meek, K. S. Nair, M. D. Jensen, Insulin regulation of regional free fatty acid metabolism. *Diabetes*. **48**, 10–14 (1999).
119. T. S. Nielsen, N. Jessen, J. O. L. Jørgensen, N. Møller, S. Lund, Dissecting adipose tissue lipolysis: Molecular regulation and implications for metabolic disease. *J. Mol.*

Endocrinol. **52** (2014), doi:10.1530/JME-13-0277.

120. K. N. Manolopoulos, F. Karpe, K. N. Frayn, Gluteofemoral body fat as a determinant of metabolic health. *Int. J. Obes.* **34**, 949–959 (2010).
121. J. Laurencikiene *et al.*, Regulation of lipolysis in small and large fat cells of the same subject. *J. Clin. Endocrinol. Metab.* **96**, 2045–2049 (2011).
122. F. Karpe, K. E. Pinnick, Biology of upper-body and lower-body adipose tissue - Link to whole-body phenotypes. *Nat. Rev. Endocrinol.* **11**, 90–100 (2015).
123. H. Ray, C. Pinteur, V. Frering, M. Beylot, V. Large, Depot-specific differences in perilipin and hormone-sensitive lipase expression in lean and obese. *Lipids Health Dis.* **8**, 1–10 (2009).
124. L. Heilbronn, S. R. Smith, E. Ravussin, Failure of fat cell proliferation, mitochondrial function and fat oxidation results in ectopic fat storage, insulin resistance and type II diabetes mellitus. *Int. J. Obes.* **28**, 12–21 (2004).
125. P. Trayhurn, Adipocyte Biology. *Clin. Obes. Adults Child.* **8**, 103–114 (2010).
126. V. Rakotoarivelo *et al.*, Inflammatory Cytokine Profiles in Visceral and Subcutaneous Adipose Tissues of Obese Patients Undergoing Bariatric Surgery Reveal Lack of Correlation With Obesity or Diabetes. *EBioMedicine*. **30**, 237–247 (2018).
127. T. Skurk, C. Alberti-Huber, C. Herder, H. Hauner, Relationship between adipocyte size and adipokine expression and secretion. *J. Clin. Endocrinol. Metab.* **92**, 1023–1033 (2007).
128. M. jeong Lee, S. K. Fried, in *Adipose Tissue in Health and Disease*, T. Leff, J. G. Granneman, Eds. (2010), pp. 283–306.
129. B. L. Wajchenberg, Subcutaneous and Visceral Adipose Tissue : Their Relation to the Metabolic Syndrome. *Endocr. Rev.* **21**, 697–738 (2000).
130. M. Maffei *et al.*, Leptin levels in human and rodent: Measurement of plasma leptin and ob RNA in obese and weight-reduced subjects. *Nat. Med.* **1**, 1155–1161 (1997).
131. F. Lönnqvist *et al.*, Leptin secretion from adipose tissue in women: Relationship to plasma levels and gene expression. *J. Clin. Invest.* **99**, 2398–2404 (1997).
132. V. Van Harmelen *et al.*, Leptin secretion from subcutaneous and visceral adipose tissue in women. *Diabetes*. **47**, 913–917 (1998).
133. C. T. Montague, J. B. Prins, L. Sanders, J. E. Digby, S. O'Rahilly, Depot- and sex-specific differences in human leptin mRNA expression: Implications for the control of regional

fat distribution. *Diabetes*. **46**, 342–347 (1997).

134. Y. Matsuzawa, The metabolic syndrome and adipocytokines. *FEBS Lett.* **580**, 2917–2921 (2006).

135. K. Kwon, H. J. Sang, C. Choi, S. H. Park, Reciprocal association between visceral obesity and adiponectin: In healthy premenopausal women. *Int. J. Cardiol.* **101**, 385–390 (2005).

136. J. Reneau *et al.*, Effect of adiposity on tissue-specific adiponectin secretion. *PLoS One*. **13**, 1–12 (2018).

137. Y. Matsuzawa, Obesity and metabolic syndrome: the contribution of visceral fat and adiponectin. *Diabetes Manag.* **4**, 391–401 (2014).

138. J.-B. Funcke, P. E. Scherer, Beyond adiponectin and leptin: Adipose tissue-derived mediators of inter-organ communication. *J. Lipid Res.* **60**, 1648–1697 (2019).

139. M. Blüher, Do adipokines link obesity to its related metabolic and cardiovascular diseases? *Clin. Lipidol.* **5**, 95–107 (2010).

140. Y. Matsuzawa, Adiponectin: Identification, physiology and clinical relevance in metabolic and vascular disease. *Atheroscler. Suppl.* **6**, 7–14 (2005).

141. M. Ebrahimi-Mamaeghani, S. Mohammadi, S. R. Arefhosseini, P. Fallah, Z. Bazi, Adiponectin as a potential biomarker of vascular disease. *Vasc. Health Risk Manag.* **11**, 55–70 (2015).

142. J. J. Díez, P. Iglesias, The role of the novel adipocyte-derived hormone adiponectin in human disease. *Eur. J. Endocrinol.* **148**, 293–300 (2003).

143. H. K. Park, M. K. Kwak, H. J. Kim, R. S. Ahima, Linking resistin, inflammation, and cardiometabolic diseases. *Korean J. Intern. Med.* **32**, 239–247 (2017).

144. N. Klöting *et al.*, Serum Retinol-Binding Protein Is More Highly Expressed in Visceral than in Subcutaneous Adipose Tissue and Is a Marker of Intra-abdominal Fat Mass. *Cell Metab.* **6**, 79–87 (2007).

145. T. E. Graham *et al.*, Retinol-binding protein 4 and insulin resistance in lean, obese, and diabetic subjects. *N. Engl. J. Med.* **354**, 2552–2563 (2006).

146. C. M. De Souza Batista *et al.*, Omentin plasma levels and gene expression are decreased in obesity. *Diabetes*. **56**, 1655–1661 (2007).

147. B. Kumari, U. C. S. Yadav, Adipokine Visfatin's Role in Pathogenesis of Diabesity and Related Metabolic Derangements. *Curr. Mol. Med.* **18** (2018), pp. 116–125.

148. R. Shibata *et al.*, Omentin as a novel biomarker of metabolic risk factors. *Diabetol. Metab. Syndr.* **4**, 2–5 (2012).
149. M. Blüher, Adipose tissue inflammation: A cause or consequence of obesity-related insulin resistance? *Clin. Sci.* **130**, 1603–1614 (2016).
150. N. Bashan *et al.*, Mitogen-activated protein kinases, inhibitory-κB kinase, and insulin signaling in human omental versus subcutaneous adipose tissue in obesity. *Endocrinology*. **148**, 2955–2962 (2007).
151. V. Mohamed-Ali *et al.*, Subcutaneous adipose tissue releases interleukin-6, but not tumor necrosis factor-α, in vivo. *J. Clin. Endocrinol. Metab.* **82**, 4196–4200 (1997).
152. K. E. Pinnick *et al.*, Distinct developmental profile of lower-body adipose tissue defines resistance against obesity-associated metabolic complications. *Diabetes*. **63**, 3785–3797 (2014).
153. I. Harman-Boehm *et al.*, Macrophage infiltration into omental versus subcutaneous fat across different populations: Effect of regional adiposity and the comorbidities of obesity. *J. Clin. Endocrinol. Metab.* **92**, 2240–2247 (2007).
154. M. E. Frigolet, R. Gutiérrez-Aguilar, The Role of the Novel Lipokine Palmitoleic Acid in Health and Disease. *Am. Soc. Nutr.* **5**, 173–181 (2017).
155. G. Onal, O. Kutlu, D. Gozuacik, S. Dokmeci Emre, Lipid Droplets in Health and Disease. *Lipids Health Dis.* **16**, 1–15 (2017).
156. Y. Guo, K. R. Cordes, R. V. Farese, T. C. Walther, Lipid droplets at a glance. *J. Cell Sci.* **122**, 749–752 (2009).
157. T. C. Walther, R. V Farese Jr, Lipid Droplets and Cellular Lipid Metabolism. *Annu. Rev. Biochem.* **81**, 687–714 (2012).
158. A. S. Greenberg, R. A. Coleman, Expanding roles for lipid droplets. *Trends Endocrinol. Metab.* **22**, 195–196 (2011).
159. A. S. Greenberg *et al.*, Perilipin, a major hormonally regulated adipocyte-specific phosphoprotein associated with the periphery of lipid storage droplets. *J. Biol. Chem.* **266**, 11341–11346 (1991).
160. J. A. Olzmann, P. Carvalho, Dynamics and functions of lipid droplets. *Nat. Rev. Mol. Cell Biol.* **20**, 137–155 (2018).
161. A. B. Novikoff, P. M. Novikoff, O. M. Rosen, C. S. Rubin, Organelle relationships in cultured 3T3-L1 preadipocytes. *J. Cell Biol.* **87**, 180–196 (1980).

162. T. Fujimoto, Y. Ohsaki, J. Cheng, M. Suzuki, Y. Shinohara, Lipid droplets: A classic organelle with new outfits. *Histochem. Cell Biol.* **130**, 263–279 (2008).
163. N. Jacquier *et al.*, Lipid droplets are functionally connected to the endoplasmic reticulum in Saccharomyces cerevisiae. *J. Cell Sci.* **124**, 2424–2437 (2011).
164. S. Daemen, M. A. M. J. van Zandvoort, S. H. Parekh, M. K. C. Hesselink, Microscopy tools for the investigation of intracellular lipid storage and dynamics. *Mol. Metab.* **5**, 153–163 (2016).
165. V. T. Salo, E. Ikonen, Moving out but keeping in touch: contacts between endoplasmic reticulum and lipid droplets. *Curr. Opin. Cell Biol.* **57**, 64–70 (2019).
166. F. Wilfling *et al.*, Triacylglycerol synthesis enzymes mediate lipid droplet growth by relocalizing from the ER to lipid droplets. *Dev. Cell*. **24**, 384–399 (2013).
167. T. C. Walther, R. V. Farese, The life of lipid droplets. *Biochim. Biophys. Acta - Mol. Cell Biol. Lipids*. **1791**, 459–466 (2009).
168. H. L. Ploegh, A lipid-based model for the creation of an escape hatch from the endoplasmic reticulum. *Nature*. **448**, 435–438 (2007).
169. H. Robenek *et al.*, Adipophilin-enriched domains in the ER membrane are sites of lipid droplet biogenesis. *J. Cell Sci.* **119**, 4215–4224 (2006).
170. C. Thiele, J. Spandl, Cell biology of lipid droplets. *Curr. Opin. Cell Biol.* **20**, 378–385 (2008).
171. P. Boström *et al.*, SNARE proteins mediate fusion between cytosolic lipid droplets and are implicated in insulin sensitivity. *Nat. Cell Biol.* **9**, 1286–1293 (2007).
172. J. Gong *et al.*, Fsp27 promotes lipid droplet growth by lipid exchange and transfer at lipid droplet contact sites. *J. Cell Biol.* **195**, 953–963 (2011).
173. S. Jambunathan, J. Yin, W. Khan, Y. Tamori, V. Puri, FSP27 promotes lipid droplet clustering and then fusion to regulate triglyceride accumulation. *PLoS One*. **6**, 1–12 (2011).
174. N. Krahmer *et al.*, Phosphatidylcholine synthesis for lipid droplet expansion is mediated by localized activation of CTP:Phosphocholine cytidylyltransferase. *Cell Metab.* **14**, 504–515 (2011).
175. A. J. Aitchison, D. J. Arsenault, N. D. Ridgway, Nuclear-localized CTP:phosphocholine cytidylyltransferase α regulates phosphatidylcholine synthesis required for lipid droplet biogenesis. *Mol. Biol. Cell*. **26**, 2927–2938 (2015).

176. A. Haider *et al.*, PCYT1A Regulates Phosphatidylcholine Homeostasis from the Inner Nuclear Membrane in Response to Membrane Stored Curvature Elastic Stress. *Dev. Cell*. **45**, 481-495.e8 (2018).
177. A. S. Greenberg *et al.*, The role of lipid droplets in metabolic disease in rodents and humans. *J. Clin. Invest.* **121**, 2102–2110 (2011).
178. K. Bersuker *et al.*, A Proximity Labeling Strategy Provides Insights into the Composition and Dynamics of Lipid Droplet Proteomes. *Dev. Cell*. **44**, 97-112.e7 (2018).
179. E. R. Rowe *et al.*, Conserved amphipathic helices mediate lipid droplet targeting of perilipins 1-3. *J. Biol. Chem.* **291**, 6664–6678 (2016).
180. R. Bartz *et al.*, Dynamic activity of lipid droplets: Protein phosphorylation and GTP-mediated protein translocation. *J. Proteome Res.* **6**, 3256–3265 (2007).
181. S. Xu, X. Zhang, P. Liu, Lipid droplet proteins and metabolic diseases. *Biochim. Biophys. Acta - Mol. Basis Dis.* **1864**, 1968–1983 (2018).
182. A. M. Valm *et al.*, Applying systems-level spectral imaging and analysis to reveal the organelle interactome. *Nature*. **546**, 162–167 (2017).
183. A. D. Barbosa, D. B. Savage, S. Siniossoglou, Lipid droplet-organelle interactions: Emerging roles in lipid metabolism. *Curr. Opin. Cell Biol.* **35**, 91–97 (2015).
184. K. Frayn, Adipose tissue as a buffer for daily lipid flux. *Diabetologia*. **45**, 1201–1210 (2002).
185. A. R. Kimmel, C. Sztalryd, The Perilipins: Major Cytosolic Lipid Droplet–Associated Proteins and Their Roles in Cellular Lipid Storage, Mobilization, and Systemic Homeostasis. *Annu. Rev. Nutr.* **36**, 471–509 (2016).
186. K. Bersuker, J. A. Olzmann, Establishing the lipid droplet proteome: Mechanisms of lipid droplet protein targeting and degradation. *Biochim. Biophys. Acta - Mol. Cell Biol. Lipids*. **1862**, 1166–1177 (2017).
187. C. Lefèvre *et al.*, Mutations in CGI-58, the Gene Encoding a New Protein of the Esterase/Lipase/Thioesterase Subfamily, in Chanarin-Dorfman Syndrome. *Am. J. Hum. Genet.* **69**, 1002–1012 (2001).
188. A. Lass *et al.*, Adipose triglyceride lipase-mediated lipolysis of cellular fat stores is activated by CGI-58 and defective in Chanarin-Dorfman Syndrome. *Cell Metab.* **3**, 309–319 (2006).

189. R. Ross *et al.*, Sex differences in lean and adipose tissue distribution by magnetic resonance imaging: Anthropometric relationships. *Am. J. Clin. Nutr.* **59**, 1277–1285 (1994).

190. C. J. Ley, B. Lees, J. C. Stevenson, Sex- and menopause-associated in body-fat distribution. *Am. J. Clin. Nutr.* **55**, 950–954 (1992).

191. A. Pascot *et al.*, Age-Related Increase in Visceral Adipose Tissue and Body Fat and the Metabolic Risk Pro file of Premenopausal Women. *Diabetes Care*. **22**, 1471–1478 (1999).

192. O. L. Svendsen, C. Hassager, C. Christiansen, Age- and menopause-associated variations in body composition and fat distribution in healthy women as measured by dual-energy x-ray absorptiometry. *Metabolism*. **44**, 369–373 (1995).

193. P. Szulc, F. Duboeuf, R. Chapurlat, Age-Related Changes in Fat Mass and Distribution in Men—the Cross-Sectional STRAMBO Study. *J. Clin. Densitom.* **20**, 472–479 (2017).

194. H. Noppa, M. Andersson, C. Bengtsson, A. Bruce, B. Isaksson, Longitudinal studies of anthropometric data and body composition. The population study of women in Goteborg, Sweden. *Am. J. Clin. Nutr.* **33**, 155–162 (1980).

195. G. Enzi *et al.*, Subcutaneous and visceral fat distribution according to sex, age, and overweight, evaluated by computed tomography. *Am J Clin Nutr*. **44**, 739–746 (1986).

196. M. Zamboni *et al.*, Effects of age on body fat distribution and cardiovascular risk factors in women. *Am. J. Clin. Nutr.* **66**, 111–115 (1997).

197. K. Kotani *et al.*, Sexual Dimorphism of Age-Related-Changes in Whole-Body Fat Distribution in the Obese. *Int J Obes Relat Metab Disord*. **18**, 207–2 (1994).

198. B. Beaufrère, B. Morio, Fat and protein redistribution with aging: Metabolic considerations. *Eur. J. Clin. Nutr.* **54**, S48–S53 (2000).

199. G. R. Hunter, B. A. Gower, B. L. Kane, Age Related Shift in Visceral Fat. *Int. J. Body Compos. Res.* **8**, 103–108 (2010).

200. J. C. Seidell, P. Björntorp, L. Sjöström, H. Kvist, R. Sannerstedt, Visceral fat accumulation in men is positively associated with insulin, glucose, and C-peptide levels, but negatively with testosterone levels. *Metabolism*. **39**, 897–901 (1990).

201. P. Mårin, Testosterone and regional fat distribution. *Obes. Res.* **3 Suppl 4**, 609S-612S (1995).

202. M. A. Boyanov, Z. Boneva, V. G. Christov, Testosterone supplementation in men with

type 2 diabetes, visceral obesity and partial androgen deficiency. *Aging Male*. **6**, 1–7 (2003).

203. J. C. Lovejoy *et al.*, Exogenous Androgens Influence Body Composition and Regional Body Fat Distribution in Obese Postmenopausal Women--A Clinical Research Center Study. *J Clin Endocrinol Metab*. **81**, 2198–203 (1996).
204. K. Blouin, A. Boivin, A. Tchernof, Androgens and body fat distribution. *J. Steroid Biochem. Mol. Biol.* **108**, 272–280 (2008).
205. J. C. K. Wells, Sexual dimorphism of body composition. *Best Pract. Res. Clin. Endocrinol. Metab.* **21**, 415–430 (2007).
206. K. Karastergiou, S. R. Smith, A. S. Greenberg, S. K. Fried, Sex differences in human adipose tissues – the biology of pear shape. *Biol. Sex Differ.* **3**, 13 (2012).
207. M. C. Carr, The emergence of the metabolic syndrome with menopause. *J. Clin. Endocrinol. Metab.* **88**, 2404–2411 (2003).
208. A. Tchernof *et al.*, Ovarian hormone status and abdominal visceral adipose tissue metabolism. *J. Clin. Endocrinol. Metab.* **89**, 3425–3430 (2004).
209. J. M. H. Elbers, H. Asscheman, J. C. Seidell, L. J. G. Gooren, Effects of sex steroid hormones on regional fat depots as assessed by magnetic resonance imaging in transsexuals. *Am. J. Physiol. - Endocrinol. Metab.* **276**, E317-25 (1999).
210. X. Li, L. Qi, Gene – Environment Interactions on Body Fat Distribution. *Int. J. Mol. Sci.* **20**, 1–16 (2019).
211. J. Kaprio, Twins and the mystery of missing heritability: The contribution of gene-environment interactions. *J. Intern. Med.* **272**, 440–448 (2012).
212. M. C. Zillikens *et al.*, Sex-specific genetic effects influence variation in body composition. *Diabetologia*. **51**, 2233–2241 (2008).
213. A. J. Stunkard, J. R. Harris, N. L. Pedersen, G. E. McClearn, The Body-Mass Index of Twins Who Have Been Reared Apart. *New English J. Med.* **322**, 1483–7 (1990).
214. T. L. Nelson, G. P. Vogler, N. L. Pedersen, Y. Hong, T. P. Miles, Genetic and environmental influences on body fat distribution, fasting insulin levels and CVD: are the influences shared? *Twin Res.* **3**, 43–50 (2000).
215. C. Rouchard *et al.*, The Response to Long-Term Overfeeding in Identical Twins. *New English J. Med.* **323**, 1477–1482 (1990).
216. L. Pérusse *et al.*, Familial aggregation of abdominal visceral fat level: Results from the

Quebec family study. *Metabolism.* **45**, 378–382 (1996).

217. C. Malis *et al.*, Total and regional fat distribution is strongly influenced by genetic factors in young and elderly twins. *Obes. Res.* **13**, 2139–2145 (2005).
218. P. M. Visscher *et al.*, 10 Years of GWAS Discovery: Biology, Function, and Translation. *Am. J. Hum. Genet.* **101**, 5–22 (2017).
219. C. H. Sandholt, T. Hansen, O. Pedersen, Beyond the fourth wave of genome-wide obesity association studies. *Nutr. Diabetes*. **2**, e37-10 (2012).
220. G. Agha *et al.*, Adiposity is associated with DNA methylation profile in adipose tissue. *Int. J. Epidemiol.* **44**, 1277–1287 (2015).
221. X. Sun *et al.*, From genetics and epigenetics to the future of precision treatment for obesity. *Gastroenterol. Rep.* **5**, 266–270 (2017).
222. S. Gehrke *et al.*, Epigenetic regulation of depot-specific gene expression in adipose tissue. *PLoS One*. **8**, 1–11 (2013).
223. M. Keller *et al.*, Genome-wide DNA promoter methylation and transcriptome analysis in human adipose tissue unravels novel candidate genes for obesity. *Mol. Metab.* **6**, 86–100 (2017).
224. S. T. Bradford *et al.*, Methylome and transcriptome maps of human visceral and subcutaneous adipocytes reveal key epigenetic differences at developmental genes. *Sci. Rep.* **9**, 1–13 (2019).
225. G. Campanella *et al.*, Epigenome-wide association study of adiposity and future risk of obesity-related diseases. *Int. J. Obes.* **42**, 2022–2035 (2018).
226. S. Wahl *et al.*, Epigenome-wide association study of body mass index, and the adverse outcomes of adiposity. *Nature*. **541**, 81–86 (2017).
227. M. C. Benton *et al.*, An analysis of DNA methylation in human adipose tissue reveals differential modification of obesity genes before and after gastric bypass and weight loss. *Genome Biol.* **16**, 1–21 (2015).
228. I. Dahlman *et al.*, The fat cell epigenetic signature in post-obese women is characterized by global hypomethylation and differential DNA methylation of adipogenesis genes. *Int. J. Obes.* **39**, 910–919 (2015).
229. H. Giral, U. Landmesser, A. Kratzer, Into the Wild: GWAS Exploration of Non-coding RNAs. *Front. Cardiovasc. Med.* **5** (2018), doi:10.3389/fcvm.2018.00181.
230. A. Y. Chu *et al.*, Multiethnic genome-wide meta-analysis of ectopic fat depots

identifies loci associated with adipocyte development and differentiation. *Nat. Genet.* **49**, 125–130 (2017).

231. G. Povysil *et al.*, Rare-variant collapsing analyses for complex traits: guidelines and applications. *Nat. Rev. Genet.* **20** (2019), doi:10.1038/s41576-019-0177-4.
232. Y. Tanigawa *et al.*, Components of genetic associations across 2,138 phenotypes in the UK Biobank highlight adipocyte biology. *Nat. Commun.* **10** (2019), doi:10.1038/s41467-019-11953-9.
233. T. M. Frayling *et al.*, A common variant in the FTO gene is associated with body mass index and predisposes to childhood and adult obesity. *Science (80-.).* **316**, 889–894 (2007).
234. M. O. Goodarzi, Genetics of obesity: what genetic association studies have taught us about the biology of obesity and its complications. *Lancet Diabetes Endocrinol.* **6**, 223–236 (2018).
235. C. M. Lindgren *et al.*, Genome-wide association scan meta-analysis identifies three loci influencing adiposity and fat distribution. *PLoS Genet.* **5** (2009), doi:10.1371/journal.pgen.1000508.
236. A. Buniello *et al.*, The NHGRI-EBI GWAS Catalog of published genome-wide association studies, targeted arrays and summary statistics 2019. *Nucleic Acids Res.* **47**, D1005–D1012 (2019).
237. A. E. Locke *et al.*, Genetic studies of body mass index yield new insights for obesity biology. *Nature*. **518**, 197–206 (2015).
238. D. Shungin *et al.*, New genetic loci link adipose and insulin biology to body fat distribution. *Nature*. **518**, 187–196 (2015).
239. W. Bodmer, C. Bonilla, Common and rare variants in multifactorial susceptibility to common diseases. *Nat. Genet.* **40**, 695–701 (2008).
240. N. E. Allen, C. Sudlow, T. Peakman, R. Collins, UK biobank data: Come and get it. *Sci. Transl. Med.* **6**, 4–7 (2014).
241. C. Bycroft *et al.*, The UK Biobank resource with deep phenotyping and genomic data. *Nature*. **562**, 203–209 (2018).
242. A. Weiss, L. Attisano, The TGFbeta superfamily signaling pathway. *Wiley Interdiscip. Rev. Dev. Biol.* **2**, 47–63 (2013).
243. A. P. Hinck, Structural studies of the TGF-βs and their receptors - Insights into

evolution of the TGF-β superfamily. *FEBS Lett.* **586**, 1860–1870 (2012).

244. A. Chaikuad, A. N. Bullock, Structural basis of intracellular TGF-β signaling: Receptors and smads. *Cold Spring Harb. Perspect. Biol.* **8**, 1–18 (2016).

245. J. L. Wrana *et al.*, TGF beta signals through a heteromeric protein kinase receptor complex. *Cell*. **71**, 1003–14 (1992).

246. M. De Caestecker, The transforming growth factor-β superfamily of receptors. *Cytokine Growth Factor Rev.* **15**, 1–11 (2004).

247. M. Lorentzon, B. Hoffer, T. Ebendal, L. Olson, A. Tomac, Habrec1, a novel serine/threonine kinase TGF-β type I-like receptor, has a specific cellular expression suggesting function in the developing organism and adult brain. *Exp. Neurol.* **142**, 351–360 (1996).

248. K. Tsuchida, P. E. Sawchenko, S. I. Nishikawa, W. W. Vale, Molecular cloning of a novel type I receptor serine/threonine kinase for the TGFβ superfamily from rat brain. *Mol. Cell. Neurosci.* **7**, 467–478 (1996).

249. M. Rydén *et al.*, A novel type I receptor serine-threonine kinase predominantly expressed in the adult central nervous system. *J. Biol. Chem.* **271**, 30603–30609 (1996).

250. M. Murakami *et al.*, Expression of activin receptor-like kinase 7 in adipose tissues. *Biochem. Genet.* **51**, 202–210 (2013).

251. J. Bondestam *et al.*, cDNA cloning, expression studies and chromosome mapping of human type I serine/threonine kinase receptor ALK7 (ACVR1C). *Cytogenet Cell Genet.* **95**, 157–162 (2001).

252. L. M. S. Carlsson *et al.*, ALK7 expression is specific for adipose tissue, reduced in obesity and correlates to factors implicated in metabolic disease. *Biochem. Biophys. Res. Commun.* **382**, 309–314 (2009).

253. H. J. Roberts *et al.*, Identification of Novel Isoforms of Activin Receptor-Like Kinase 7 (ALK7) Generated by Alternative Splicing and Expression of ALK7 and Its Ligand, Nodal, in Human Placenta. *Biol. Reprod.* **68**, 1719–1726 (2003).

254. C. Wang *et al.*, GPS 5.0: An Update on the Prediction of Kinase-specific Phosphorylation Sites in Proteins. *Genomics. Proteomics Bioinformatics*. **18**, 72–80 (2020).

255. A. P. Hinck, T. D. Mueller, T. A. Springer, Structural biology and evolution of the TGF-β

family. *Cold Spring Harb. Perspect. Biol.* **8**, 1–52 (2016).

256. J. Greenwald, W. H. Fischer, W. W. Vale, S. Choe, Three-finger toxin fold for the extracellular ligand-binding domain of the type II activin receptor serine kinase. *Nat. Struct. Biol.* **6**, 18–22 (1999).

257. J. Groppe *et al.*, Cooperative Assembly of TGF-β Superfamily Signaling Complexes Is Mediated by Two Disparate Mechanisms and Distinct Modes of Receptor Binding. *Mol. Cell*. **29**, 157–168 (2008).

258. M. Huse, Y. G. Chen, J. Massagué, J. Kuriyan, Crystal structure of the cytoplasmic domain of the type I TGFβ receptor in complex with FKBP12. *Cell*. **96**, 425–436 (1999).

259. M. Huse *et al.*, The TGFβ receptor activation process: An inhibitor- to substrate-binding switch. *Mol. Cell*. **8**, 671–682 (2001).

260. R. Wieser, J. L. Wrana, J. Massagué, GS domain mutations that constitutively activate TβR-I, the downstream signaling component in the TGF-β receptor complex. *EMBO J.* **14**, 2199–2208 (1995).

261. U. Persson *et al.*, The L45 loop in type I receptors for TGF-β family members is a critical determinant in specifying Smad isoform activation. *FEBS Lett.* **434**, 83–87 (1998).

262. Y. G. Chen, J. Massagué, Smad1 recognition and activation by the ALK1 group of transforming growth factor-β family receptors. *J. Biol. Chem.* **274**, 3672–3677 (1999).

263. Y.-G. Chen *et al.*, Determinants of specificity in TGF-β signal transduction. *Genes Dev.* **12**, 2144–2152 (1998).

264. X. H. Feng, R. Derynck, A kinase subdomain of transforming growth factor-β (TGF-β) type I receptor determines the TGF-β intracellular signaling specificity. *EMBO J.* **16**, 3912–3923 (1997).

265. R. S. Lo, Y. G. Chen, Y. Shi, N. P. Pavletich, J. Massagué, The L3 loop: A structural motif determining specific interactions between SMAD proteins and TGF-β receptors. *EMBO J.* **17**, 996–1005 (1998).

266. N. Zhang *et al.*, Activin receptor-like kinase 7 induces apoptosis of pancreatic beta cells and beta cell lines. *Diabetologia*. **49**, 506–518 (2006).

267. M. Kogame *et al.*, ALK7 is a novel marker for adipocyte differentiation. *J. Med. Invest.* **53**, 238–45 (2006).

268. O. Andersson, M. Korach-Andre, E. Reissmann, C. F. Ibáñez, P. Bertolino,

Growth/differentiation factor 3 signals through ALK7 and regulates accumulation of adipose tissue and diet-induced obesity. *Proc. Natl. Acad. Sci. U. S. A.* **105**, 7252–6 (2008).

269. F. Zhao *et al.*, Nodal induces apoptosis through activation of the ALK7 signaling pathway in pancreatic INS-1 -cells. *AJP Endocrinol. Metab.* **303**, E132–E143 (2012).
270. Y. Bu *et al.*, Insulin Regulates Lipolysis and Fat Mass by Upregulating Growth/Differentiation Factor 3 in Adipose Tissue Macrophages. *Diabetes*, db171201 (2018).
271. O. Hashimoto *et al.*, Activin E Controls Energy Homeostasis in Both Brown and White Adipose Tissues as a Hepatokine. *Cell Rep.* **25**, 1193–1203 (2018).
272. M. Whitman, Nodal Signaling in Early Vertebrate Embryos: Themes and Variations. *Dev. Cell*. **1**, 605–617 (2001).
273. P. C. Gray, C. A. Harrison, W. Vale, Cripto forms a complex with activin and type II activin receptors and can block activin signaling. *Proc. Natl. Acad. Sci. U. S. A.* **100**, 5193–5198 (2003).
274. E. Reissmann *et al.*, The orphan receptor ALK7 and the Activin receptor ALK4 mediate signaling by Nodal proteins during vertebrate development. *Genes Dev.* **15**, 2010–2022 (2001).
275. H. Jörnvall, E. Reissmann, O. Andersson, M. Mehrkash, C. F. Ibáñez, ALK7, a Receptor for Nodal, Is Dispensable for Embryogenesis and Left-Right Patterning in the Mouse. *Mol. Cell. Biol.* **24**, 9383–9389 (2004).
276. G. Xu *et al.*, Nodal Induces Apoptosis and Inhibits Proliferation in Human Epithelial Ovarian Cancer Cells via Activin Receptor-Like Kinase 7. *J. Clin. Endocrinol. Metab.* **89**, 5523–5534 (2004).
277. T. Guo *et al.*, Adipocyte ALK7 links nutrient overload to catecholamine resistance in obesity. *Elife*. **3**, e03245 (2014).
278. A. Balkow *et al.*, A novel crosstalk between Alk7 and cGMP signaling differentially regulates brown adipocyte function. *Mol. Metab.* **4**, 576–583 (2015).
279. P. Marmol-Carrasco, F. Krapacher, C. F. Ibáñez, Control of brown adipose tissue adaptation to nutrient stress by the activin receptor ALK7. *Elife*. **9** (2020), doi:10.7554/eLife.54721.
280. P. Bertolino *et al.*, Activin B receptor ALK7 is a negative regulator of pancreatic beta-

cell function. *Proc Natl Acad Sci U S A*. **105**, 7246–7251 (2008).

281. H. Huang *et al.*, ALK7 protects against pathological cardiac hypertrophy in mice. *Cardiovasc. Res.* **108**, 50–61 (2015).

282. T. Hu, F. Su, W. Jiang, D. A. Dart, Overexpression of activin receptor-like kinase 7 in breast cancer cells is associated with decreased cell growth and adhesion. *Anticancer Res.* **37**, 3441–3451 (2017).

283. S. Munir *et al.*, Nodal and ALK7 inhibit proliferation and induce apoptosis in human trophoblast cells. *J. Biol. Chem.* **279**, 31277–31286 (2004).

284. I. P. Michael *et al.*, ALK7 Signaling Manifests a Homeostatic Tissue Barrier That Is Abrogated during Tumorigenesis and Metastasis. *Dev. Cell*. **49**, 409-424.e6 (2019).

285. X. Ni *et al.*, YAP is essential for treg-mediated suppression of antitumor immunity. *Cancer Discov.* **8**, 1026–1043 (2018).

286. J. Barwell *et al.*, Calcitonin and calcitonin receptor-like receptors: Common themes with family B GPCRs? *Br. J. Pharmacol.* **166**, 51–65 (2012).

287. T. A. Lutz, R. Rossi, J. Althaus, E. Del Prete, E. Scharrer, Evidence for a physiological role of central calcitonin gene-related peptide (CGRP) receptors in the control of food intake in rats. *Neurosci. Lett.* **230**, 159–162 (1997).

288. A. J. Felsenfeld, B. S. Levine, Calcitonin, the forgotten hormone: Does it deserve to be forgotten? *Clin. Kidney J.* **8**, 180–187 (2015).

289. D. L. Hay, M. L. Garelja, D. R. Poyner, C. S. Walker, Update on the pharmacology of calcitonin/CGRP family of peptides: IUPHAR Review 25. *Br. J. Pharmacol.* **175**, 3–17 (2018).

290. D. L. Hay, S. Chen, T. A. Lutz, D. G. Parkes, J. D. Roth, Amylin : Pharmacology , Physiology , and Clinical Potential. *Pharmacol. Rev.* **67**, 564–600 (2015).

291. F. A. Russell, R. King, S.-J. Smillie, X. Kodji, S. D. Brain, Calcitonin Gene-Related Peptide: Physiology and Pathophysiology. *Physiol. Rev.* **94**, 1099–1142 (2014).

292. B. N. Evans, M. I. Rosenblatt, L. O. Mnayer, K. R. Oliver, I. M. Dickerson, CGRP-RCP, a novel protein required for signal transduction at calcitonin gene-related peptide and adrenomedullin receptors. *J. Biol. Chem.* **275**, 31438–31443 (2000).

293. A. A. Tolun, I. M. Dickerson, A. Malhotra, Overexpression and purification of human calcitonin gene-related peptide-receptor component protein in Escherichia coli. *Protein Expr. Purif.* **52**, 167–174 (2007).

294. A. C. Conner, J. Simms, S. G. Howitt, M. Wheatley, D. R. Poyner, The second intracellular loop of the calcitonin gene-related peptide receptor provides molecular determinants for signal transduction and cell surface expression. *J. Biol. Chem.* **281**, 1644–1651 (2006).

295. S. Kapas, K. J. Catt, A. J. L. Clark, Cloning and expression of cDNA encoding a rat adrenomedullin receptor. *J. Biol. Chem.* **270**, 25344–25347 (1995).

296. B. Flühmann, R. Muff, W. Hunziker, J. A. Fischer, W. Born, A human orphan calcitonin receptor like structure. *Biochem. Biophys. Res. Commun.* **206**, 341–347 (1995).

297. N. Aiyar *et al.*, A cDNA Encoding the Calcitonin Gene-related Peptide Type 1 Receptor. *J. Biol. Chem.* **271**, 11325–11329 (1996).

298. L. M. McLatchie *et al.*, RAMPS regulate the transport and ligand specificity of the calcitonin- receptor-like receptor. *Nature*. **393**, 333–339 (1998).

299. H. A. Watkins *et al.*, Receptor activity-modifying proteins 2 and 3 generate adrenomedullin receptor subtypes with distinct molecular properties. *J. Biol. Chem.* **291**, 11657–11675 (2016).

300. S. Kusano *et al.*, Structural basis for extracellular interactions between calcitonin receptor-like receptor and receptor activity-modifying protein 2 for adrenomedullin-specific binding. *Protein Sci.* **21**, 199–210 (2012).

301. W. Born, R. Muff, J. A. Fischer, Functional interaction of G protein-coupled receptors of the adrenomedullin peptide family with accessory Receptor-activity-modifying proteins (RAMP). *Microsc. Res. Tech.* **57**, 14–22 (2002).

302. A. Bortolato *et al.*, Structure of Class B GPCRs: New horizons for drug discovery. *Br. J. Pharmacol.* **171**, 3132–3145 (2014).

303. M. Chauhan, K. Rajarathnam, C. Yallampalli, Role of the N-terminal domain of the calcitonin receptor-like receptor in ligand binding. *Biochemistry*. **44**, 782–789 (2005).

304. U. Omasits, C. H. Ahrens, S. Müller, B. Wollscheid, Protter: interactive protein feature visualization and integration with experimental proteomic data. *Bioinformatics*. **30**, 884–886 (2014).

305. J. M. Booe *et al.*, Structural Basis for Receptor Activity-Modifying Protein-Dependent Selective Peptide Recognition by a G Protein-Coupled Receptor. *Mol. Cell*. **58**, 1040–1052 (2015).

306. E. ter Haar *et al.*, Crystal structure of the ectodomain complex of the CGRP receptor,

a class-B GPCR, reveals the site of drug antagonism. *Structure*. **18**, 1083–1093 (2010).

307. Y. L. Liang *et al.*, Cryo-EM structure of the active, G s -protein complexed, human CGRP receptor. *Nature*. **561**, 492–497 (2018).
308. J. Barwell, P. S. Miller, D. Donnelly, D. R. Poyner, Mapping interaction sites within the N-terminus of the calcitonin gene-related peptide receptor; the role of residues 23-60 of the calcitonin receptor-like receptor. *Peptides*. **31**, 170–176 (2010).
309. S. Kamitani, T. Sakata, Glycosylation of human CRLR at Asn123 is required for ligand binding and signaling. *Biochim. Biophys. Acta - Mol. Cell Res.* **1539**, 131–139 (2001).
310. K. Kuwasako, K. Kitamura, S. Nagata, J. Kato, Flow cytometric analysis of the calcitonin receptor-like receptor domains responsible for cell-surface translocation of receptor activity-modifying proteins. *Biochem. Biophys. Res. Commun.* **384**, 249–254 (2009).
311. K. Kuwasako *et al.*, The third extracellular loop of the human calcitonin receptor-like receptor is crucial for the activation of adrenomedullin signalling. *Br. J. Pharmacol.* **166**, 137–150 (2012).
312. K. Kuwasako, K. Kitamura, S. Nagata, T. Hikosaka, J. Kato, Function of the cytoplasmic tail of human calcitonin receptor-like receptor in complex with receptor activity-modifying protein 2. *Biochem. Biophys. Res. Commun.* **392**, 380–385 (2010).
313. K. Kuwasako, K. Kitamura, S. Nagata, T. Hikosaka, J. Kato, Structure-function analysis of helix 8 of human calcitonin receptor-like receptor within the adrenomedullin 1 receptor. *Peptides*. **32**, 144–149 (2011).
314. R. Harmancey *et al.*, The vasoactive peptide adrenomedullin is secreted by adipocytes and inhibits lipolysis through NO-mediated beta-adrenergic agonist oxidation. *FASEB J.* **19**, 1045–7 (2005).
315. H. K. Wong, T. T. Cheung, B. M. Y. Cheung, Adrenomedullin and cardiovascular diseases. *JRSM Cardiovasc. Dis.* **1**, 14 (2012).
316. Y. Nagoshi *et al.*, Tumor necrosis factor-α downregulates adrenomedullin receptors in human coronary artery smooth muscle cells. *Peptides*. **25**, 1115–1121 (2004).
317. S. Frayon, C. Cueille, S. Gnidéhou, M. C. De Vernejoul, J. M. Garel, Dexamethasone increases RAMP1 and CRLR mRNA expressions in human vascular smooth muscle cells. *Biochem. Biophys. Res. Commun.* **270**, 1063–1067 (2000).
318. M. L. Garelja *et al.*, Molecular Mechanisms of Class B GPCR Activation: Insights from Adrenomedullin Receptors. *ACS Pharmacol. Transl. Sci.* **3**, 246–262 (2020).

319. S. Ghatta, D. Nimmagadda, Calcitonin gene-related peptide : Understanding its role. **36**, 277–283 (2004).
320. A. F. Russo, Calcitonin Gene-Related Peptide (CGRP): A New Target for Migraine. *Annu. Rev. Pharmacol. Toxicol.* **55**, 533–552 (2015).
321. K. Miyashita *et al.*, Adrenomedullin provokes endothelial Akt activation and promotes vascular regeneration both in vitro and in vivo. *FEBS Lett.* **544**, 86–92 (2003).
322. C. Iemura-Inaba *et al.*, Role of adrenomedullin system in lipid metabolism and its signaling mechanism in cultured adipocytes. *Am. J. Physiol. Regul. Integr. Comp. Physiol.* **295**, R1376–R1384 (2008).
323. J. J. Gingell *et al.*, An allosteric role for receptor activity-modifying proteins in defining GPCR pharmacology. *Cell Discov.* **2** (2016), doi:10.1038/celldisc.2016.12.
324. S. Hilairet, S. M. Foord, F. H. Marshall, M. Bouvier, Protein-Protein Interaction and Not Glycosylation Determines the Binding Selectivity of Heterodimers between the Calcitonin Receptor-like Receptor and the Receptor Activity-modifying Proteins. *J. Biol. Chem.* **276**, 29575–29581 (2001).
325. E. J. Visser, A review of calcitonin and its use in the treatment of acute pain. *Acute Pain*. **7**, 185–189 (2005).
326. J. J. Gingell *et al.*, Distinct Patterns of Internalization of Different Calcitonin Gene-Related Peptide Receptors. *ACS Pharmacol. Transl. Sci.* **3**, 296–304 (2020).
327. T. Mavridis, C. Koniari, N. Fakas, D. D. Mitsikostas, Anti-Calcitonin Gene-Related Peptide Monoclonal Antibodies : Adverse Effects . What Do We Really Know ? A Literature Review. *EMJ Innov.* **3**, 64–72 (2019).
328. D. X. Gram *et al.*, Plasma calcitonin gene-related peptide is increased prior to obesity, and sensory nerve desensitization by capsaicin improves oral glucose tolerance in obese Zucker rats. *Eur. J. Endocrinol.* **153**, 963–969 (2005).
329. C. S. Walker *et al.*, Mice lacking the neuropeptide α-calcitonin gene-related peptide are protected against diet-induced obesity. *Endocrinology*. **151**, 4257–4269 (2010).
330. T. Koyama *et al.*, Genetic variants of RAMP2 and CLR are associated with stroke. *J. Atheroscler. Thromb.* **24**, 1267–1281 (2017).
331. C. Sztalryd, D. L. Brasaemle, The perilipin family of lipid droplet proteins: Gatekeepers of intracellular lipolysis. *Biochim. Biophys. Acta - Mol. Cell Biol. Lipids*. **1862**, 1221–1232 (2017).

332. C. Sztalryd, A. R. Kimmel, Perilipins: Lipid droplet coat proteins adapted for tissue-specific energy storage and utilization, and lipid cytoprotection. *Biochimie*. **96**, 96–101 (2014).

333. A. S. Greenberg *et al.*, Isolation of cDNAs for perilipins A and B: sequence and expression of lipid droplet-associated proteins of adipocytes. *Proc. Natl. Acad. Sci. U. S. A.* **90**, 12035–9 (1993).

334. J. Nishiu, T. Tanaka, Y. Nakamura, Isolation and chromosomal mapping of the human homolog of perilipin (PLIN), a rat adipose tissue-specific gene, by differential display method. *Genomics*. **48**, 254–257 (1998).

335. A. R. Kimmel, D. L. Brasaemle, M. McAndrews-Hill, C. Sztalryd, C. Londos, Adoption of PERILIPIN as a unifying nomenclature for the mammalian PAT-family of intracellular lipid storage droplet proteins. *J. Lipid Res.* **51**, 468–471 (2010).

336. D. A. Servetnick *et al.*, Perilipins are associated with cholesteryl ester droplets in steroidogenic adrenal cortical and Leydig cells. *J. Biol. Chem.* **270** (1995), pp. 16970–16973.

337. M. Rogne *et al.*, OPA1-anchored PKA phosphorylates perilipin 1 on S522 and S497 in adipocytes differentiated from human adipose stem cells. *Mol. Biol. Cell*. **29** (2018), doi:10.1091/mbc.E17-09-0538.

338. A. Garcia, A. Sekowski, V. Subramanian, D. L. Brasaemle, The central domain is required to target and anchor perilipin A to lipid droplets. *J. Biol. Chem.* **278**, 625–635 (2003).

339. V. Subramanian, A. Garcia, A. Sekowski, D. L. Brasaemle, Hydrophobic sequences target and anchor perilipin A to lipid droplets. *J. Lipid Res.* **45**, 1983–1991 (2004).

340. A. Garcia *et al.*, The Amino and Carboxyl Termini of Perilipin A Facilitate the Storage of Triacylglycerols. *J. Biol. Chem.* **279**, 8409–8416 (2004).

341. H. H. Zhang *et al.*, Lipase-selective Functional Domains of Perilipin A Differentially Regulate Constitutive and Protein Kinase A-stimulated Lipolysis. *J. Biol. Chem.* **278**, 51535–51542 (2003).

342. H. Wang *et al.*, Activation of hormone-sensitive lipase requires two steps, protein phosphorylation and binding to the PAT-1 domain of lipid droplet coat proteins. *J. Biol. Chem.* **284**, 32116–32125 (2009).

343. W.-J. Shen, S. Patel, H. Miyoshi, A. S. Greenberg, F. B. Kraemer, Functional interaction

of hormone-sensitive lipase and perilipin in lipolysis. *J. Lipid Res.* **50**, 2306–2313 (2009).

344. P. E. Bickel, J. T. Tansey, M. A. Welte, PAT proteins, an ancient family of lipid droplet proteins that regulate cellular lipid stores. *Biochim. Biophys. Acta - Mol. Cell Biol. Lipids*. **1791**, 419–440 (2009).
345. C. Sztalryd *et al.*, Perilipin A is essential for the translocation of hormone-sensitive lipase during lipolytic activation. *J. Cell Biol.* **161**, 1093–1103 (2003).
346. Z. Sun *et al.*, Perilipin1 promotes unilocular lipid droplet formation through the activation of Fsp27 in adipocytes. *Nat. Commun.* **4**, 1514–1594 (2013).
347. S. J. Hickenbottom, A. R. Kimmel, C. Londos, J. H. Hurley, Structure of a lipid droplet protein: The PAT family member TIP47. *Structure*. **12**, 1199–1207 (2004).
348. D. L. Brasaemle, V. Subramanian, A. Garcia, A. Marcinkiewicz, A. Rothenberg, Perilipin A and the control of triacylglycerol metabolism. *Mol. Cell. Biochem.* **326**, 15–21 (2009).
349. S. Patel, W. Yang, K. Kozusko, V. Saudek, D. B. Savage, Perilipins 2 and 3 lack a carboxy-terminal domain present in perilipin 1 involved in sequestering ABHD5 and suppressing basal lipolysis. *Proc. Natl. Acad. Sci.* **111**, 9163–9168 (2014).
350. V. Subramanian *et al.*, Perilipin A mediates the reversible binding of CGI-58 to lipid droplets in 3T3-L1 adipocytes. *J. Biol. Chem.* **279**, 42062–42071 (2004).
351. J. G. Granneman, H. P. H. Moore, R. Krishnamoorthy, M. Rathod, Perilipin controls lipolysis by regulating the interactions of AB-hydrolase containing 5 (Abhd5) and adipose triglyceride lipase (Atgl). *J. Biol. Chem.* **284**, 34538–34544 (2009).
352. H. Miyoshi *et al.*, Control of adipose triglyceride lipase action by serine 517 of perilipin A globally regulates protein kinase a-stimulated lipolysis in adipocytes. *J. Biol. Chem.* **282**, 996–1002 (2007).
353. A. Marcinkiewicz, D. Gauthier, A. Garcia, D. L. Brasaemle, The phosphorylation of serine 492 of perilipin A directs lipid droplet fragmentation and dispersion. *J. Biol. Chem.* **281**, 11901–11909 (2006).
354. D. L. Brasaemle *et al.*, Perilipin A increases triacylglycerol storage by decreasing the rate of triacylglycerol hydrolysis. *J. Biol. Chem.* **275**, 38486–38493 (2000).
355. G. F. Grabner, R. Zimmermann, R. Schicho, U. Taschler, Monoglyceride lipase as a drug target: At the crossroads of arachidonic acid metabolism and endocannabinoid

signaling. *Pharmacol. Ther.* **175**, 35–46 (2017).

356. T. H. M. Grahn *et al.*, FSP27 and PLIN1 interaction promotes the formation of large lipid droplets in human adipocytes. *Biochem. Biophys. Res. Commun.* **432**, 296–301 (2013).
357. T. Sawada *et al.*, Perilipin overexpression in white adipose tissue induces a brown fat-like phenotype. *PLoS One*. **5** (2010), doi:10.1371/journal.pone.0014006.
358. J. Martinez-Botas *et al.*, Absence of perilipin results in leanness and reverses obesity in Lepr(db/db) mice. *Nat. Genet.* **26**, 474–479 (2000).
359. J. T. Tansey *et al.*, Perilipin ablation results in a lean mouse with aberrant adipocyte lipolysis, enhanced leptin production, and resistance to diet-induced obesity. *Proc. Natl. Acad. Sci.* **98**, 6494–6499 (2001).
360. S. Gandotra *et al.*, Human frame shift mutations affecting the carboxyl terminus of perilipin increase lipolysis by failing to sequester the adipose triglyceride lipase (ATGL) coactivator AB-hydrolase-containing 5 (ABHD5). *J. Biol. Chem.* **286**, 34998–35006 (2011).
361. K. Kozusko *et al.*, Clinical and Molecular Characterization of a Novel PLIN1 Frameshift Mutation Identified in Patients With Familial Partial Lipodystrophy. *Diabetes*. **64**, 299–310 (2015).
362. S. Gandotra *et al.*, Perilipin Deficiency and Autosomal Dominant Partial Lipodystrophy. *N. Engl. J. Med.* **364**, 740–748 (2011).
363. R. X. Chen *et al.*, The renal manifestations of type 4 familial partial lipodystrophy: A case report and review of literature. *BMC Nephrol.* **19**, 1–7 (2018).
364. I. Jéru *et al.*, Diagnostic challenge in PLIN1-associated Familial Partial Lipodystrophy. *J. Clin. Endocrinol. Metab.* **104**, 6025–6032 (2019).
365. T. W. Laver *et al.*, *J. Clin. Endocrinol. Metab.*, in press, doi:10.1210/jc.2017-02662.
366. M. Conti, J. Beavo, Biochemistry and Physiology of Cyclic Nucleotide Phosphodiesterases: Essential Components in Cyclic Nucleotide Signaling. *Annu. Rev. Biochem.* **76**, 481–511 (2007).
367. E. Degerman *et al.*, From PDE3B to the regulation of energy homeostasis. *Curr. Opin. Pharmacol.* **11**, 676–682 (2011).
368. F. Ahmad *et al.*, Cyclic nucleotide phosphodiesterases: Important signaling modulators and therapeutic targets. *Oral Dis.* **21**, e25–e50 (2015).

369. A. C. Newton, M. D. Bootman, J. Scott, Second messengers. *Cold Spring Harb. Perspect. Biol.* **8**, 1–14 (2016).

370. S. Francis, M. Blount, J. Corbin, Mammalian cyclic nucleotide phosphodiesterases: molecular mechanisms and physiological functions. *Physiol. Rev.* **91**, 651–690 (2011).

371. A. T. Bender, J. A. Beavo, Cyclic nucleotide phosphodiesterases: Molecular regulation to clinical use. *Pharmacol. Rev.* **58**, 488–520 (2006).

372. V. Vasta, C. J. Smith, J. Calvo, P. Belfrage, V. C. Manganiello, Insulin and isoproterenol induced phosphorylation of the particulate cGMP-inhibited, low Km cGI PDE in 3T3-L1 adipocytes. *Biochem. Biophys. Res. Commun.* **183**, 1070–1075 (1992).

373. R. R. Reinhardt *et al.*, Distinctive anatomical patterns of gene expression for cGMP-inhibited cyclic nucleotide phosphodiesterases. *J. Clin. Invest.* **95**, 1528–1538 (1995).

374. T. Rahn *et al.*, Identification of the site in the cGMP-inhibited phosphodiesterase phosphorylated in adipocytes in response to insulin and isoproterenol. *J. Biol. Chem.* **271**, 11575–11580 (1996).

375. E. Degerman, P. Belfrage, V. C. Manganiello, Structure, Localization, and Regulation of cGMP-inhibited Phosphodiesterase (PDE3). *J. Biol. Chem.* **272**, 6823–6826 (1997).

376. E. Heimann *et al.*, Expression and regulation of cyclic nucleotide phosphodiesterases in human and rat pancreatic islets. *PLoS One*. **5**, 1–8 (2010).

377. F. Ahmad *et al.*, Phosphodiesterase 3B (PDE3B) regulates NLRP3 inflammasome in adipose tissue. *Sci. Rep.* **6**, 1–13 (2016).

378. T. Miki *et al.*, Characterization of the cDNA and gene encoding human PDE3B, the cGIP1 isoform of the human cyclic GMP-inhibited cyclic nucleotide phosphodiesterase family. *Genomics*. **36**, 476–485 (1996).

379. G. Scapin *et al.*, Crystal structure of human phosphodiesterase 3B: Atomic basis for substrate and inhibitor specificity. *Biochemistry*. **43**, 6091–6100 (2004).

380. T. Keravis, C. Lugnier, Cyclic Nucleotide Phosphodiesterases (PDE) and Peptide Motifs. *Curr. Pharm. Des.* **16**, 1114–1125 (2010).

381. T. Murata, M. Taira, V. C. Manganiello, Differential expression of cGMP-inhibited cyclic nucleotide phosphodiesterases in human hepatoma cell lines. *FEBS Lett.* **390**, 29–33 (1996).

382. Y. Shakur *et al.*, Membrane localization of cyclic nucleotide phosphodiesterase 3 (PDE3). Two n-terminal domains are required for the efficient targeting to, and

association of, PDE3 with endoplasmic reticulum. *J. Biol. Chem.* **275**, 38749–38761 (2000).

383. R. Nilsson *et al.*, Plasma membrane cyclic nucleotide phosphodiesterase 3B (PDE3B) is associated with caveolae in primary adipocytes. *Cell. Signal.* **18**, 1713–1721 (2006).
384. Y. W. Chung *et al.*, Targeted disruption of PDE3B, but not PDE3A, protects murine heart from ischemia/reperfusion injury. *Proc. Natl. Acad. Sci.* **112**, E2253–E2262 (2015).
385. K. Berger *et al.*, Phosphodiesterase 3B is localized in caveolae and smooth ER in mouse hepatocytes and is important in the regulation of glucose and lipid metabolism. *PLoS One*. **4** (2009), doi:10.1371/journal.pone.0004671.
386. Y. Shakur *et al.*, Regulation and function of the cyclic nucleotide phosphodiesterase (PDE3) gene family. *Prog. Nucleic Acid Res. Mol. Biol.* **66**, 241–277 (2000).
387. K. Omori, J. Kotera, Overview of PDEs and their regulation. *Circ. Res.* **100**, 309–327 (2007).
388. S. H. Francis, I. V Turko, J. D. Corbin, Cyclic Nucleotide Phosphodiesterases: Relating Structure and Function. *Prog. Nucleic Acid Res. Mol. Biol.* **65**, 1–52 (2000).
389. R. Lindh *et al.*, Multisite phosphorylation of adipocyte and hepatocyte phosphodiesterase 3B. *Biochim. Biophys. Acta - Mol. Cell Res.* **1773**, 584–592 (2007).
390. T. W. Gettys, A. J. Vine, M. F. Simonds, J. D. Corbin, Activation of the particulate low K(m) phosphodiesterase of adipocytes by addition of cAMP-dependent protein kinase. *J. Biol. Chem.* **263**, 10359–10363 (1988).
391. D. Palmer *et al.*, Protein kinase A phosphorylation of human phosphodiesterase 3B promotes 14-3-3 protein binding and inhibits phosphatase-catalyzed inactivation. *J. Biol. Chem.* **282**, 9411–9419 (2007).
392. B. Omar, E. Banke, M. Ekelund, S. Frederiksen, E. Degerman, Alterations in cyclic nucleotide phosphodiesterase activities in omental and subcutaneous adipose tissues in human obesity. *Nutr. Diabetes*. **1**, e13-6 (2011).
393. A. Z. Zhao, H. Zhao, J. Teague, W. Fujimoto, J. A. Beavo, Attenuation of insulin secretion by insulin-like growth factor 1 is mediated through activation of phosphodiesterase 3B. *Proc. Natl. Acad. Sci. U. S. A.* **94**, 3223–8 (1997).
394. M. Ahmad, P. R. Flatt, B. L. Furman, N. J. Pyne, The role of the cyclic GMP-inhibited cyclic AMP-specific phosphodiesterase (PDE3) in regulating clonal BRIN-BD11 insulin

secreting cell survival. *Cell. Signal.* **12**, 541–548 (2000).

395. A. Z. Zhao, J. N. Huan, S. Gupta, R. Pal, A. Sahu, A phosphatidylinositol 3-kinase-phosphodiesterase 3b-cyclic AMP pathway in hypothalamic action of leptin on feeding. *Nat. Neurosci.* **5**, 727–728 (2002).
396. A. Sahu, A. S. Metlakunta, Hypothalamic phosphatidylinositol 3-kinase-phosphodiesterase 3B-cyclic AMP pathway of leptin signalling is impaired following chronic central leptin infusion. *J. Neuroendocrinol.* **17**, 720–726 (2005).
397. A. Sahu, A role of phosphodiesterase-3B pathway in mediating leptin action on proopiomelanocortin and neurotensin neurons in the hypothalamus. *Neurosci. Lett.* **479**, 18–21 (2010).
398. Y. W. Chung *et al.*, White to beige conversion in PDE3B KO adipose tissue through activation of AMPK signaling and mitochondrial function. *Sci. Rep.* **7**, 1–13 (2017).
399. P. Thompson, V. Manganiello, E. Degerman, Re-Discovering PDE3 Inhibitors - New Opportunities for a Long Neglected Target. *Curr. Top. Med. Chem.* **7**, 421–436 (2007).
400. G. S. Baillie, G. S. Tejeda, M. P. Kelly, Therapeutic targeting of 3’,5’-cyclic nucleotide phosphodiesterases: inhibition and beyond. *Nat. Rev. Drug Discov.* **18** (2019), doi:10.1038/s41573-019-0033-4.
401. F. B. Kraemer, W.-J. Shen, Hormone-Sensitive Lipase: control of intracellular tri-(di-)acylglycerol and cholesteryl ester hydrolysis Fredric. *J. Lipid Res.* **43**, 1585–1594 (2002).
402. G. Haemmerle *et al.*, Hormone-sensitive lipase deficiency in mice causes diglyceride accumulation in adipose tissue, muscle, and testis. *J. Biol. Chem.* **277**, 4806–4815 (2002).
403. E. Smirnova *et al.*, ATGL has a key role in lipid droplet/adiposome degradation in mammalian cells. *EMBO Rep.* **7**, 106–113 (2006).
404. J. Osuga *et al.*, Targeted disruption of hormone-sensitive lipase results in male sterility and adipocyte hypertrophy, but not in obesity. *Proc. Natl. Acad. Sci. U. S. A.* **97**, 787–92 (2000).
405. J. A. Villena, S. Roy, E. Sarkadi-Nagy, K. H. Kim, S. S. Hei, Desnutrin, an adipocyte gene encoding a novel patatin domain-containing protein, is induced by fasting and glucocorticoids: Ectopic expression of desnutrin increases triglyceride hydrolysis. *J. Biol. Chem.* **279**, 47066–47075 (2004).

406. C. M. Jenkins *et al.*, Identification, cloning, expression, and purification of three novel human calcium-independent phospholipase A2family members possessing triacylglycerol lipase and acylglycerol transacylase activities. *J. Biol. Chem.* **279**, 48968–48975 (2004).

407. R. Zimmermann *et al.*, Fat mobilization in adipose rissue is promoted by adipose triglyceride lipase. *Science*. **306**, 1383–1386 (2004).

408. P. C. Kienesberger, M. Oberer, A. Lass, R. Zechner, Mammalian patatin domain containing proteins: a family with diverse lipolytic activities involved in multiple biological functions. *J. Lipid Res.* **50**, S63–S68 (2009).

409. I. Cornaciu *et al.*, The minimal domain of adipose triglyceride lipase (ATGL) ranges until leucine 254 and can be activated and inhibited by CGI-58 and G0S2, respectively. *PLoS One*. **6**, 0–10 (2011).

410. X. Lu, X. Yang, J. Liu, Differential control of ATGL-mediated lipid droplet degradation by CGI-58 and G0S2. *Cell Cycle*. **9**, 2791–2797 (2010).

411. K. G. Soni *et al.*, Coatomer-dependent protein delivery to lipid droplets. *J. Cell Sci.* **122**, 1834–1841 (2009).

412. X. Yang *et al.*, The G0/G1 Switch Gene 2 Regulates Adipose Lipolysis through Association with Adipose Triglyceride Lipase. *Cell Metab.* **11**, 194–205 (2010).

413. A. Dessen *et al.*, Crystal structure of human cytosolic phospholipase A2 reveals a novel topology and catalytic mechanism. *Cell*. **97**, 349–360 (1999).

414. T. J. Rydel *et al.*, The crystal structure, mutagenesis, and activity studies reveal that patatin is a lipid acyl hydrolase with a Ser-Asp catalytic dyad. *Biochemistry*. **42**, 6696–6708 (2003).

415. S. J. Wijeyesakere, R. J. Richardson, J. A. Stuckey, Crystal structure of Patatin-17 in complex with aged and non-aged organophosphorus compounds. *PLoS One*. **9** (2014), doi:10.1371/journal.pone.0108245.

416. M. Schweiger *et al.*, The C-terminal region of human adipose triglyceride lipase affects enzyme activity and lipid droplet binding. *J. Biol. Chem.* **283**, 17211–17220 (2008).

417. A. C. Lake *et al.*, Expression, regulation, and triglyceride hydrolase activity of Adiponutrin family members. *J. Lipid Res.* **46**, 2477–2487 (2005).

418. K. M. Padmanabha Das *et al.*, Hypoxia-inducible lipid droplet-associated protein

inhibits adipose triglyceride lipase. *J. Lipid Res.* **59**, 531–541 (2018).

419. S. Murugesan, E. B. Goldberg, E. Dou, W. J. Brown, Identification of Diverse Lipid Droplet Targeting Motifs in the PNPLA Family of Triglyceride Lipases. *PLoS One*. **8** (2013), doi:10.1371/journal.pone.0064950.
420. X. Xie *et al.*, Identification of a novel phosphorylation site in adipose triglyceride lipase as a regulator of lipid droplet localization. *Am. J. Physiol. - Endocrinol. Metab.* **306**, 1449–1459 (2014).
421. J. Pagnon *et al.*, Identification and functional characterization of protein kinase A phosphorylation sites in the major lipolytic protein, adipose triglyceride lipase. *Endocrinology*. **153**, 4278–4289 (2012).
422. M. Ahmadian *et al.*, Desnutrin/ATGL is regulated by AMPK and is required for a brown adipose phenotype. *Cell Metab.* **13**, 739–748 (2011).
423. K. T. Ong, M. T. Mashek, S. Y. Bu, A. S. Greenberg, D. G. Mashek, Adipose triglyceride lipase is a major hepatic lipase that regulates triacylglycerol turnover and fatty acid signaling and partitioning. *Hepatology*. **53**, 116–126 (2011).
424. P. C. Kienesberger *et al.*, Early structural and metabolic cardiac remodelling in response to inducible adipose triglyceride lipase ablation. *Cardiovasc. Res.* **99**, 442–451 (2013).
425. M. Schweiger *et al.*, G0/G1 switch gene-2 regulates human adipocyte lipolysis by affecting activity and localization of adipose triglyceride lipase. *J. Lipid Res.* **53**, 2307–2317 (2012).
426. T. H. M. Grahn *et al.*, Fat-specific protein 27 (FSP27) interacts with adipose triglyceride lipase (ATGL) to regulate lipolysis and insulin sensitivity in human adipocytes. *J. Biol. Chem.* **289**, 12029–12039 (2014).
427. W. C. Liang, I. Nishino, Lipid storage myopathy. *Curr. Neurol. Neurosci. Rep.* **11**, 97–103 (2011).
428. K. Kaneko *et al.*, A novel mutation in PNPLA2 causes neutral lipid storage disease with myopathy and triglyceride deposit cardiomyovasculopathy: A case report and literature review. *Neuromuscul. Disord.* **24**, 634–641 (2014).
429. J. Fischer *et al.*, The gene encoding adipose triglyceride lipase (PNPLA2) is mutated in neutral lipid storage disease with myopathy. *Nat. Genet.* **39**, 28–30 (2007).
430. P. Reilich *et al.*, The phenotypic spectrum of neutral lipid storage myopathy due to

mutations in the PNPLA2 gene. *J. Neurol.* **258**, 1987–1997 (2011).

431. R. Schreiber, H. Xie, M. Schweiger, Of mice and men: The physiological role of adipose triglyceride lipase (ATGL). *Biochim. Biophys. Acta - Mol. Cell Biol. Lipids*. **1864**, 880–899 (2019).
432. R. Schreiber *et al.*, Hypophagia and metabolic adaptations in mice with defective ATGL-mediated lipolysis cause resistance to HFD-induced obesity. *Proc. Natl. Acad. Sci.* **112**, 13850–13855 (2015).
433. M. Schweiger *et al.*, Pharmacological inhibition of adipose triglyceride lipase corrects high-fat diet-induced insulin resistance and hepatosteatosis in mice. *Nat. Commun.* **8** (2017), doi:10.1038/ncomms14859.
434. N. Mayer *et al.*, Development of small-molecule inhibitors targeting adipose triglyceride lipase. *Nat. Chem. Biol.* **9**, 785–787 (2013).
435. H. Miyoshi *et al.*, Perilipin promotes hormone-sensitive lipase-mediated adipocyte lipolysis via phosphorylation-dependent and -independent mechanisms. *J. Biol. Chem.* **281**, 15837–15844 (2006).
436. T. K. Kerppola, Visualization of molecular interactions by fluorescence complementation. *Nat. Rev. Mol. Cell Biol.* **7**, 449–456 (2006).
437. T. K. Kerppola, Design and implementation of bimolecular fluorescence complementation (BiFC) assays for the visualization of protein interactions in living cells. *Nat. Protoc.* **1**, 1278–1286 (2006).
438. R. M. Wachter, M.-A. Elsliger, K. Kallio, G. T. Hanson, S. J. Remington, Structural basis of spectral shifts in the yellow-emission variants of green fluorescent protein. *Structure*. **6**, 1267–1277 (1998).
439. Sigma-Aldrich, Free Glycerol Reagent Technical Bulletin, 6–7 (2003).
440. G. J. Todaro, H. Green, Quantitative Studies of the Growth of Mouse Embryo Cells in Culture and Their Development Into Established Lines. *J. Cell Biol.* **17**, 299–313 (1963).
441. H. Green, O. Kehinde, An established preadipose cell line and its differentiation in culture II. Factors affecting the adipose conversion. *Cell*. **5**, 19–27 (1975).
442. C. S. Rubin, A. Hirsch, C. Fung, O. M. Rosen, Development of hormone receptors and hormonal responsiveness in vitro. *J.Biol.Chem.* **253**, 7570–7578 (1978).
443. H. Hauner, Complete adipose differentiation of 3T3 L1 cells in a chemically defined medium: Comparison to serum- containing culture conditions. *Endocrinology*. **127**,

865–872 (1990).

444. F. J. Ruiz-Ojeda, A. I. Rupérez, C. Gomez-Llorente, A. Gil, C. M. Aguilera, Cell models and their application for studying adipogenic differentiation in relation to obesity: A review. *Int. J. Mol. Sci.* **17**, 1–26 (2016).

445. H. Jörnvall, A. Blokzijl, P. Ten Dijke, C. F. Ibáñez, The Orphan Receptor Serine/Threonine Kinase ALK7 Signals Arrest of Proliferation and Morphological Differentiation in a Neuronal Cell Line. *J. Biol. Chem.* **276**, 5140–5146 (2001).

446. B. C. Kim *et al.*, Activin receptor-like kinase-7 induces apoptosis through activation of MAPKs in a Smad3-dependent mechanism in hepatoma cells. *J. Biol. Chem.* **279**, 28458–28465 (2004).

447. S. Yogosawa, T. Izumi, Roles of activin receptor-like kinase 7 signaling and its target, peroxisome proliferator-activated receptor γ, in lean and obese adipocytes. *Adipocyte*. **2**, 246–250 (2013).

448. S. Yogosawa, S. Mizutani, Y. Ogawa, T. Izumi, Activin receptor-like kinase 7 suppresses lipolysis to accumulate fat in obesity through downregulation of peroxisome proliferator-activated receptor γ and C/EBPα. *Diabetes*. **62**, 115–123 (2013).

449. R. Srivastava, E.-S. Lee, E. Sim, C.-S. New, C. F. Ibañez, Sustained anti-obesity effects of life-style change and anti-inflammatory interventions after conditional inactivation of the activin receptor ALK7. *bioRxiv* (2020), doi:10.1101/2020.07.28.224881.

450. W. Zhang *et al.*, ALK7 Gene Polymorphism is Associated with Metabolic Syndrome Risk and Cardiovascular Remodeling. *Arq. Bras. Cardiol.* **101**, 134–140 (2013).

451. A. E. Justice *et al.*, Protein-coding variants implicate novel genes related to lipid homeostasis contributing to body-fat distribution. *Nat. Genet.* **51**, 452–469 (2019).

452. S. Ying *et al.*, Alk7 Depleted Mice Exhibit Prolonged Cardiac Repolarization and Are Predisposed to Ventricular Arrhythmia. *PLoS One*. **11**, 1–14 (2016).

453. W. bo Li *et al.*, Silencing of activin receptor-like kinase 7 alleviates aortic stiffness in type 2 diabetic rats. *Acta Diabetol.* **52**, 717–726 (2015).

454. N. R. A. Beeley, K. S. Prickett, Section review oncologic, endocrine & metabolic: The amylin, CGRP and calcitonin family of peptides. *Expert Opin. Ther. Pat.* **6**, 555–567 (1996).

455. T. Liu *et al.*, Endogenous calcitonin gene-related peptide regulates lipid metabolism and energy homeostasis in male mice. *Endocrinology*. **158**, 1194–1206 (2017).

456. R. Harmancey, J. M. Senard, P. Rouet, A. Pathak, F. Smih, Adrenomedullin inhibits adipogenesis under transcriptional control of insulin. *Diabetes*. **56**, 553–563 (2007).
457. R. T. Dackor *et al.*, Hydrops Fetalis, Cardiovascular Defects, and Embryonic Lethality in Mice Lacking the Calcitonin Receptor-Like Receptor Gene. *Mol. Cell. Biol.* **26**, 2511–2518 (2006).
458. K. L. Fritz-Six, W. P. Dunworth, M. Li, K. M. Caron, Adrenomedullin signaling is necessary for murine lymphatic vascular development. *J. Clin. Invest.* **118**, 40–50 (2008).
459. S. L. Hoopes, H. H. Willcockson, K. M. Caron, Characteristics of Multi-Organ Lymphangiectasia Resulting from Temporal Deletion of Calcitonin Receptor-Like Receptor in Adult Mice. *PLoS One*. **7**, e45261 (2012).
460. R. B. Davis, D. O. Kechele, E. S. Blakeney, J. B. Pawlak, K. M. Caron, Lymphatic deletion of calcitonin receptor–like receptor exacerbates intestinal inflammation. *JCI Insight*. **2**, e92465 (2017).
461. N. Fukai *et al.*, Concomitant expression of adrenomedullin and its receptor components in rat adipose tissues. *Am. J. Physiol. - Endocrinol. Metab.* **288**, 56–62 (2005).
462. P. M. Zelissen, H. P. Koppeschaar, C. J. Lips, W. H. Hackeng, Calcitonin gene-related peptide in human obesity. *Peptides*. **12**, 861–3 (1991).
463. M. T. García-Unzueta, C. Montalban, C. Pesquera, J. R. Berrazueta, J. A. Amado, Plasma Adrenomedullin Levels in Type 1 Diabetes. *Diabetes Care*. **21**, 999–1003 (1998).
464. J. P. Hinson, S. Kapas, D. M. Smith, Adrenomedullin, a multifunctional regulatory peptide. *Endocr. Rev.* **21**, 138–167 (2000).
465. A. Martínez *et al.*, Is adrenomedullin a causal agent in some cases of type 2 diabetes? *Peptides*. **20**, 1471–1478 (1999).
466. H. M. Turk *et al.*, Relationship between plasma adrenomedullin levels and metabolic control, risk factors, and diabetic microangiopathy in patients with type 2 diabetes. *Diabetes Care*. **23**, 864–867 (2000).
467. O. Paulmyer-Lacroix *et al.*, Expression of adrenomedullin in adipose tissue of lean and obese women. *Eur. J. Endocrinol.* **155**, 177–185 (2006).
468. Y. Dong, A. Betancourt, M. Belfort, C. Yallampalli, Targeting Adrenomedullin to

Improve Lipid Homeostasis in Diabetic Pregnancies. *J. Clin. Endocrinol. Metab.* **102**, 3425–3436 (2017).

469. Y. Lv *et al.*, Adrenomedullin 2 enhances beiging in white adipose tissue directly in an adipocyte-autonomous manner and indirectly through activation of M2 macrophages. *J. Biol. Chem.* **291**, 23390–23402 (2016).
470. C. M. Aguilera *et al.*, Genome-wide expression in visceral adipose tissue from obese prepubertal children. *Int. J. Mol. Sci.* **16**, 7723–7737 (2015).
471. X. Zhang, L. A. Cupples, C.-T. Liu, A fine-mapping study of central obesity loci incorporating functional annotation and imputation. *Eur. J. Hum. Genet.* **8** (2018), doi:10.1038/s41431-018-0168-5.
472. I. Dahlman *et al.*, Numerous genes in loci associated with body fat distribution are linked to adipose function. *Diabetes*. **65**, 433–437 (2016).
473. A. M. Waterhouse, J. B. Procter, D. M. A. Martin, M. Clamp, G. J. Barton, Jalview Version 2—a multiple sequence alignment editor and analysis workbench. *Bioinformatics*. **25**, 1189–1191 (2009).
474. N. Arimura, T. Horiba, M. Imagawa, M. Shimizu, R. Sato, The Peroxisome Proliferator-activated Receptor γ Regulates Expression of the Perilipin Gene in Adipocytes. *J. Biol. Chem.* **279**, 10070–10076 (2004).
475. M. H. Akter, T. Yamaguchi, F. Hirose, T. Osumi, Perilipin, a critical regulator of fat storage and breakdown, is a target gene of estrogen receptor-related receptor α. *Biochem. Biophys. Res. Commun.* **368**, 563–568 (2008).
476. D. Li, Q. Kang, D. M. Wang, Constitutive coactivator of peroxisome proliferator-activated receptor (PPARγ), a novel coactivator of PPARγ that promotes adipogenesis. *Mol. Endocrinol.* **21**, 2320–2333 (2007).
477. Y. Takahashi, N. Ohoka, H. Hayashi, R. Sato, TRB3 suppresses adipocyte differentiation by negatively regulating PPARγ transcriptional activity. *J. Lipid Res.* **49**, 880–892 (2008).
478. S. C. Souza *et al.*, TNF-α induction of lipolysis is mediated through activation of the extracellular signal related kinase pathway in 3T3-L1 adipocytes. *J. Cell. Biochem.* **89**, 1077–1086 (2003).
479. J. Laurencikiene *et al.*, NF-κB is important for TNF-α-induced lipolysis in human adipocytes. *J. Lipid Res.* **48**, 1069–1077 (2007).

480. M. Rydén *et al.*, Targets for TNF-α-induced lipolysis in human adipocytes. *Biochem. Biophys. Res. Commun.* **318**, 168–175 (2004).
481. H. Miyoshi *et al.*, Perilipin overexpression in mice protects against diet-induced obesity. *J. Lipid Res.* **51**, 975–982 (2010).
482. S. Liu *et al.*, Development of hypertrophic cardiomyopathy in perilipin-1 null mice with adipose tissue dysfunction. *Cardiovasc. Res.* **105**, 20–30 (2015).
483. P. K. Saha, H. Kojima, J. Martinez-Botas, A. L. Sunehag, L. Chan, Metabolic adaptations in the absence of perilipin: Increased β-oxidation and decreased hepatic glucose production associated with peripheral insulin resistance but normal glucose tolerance in perilipin-null mice. *J. Biol. Chem.* **279**, 35150–35158 (2004).
484. Y. Takahashi *et al.*, Perilipin-Mediated Lipid Droplet Formation in Adipocytes Promotes Sterol Regulatory Element-Binding Protein-1 Processing and Triacylglyceride Accumulation. *PLoS One*. **8** (2013), doi:10.1371/journal.pone.0064605.
485. Y. Lyu *et al.*, Defective differentiation of adipose precursor cells from lipodystrophic mice lacking perilipin 1. *PLoS One*. **10**, 1–18 (2015).
486. J. H. Sohn *et al.*, Perilipin 1 (Plin1) deficiency promotes inflammatory responses in lean adipose tissue through lipid dysregulation. *J. Biol. Chem.* **293**, 13947–13988 (2018).
487. Y. Wang *et al.*, Perilipin Expression in Human Adipose Tissues: Effects of Severe Obesity, Gender, and Depot. *Obes. Res.* **11**, 930–936 (2003).
488. P. A. Kern, G. Di Gregorio, T. Lu, N. Rassouli, G. Ranganathan, Perilipin expression in human adipose tissue is elevated with obesity. *J. Clin. Endocrinol. Metab.* **89**, 1352–1358 (2004).
489. S. Mottagui-Tabar *et al.*, Evidence for an important role of perilipin in the regulation of human adipocyte lipolysis. *Diabetologia*. **46**, 789–797 (2003).
490. V. Puri *et al.*, Cidea is associated with lipid droplets and insulin sensitivity in humans. *Proc. Natl. Acad. Sci.* **105**, 7833–7838 (2008).
491. S. G. Yılmaz *et al.*, Childhood Obesity Risk in Relationship to Perilipin 1 (PLIN1) Gene Regulation by Circulating microRNAs 1. *OMICS*. **24**, 1–8 (2020).
492. C. E. Smith, J. M. Ordovás, Update on perilipin polymorphisms and obesity. *Nutr. Rev.* **70**, 611–621 (2012).

493. I. Jéru, C. Vatier, D. Araujo-Vilar, C. Vigouroux, O. Lascols, Clinical Utility Gene Card for: Familial partial lipodystrophy. *Eur. J. Hum. Genet.* **25**, 1–5 (2017).
494. S. Soenen *et al.*, Relationship between perilipin gene polymorphisms and body weight and body composition during weight loss and weight maintenance. *Physiol. Behav.* **96**, 723–728 (2009).
495. S. Deram *et al.*, Effects of perilipin (PLIN) gene variation on metabolic syndrome risk and weight loss in obese children and adolescents. *J. Clin. Endocrinol. Metab.* **93**, 4933–4940 (2008).
496. Y. Jang *et al.*, Genetic variation at the perilipin locus is associated with changes in serum free fatty acids and abdominal fat following mild weight loss. *Int. J. Obes.* **30**, 1601–1608 (2006).
497. L. Qi *et al.*, Intragenic linkage disequilibrium structure of the human perilipin gene (PLIN) and haplotype association with increased obesity risk in a multiethnic Asian population. *J. Mol. Med.* **83**, 448–456 (2005).
498. L. Qi *et al.*, Genetic variation at the perilipin (PLIN) locus is associated with obesity-related phenotypes in White women. *Clin. Genet.* **66**, 299–310 (2004).
499. E. E. J. G. Aller, E. C. M. Mariman, F. G. Bouwman, M. A. Van Baak, Genetic predictors of ≥5% weight loss by multidisciplinary advice to severely obese subjects. *J. Nutrigenet. Nutrigenomics*. **10**, 32–42 (2017).
500. L. Qi, C. Zhang, A. Greenberg, F. B. Hu, Common variations in perilipin gene, central obesity, and risk of type 2 diabetes in US women. *Obesity*. **16**, 1061–1065 (2008).
501. T. Niiya *et al.*, Activation of mouse phosphodiesterase 3B gene promoter by adipocyte differentiation in 3T3-L1 cells. *FEBS Lett.* **505**, 136–140 (2001).
502. T. Rahn Landström, J. Mei, M. Karlsson, V. Manganiello, E. Degerman, Down-regulation of cyclic-nucleotide phosphodiesterase 3B in 3T3-L1 adipocytes induced by tumour necrosis factor alpha and cAMP. *Biochem. J.* **346 Pt 2**, 337–343 (2000).
503. T. Ogura *et al.*, Reduction of phosphodiesterase 3B gene expression in peroxisome proliferator-activated receptor γ (+/-) mice independent of adipocyte size. *FEBS Lett.* **542**, 65–68 (2003).
504. H. Liu *et al.*, Importance of cAMP-response element-binding protein in regulation of expression of the murine cyclic nucleotide phosphodiesterase 3B (Pde3b) gene in differentiating 3T3-L1 preadipocytes. *J. Biol. Chem.* **281**, 21096–21113 (2006).

505. F. Hube, M. Birgel, Y. M. Lee, H. Hauner, Expression pattern of tumour necrosis factor receptors in subcutaneous and omental human adipose tissue: Role of obesity and non-insulin-dependent diabetes mellitus. *Eur. J. Clin. Invest.* **29**, 672–678 (1999).

506. T. Tzanavari, P. Giannogonas, K. P. Karalis, TNF-αlpha and obesity. *Curr. Dir. Autoimmun.* **11**, 145–156 (2010).

507. H. H. Zhang, M. Halbleib, F. Ahmad, V. C. Manganiello, A. S. Greenberg, Differentiated Human Adipocytes Through Activation of Extracellular Signal – Related Kinase and Elevation of Intracellular cAMP. *Diabetes*. **51**, 2929–2935 (2002).

508. Y. H. Choi *et al.*, Alterations in Regulation of Energy Homeostasis in Cyclic Nucleotide Phosphodiesterase 3B-null Mice_supp. *Library (Lond).*, 1–17 (2006).

509. Y. H. Choi *et al.*, Alterations in regulation of energy homeostasis in cyclic nucleotide phosphodiesterase 3B – null mice. *J. Clin. Invest.* **116**, 3240–3251 (2006).

510. E. Guirguis *et al.*, A role for phosphodiesterase 3B in acquisition of brown fat characteristics by white adipose tissue in male mice. *Endocrinology*. **154**, 3152–3167 (2013).

511. L. Härndahl *et al.*, β-Cell-targeted Overexpression of Phosphodiesterase 3B in Mice Causes Impaired Insulin Secretion, Glucose Intolerance, and Deranged Islet Morphology. *J. Biol. Chem.* **279**, 15214–15222 (2004).

512. J. Söhle *et al.*, Identification of new genes involved in human adipogenesis and fat storage. *PLoS One*. **7** (2012), doi:10.1371/journal.pone.0031193.

513. C. A. Emdin *et al.*, Analysis of predicted loss-of-function variants in disease. *Nat. Commun.* **9**, 1613 (2018).

514. J. Y. Kim, K. Tillison, J. H. Lee, D. a Rearick, C. M. Smas, The adipose tissue triglyceride lipase ATGL / PNPLA2 is downregulated by insulin and TNF {alpha} in 3T3-L1 adipocytes and is a target for transactivation by PPAR {gamma}. *Am. J. Physiol.* **291**, E115–E127 (2006).

515. E. E. Kershaw *et al.*, PPARγ regulates adipose triglyceride lipase in adipocytes in vitro and in vivo. *Am. J. Physiol. - Endocrinol. Metab.* **293**, 1736–1745 (2007).

516. P. Chakrabarti, K. V. Kandror, FoxO1 controls insulin-dependent adipose triglyceride lipase (ATGL) expression and lipolysis in adipocytes. *J. Biol. Chem.* **284**, 13296–13300 (2009).

517. P. Chakrabarti *et al.*, SIRT1 controls lipolysis in adipocytes via FOXO1-mediated

expression of ATGL. *J. Lipid Res.* **52**, 1693–1701 (2011).

518. S. Kralisch *et al.*, Isoproterenol, TNFα, and insulin downregulate adipose triglyceride lipase in 3T3-L1 adipocytes. *Mol. Cell. Endocrinol.* **240**, 43–49 (2005).
519. P. Chakrabarti, T. English, J. Shi, C. M. SMAS, K. V. Kandror, Mammalian Target of Rapamycin Complex 1 Suppresses Lipolysis, Stimulates Lipogenesis, and Promotes Fat Storage. *Diabetes*. **59**, 775–781 (2010).
520. H. M. Nagy *et al.*, Adipose triglyceride lipase activity is inhibited by long-chain acyl-coenzyme A. *Biochim. Biophys. Acta - Mol. Cell Biol. Lipids*. **1841**, 588–594 (2014).
521. S. Coassin *et al.*, Investigation and functional characterization of rare genetic variants in the adipose triglyceride lipase in a large healthy working population. *PLoS Genet.* **6**, 1–13 (2010).
522. V. Schoenborn *et al.*, The ATGL gene is associated with free fatty acids, triglycerides, and type 2 diabetes. *Diabetes*. **55**, 1270–1275 (2006).
523. G. Haemmerle *et al.*, Defective lipolysis and altered energy metabolism in mice lacking adipose triglyceride lipase_supp. *Science (80-.).* **312**, 734–737 (2006).
524. M. L. Peyot *et al.*, Adipose triglyceride lipase is implicated in fuel-and non-fuel-stimulated insulin secretion. *J. Biol. Chem.* **284**, 16848–16859 (2009).
525. P. C. Kienesberger *et al.*, Adipose triglyceride lipase deficiency causes tissue-specific changes in insulin signaling. *J. Biol. Chem.* **284**, 30218–30229 (2009).
526. P. M. Nunes *et al.*, Increased intramyocellular lipids but unaltered in vivo mitochondrial oxidative phosphorylation in skeletal muscle of adipose triglyceride lipase-deficient mice. *Am. J. Physiol. - Endocrinol. Metab.* **303**, 71–81 (2012).
527. G. Schoiswohl *et al.*, Adipose triglyceride lipase plays a key role in the supply of the working muscle with fatty acids. *J. Lipid Res.* **51**, 490–499 (2010).
528. R. Schreiber *et al.*, Cold-Induced Thermogenesis Depends on ATGL-Mediated Lipolysis in Cardiac Muscle, but Not Brown Adipose Tissue. *Cell Metab.* **26**, 753-763.e7 (2017).
529. J. W. Wu *et al.*, Fasting energy homeostasis in mice with adipose deficiency of desnutrin/adipose triglyceride lipase. *Endocrinology*. **153**, 2198–2207 (2012).
530. G. Schoiswohl *et al.*, Impact of reduced ATGL-mediated adipocyte lipolysis on obesity-associated insulin resistance and inflammation in male mice. *Endocrinology*. **156**, 3610–3624 (2015).
531. J. W. Wu *et al.*, Deficiency of liver adipose triglyceride lipase in mice causes

progressive hepatic steatosis. *Hepatology*. **54**, 122–132 (2011).

532. T. Tang *et al.*, Desnutrin/ATGL activates PPARδ to promote mitochondrial function for insulin secretion in islet β cells. *Cell Metab.* **18**, 883–895 (2013).
533. C. Attané *et al.*, A beta cell ATGL-lipolysis/adipose tissue axis controls energy homeostasis and body weight via insulin secretion in mice. *Diabetologia*. **59**, 2654–2663 (2016).
534. P. Jha *et al.*, Role of adipose triglyceride lipase (PNPLA2) in protection from hepatic inflammation in mouse models of steatohepatitis and endotoxemia. *Hepatology*. **59**, 858–869 (2014).
535. M. T. Sitnick *et al.*, Skeletal muscle triacylglycerol hydrolysis does not influence metabolic complications of obesity. *Diabetes*. **62**, 3350–3361 (2013).
536. S. Obrowsky *et al.*, Adipose triglyceride lipase is a TG hydrolase of the small intestine and regulates intestinal PPARα signaling. *J. Lipid Res.* **54**, 425–435 (2013).
537. B. N. Reid *et al.*, Hepatic overexpression of hormone-sensitive lipase and adipose triglyceride lipase promotes fatty acid oxidation, stimulates direct release of free fatty acids, and ameliorates steatosis. *J. Biol. Chem.* **283**, 13087–13099 (2008).
538. M. Ahmadian *et al.*, Adipose overexpression of desnutrin promotes fatty acid use and attenuates diet-induced obesity. *Diabetes*. **58**, 855–866 (2009).
539. J. W. Wu *et al.*, Epistatic interaction between the lipase-encoding genes Pnpla2 and Lipe causes liposarcoma in mice. *PLoS Genet.* **13**, 1–15 (2017).
540. M. Korbelius *et al.*, ATGL/CGI-58-Dependent Hydrolysis of a Lipid Storage Pool in Murine Enterocytes. *Cell Rep.* **28**, 1923-1934.e4 (2019).
541. U. Arulmani, A. MaassenVanDenBrink, C. M. Villalón, P. R. Saxena, Calcitonin gene-related peptide and its role in migraine pathophysiology. *Eur. J. Pharmacol.* **500**, 315–330 (2004).
542. Y. Song, J. Ahn, Y. Suh, M. E. Davis, K. Lee, Identification of Novel Tissue-Specific Genes by Analysis of Microarray Databases: A Human and Mouse Model. *PLoS One*. **8**, 1–17 (2013).
543. M. J. Lee, Transforming growth factor beta superfamily regulation of adipose tissue biology in obesity. *Biochim. Biophys. Acta - Mol. Basis Dis.* **1864**, 1160–1171 (2018).
544. J. Hino, T. Miyazawa, M. Miyazato, K. Kangawa, Bone morphogenetic protein-3b (BMP-3b) is expressed in adipocytes and inhibits adipogenesis as a unique complex.

Int. J. Obes. **36**, 725–734 (2012).

545. J. Hino *et al.*, Overexpression of bone morphogenetic protein-3b (BMP-3b) in adipose tissues protects against high-fat diet-induced obesity. *Int. J. Obes.* **41**, 483–488 (2017).
546. A. Hammarstedt *et al.*, WISP2 regulates preadipocyte commitment and PPARγ activation by BMP4. *Proc. Natl. Acad. Sci. U. S. A.* **110**, 2563–2568 (2013).
547. S. Aykul, J. Maust, M. Floer, E. Martinez-Hackert, *bioRxiv*, in press, doi:10.1101/2020.03.12.988568.
548. N. E. Wolins *et al.*, OP9 mouse stromal cells rapidly differentiate into adipocytes: Characterization of a useful new model of adipogenesis. *J. Lipid Res.* **47**, 450–460 (2006).
549. K. Zebisch, V. Voigt, M. Wabitsch, M. Brandsch, Protocol for effective differentiation of 3T3-L1 cells to adipocytes. *Anal. Biochem.* **425**, 88–90 (2012).
550. B. Magnusson, P. A. Svensson, L. M. S. Carlsson, K. Sjöholm, Activin B inhibits lipolysis in 3T3-L1 adipocytes. *Biochem. Biophys. Res. Commun.* **395**, 373–376 (2010).
551. C. Rodgarkia-Dara *et al.*, The activin axis in liver biology and disease. *Mutat. Res. - Rev. Mutat. Res.* **613**, 123–137 (2006).
552. D. J. Bernard, K. B. Lee, M. M. Santos, Activin B can signal through both ALK4 and ALK7 in gonadotrope cells. *Reprod. Biol. Endocrinol.* **4**, 1–8 (2006).
553. K. Kuwasako *et al.*, Characterization of the Human Calcitonin Gene-Related Peptide Receptor Subtypes Associated with Receptor Activity-Modifying Proteins. *Mol. Pharmacol.* **65**, 207–213 (2004).
554. P. Linscheid, D. Seboek, H. Zulewski, U. Keller, B. Müller, Autocrine/paracrine role of inflammation-mediated calcitonin gene-related peptide and adrenomedullin expression in human adipose tissue. *Endocrinology*. **146**, 2699–2708 (2005).
555. K. T. Dalen *et al.*, Adipose Tissue Expression of the Lipid Droplet-Associating Proteins S3-12 and Perilipin Is Controlled by Peroxisome Proliferator-Activated Receptor-γ. *Diabetes*. **53**, 1243–1252 (2004).
556. D. L. Brasaemle, T. Barber, A. R. Kimmel, C. Londos, Post-translational regulation of perilipin expression: Stabilization by stored intracellular neutral lipids. *J. Biol. Chem.* **272**, 9378–9387 (1997).
557. P. Ferré, F. Foufelle, SREBP-1c transcription factor and lipid homeostasis: Clinical

perspective. *Horm. Res.* **68**, 72–82 (2007).

558. L. M. DiPilato *et al.*, The Role of PDE3B Phosphorylation in the Inhibition of Lipolysis by Insulin. *Mol. Cell. Biol.* **35**, 2752–2760 (2015).

559. J. Stöckli *et al.*, ABHD15 regulates adipose tissue lipolysis and hepatic lipid accumulation. *Mol. Metab.* **25**, 83–94 (2019).

560. D. Roy *et al.*, Coordinated transcriptional control of adipocyte triglyceride lipase (Atgl) by transcription factors Sp1 and peroxisome proliferator-activated receptor γ (PPARγ) during adipocyte differentiation. *J. Biol. Chem.* **292**, 14827–14835 (2017).

561. X. Yang, B. L. Heckmann, X. Zhang, C. M. Smas, J. Liu, Distinct Mechanisms Regulate ATGL-Mediated Adipocyte Lipolysis by Lipid Droplet Coat Proteins. *Mol. Endocrinol.* **27**, 116–126 (2013).

562. M. Morikawa, D. Koinuma, K. Miyazono, C. H. Heldin, Genome-wide mechanisms of Smad binding. *Oncogene*. **32**, 1609–1615 (2013).

563. L. Zawel *et al.*, Human Smad3 and Smad4 Are Sequence-Specific Transcription Activators. *Mol. Cell*. **1**, 611–617 (1998).

564. C. J. David, J. Massagué, Contextual determinants of TGFβ action in development, immunity and cancer. *Nat. Rev. Mol. Cell Biol.* **19**, 419–435 (2018).

565. P. Martin-Malpartida *et al.*, Structural basis for genome wide recognition of 5-bp GC motifs by SMAD transcription factors. *Nat. Commun.* **8**, 1–15 (2017).

566. J. Massagué, J. Seoane, D. Wotton, Smad transcription factors. *Genes Dev.* **19**, 2783–2810 (2005).

567. S. P. Lakshmi, A. T. Reddy, R. C. Reddy, Transforming growth factor β suppresses peroxisome proliferator-activated receptor γ expression via both SMAD binding and novel TGF-β inhibitory elements. *Biochem. J.* **474**, 1531–1546 (2017).

568. L. Choy, R. Derynck, Transforming growth factor-β inhibits adipocyte differentiation by Smad3 interacting with CCAAT/enhancer-binding protein (C/EBP) and repressing C/EBP transactivation function. *J. Biol. Chem.* **278**, 9609–9619 (2003).

569. P. Oliver, B. Reynés, A. Caimari, A. Palou, Peripheral blood mononuclear cells: A potential source of homeostatic imbalance markers associated with obesity development. *Pflugers Arch. Eur. J. Physiol.* **465**, 459–468 (2013).

570. C. C. Liew, J. Ma, H. C. Tang, R. Zheng, A. A. Dempsey, The peripheral blood transcriptome dynamically reflects system wide biology: A potential diagnostic tool. *J.*

Lab. Clin. Med. **147**, 126–132 (2006).

571. M. E. Burczynski, A. J. Dorner, Transcriptional profling of peripheral blood cells in clinical pharmacogenomic studies. *Pharmacogenomics*. **7**, 187–202 (2006).
572. A. Samara, B. Marie, M. Pfister, S. Visvikis-Siest, Leptin expression in Peripheral Blood Mononuclear Cells (PBMCs) is related with blood pressure variability. *Clin. Chim. Acta*. **395**, 47–50 (2008).
573. A. Caimari, P. Oliver, W. Rodenburg, J. Keijer, A. Palou, Slc27a2 expression in peripheral blood mononuclear cells as a molecular marker for overweight development. *Int. J. Obes.* **34**, 831–839 (2010).
574. H. Ghanim *et al.*, Circulating mononuclear cells in the obese are in a proinflammatory state. *Circulation*. **110**, 1564–1571 (2004).
575. C. Zhao *et al.*, Quantification of allelic differential expression using a simple Fluorescence primer PCR-RFLP-based method. *Sci. Rep.* **9**, 1–8 (2019).
576. H. B. Lee *et al.*, Allele-specific quantitative PCR for accurate, rapid, and cost-effective genotyping. *Hum. Gene Ther.* **27**, 425–435 (2016).
577. F. O. Desmet *et al.*, Human Splicing Finder: An online bioinformatics tool to predict splicing signals. *Nucleic Acids Res.* **37**, 1–14 (2009).
578. Y. Lee, D. C. Rio, Mechanisms and regulation of alternative Pre-mRNA splicing. *Annu. Rev. Biochem.* **84**, 291–323 (2015).
579. Y. WANG *et al.*, Mechanism of alternative splicing and its regulation. *Biomed. Reports*. **3**, 152–158 (2015).
580. E. Scotto-Lavino, G. Du, M. A. Frohman, 3’ end cDNA amplification using classic RACE. *Nat. Protoc.* **1**, 2742–2745 (2006).
581. S. Zhang *et al.*, Base-specific mutational intolerance near splice-sites clarifies role of non-essential splice nucleotides. *Genome Res.* **28**, 968–974 (2018).
582. M. A. Rivas *et al.*, Effect of predicted protein-truncating genetic variants on the human transcriptome. *Science (80-.).* **348**, 666–669 (2015).
583. M. B. Shapiro, P. Senapathy, RNA splice junctions of different classes of eukaryotes: Sequence statistics and functional implications in gene expression. *Nucleic Acids Res.* **15**, 7155–7174 (1987).
584. M. Krawczak *et al.*, Single base-pair substitutions in exon-intron junctions of human genes: Nature, distribution, and consequences for mRNA splicing. *Hum. Mutat.* **28**,

150–158 (2007).

585. G. Vieyres, I. Reichert, A. Carpentier, F. W. R. Vondran, T. Pietschmann, *The ATGL lipase cooperates with ABHD5 to mobilize lipids for hepatitis C virus assembly* (2020; http://dx.doi.org/10.1371/journal.ppat.1008554), vol. 16.

586. M. Schweiger *et al.*, Measurement of Lipolysis. *Methods Enzym.* **538**, 171–193 (2014).

587. Promega Corporation, Dual-Luciferase ® Reporter Assay System - Technical Manual, 608–277 (2015).

588. J. M. Topczewska *et al.*, Dual roles of Cripto as a ligand and coreceptor. *Nat. Med.* **12**, 1–4 (2006).

589. A. Boulling *et al.*, Functional analysis of pancreatitis-associated missense mutations in the pancreatic secretory trypsin inhibitor (SPINK1) gene. *Eur. J. Hum. Genet.* **15**, 936–942 (2007).

590. W. Shi *et al.*, GADD34-PP1c recruited by Smad7 dephosphorylates TGFβ type I receptor. *J. Cell Biol.* **164**, 291–300 (2004).

591. F. Huang, Y.-G. Chen, Regulation of TGF-β receptor activity. *Cell Biosci.* **2**, 9 (2012).

592. S. Itoh, P. ten Dijke, Negative regulation of TGF-β receptor/Smad signal transduction. *Curr. Opin. Cell Biol.* **19**, 176–184 (2007).

593. P. Lönn, A. Morén, E. Raja, M. Dahl, A. Moustakas, Regulating the stability of TGFβ receptors and Smads. *Cell Res.* **19**, 21–35 (2009).

594. L. Zhang *et al.*, Zebrafish Dpr2 inhibits mesoderm induction by promoting degradation of nodal receptors. *Science (80-.).* **306**, 114–117 (2004).

595. C.-Y. Yeo, M. Whitman, Nodal Signals to Smads through Cripto-Dependent and Cripto-Independent Mechanisms. *Mol. Cell*. **7**, 949–957 (2001).

596. K. J. Shin *et al.*, A single lentiviral vector platform for microRNA-based conditional RNA interference and coordinated transgene expression. *Proc. Natl. Acad. Sci. U. S. A.* **103**, 13759–13764 (2006).

597. T. Higashimoto *et al.*, The woodchuck hepatitis virus post-transcriptional regulatory element reduces readthrough transcription from retroviral vectors. *Gene Ther.* **14**, 1298–1304 (2007).

598. N. J. Arhel, S. Souquere-Besse, P. Charneau, Wild-type and central DNA flap defective HIV-1 lentiviral vector genomes: Intracellular visualization at ultrastructural resolution levels. *Retrovirology*. **3**, 1–7 (2006).

599. A. T. Das *et al.*, Viral Evolution as a Tool to Improve the Tetracycline-regulated Gene Expression System. *J. Biol. Chem.* **279**, 18776–18782 (2004).
600. R. F. Shearer, D. N. Saunders, Experimental design for stable genetic manipulation in mammalian cell lines: Lentivirus and alternatives. *Genes to Cells*. **20**, 1–10 (2015).
601. M. Gossen, H. Bujard, Tight control of gene expression in mammalian cells by tetracycline-responsive promoters. *Proc. Natl. Acad. Sci. U. S. A.* **89**, 5547–5551 (1992).
602. D. Ajjajia *et al.*, Dual binding motifs underpin the hierarchical association of perilipins1-3 with lipid droplets. *Mol. Biol. Cell*. **30**, 703–716 (2019).
603. J. S. Hansen, S. De Maré, H. A. Jones, O. Göransson, K. Lindkvist-Petersson, Visualization of lipid directed dynamics of perilipin 1 in human primary adipocytes. *Sci. Rep.* **7**, 1–14 (2017).
604. A. Sahu-Osen *et al.*, CGI-58/ABHD5 is phosphorylated on Ser239 by protein kinase A: control of subcellular localization. *J. Lipid Res.* **56**, 109–121 (2015).
605. J. G. Granneman *et al.*, Analysis of lipolytic protein trafficking and interactions in adipocytes. *J. Biol. Chem.* **282**, 5726–5735 (2007).
606. M. Daval *et al.*, Anti-lipolytic action of AMP-activated protein kinase in rodent adipocytes. *J. Biol. Chem.* **280**, 25250–25257 (2005).
607. M. W. Anthonsen, L. Rönnstrand, C. Wernstedt, E. Degerman, C. Holm, Identification of novel phosphorylation sites in hormone-sensitive lipase that are phosphorylated in response to isoproterenol and govern activation properties in vitro. *J. Biol. Chem.* **273**, 215–221 (1998).
608. H. Venselaar, T. A. H. te Beek, R. K. P. Kuipers, M. L. Hekkelman, G. Vriend, Protein structure analysis of mutations causing inheritable diseases. An e-Science approach with life scientist friendly interfaces. *BMC Bioinformatics*. **11**, 548 (2010).
609. M. Ueno *et al.*, Fat-specific protein 27 modulates nuclear factor of activated T cells 5 and the cellular response to stress. *J. Lipid Res.* **54**, 734–743 (2012).
610. H. P. H. Moore, R. B. Silver, E. P. Mottillo, D. A. Bernlohr, J. G. Granneman, Perilipin targets a novel pool of lipid droplets for lipolytic attack by hormone-sensitive lipase. *J. Biol. Chem.* **280**, 43109–43120 (2005).
611. C. Morimoto, K. Kameda, T. Tsujita, H. Okuda, Relationships between lipolysis induced by various lipolytic agents and hormone-sensitive lipase in rat fat cells. *J.*

Lipid Res. **42**, 120–127 (2001).

612. M. Morell, A. Espargaro, F. X. Aviles, S. Ventura, Study and selection of in vivo protein interactions by coupling bimolecular fluorescence complementation and flow cytometry. *Nat. Protoc.* **3**, 22–33 (2008).

613. D. L. Brasaemle, D. M. Levin, D. C. Adler-Wailes, C. Londos, The lipolytic stimulation of 3T3-L1 adipocytes promotes the translocation of hormone-sensitive lipase to the surfaces of lipid storage droplets. *Biochim. Biophys. Acta - Mol. Cell Biol. Lipids*. **1483**, 251–262 (2000).

614. T. K. Kerppola, BiFC analysis as a probe of protein interactions in living cells. *Annu Rev Biophys*, 465–487 (2008).

615. PromegaCorporation, NanoBiT® Protein:Protein Interaction System. *Tm439*. **4**, 1–28 (2015).

616. L. J. Syu, A. R. Saltiel, Lipotransin: A novel docking protein for hormone-sensitive lipase. *Mol. Cell*. **4**, 109–115 (1999).

617. G. Xu, C. Sztalryd, C. Londos, Degradation of perilipin is mediated through ubiquitination-proteasome pathway. *Biochim. Biophys. Acta - Mol. Cell Biol. Lipids*. **1761**, 83–90 (2006).

618. J. Kovsan, R. Ben-Romano, S. C. Souza, A. S. Greenberg, A. Rudich, Regulation of adipocyte lipolysis by degradation of the perilipin protein: Nelfinavir enhances lysosome-mediated perilipin proteolysis. *J. Biol. Chem.* **282**, 21704–21711 (2007).

619. L. Ju *et al.*, Obesity-associated inflammation triggers an autophagy–lysosomal response in adipocytes and causes degradation of perilipin 1. *Cell Death Dis.* **10**, 121 (2019).

620. T. Schneider-Poetsch *et al.*, Inhibition of eukaryotic translation elongation by cycloheximide and lactimidomycin. *Nat. Chem. Biol.* **6**, 209–217 (2010).

621. D. C. Adler-Wailes *et al.*, Effects of the human immunodeficiency virus-protease inhibitor, ritonavir, on basal and catecholamine-stimulated lipolysis. *J. Clin. Endocrinol. Metab.* **90**, 3251–3261 (2005).

622. J. T. Tansey *et al.*, Functional studies on native and mutated forms of perilipins: A role in protein kinase a-mediated lipolysis of triacylglycerols in Chinese hamster ovary cells. *J. Biol. Chem.* **278**, 8401–8406 (2003).

623. S. C. Souza *et al.*, Modulation of hormone-sensitive lipase and protein kinase A-

mediated lipolysis by perilipin A in an adenoviral reconstituted system. *J. Biol. Chem.* **277**, 8267–8272 (2002).

624. Addgene, Viral Vectors 101: A Desktop Resource. **2018** (2018), doi:10.1016/j.pepi.2014.08.002.
625. J. B. Connoly, Lentiviruses in gene therapy clinical reseach. *Gene Ther.* **9**, 1730–1734 (2002).
626. D. Schleinitz, Y. Böttcher, M. Blüher, P. Kovacs, The genetics of fat distribution. *Diabetologia*. **57**, 1276–1286 (2014).
627. S. Kathiresan, Putative medicines that mimic mutations. *Nature*. **548**, 530–531 (2017).
628. A. Ghorbani, M. Abedinzade, Comparison of In Vitro and In Situ Methods for Studying Lipolysis. *ISRN Endocrinol.* **2013**, 1–6 (2013).
629. A. Armani *et al.*, Cellular models for understanding adipogenesis, adipose dysfunction, and obesity. *J. Cell. Biochem.* **110**, 564–572 (2010).
630. S. Morrison, S. L. McGee, 3T3-L1 adipocytes display phenotypic characteristics of multiple adipocyte lineages. *Adipocyte*. **3945**, 295–302 (2015).
631. A. M. Zimmer, Y. K. Pan, T. Chandrapalan, R. W. M. Kwong, S. F. Perry, Loss-of-function approaches in comparative physiology: Is there a future for knockdown experiments in the era of genome editing? *J. Exp. Biol.* **222** (2019), doi:10.1242/jeb.175737.
632. S. Mocellin, M. Provenzano, RNA interference: Learning gene knock-down from cell physiology. *J. Transl. Med.* **2**, 1–6 (2004).
633. J. W. Zhang, D. J. Klemm, C. Vinson, M. D. Lane, Role of CREB in Transcriptional Regulation of CCAAT/Enhancer-binding Protein β Gene during Adipogenesis. *J. Biol. Chem.* **279**, 4471–4478 (2004).
634. Y. Li *et al.*, Adrenomedullin is a novel adipokine: Adrenomedullin in adipocytes and adipose tissues. *Peptides*. **28**, 1129–1143 (2007).
635. H. Zhang *et al.*, Intermedin/adrenomedullin 2 polypeptide promotes adipose tissue browning and reduces high-fat diet-induced obesity and insulin resistance in mice. *Int. J. Obes.* **40**, 852–860 (2016).
636. K. A. Metwalley, H. S. Farghaly, T. Sherief, Plasma adrenomedullin level in children with obesity: relationship to left ventricular function. *World J. Pediatr.* **14**, 84–91 (2018).

637. L. H. Wang *et al.*, Serum levels of calcitonin gene-related peptide and substance P are decreased in patients with diabetes mellitus and coronary artery disease. *J. Int. Med. Res.* **40**, 134–140 (2012).

638. H. B. Dai *et al.*, Adrenomedullin Attenuates Inflammation in White Adipose Tissue of Obese Rats Through Receptor-Mediated PKA Pathway. *Obesity*. **00**, 1–12 (2020).

639. A. Guilherme, F. Henriques, A. H. Bedard, M. P. Czech, Molecular pathways linking adipose innervation to insulin action in obesity and diabetes mellitus. *Nat. Rev. Endocrinol.* **15**, 207–225 (2019).

640. T. J. Bartness, Y. Liu, Y. B. Shrestha, V. Ryu, Neural innervation of white adipose tissue and the control of lipolysis. *Front. Neuroendocrinol.* **35**, 473–493 (2014).

641. T. J. Bartness, Y. B. Shrestha, C. H. Vaughan, G. J. Schwartz, C. K. Song, Sensory and sympathetic nervous system control of white adipose tissue lipolysis. *Mol. Cell. Endocrinol.* **318**, 34–43 (2010).

642. H. Sadie-Van Gijsen, Adipocyte biology: It is time to upgrade to a new model. *J. Cell. Physiol.* **234**, 2399–2425 (2019).

643. K. Karastergiou *et al.*, Growth hormone receptor expression in human gluteal versus abdominal subcutaneous adipose tissue: Association with body shape. *Obesity*. **24**, 1090–1096 (2016).

644. Q. Wu *et al.*, Translation affects mRNA stability in a codon-dependent manner in human cells. *Elife*. **8**, 1–22 (2019).

645. S. H. Boo, Y. K. Kim, The emerging role of RNA modifications in the regulation of mRNA stability. *Exp. Mol. Med.* **52**, 400–408 (2020).

646. A. Narula, J. Ellis, J. M. Taliaferro, O. S. Rissland, Coding regions affect mRNA stability in human cells. *Rna*. **25**, 1751–1764 (2019).

647. E. M. Pennisi *et al.*, Neutral Lipid Storage Diseases: clinical/genetic features and natural history in a large cohort of Italian patients. *Orphanet J. Rare Dis.* **12**, 1–10 (2017).

648. S. Missaglia, R. Coleman, A. Mordente, D. Tavian, Neutral Lipid Storage Diseases as Cellular Model to Study Lipid Droplet Function. *Cells*. **8**, 187 (2019).

649. H. Miyoshi, J. W. Perfield II, M. S. Obin, A. S. Greenberg, Adipose Triglyceride Lipase Regulates Basal Lipolysis and Lipid Droplet Size in Adipocytes. *J Cell Biochem*. **105**, 1430–1436 (2009).

650. E. Arvidsson, L. Blomqvist, M. Rydén, Depot-specific differences in perilipin mRNA but not protein expression in obesity. *J. Intern. Med.* **255**, 595–601 (2004).
651. M. R. Nelson *et al.*, The support of human genetic evidence for approved drug indications. *Nat. Genet.* **47**, 856–860 (2015).
652. Y. Momozawa, K. Mizukami, Unique roles of rare variants in the genetics of complex diseases in humans. *J. Hum. Genet.* **66**, 11–23 (2021).
653. R. M. Plenge, E. M. Scolnick, D. Altshuler, Validating therapeutic targets through human genetics. *Nat. Rev. Drug Discov.* **12**, 581–594 (2013).
654. J. Cohen *et al.*, Low LDL cholesterol in individuals of African descent resulting from frequent nonsense mutations in PCSK9. *Nat. Genet.* **37**, 161–165 (2005).
655. J. C. Cohen, E. Boerwinkle, T. H. Mosley, H. H. Hobbs, Sequence Variations in PCSK9, Low LDL, and Protection against Coronary Heart Disease. *Hear. Dis.* **354**, 1264–1272 (2006).
656. M. S. Sabatine *et al.*, Evolocumab and Clinical Outcomes in Patients with Cardiovascular Disease. *N. Engl. J. Med.* **376**, 1713–1722 (2017).
657. G. R. Cutter, Y. Liu, Personalized medicine: The return of the house call? *Neurol. Clin. Pract.* **2**, 343–351 (2012).
658. C. Cain, ALK7's obese functions. *Sci. Exch.* **7**, 1090 (2014).
659. I. K. Cerk *et al.*, A peptide derived from G0/G1 switch gene 2 acts as noncompetitive inhibitor of adipose triglyceride lipase. *J. Biol. Chem.* **289**, 32559–32570 (2014).
660. A. Ghorbani, M. Abedinzade, Comparison of in vitro and in situ methods for studying lipolysis. *ISRN Endocrinol.* **2013**, 205385 (2013).
661. M. Blüher, Transgenic animal models for the study of adipose tissue biology. *Best Pract. Res. Clin. Endocrinol. Metab.* **19**, 605–623 (2005).
662. Q. A. Wang, P. E. Scherer, R. K. Gupta, Improved methodologies for the study of adipose biology: Insights gained and opportunities ahead. *J. Lipid Res.* **55**, 605–624 (2014).
663. A. Kulyté *et al.*, Genome-wide association study of adipocyte lipolysis in the GENetics of adipocyte lipolysis (GENiAL) cohort. *Mol. Metab.* **34**, 85–96 (2020).
664. P. Djian, D. A. K. Roncari, C. H. Hollenberg, Influence of anatomic site and age on the replication and differentiation of rat adipocyte precursors in culture. *J. Clin. Invest.* **72**, 1200–1208 (1983).

Appendices

Appendix 1. Primers for cloning

Name	Type	Sequence (5’ to 3’)
SpeI-myc-Plin1_Fwd	Forward	TTTTTTTACTAGTACCATGGAACAGAAACTCATCTCAGAAG
Plin1-NotI_Rev	Reverse	TTTTTTTGCGGCCGCTCAGCTCTTCTTGCGCAGCTGG

Appendix 2. Primers for site-directed mutagenesis

Name	Type	Sequence (5’ to 3’)
PLIN1_L90P_Fwd	Forward	CTGCCAATGAGCCGGCCTGCCGAGG
PLIN1_L90P_Rev	Reverse	CCTCGGCAGGCCGGCTCATTGGCAG
PNPLA2_S47A_Fwd	Forward	CTACGGCGCCGCGGCCGGGGC
PNPLA2_S47A_Rev	Reverse	GCCCCGGCCGCGGCGCCGTAG

Appendix 3. siRNAs for knockdown studies

Target gene	Catalogue No
Acvr1c	L-045747-01-0005
Calcrl	L-045370-00-0005
Plin1	L-056623-01-0005
Pde3b	L-043781-00-0005
Pnpla2	L-040220-01-0005
Non-targeting pool (NC)	D-001810-10-20

Appendix 4. Primers for qPCR

Gene	Species	TaqMan gene expression assay	Type	Primer sequences (5' to 3')
Acvr1c	Mouse	Mm03023957_m1		
Calcrl	Mouse	Mm00516986_m1		
Plin1	Mouse	Mm00558672_m1		
Pde3b	Mouse	Mm00691635_m1		
Pnpla2	Mouse	Mm00503040_m1		
Pparg2	Mouse		Forward	GATGCACTGCCTATGAGCACTT
			Reverse	AGAGGTCCACAGAGCTGATTCC
			Probe	6FAM-AGAGATGCCATTCTGGCCCAC-TAMRA
Ppia	Mouse		Forward	TTCCTCCTTTCACAGAATTATTCCA
			Reverse	CCGCCAGTGCCATTATGG
			Probe	6FAM-ATTCATGTGCCAGGGTGGTGACTTTACAC-TAMRA
Adipoq	Mouse		Forward	GTTGCAAGCTCTCCTGTTCC
			Reverse	ATCCAACCTGCACAAGTTCC
			Probe	6FAM-TCATGCCGAAGATGACGTTA-TAMRA
Lep	Mouse		Forward	CCAGGATGACACCAAAACCCT
			Reverse	GATACCGACTGCGTGTGTGA
Slc2a4	Mouse		Forward	TTATTGCAGCGCCTGAGTCT
			Reverse	GGGTTCCCCATCGTCAGAG
			Probe	6FAM-TAAAACAAGATGCCGTCGGG-TAMRA
HPRT1	Human	Hs02800695_m1		
PNPLA2	Human	Hs00386101_m1		
B2m	Mouse		Forward	ACCGGCCTGTATGCTATCCAG
			Reverse	GTAGCAGTTCAGTATGTTCGGCTTC
PLIN1	Human		Forward	CCCCCTGAAAAGATTGCTTCT
			Reverse	GGAACGCTGATGCTGTTTCTG
			Probe	6FAM-CATCTCCACCCGCCTCCGCA-TAMRA

Appendix 5. Antibodies and fluorescent dyes for Western blotting and immunofluorescence

Target protein	Host	Application	Dilution	Supplier	Catalogue No
Primary antibodies					
ACVR1C (A-1)	Mouse	WB	1:1000	Santa Cruz Biotechnology, USA	sc-374538
Myc tag (clone 4A6)	Mouse	WB/IF	1:1000	Millipore, USA	05-724
PLIN1	Mouse	WB	1:1000	Vala Sciences, USA	4854
PLIN1 (K117)	Rabbit	IF	1:50	Cell Signalling Technology, USA	3467
p-PLIN1 (Ser522)	Mouse	WB	1:1000	Vala Sciences, USA	4856
HSL	Rabbit	WB	1:1000	Cell Signalling Technology, USA	4107
p-HSL (Ser660)	Rabbit	WB	1:1000	Cell Signalling Technology, USA	4126
Smad2	Rabbit	WB	1:5000	Cell Signalling Technology, USA	3122
p-Smad2 (Ser465/467)	Rabbit	WB	1:500	Cell Signalling Technology, USA	3108
GFP	Mouse	WB	1:1000	Roche, Switzerland	11814460001
ABHD5	Rabbit	WB	1:1000	Proteintech, USA	12201-1-AP
PNPLA2	Rabbit	WB	1:1000	Cell Signalling Technology, USA	2138
PPARγ (C26H12)	Rabbit	WB	1:1000	Cell Signalling Technology, USA	2435
FABP4 (C-15)	Goat	WB	1:5000	Santa Cruz Biotechnology, USA	sc-18661
Calnexin	Rabbit	WB	1:4000	Abcam, UK	ab22595
GAPDH	Rabbit	WB	1:10000	GeneTex, USA	GTX100118
HRP-linked secondary antibodies					
Mouse IgG	Horse	WB	1:5000	Cell Signalling Technology, USA	7076
Rabbit IgG	Goat	WB	1:5000	Cell Signalling Technology, USA	7074
Goat IgG	Rabbit	WB	1:5000	Thermo Fisher Scientific, USA	81-1620
Fluorescent probe-linked secondary antibody					
Mouse IgG Alexa Fluor 405	Goat	IF	1:1000	Thermo Fisher Scientific, USA	A31553
Mouse IgG Alexa Fluor 488	Goat	IF	1:1000	Thermo Fisher Scientific, USA	A11029
Mouse IgG Alexa Fluor 647	Goat	IF	1:1000	Thermo Fisher Scientific, USA	A28181

Appendix 5. Antibodies and fluorescent dyes for Western blotting and immunofluorescence (continued)

Target protein	Host	Application	Dilution	Supplier	Catalogue No
Fluorescent dyes					
BODIPY 493/503	N/A	IF	1:1000	Thermo Fisher Scientific, USA	D3922
HCS LipidTox Deep Red	N/A	IF	1:1000	Thermo Fisher Scientific, USA	H34477
ProLong Gold Antifade Mountant	N/A	IF	N/A	Thermo Fisher Scientific, USA	P36930
ProLong Gold Antifade Mountant with DAPI	N/A	IF	N/A	Thermo Fisher Scientific, USA	P36931
ProLong Diamond Antifade Mountant with DAPI	N/A	IF	N/A	Thermo Fisher Scientific, USA	P36966